The adsorption of binary and ternary gaseous mixtures on molecular sieves.

Al-Qassab, Azzam Abdul-Aziz-Ismail

Award date:
1984

Awarding institution:
University of Bath

THE ADSORPTION OF BINARY AND TERNARY

GASEOUS MIXTURES ON MOLECULAR SIEVES

submitted by Azzam Abdul-Aziz Ismail Al-Qassab

for the degree of PhD

of the University of Bath,

1984

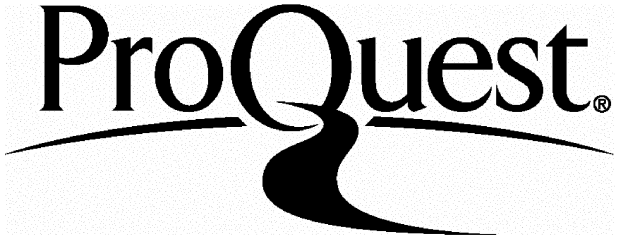

ACKNOWLEDGEMENTS

I have much pleasure in acknowledging my sincere gratitude to Professor W.J. Thomas for his generous and patient supervision in every phase of the preparation of the work. I am greatly indebted to the staff of the School of Chemical Engineering, especially Dr. Usman Ullah and Mr. T. Walton, for their valuable help. Many thanks, also, go to Mr. K.G. Blackmore and David Sirl for their help.

I must make special mention of the Foundation of the Technical Institute, Iraq, without whose grant this research would not have been possible. I am also indebted to my colleagues of the Department of Chemical Industries, Institute of Technology, Baghdad, whose kindness and co-operation have been a constant encouragement. I should like to thank Mrs. Paula Keilthy, who helpfully typed the thesis.

Finally, I owe a special debt of gratitude to my family, who have supported me in countless ways. I am particularly grateful to my brother, Natiq, for much practical assistance.

To my Family

CONTENTS

NOMENCLATURE

Symbol	Description	Units
A	Cross-sectional area of adsorption column	cm^2
a	Coefficient in empirical Langmuir equation	$mol\ g^{-1}$
b	Coefficient in empirical Langmuir equation	$cm^3\ mol^{-1}$
b'	Empirical coefficient in modified extended Langmuir equation	$cm^3\ mol^{-1}$
C	Total gas phase concentration	$mol\ cm^{-3}$
c	Gas phase concentration	$mol\ cm^{-3}$
c^*	Gas phase concentration at equilibrium	$mol\ cm^{-3}$
D_c	Crystal diffusion coefficient	$cm^2\ sec^{-1}$
D_m	Micropore diffusion coefficient	$cm^2\ sec^{-1}$
D_s	Surface diffusion coefficient	$cm^2\ sec^{-1}$
F	Molar flowrate	$mol\ min^{-1}$
K	Henry's law constant	$molecule\ cavity^{-1}\ bar^{-1}$
K_0	Henry's law constant	$molecule\ cavity^{-1}\ bar^{-1}$
$K_{1,2}$	Separation factor	
K_0, K_{10}, K_{12}, K_{13}, K_{20}, K_{21}, K_{23}, K_{30}, K_{31}, K_{32}	Constants in Freundlich-type multicomponent equations	

Symbol	Description	Units
K_f	Empirical constant in Freundlich equation (for n = 1)	$cm^3\ g^{-1}$
K_G	Kinetic parameter in linear driving force model	sec^{-1}
$K_g a$	Mass transfer film resistance	sec^{-1}
l	Adsorbent bed length	cm
m	Mass of adsorbent OR saturation limit (an integer, statistical thermodynamic model)	g
n	Freundlich constant	
n_{10} n_{20} n_{30}	Constant in Freundlich-type multicomponent equation	
p	Adsorbate partial pressure	bar
Q	Total adsorbed phase concentration (separation factor)	$mol\ g^{-1}$
	OR	
	average number of molecules per cavity (statistical thermodynamic model)	$molecule\ cavity^{-1}$
q	Adsorbed phase concentration	$mol\ g^{-1}$
q^*	Adsorbed phase concentration in equilibrium with concentration c	$mol\ g^{-1}$
R	Instantaneous rate of adsorption or gas constant	$mol\ sec^{-1}$
r	5A molecular sieve crystal equivalent radius	cm
T	Temperature	°K
t_0	Stoichiometric time	sec
t_e	Time at which the bed is at equilibrium	sec
t_n	Time at which transfer zone flattens out to plateau zone	sec
u	Interstitial flowrate	$cm^3\ sec^{-1}$

Symbol	Description	Units
v_b	Bed volume	
y	Mole fraction of component in total gas phase	
β	Effective molecular volume of adsorbate	$\mathring{A}$ molecule^{-1}
ν	Effective volume of molecular sieve cavity	$\mathring{A}^3$
θ	Film resistance parameter (Rosen) dimensionless	
μ	Bed length parameter (Rosen) dimensionless	
τ	Time parameter (Rosen) dimensionless	
ρ_{bulk}	Bulk density of adsorbent bed	g cm^{-3}
ρ_{pellet}	Adsorbent pellet density	g cm^{-3}
ε	Total bed voidage	
ε_{IG}	Intergranular voidage	
ε_{macro}	Adsorbent macro-pore voidage	

Subscripts

M	Methane
E	Ethane
p	Propane
i	Condition at bed inlet or component i
o	Condition at bed outlet
j	Component j

SUMMARY

Equilibrium adsorption isotherms were obtained for methane, ethane and propane in nitrogen on a 5A molecular sieve and also for methane and carbon dioxide on 5A and 4A molecular sieves at 25° C. The single component experimental data of these gases agreed well with the empirical Langmuir and Freundlich models. A statistical thermodynamic model also represented the data fairly well.

Ternary isotherms for methane, ethane and propane mixtures and binary isotherms for methane and carbon dioxide mixtures were obtained experimentally. A modified extended Langmuir model correlated the adsorption of ternary and binary mixtures fairly well. The Freundlich-type multicomponent model gave a reasonable fit for ternary mixtures and represented the adsorption of binary mixtures fairly well. Other models were also considered for both ternary and binary mixtures.

Breakthrough curves for single and multicomponent mixtures were obtained and mathematical models investigated to establish which was the most suitable model. A finite difference technique was used to solve the mathematical models. Surface diffusion resistance was found to play a dominant role and could be the rate controlling step for single component adsorption. An equilibrium control model does not predict the breakthrough curve for a ternary mixture of methane, ethane and propane very well, but did give a reasonable fit for binary mixtures of methane and carbon dioxide.

Experimental adsorption-desorption cycles showed that this technique could be used to separate ethane as well as propane from a ternary mixture of methane-ethane and propane, and to separate carbon dioxide from a binary

mixture of methane and carbon dioxide. Adsorption-desorption cycles showed that separation was achieved and that it depends strongly upon the instant at which desorption is commenced. The equilibrium model was used to describe both adsorption-desorption cycles for binary and ternary mixtures.

CHAPTER 1

INTRODUCTION

As a result of rapid development in the field of petrochemicals, the procurement of raw materials such as methane, ethane and propane has become necessary. As natural gas contains proportions of these gases, it is well justified to exploit this source. Ethane and propane thus recovered from natural gas constitute an important source of supply for the manufacture of polyethylene and polypropylene.[1] Recently, a technique involving the injection of carbon dioxide into an almost exhausted well has received considerable attention for enhancing oil recovery. Carbon dioxide is miscible with most reservoir oils at high pressures. This causes appreciable swelling and reduction in the viscosity of the oils with attendant benefits to recovery efficiency. Moreover, mass transfer between the carbon dioxide and reservoir oil enhances extraction of the light hydrocarbons in the CO_2 rich oil phase.

Recently, natural gas has become very important from a commercial point of view and considerable research is being done to make use of this source. Many ways of separating the component gases are available, such as absorption, cryogenic distillation and adsorption. The main advantages of adsorption as a separation technique, compared with the other processes, are that in many cases a much higher selectivity can be obtained by adsorption than by any of the other techniques, and adsorbents have a relatively high capacity for volatile materials, even at low partial pressure.[2] Separation of gas mixtures in adsorbers can be based on steric effects, equilibrium effects and kinetic effects. In the case of steric effects, the only molecules which pass through the adsorbent are those of smaller

diameter than the micropores within the adsorbent. Hence, a screening effect comes into play. The utilisation of the steric effect requires an adsorbent with a very narrow and uniform size distribution of micropores. In addition, the components to be separated must differ in their molecular diameters. For separation purposes, an adsorbent is necessary with a mean micropore diameter lying between the molecular diameters of the components. These strict requirements are fulfilled only by zeolites and partly by the so-called carbon molecular sieves. Zeolite molecular sieves are much more favourable with respect to steric effects. They have intracrystalline channels of uniform size (3-10 Å), which are uniquely determined by the unit structure of the crystal. These channels will completely exclude molecules which are larger than the channel diameters. Molecular sieves are crystalline hydrated metal aluminosilicates, characterised by a three-dimensional framework of alumina and silica tetrahedra, *e.g.*, AlO_4 and SiO_4. Breck and Reed[3] assumed the following composition for the elementary cells of completely hydrated A type sieves in the sodium form (NaA) and calcium form (CaA):

$Na_{12}[(AlO_2)_{12}(SiO_2)_{12}].27H_2O$	Zeolite NaA (channel diameter 4 Å)
$Ca_6[(AlO_2)_{12}(SiO_2)_{12}].30H_2O$	Zeolite CaA (channel diameter 5 Å)

One of the important characteristic features of 5A molecular sieves is that they can adsorb *n*-paraffins and other straight chain hydrocarbons, but not *iso*-paraffins, cyclo-paraffins or aromatic hydrocarbons.[4,5] This property has resulted in extensive commercial use of this adsorbent for separating and obtaining high purity fractions of *n*-paraffins, which are used for subsequent processing. Molecular sieves are used in many installations. For example, they are used to purify gas streams containing carbon dioxide in cryogenic applications where freeze-out of carbon dioxide

would cause fouling of low temperature equipment, or to adsorb carbon dioxide and water from ethylene gas, which is used for the production of polyethylene plastics.[6,7]

The objectives of this investigation were to study:

(1) The equilibrium isotherms of methane, ethane and propane, as well as mixtures of these gases on a 5A molecular sieve at 25° C and at pressures ranging from 0.5-12 atmos gauge.

(2) The equilibrium isotherms of methane and carbon dioxide and their mixtures on 5A and 4A molecular sieves at 25° C and at pressures ranging from 14-82 atmos gauge.

(3) Breakthrough curves for single and multi-component adsorbates. These were to be interpreted by recasting the differential equation describing the bed material balance into difference form and coupling this with the equilibrium relationships found between adsorbate and adsorbed phase concentration.

(4) Experimental adsorption-desorption cycles for multi-component mixtures, to investigate the feasibility of separation of these mixtures, and computer modelling of these cycles.

1. Adsorption and Mathematical Modelling of a Fixed Bed

1.1 Adsorption in a fixed bed

Physical adsorption, like condensation, requires no activation energy and therefore can occur nearly as fast as molecules strike the surface of an adsorbent. The adsorbate undergoing adsorption is removed continuously from the carrier gas and accumulates upon the surface of the adsorbent. Such transfer proceeds until the concentration on the adsorbent reaches eqiulibrium with the gas phase, and the column effluent reaches the feed concentration. The concentration profile of an adsorbed component in a bed is determined by the interaction between the fluid-solid equilibrium and the mass transfer processes taking place. The concentration profile for the adsorption of a single component with no mass transfer resistance

would be a step function advancing through the column at constant velocity. The effect of mass transfer resistance is to make the concentration change less abrupt. With a linear equilibrium relation, the concentration profile assumes a "proportional pattern" - that is to say, the form of the profile is maintained, but the profile broadens continuously in proportion to the distance travelled along the column. In most practical cases, although the equilibrium relationship may be linear at low gas phase concentrations, the amount adsorbed on the solid approaches an upper limit as the gas phase concentration increases. For this so-called "favourable equilibrium"the concentration profile is "self-sharpening", assuming a "constant pattern" in which the length remains the same as it moves through the bed at a constant velocity. The length of the pattern and the length of bed required to reach the constant pattern shape depend upon the transfer resistance. For multicomponent adsorption, the equilibrium relationships for the various components will be inter-dependent, and in the absence of mass transfer resistance, the equilibrium model already referred to predicts that wave fronts (or step changes in concentration) equal in number to the number of components being adsorbed will pass through the bed. Each of these wave fronts will have its own characteristic constant velocity, with the result that the concentration pattern as a whole will spread continuously in proportion to the distance travelled along the bed. Figure 1 shows a breakthrough curve for a ternary mixture according to equilibrium theory. The operation of a fixed bed adsorber can perhaps best be understood by considering a ternary mixture containing components A, B, and C (component A being more readily adsorbed than B, and B being more readily adsorbed than C). This ternary mixture is then passed continuously through the adsorbent bed. This can be illustrated

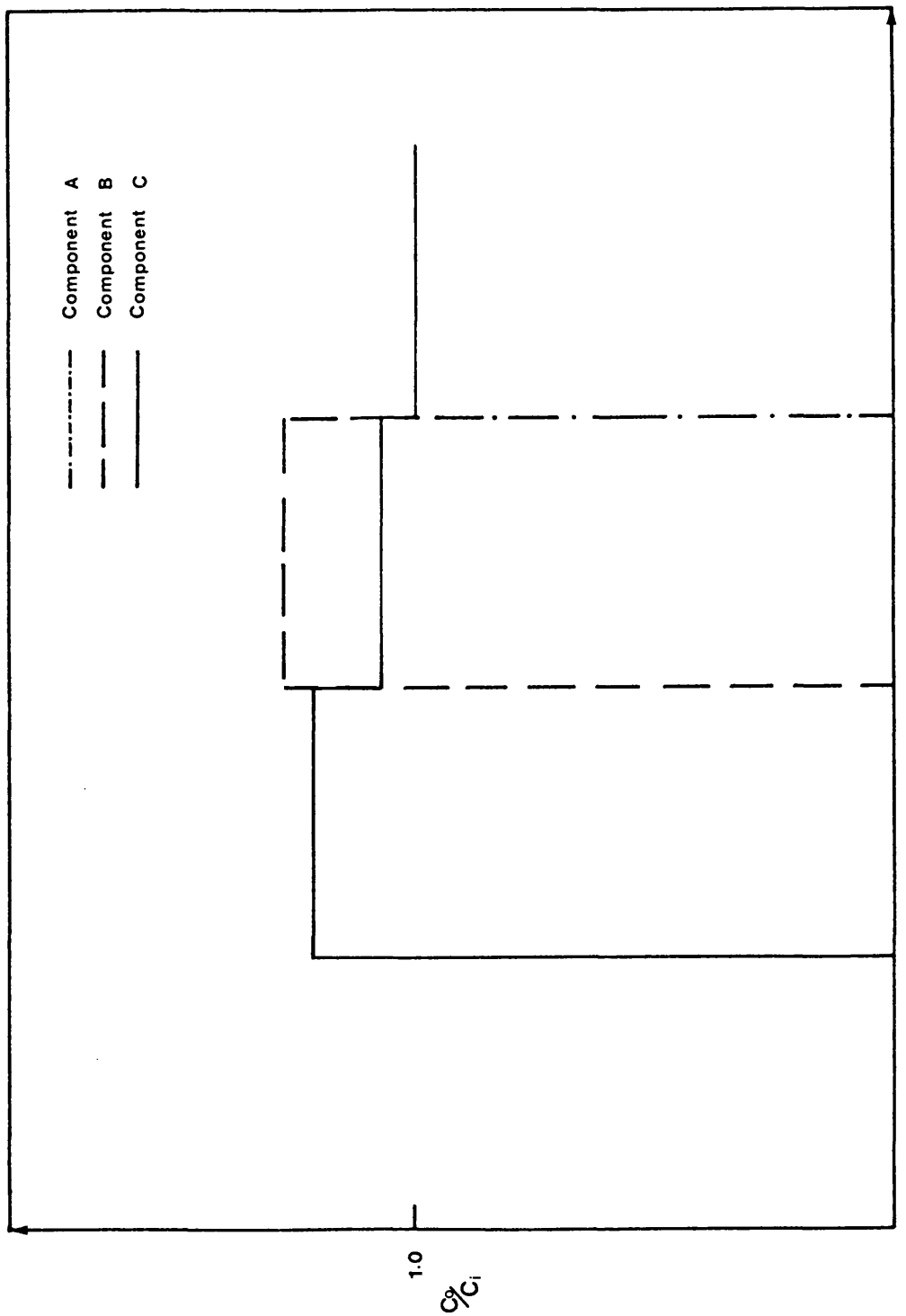

Figure 1 Breakthrough curve for a ternary mixture according to equilibrium theory.

by considering Figure 2. At the beginning, there will be a region (plateau zone 1, or feed zone) in which the adsorbent is saturated and the concentration of components is the same as in the feed. Zone 2 in Figure 2 is the first transfer zone (sorption zone), in which the strongest component, A, is adsorbed by the solid, causing an increase in concentration of components B and C in the gas phase. Zone 3 is again a plateau zone, where components B and C are in equilibrium with the adsorbed phase. Zone 4 is the second transfer zone, in which the second strongest component, B, is adsorbed, causing an increase in concentration of component C in the gas phase. Zone 5 is again a plateau zone, where component C is in equilibrium with the adsorbed phase. Zone 6 is the third transfer zone, in which the last component (most weakly adsorbed), C, is adsorbed. Zone 7 is a plateau zone, in which there is still a residual capacity for adsorption of further gas. The system of zones travels along the bed, until the plateau zone, corresponding to the feed composition, reaches the end of the bed (*i.e.*, equilibrium is reached). In the light of the above discussion, it can be concluded that the number of transfer zones is equal to the number of components being adsorbed (*i.e.*, three transfer zones exist in the case of ternary mixtures, and only two in the case of binary mixtures).

Concentration profile histories within the bed are simply records of what has occurred within the bed and one constructed from material balance considerations. Their form is illustrated in Figure 2(b) and it can be seen that they are mirror images of concentration profiles.

1.2 Adsorption equilibrium

When a gas or liquid is exposed to the adsorbent, a certain amount of the fluid is adsorbed by the solid. The amount adsorbed when equilibrium is established is a function of the final pressure (p), or concentration (c)

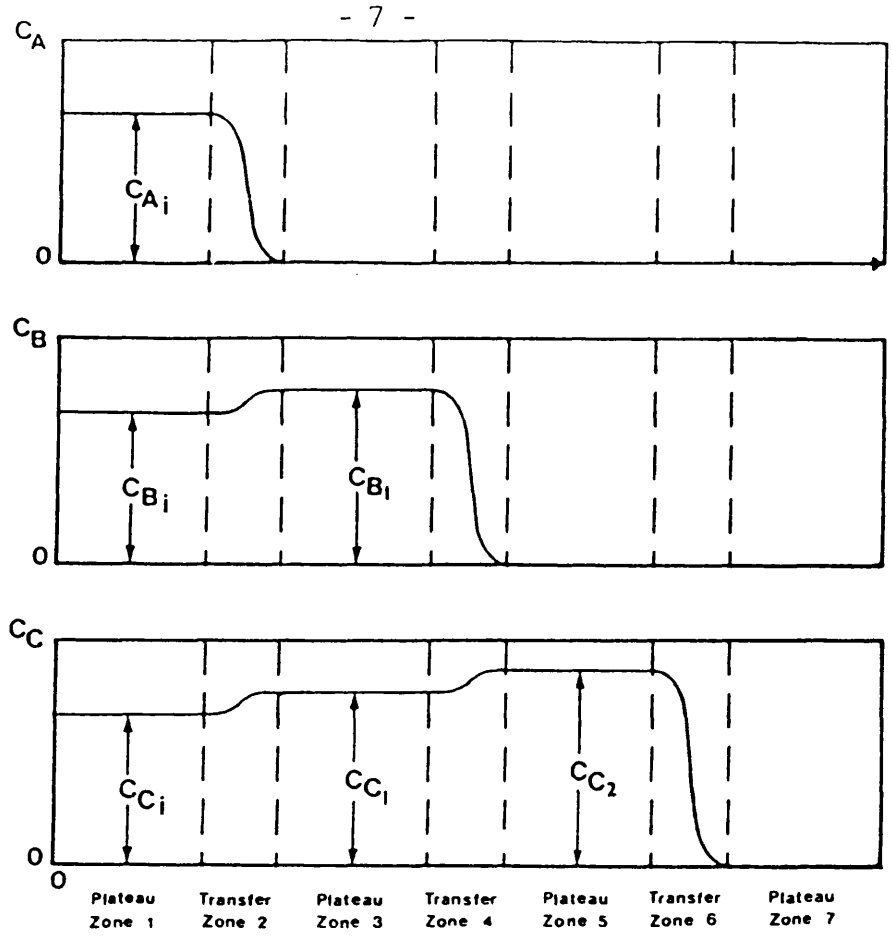

(a) Concentration profiles for components A, B and C.

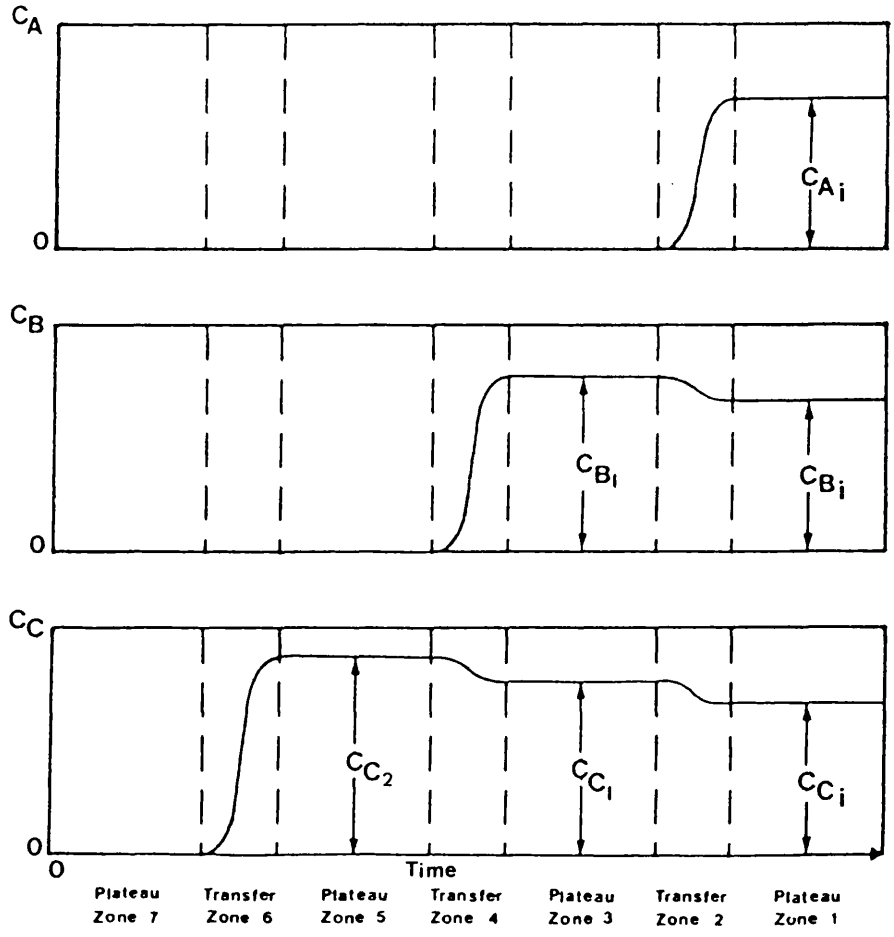

(b) Concentration histories for components A, B and C.

Figure 2 Breakthrough curve for a ternary mixture.

and temperature (T) and is given by:

$$q^* = f(p \text{ or } c, T) \qquad (1.1)$$

An adsorption isotherm would, for example, be represented:

$$q^* = f(p \text{ or } c) \quad T = \text{constant} \qquad (1.2)$$

where q^* is the adsorbed phase concentration in equilibrium with vapour phase concentration c.

The shape of an equilibrium adsorption isotherm depends on the interactions between adsorbate and the solid adsorbent, as well as on the chemical and structural nature of the adsorbent and adsorbate.

1.2.1 Single component adsorption

Several theories have been proposed to account for the physical adsorption equilibria for single gases and vapours on solids by Henry, Freundlich, Langmuir, Polanyi and others.[8-11] Single component adsorption has been studied quite extensively and abundant data exist in the literature for various adsorbates and adsorbent pairs. Many investigators have used the theories mentioned above for single component equilibria and there has been much success in the correlation of experimental data.

1.2.2 Multi-component adsorption

The amount of gas or liquid adsorbed in the mixture is a function of the concentration of its constituents, *i.e.*,

$$q_1^* = f(c_1, c_2 - c_n) \qquad (1.3)$$

where c_1, $c_2 - c_n$ are the concentration of components 1,2 - n in the fluid phase. There are analogous equations for each of the components of the adsorbing mixtures. The increased use of solid adsorbents in separation

processes has led to the need for methods for predicting the equilibria of multi-component mixtures from a knowledge of the equilibrium adsorption for a single component. Various theories have been proposed to predict the adsorption equilibria for mixtures. Markham and Benton[12] extended Langmuir's theory to multi-component mixtures. Grant and Manes[13,14] proposed a correlation method, based on the Polanyi potential theory to gas mixture adsorption, by considering the liquid-like adsorbate as a mixture in which the adsorption potential of each single adsorbed component is determined by the adsorbate volume of the mixture. Myers and Prausnitz[15-17] described a method for calculating the adsorption equilibria of components in a gaseous mixture, using only data for the single component adsorption equilibria at the same temperature and on the same adsorbent. Ruthven[18-20] developed a statistical thermodynamic model for binary mixtures. In this model, it is assumed that the adsorbed molecules are confined within the molecular sieve cavities, rather than at localised sites and that the sorbate-sorbent interaction potential is independent of the number of sorbate molecules present within a cavity. The interaction between an adsorbed molecule and the sieve is characterised by a Henry's law constant.

Recently, two methods have been proposed to extend Freundlich's isotherm to multi-component adsorption isotherms of liquid on activated carbon in which each component individually obeys the Freundlich isotherm:
(a) Fritz and Schluender[21] proposed a relationship for multi-component adsorption equilibria to predict the adsorption of organic mixtures from aqueous solution on to activated carbon in the following form:

$$q_i = \frac{K_{io} c_i^{n_{io}}}{K_i' + \sum_{j=1} K_{ij} c_j^{n_{ij}}} = f_i(c_1, c_2 - c_n) \qquad (1.4)$$

The Langmuir, Freundlich and other well-known isotherms[22-24] can be deduced as special cases of equation (1.4). This equation has been used to fit

the experimental data for equilibrium adsorption of two and three solutes with satisfactory results.[25-28] For $K_i' = 0$ and $K_{ii} = 1.0$, equation (1.4) becomes the extended Freundlich equation:

$$q_i = \frac{K_{io} c_i^{n_{io}}}{\sum_{j=1} K_{ij} c_j^{n_{io}}} \qquad (1.5)$$

where K_{io} and n_{io} are single component parameters. The other constants can be determined from the multi-component mixture data.

(b) Sheindorf *et al.*[29] derived a Freundlich type multi-component adsorption isotherm and employed it successfully to describe adsorption data of various two component and multi-solute mixtures on activated carbon.[30,31] The adsorption of component i in the mixture is given as:

$$q_i = K_i c_i (\Sigma K_{ij} c_j)^{n_i - 1} \qquad (1.6)$$

where K_i and n_i are the parameters of the single component isotherm, and the competition coefficients are defined as:

$$K_{ii} = 1, \quad K_{ij} = \frac{b_{oj}}{b_{oi}}, \quad K_{ij} = \frac{1}{K_{ji}} \qquad (1.7)$$

where b is the adsorption coefficient in the corresponding Langmuir isotherm.

Many publications are available for systems involving two components correlated with the previously mentioned models, while few publications exist for systems involving three components.

2. Data Analysis

2.1 Breakthrough curves

The breakthrough curve for a particular component is obtained by measuring its concentration in the effluent stream as a function of time

until equilibrium is obtained. The concentration of a component in the effluent stream at the beginning is zero until breakpoint, at which the concentration rises gradually to the initial value of the inlet stream. The adsorbed phase concentration in equilibrium with the inlet gas phase concentration may be calculated either in terms of the instantaneous rate of adsorption, or by utilising the concept of the stoichiometric time.

2.1.1 Instantaneous rates of adsorption

The amount of each component adsorbed during an experiment is determined by first obtaining the instantaneous rate of adsorption of each component over the total time interval for equilibrium to be reached. Using a side-stream to represent the amount of adsorbate adsorbed and accumulated:

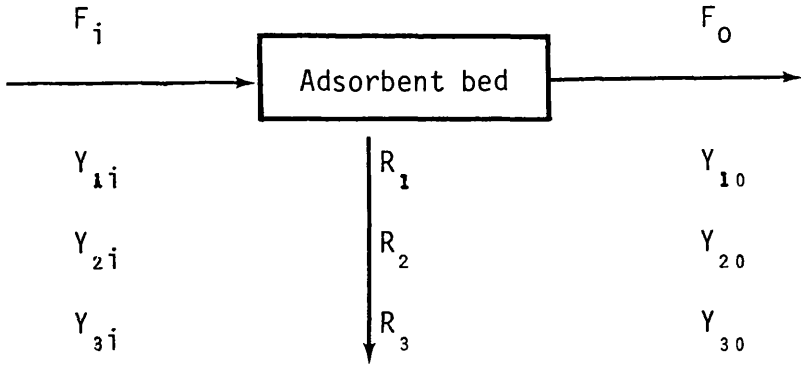

A material balance for component 1 in the mixture over the bed at any time is given by:

$$Y_{1i} \times F_i = R_1 + Y_{10} \times F_0 \qquad (1.8)$$

Similarly for components 2 and 3:

$$Y_{2i} \times F_i = R_2 + Y_{20} \times F_0 \qquad (1.9)$$

$$Y_{3i} \times F_i = R_3 + Y_{30} \times F_0 \qquad (1.10)$$

The overall balance is given by:

$$F_i = F_0 + R_1 + R_2 + R_3 \qquad (1.11)$$

Substituting equations (1.8)-(1.10) into equation (1.11) and with some algebraic manipulation, the following relation is obtained:

$$F_0 = F_i \frac{[1 - (Y_{1i}+Y_{2i}+Y_{3i})]}{[1 - (Y_{10}+Y_{20}+Y_{30}]} \qquad (1.12)$$

where R is the instantaneous rate of adsorption and Y_i, Y_0 are the mole fractions of each component in the gas phase, at bed inlet and outlet respectively. F_i and F_0 are the molar flowrate, at bed inlet and outlet respectively.

Knowing the molar composition of the mixture at the inlet and outlet and the initial molar flowrate, the final molar flowrate can be calculated over the whole time range. Equations (1.8)-(1.10) can then be used for finding the instantaneous rate of adsorption of each component over the whole of the experimental time. Knowing the instantaneous rate of adsorption of each component at any time interval during adsorption, and integrating the instantaneous rates of adsorption over the total time, will give the amount adsorbed of each component during the experiment. This method was used to calculate the quantity adsorbed for a single component and for mixtures.

2.1.2 Stoichiometric time

The stoichiometric time is the time required for a transfer zone (in which mass transfer occurs) to traverse the length of the bed if the concentration were a step function of time,[32-34] as shown in Figure 3. A mass balance over the whole bed, assuming a single transfer zone, is given by:

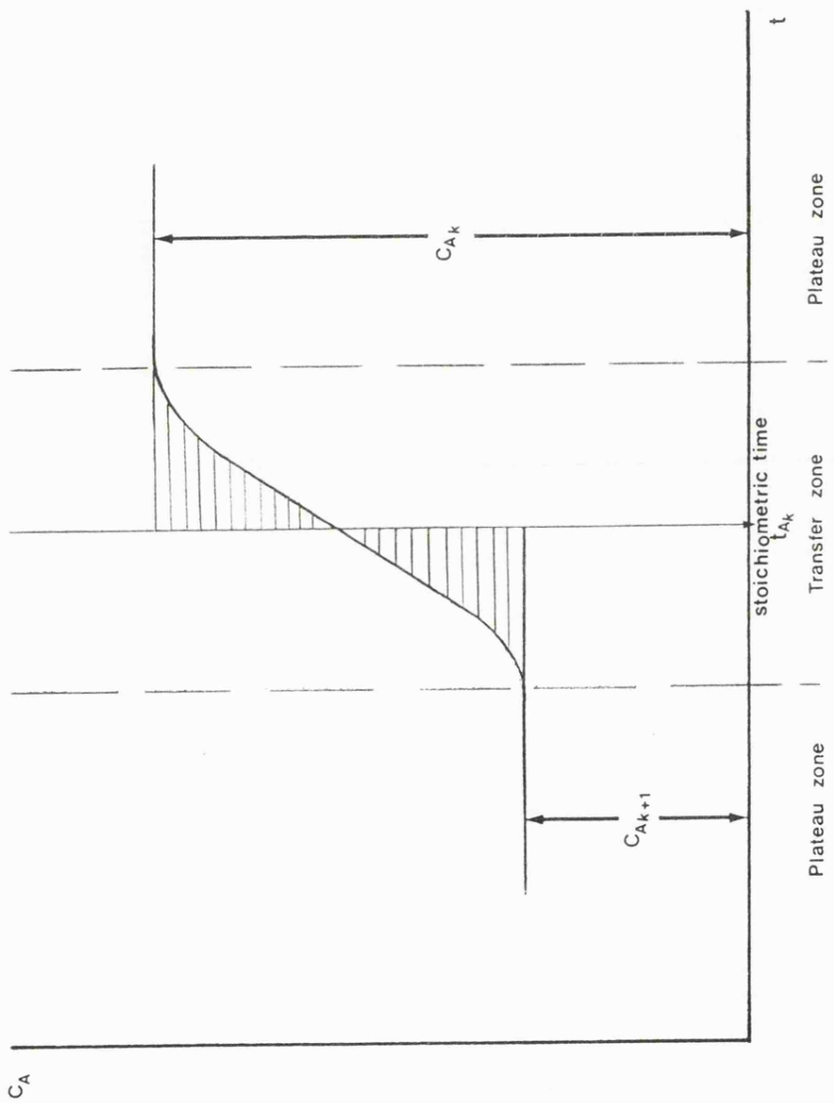

Figure 3 Stoichiometric time.

$$\text{input - output} = \text{accumulation + loss by sorption} \tag{1.13}$$

For component A:

$$\text{mass input} = uc_{A_i} t_{A_e} \tag{1.14}$$

$$\text{mass output} = uc_{A_i}(t_{A_e} - t_{A_o}) \tag{1.15}$$

$$\text{accumulation} = mq_{A_o} + \varepsilon v_b c_{A_i} \tag{1.16}$$

$$\text{loss by sorption} = 0 \tag{1.17}$$

Combining equations (1.14)-(1.17) gives:

$$uc_{A_i} t_{A_o} = mq_{A_o} + \varepsilon v_b c_{A_i} \tag{1.18}$$

where

$$t_{A_o} = t_n - \frac{\int_0^{t_n} c_A(t)\,dt}{c_{A_i}} \tag{1.19}$$

where u is the volumetric flowrate;

c_{A_i} is the gas phase concentration;

t_{A_o} is the stoichiometric time; and

t_{A_e} is the time at which the bed reaches equilibrium.

This method has also been used to calculate the quantity adsorbed for a single component.

3. Mathematical Models Describing Breakthrough in Fixed Beds

The problem of the evaluation of the performance of fixed bed adsorbers has received a great deal of attention in recent years by workers interested in ion exchange, gas chromatography and reactor design, as well as those primarily interested in gas adsorption dynamics and equilibria. A complete solution to the problem must at least correlate the effects of sorption capacity, mass transfer, sorption kinetics, particle size, bed geometry and flowrates with the concentration history of the adsorbate in effluent streams from sorption beds.

The funadmental equation describing an adsorption system is obtained by taking a mass balance over a differential volume element of the packed column for both the gas stream and the adsorbing solid and is given as:

$$\text{input - output} = \text{accumulation + loss by sorption} \tag{1.20}$$

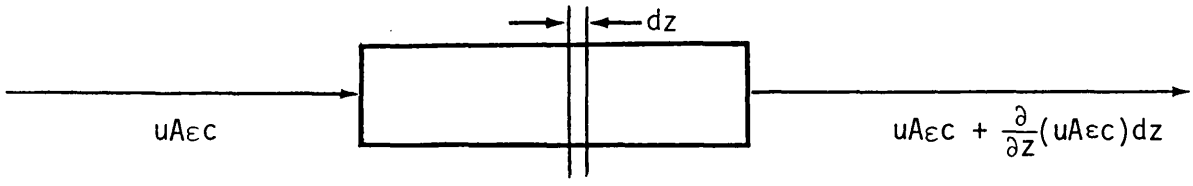

$$\text{input} = uA\varepsilon c \tag{1.21}$$

$$\text{output} = uA\varepsilon c + \frac{\partial}{\partial z}(uA\varepsilon c)dz \tag{1.22}$$

$$\text{accumulation} = \frac{\partial}{\partial t}(A\rho_b q)dz + \frac{\partial}{\partial t}(A\varepsilon c)dz \tag{1.23}$$

$$\text{loss by sorption} = 0 \tag{1.24}$$

Combining equations (1.21)-(1.24) and with further algebraic manipulation, the following relation is obtained:

$$u\left(\frac{\partial c}{\partial z}\right)_t + \left(\frac{\partial c}{\partial t}\right)_z + \frac{\rho_b}{\varepsilon}\left(\frac{\partial q}{\partial t}_z\right) = 0 \tag{1.25}$$

where u is the linear interstitial fluid velocity;

ε is the total bed voidage; and

ρ_b is the bed density.

The major assumptions made in this development are:

(1) The pressure drop through the adsorbent bed is negligible, so that the velocity and density of the fluid phase are constant.

(2) The adsorbate is dilute. This assumption implies isothermal operation as the amount of material adsorbed is assumed to be small enough for heat effects to be neglected. This permits the exclusion of the equation for conservation of energy from the mathematical analysis.

(3) The adsorbent particles are spherical.

(4) The velocity profile is flat and longitudinal dispersion in the bed is insignificant.

(5) Finally, the bed porosity is uniform.

The transport of adsorbate from the bulk gas stream to adsorbent is usually described by one of the following transport mechanisms, or by a combination of them.

3.1 External mass transfer control

The rate of adsorbate transport from the bulk of the gas phase to the surface of the adsorbent particle, as derived from the "film" theory of mass transfer, is given by:

$$\left(\frac{\partial q}{\partial t}\right)_z = \frac{Kg.a}{\rho_b}(c - c^*) \qquad (1.26)$$

3.2 Pore diffusion control

The rate of diffusion of the molecules in the channels or pores of the solid is given by:

$$\left(\frac{\partial q}{\partial t}\right)_z = \frac{D_m}{r^2\rho_b} \frac{\partial}{\partial r}\left(r^2\frac{\partial c}{\partial r}\right) \qquad (1.27)$$

3.3 Surface diffusion control

The rate of internal mass transfer along the solid surface of the pores of the absorbent is given by:

$$\left(\frac{\partial q}{\partial t}\right)_z = \frac{D_s}{r^2} \frac{\partial}{\partial r}\left(r^2\frac{\partial q}{\partial r}\right) \qquad (1.28)$$

3.4 Simple lumped model

A number of approximate single parameter models have been described in the literature for representing mass transfer effects in adsorption. These are "lumped" models in the sense that the rate of transfer of material into the adsorbent particles is given explicitly in terms of the gas phase concentration and some average concentration within the particles, thus solution of partial differential equations for diffusion into the particles is not required.

Glueckauf[35] assumed that the rate of adsorption into the solid particles is proportional to the difference between the concentration (q) of the component in the solid phase and the solid phase concentration (q*) that would be in equilibrium with the fluid phase outside the particle. Mass transfer is thus described by the relationship:

$$\frac{\partial q}{\partial t} = K_G(q^* - q) \qquad (1.29)$$

3.5 Equilibrium model

Equilibrium between solid and gas phases is assumed to be established at any point in the bed at all times. The effect of all resistance due to mass transfer is neglected.[36]

All the previous models, other models and several other possible combinations, have been used to describe fixed bed behaviour. These models can be solved by one of two methods: analytical or numerical solutions. The analytical or numerical solutions obtained generally fall into two categories. The first category, that of the asymptotic or constant pattern breakthrough solution, is obtained by making the additional assumption that the shape of the breakthrough curve is independent

of the distance along the bed (see, for example, references 37-41). This assumption is valid only for favourable equilibrium isotherms. In some cases, the solution is not applicable at small values of X,[42,43] where X = length of bed/velocity, or in a "shallow" bed.[38,39,71,73] The second solution is obtained without making this assumption and is therefore valid for all values of X (see, for example, references 44-48). The general solution method was chosen to solve the fixed bed partial differential equations for breakthrough, as this method offered greater flexibility than the asymptotic method.

CHAPTER 2

APPARATUS AND EXPERIMENTAL PROCEDURES

This chapter describes the experimental procedure used in carrying out the isothermal adsorption experiments. The adsorbates used were as follows:-

(a)
1. Methane
2. Ethane
3. Propane
4. Methane-ethane-propane mixtures using 5A molecular sieves at 25^0 C.

(b)
1. Methane
2. Carbon dioxide
3. Methane-carbon dioxide mixtures using 5A and 4A molecular sieves at 25^0 C.

A flow diagram of the experimental apparatus used for the investigation is shown in Figure 4. The apparatus used for the experimental study is described in the following section.

1. Apparatus

The equipment was built from a mild steel[1] with auxiliary tubing. An adsorption column,[7] immersed in a water bath[3] with auxiliary piping constitutes the adsorption section. The column effluent was analysed in the analysis section which consisted of a flame ionisation detector (FID), linked with a recorder[13] and coupled with an integrator.[14] The regenerator section had a temperature controlled furnace[16] for desorption. The outlet flowrate was set by a needle valve (NV_2) and measured by a bubble flowmeter.[10] The pressure in the sample loop upstream of the outlet flow control valve was maintained constant at 10 psig by a pressure regulator (PR_2)

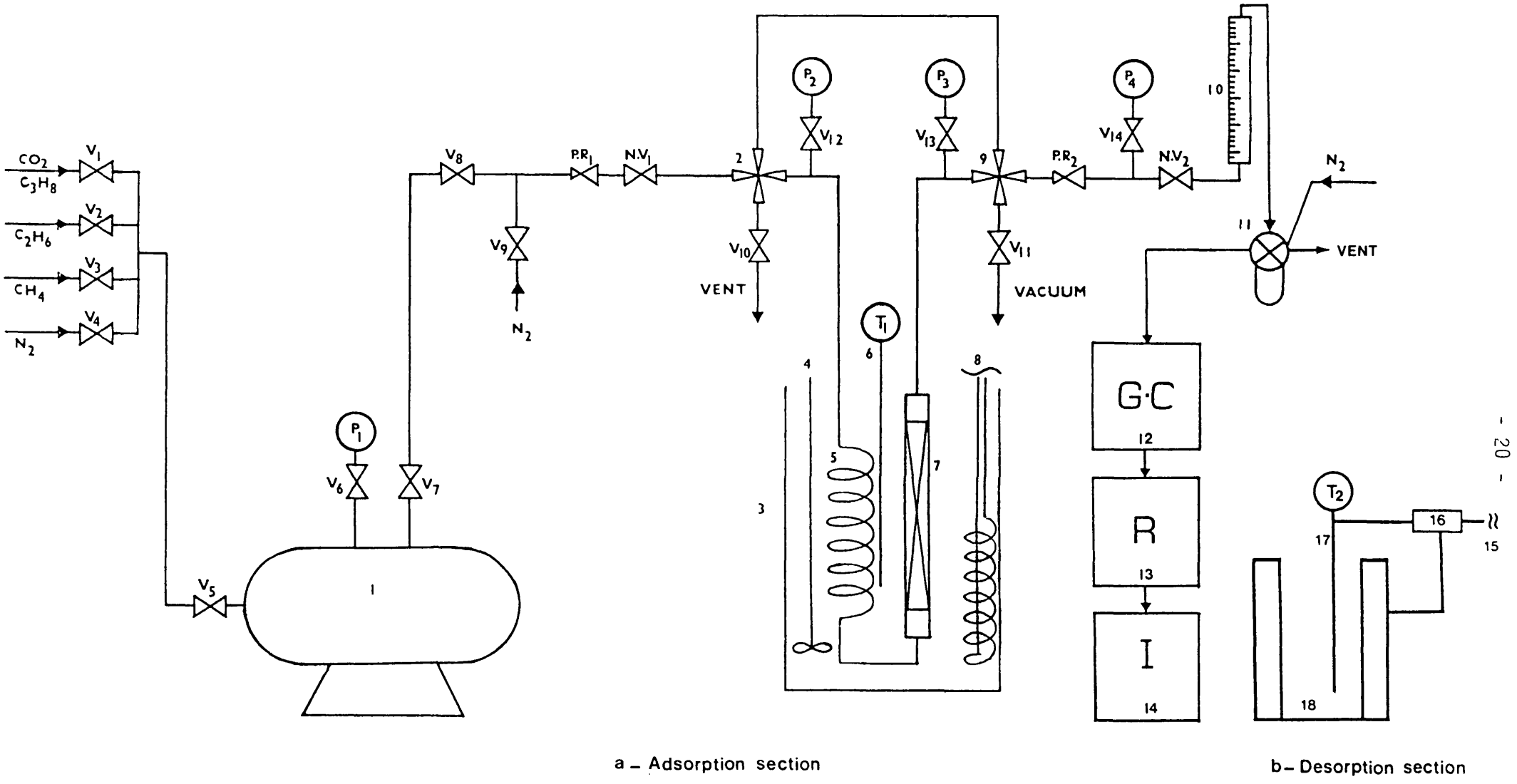

a – Adsorption section

b – Desorption section

Figure 4 Schematic diagram of apparatus.

1 Sampling tank

2 4-Way valve

3 Water bath

4 Stirrer

5 Preheated coil

6 Temperature controller

7 Adsorption column

8 Heater

9 4-Way valve

10 Bubble flowmeter

11 Sample loop

12 Gas chromatography

13 Recorder

14 Integrater

15 Electric time switch

16 Eurotherm temperature regulator

17 Chromel-alumel thermocouple

18 Regeneration furnace

to minimise surges in the flow when injecting samples or taking samples. All the tubes from the gas sample cylinder to the pressure regulator (PR_2) are ($\frac{1}{8}$" OD and 0.937"ID) and were made of stainless steel to withstand the high pressures and temperatures used. The adsorbent was regenerated by allowing movement of the adsorption tube between the water bath[3] and the regeneration furnace.[18] The adsorption column[7] used was a stainless steel tube of 50 cm in length and 0.493 cm internal diameter. The ends were plugged with glass wool and any dead space remaining after the addition of the adsorbent was filled with 30-60 mesh glass beads. All the equipment used for high temperature work was first tested for leaks in a furnace at 500^0 C. All equipment to be used at high pressure was tested for leaks at high pressure (up to 95 atmos), after which it was set aside for one day (to ensure that there were no leaks).

The adsorption column was immersed in a continuously stirred water bath.[3] The water bath temperature was kept constant, by means of a Fison Fi-Monitor regulator[6] and coil immersion heater,[8] at 25 ± 0.5^0 C, measured by a mercury in glass thermometer (T_1). When the adsorption tube was placed in the water bath, the excess (approximately 60 cm long[5]) was coiled and immersed in the bath to preheat the inlet gas stream. The temperature (T_2) of the regeneration furnace was controlled with a Eurotherm temperature regulator[16] using a chromel-alumel thermocouple.[17] After 12 hours, regeneration under vacuum overnight, the furnace was automatically switched off using an electric time switch.[15] The adsorbent bed was therefore cool and ready for use the next morning. The inlet pressure of the gas sample, which was fed to the adsorption column, was controlled by a pressure regulator (PR_1) (Tescom model 44-1113-24, inlet pressure 6000 psi max and outlet pressure 10-1500 psi), which was adjusted to the

required pressure for the experiment. The outlet pressure of the gas sample from the adsorption column was controlled by the pressure regulator (PR_2) (Tescom model 26-1610-24, inlet pressure 5000 psi max and outlet pressure 0-50 psi), by adjusting the regulator to the required pressure. The adsorption column effluent was sampled using a Pye six port rotary sampling valve (v_{15}), with a 0.5 cm^3 sample loop.[11]

2. Gas Sample Preparation

Gas mixtures were prepared in a cylindrical mild steel mixing vessel.[1] Before preparing a gas sample, the vessel and its feed lines were flushed out to remove water vapour and the whole apparatus was evacuated for 48 hours. The samples were prepared as follows:-

(1) Valves v_1, v_2, v_4 were closed and valve v_3 was opened and subsequently valve v_5 was opened. The sample cylinder was filled with methane through valve v_5.

(2) Valves v_1, v_3, v_4 were closed and valve v_2 was opened and subsequently valve v_5 was opened. The sample cylinder was filled with ethane through valve v_5.

(3) Valves v_2, v_3, v_4 were closed and valve v_1 was opened, then subsequently valve v_5 was opened. The sample cylinder was filled with propane through valve v_5.

(4) Valves v_1, v_2, v_3 were closed and valve v_4 was opened and subsequently valve v_5 was opened. The sample cylinder was filled with nitrogen to the required pressure.

For the methane-carbon dioxide mixutres, the same procedure was used, except for (2) (*i.e.*, steps 1, 3, 4 and 5) and carbon dioxide was connected in place of propane. The sample was then analysed to ensure the thoroughness of mixing using either an FID or TC detector.

3. Gas Analysis

Two techniques were used to determine the adsorbate concentration in the effluent stream. Both methods responded quickly and accurately to changes in concentration. These methods are described below.

3.1 Direct method

For the single component experiments, a fraction of the effluent from the adsorption column was directed to the chromatograph in order to prevent damage to the detector. A splitter was used to divide the flow-rate in the ratio 1:10. The signal produced, proportional to the outlet concentration, was amplified and recorded. This provided continuous monitoring of the effluent concentration, as shown in Figure 5. The process conditions were chosen after trials in order to attain both higher sensitivity and good stability. These conditions are shown in Tables 1 and 2. For the single component experiments with methane, ethane or propane, a flame ionisation detector (FID) was used. For methane and carbon dioxide, a thermal conductivity (TC) was employed.

3.2 Chromatographic system

For a ternary component gas adsorption, the direct method was initially used (see section 3.1). In this method, the least adsorbed component, methane, breaks through first, followed by a mixture of methane and ethane, and finally, when the column is saturated, a mixture of methane, ethane and propane appears in the same concentrations as in the inflowing adsorbates. This is shown in Figure 6. This type of chromatography is called frontal analysis. It is not suitable for analysis purposes, since only part of the first component is obtained in pure form by this method, and the errors are rather large and cumulative. Therefore, gas-solid chromatography, based on a Pye 104 unit, was used for the adsorption

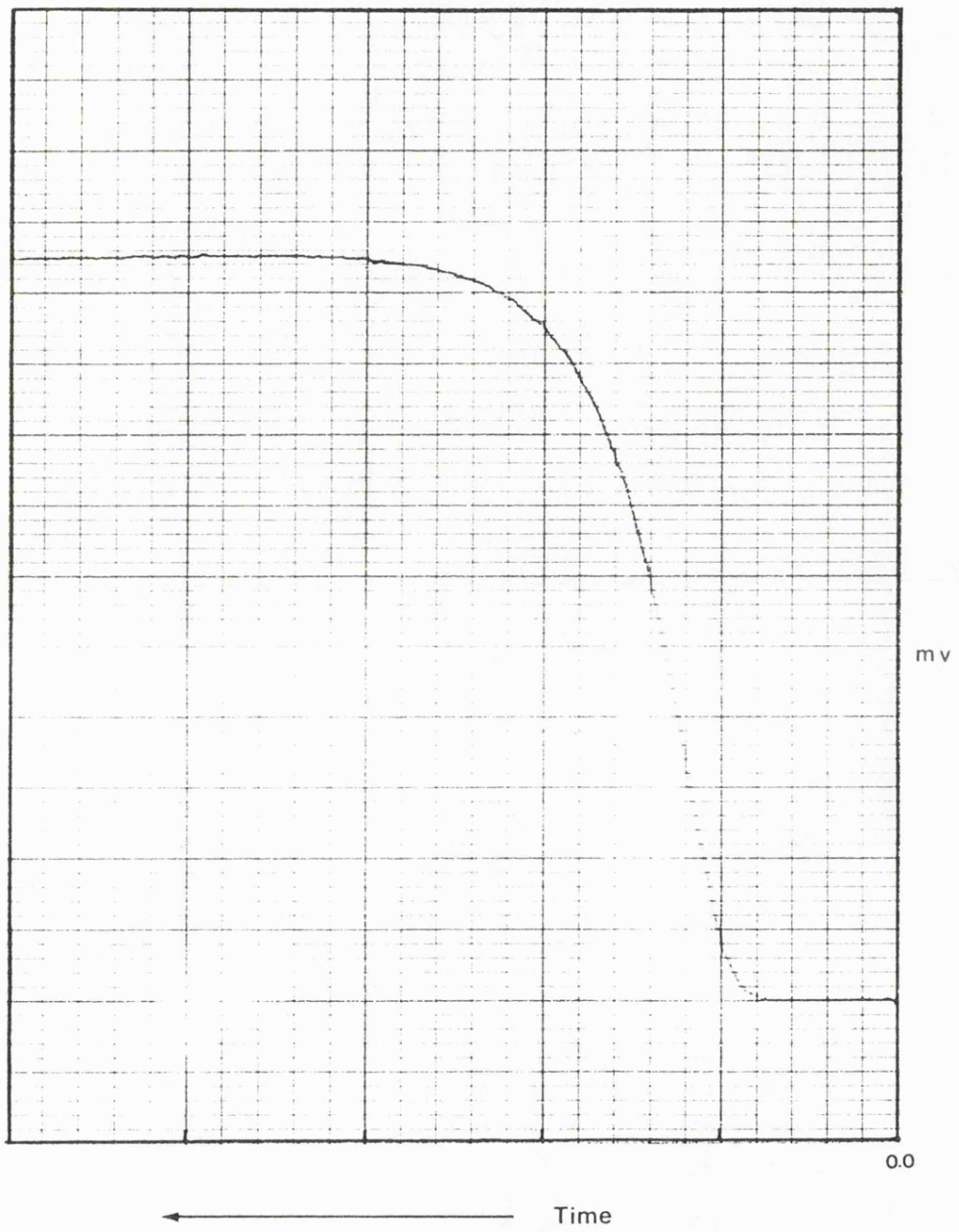

Figure 5 Typical recorded breakthrough curve for the direct method of analysis (single component).

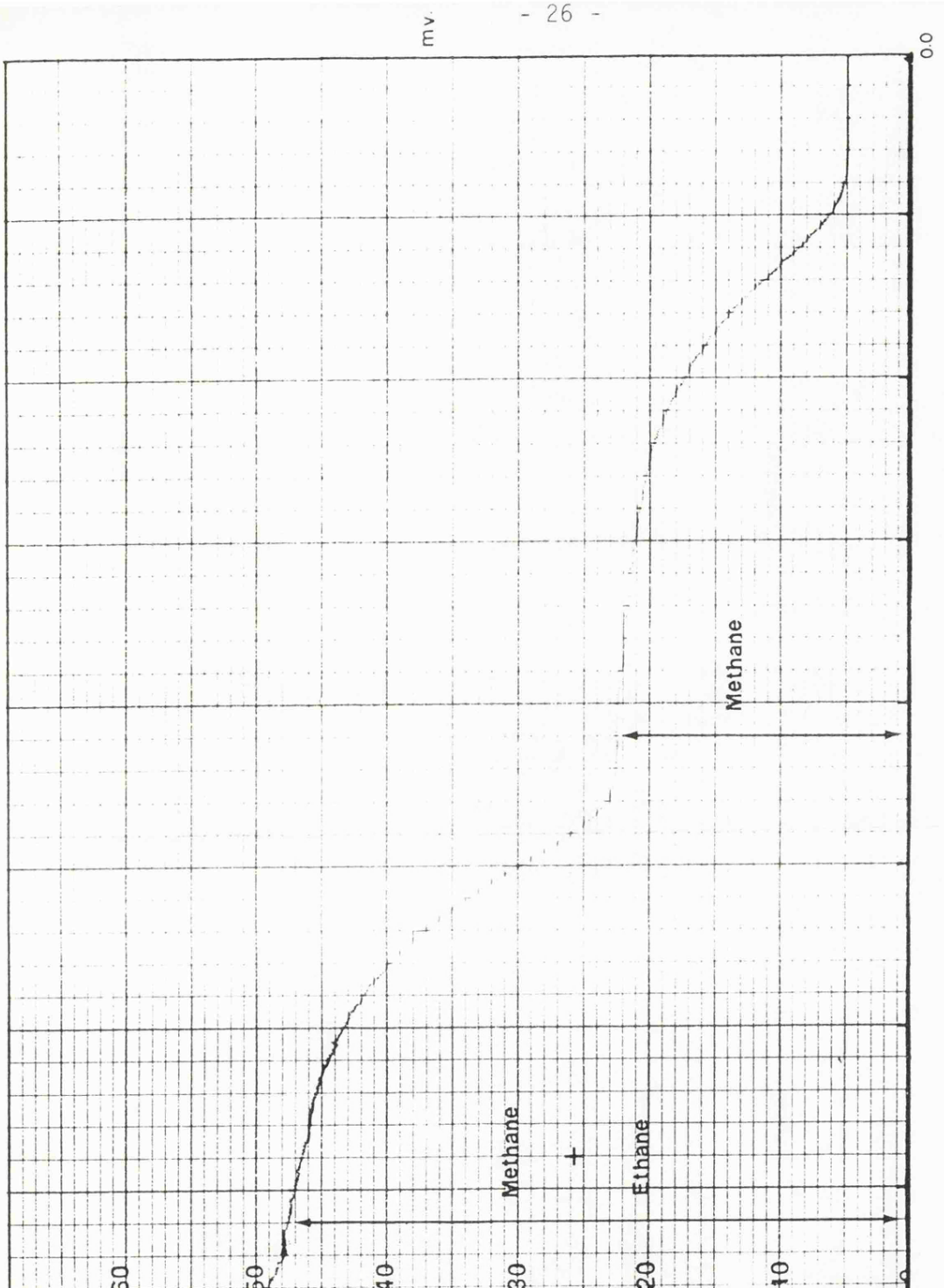

Figure 6 Typical recorded breakthrough curve for the direct method of analysis (ternary component).

mixtures. The effluent from the adsorption column was passed through a 0.5 cm^3 sample loop *via* a sample valve to the exhaust. Nitrogen carrier gas was circulated in the chromatographic column (50 cm length, 0.35 cm inside diameter) containing Porapak Q as the stationary phase and located in the oven of the gas chromatograph. For analysis, a sample was introduced into the chromatographic column by the carrier gas, while the effluent from the adsorption column was connected to the exhaust. The sample was analysed, and the corresponding signals were recorded and integrated by a digital integrator. In order to obtain a well defined breakthrough curve, it is necessary to minimise the time which elapses between samples. Overlapping of peaks from different samples should be avoided, by choosing a time corresponding to the slowest moving component. The process conditions were selected after experimenting with different packings and lengths of the chromatographic column and by varying the carrier gas flowrate and temperature. Figure 7 shows a typical recorded breakthrough curve by gas sampling for a ternary mixture (methane, ethane and propane).

For bindary adsorption (methane and carbon dioxide mixtures), thermal conductivity was employed. Silica gel was used as the stationary phase. Figure 8 shows the separation of binary mixtures (methane and carbon dioxide). The chromatographic conditions for gas analysis are summarised in Tables 2.1 and 2.2 for flame ionisation and thermal conductivity respectively.

4. Adsorbent Regeneration

A weighed sample of adsorbent was placed in the adsorption column which was put into the regeneration furnace. A slow nitrogen purge was passed through the apparatus, until the regeneration temperature (450^0 C) had been reached and the adsorbent was degassed for about 12 hours.

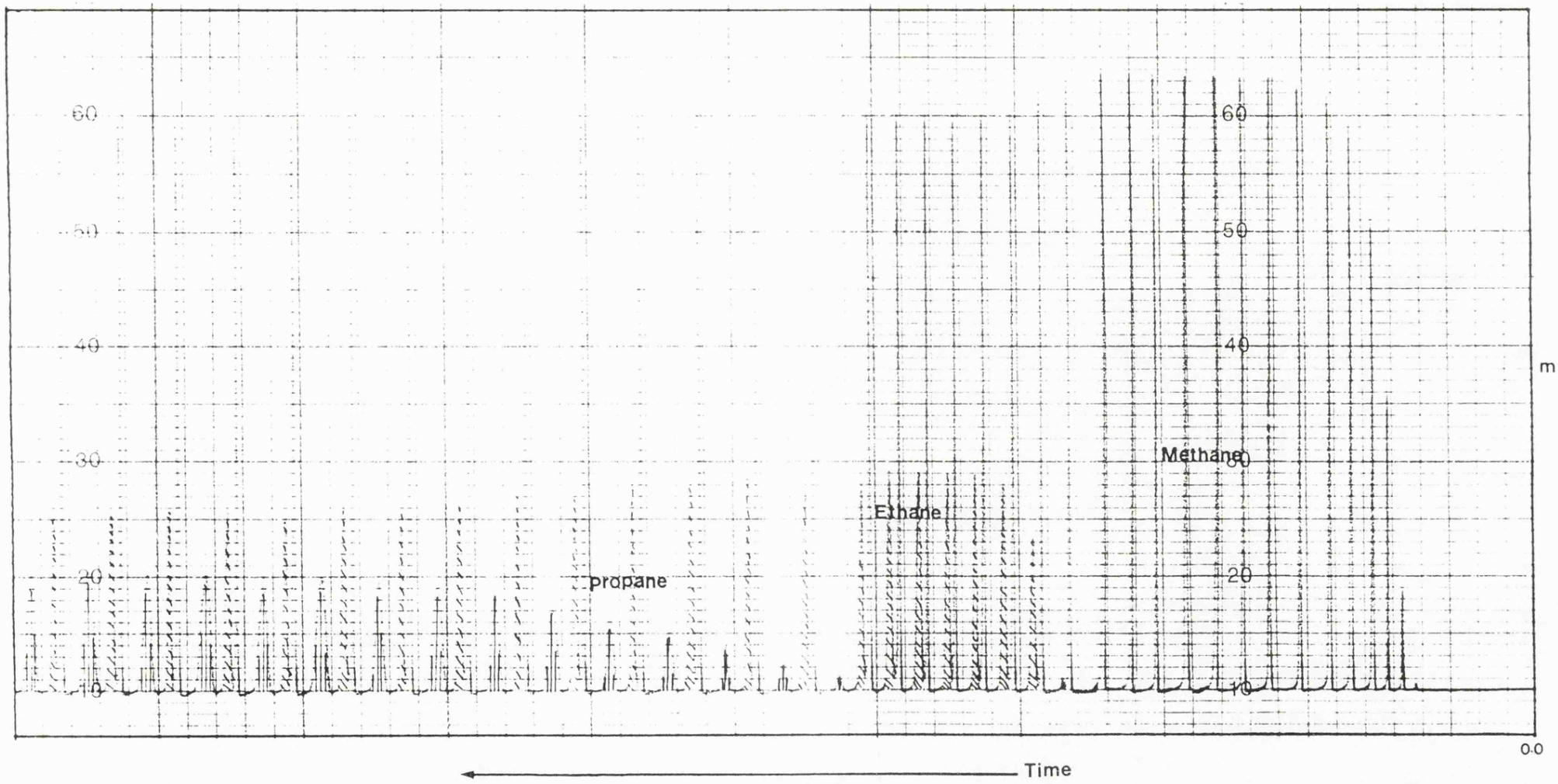

Figure 7 Typical recorded breakthrough curve by gas sampling. Ternary adsorption (methane, ethane and propane).

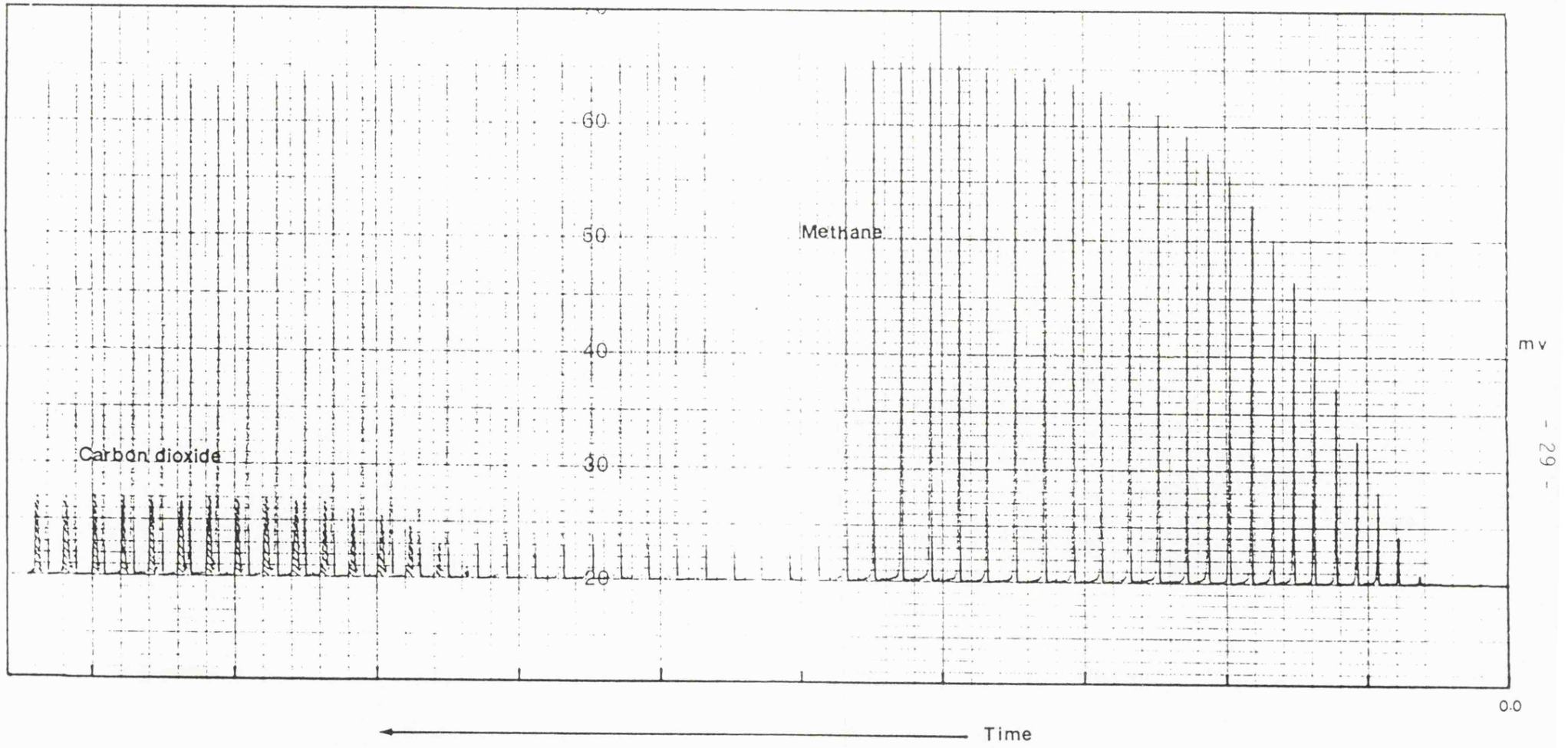

Figure 8 Typical recorded breakthrough curve by sampling. Binary mixture (methane and carbon dioxide).

Table 2.1

Chromatography conditions for gas analysis - flame ionisation detector (FID)

Flame ionisation detector (FID)	Direct method	Chromatographic method
Hydrogen flowrate (cm^3 min^{-1})	40.0	40.0
Air flowrate (cm^3 min^{-1})	600.0	600.0
Nitrogen flowrate (cm^3 min^{-1})	-	35.0
Oven temperature (^{0} C)	100.0	120.0
Detector temperature (^{0} C)	150.0	250.0

Table 2.2

Chromatography conditions for gas analysis - thermal conductivity (TC)

Thermal conductivity (TC)	Direct method	Chromatographic method
Nitrogen flowrate (cm^3 min^{-1}) (reference column)	60.0	36.0
Nitrogen flowrate (cm^3 min^{-1}) (analysing column)	-	36.0
Oven temperature (^{0} C)	100.0	180.0
Detector temperature (^{0} C)	200.0	250.0

5. Experimental procedures

After the adsorbent had been regenerated and cooled, the adsorption column was placed in the water bath and the vacuum switched off. The heater coil[8] and electrical stirrer[4] were switched on and nitrogen was continuously passed through the apparatus *via* valve v_9 for 2 hours, so that the adsorbent bed reached the temperature of the water bath. The nitrogen pressure was set by adjusting the pressure regulator (PR_1). The outlet pressure and the flowrate were set by pressure regulator (PR_2) and (NV_2) respectively. The flowrate was measured by the bubble flowmeter.[10] The chromatography unit was switched on and allowed to warm up. The nitrogen supply was switched off. Valve v_7 was then switched on to connect the sample cylinder to the feed line. The gas sample was introduced instead of nitrogen through valve v_8 into the adsorption column. Adsorption column effluent samples were then taken and analysed until breakthrough of all the adsorbate species was complete.

The interval times for a ternary mixture of methane, ethane and propane were respectively 30, 45 and 75 seconds, while the interval times for binary mixtures of methane and carbon dioxide were respectively 30 and 60 seconds.

Ambient temperature, pressure and the outlet flowrate were measured at the beginning, as well as at the end of each experiment.

Allowable gas velocities during both adsorption and regeneration were well below those which might cause attrition of the particles, or a significant pressure drop. This problem has been analysed by Ledoux,[49] and the calculation procedure is shown in Appendix 1. Taking account of these problems, the outlet flowrate employed during the experiments was between 35-100 $cm^3\ min^{-1}$.

In order to ensure safe working, the pipes used at high pressure must have a minimum wall thickness. This is calculated in Appendix 2. The actual thickness of the pipes used was much greater than the minimum value. These values are given in Table 2.3.

Table 2.3

Wall thickness of pipes

Pipe	Wall thickness used (")	Wall thcikness calculated (")
Adsorption column	0.028	0.0019
Other pipes	0.035	0.00054

6. Determination of Apparatus Dead Time

The apparatus dead time was determined with the adsorption column packed with 30-60 mesh glass beads. Dead time is the time required for the adsorbate to pass through the system and be detected by the chromatograph, when the column is packed with inert particles.

A dilute nitrogen-methane mixture was passed through the bed, and the effluent response was recorded by the direct method of analysis. It was found that the dead time varied with pressure and flowrate. Therefore, the same flowrate and pressure were used as those employed in the adsorption experiments. The process was repeated many times for each experiment at a specific pressure and flowrate. Dead times are summarised in Table 2.4.

7. Materials

Gases were supplied by Air Products Limited, at the following stated purities:-

Nitrogen 99.9%; methane 99.99%; ethane 99.70%; propane 99.50%; carbon dioxide 99.50%.

Table 2.4

Apparatus dead times

1(a) Methane, ethane and propane single components:

Pressure (atmos)	Methane (50-60 cm^3 min^{-1})	Ethane (50-60 cm^3 min^{-1})	Propane (35-40 cm^3 min^{-1})
12	6.5	7.0	10.5
10	5.5	6.5	8.6
8	5.15	5.4	7.6
6	4.15	4.4	5.5
4	3.2	3.5	5.5
2	3.5	3.4	4.84
0.5	3.3	3.5	4.5

(b) Mixtures of methane, ethane and propane

Pressure (atmos)	Mixture No.1 (50-60 cm^3 min^{-1})	Mixture No.2 (50-60 cm^3 min^{-1})
12	4.0	4.0
10	3.45	3.30
8	2.58	2.45
6	2.10	2.05
4	1.70	1.35
2	1.45	1.30
0.5	1.45	-

Table 2.4 (cont.)

Apparatus dead times

2(a) Methane and carbon dioxide single components:

(outlet flowrate for all experiments 50-60 cm^3 min^{-1})

Pressure	Methane (mol sieves)		Carbon dioxide (mol sieves)	
(psig)	(5A)	(4A)	(5A)	(4A)
1200	22.0	21.75	20.0	20.5
1000	18.0	18.25	18.0	18.0
800	14.0	14.0	14.50	13.8
600	10.50	11.0	11.50	10.0
400	7.50	7.30	7.5	8.0
200	4.30	4.25	5.0	4.0

(b) Methane and carbon dioxide mixtures:

(outlet flowrate for all experiments 50-60 cm^3 min^{-1})

Pressure	Mixture No.1 (mol sieves)		Mixture No.2 (mol sieves)	
(psig)	(5A)	(4A)	(5A)	(4A)
1200	21.0	22.5	-	-
1000	18.0	18.75	17.5	18.25
800	13.0	14.5	14.25	14.75
600	10.0	11.0	10.5	11.0
400	7.0	7.75	7.0	7.50

The molecular sieve adsorbents were supplied by Laporte Industries Limited as 1-2 mm spherical pellets, made from 1-5 μm molecular sieve crystals with approximately 20% by weight of binder, calcined at 650° C. The pellets were crushed in a ball mill and sieved to produce a 30-44 mesh cut.

5A molecular sieve pellet macropore (intercrystalline pores) and volume were determined (see Section 8 of this chapter for calculations of the total bed voidage), using a Carlo Erba 1500 mercury porosimeter. Pore diameters down to 50 $\mathring{A}$ could be determined.[46] A typical porosimeter chart is shown in Figure 9.

Average pore diameter[46] = 603 $\mathring{A}$

Total pore volume ε_{macro} = 0.28 $cm^3\ g^{-1}$

8. Determination of the Bed and Pellet Density

The density of 5A molecular sieve pellets (30-44 mesh cut) were determined experimentally using a bottle specific gravity meter (Pyknometer). Hence:

$$\rho_{pellet} = 1.18\ g\ cm^{-3}$$

The bulk density was determined by measuring the length of a certain weight of the adsorbent in a known diameter tube (glass), thus:

$$\rho_{bulk} = \frac{\omega}{\ell \times \pi r^2} \qquad (2.1)$$

Thus: $\rho_{bulk} = 0.74\ g\ cm^{-3}$

The adsorbent bed intergranular voidage (IG) was calculated from:

$$\varepsilon_{IG} = 1.0 - \frac{\rho_{bulk}}{\rho_{pellet}} \qquad (2.2)$$

1.0 g 30-44 mesh, heat treated, 5A molecuar sieve using 3 mm diameter tube.

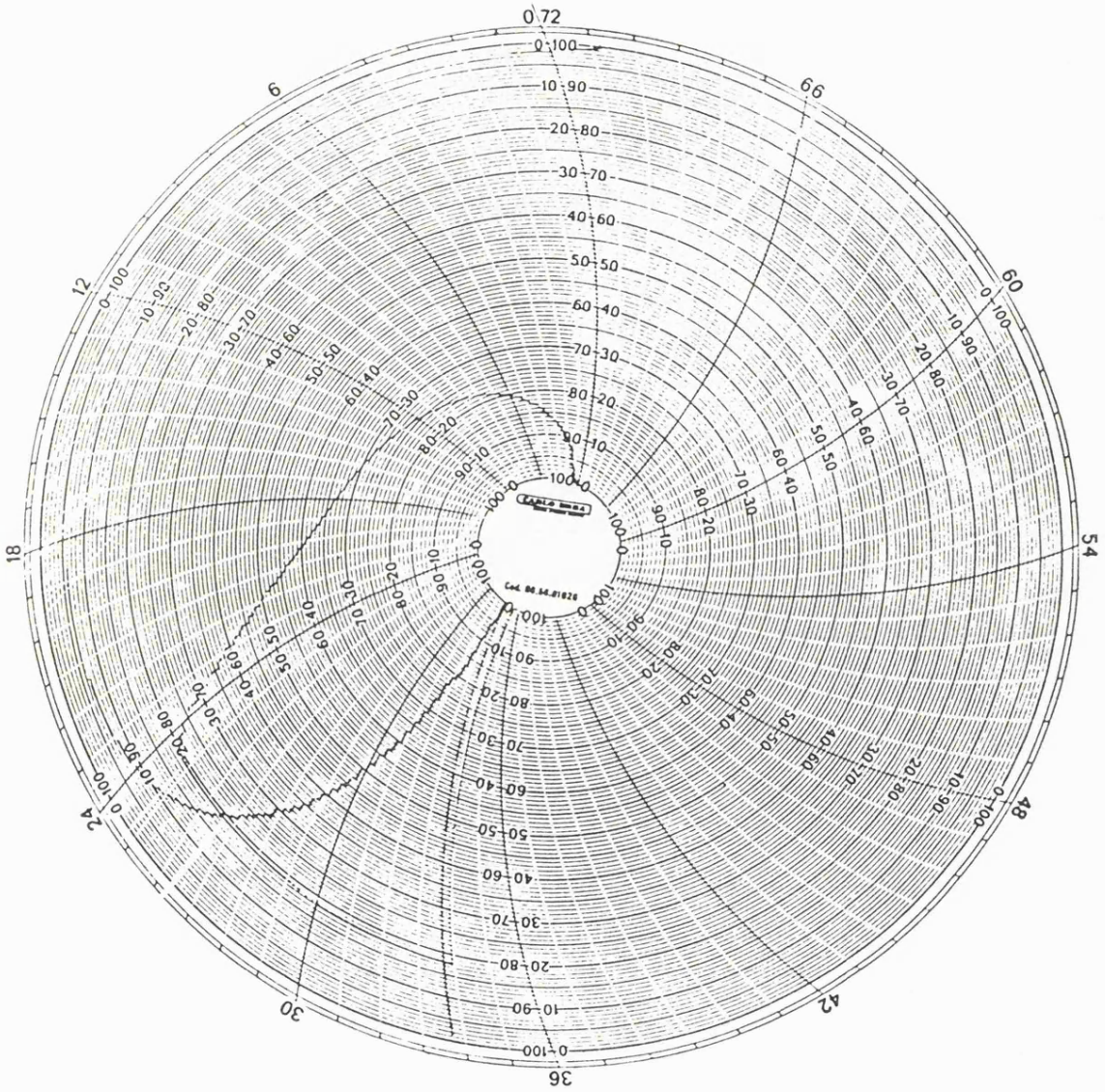

Figure 9 Porosimeter chart.

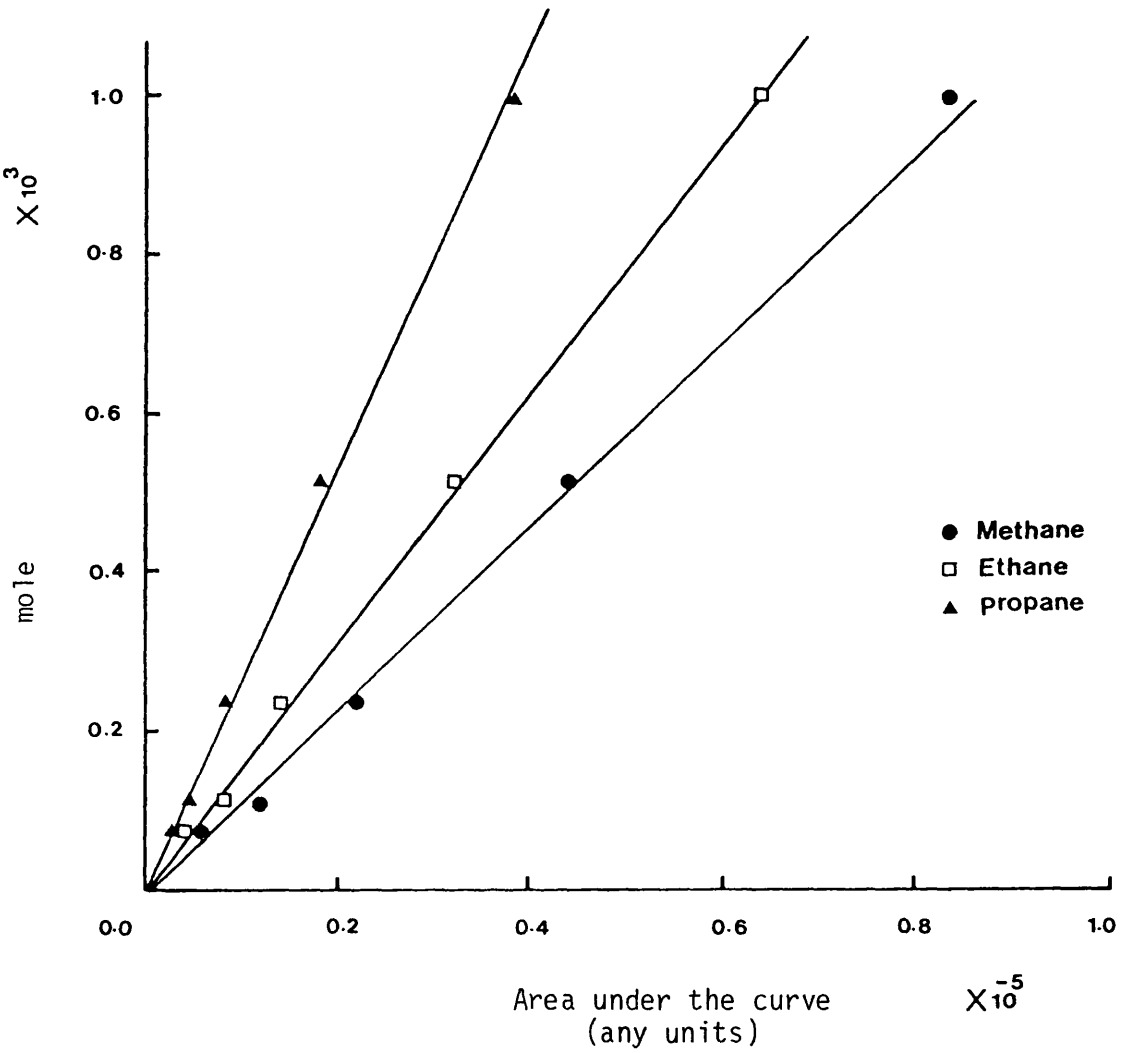

Figure 10 Calibration of F.I.D. response for methane, ethane and propane.

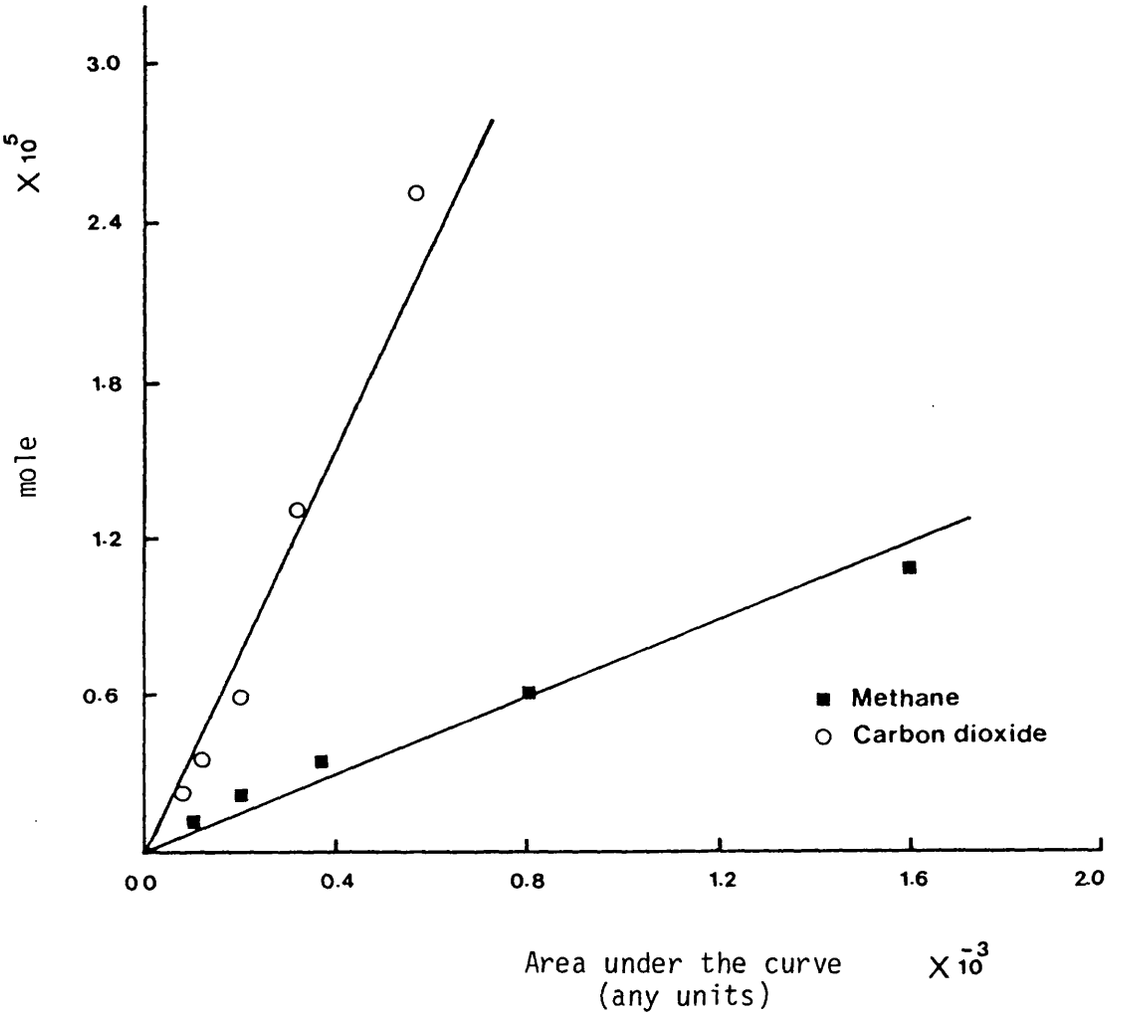

Figure 11 Calibration of T.C. response for methane and carbon dioxide.

$$\varepsilon = 1 - \frac{0.74}{1.18} \qquad (2.3)$$

therefore $\varepsilon = 0.373$

Hence, the porosity calculated above was used in equation (1.25).

9. Calibration

The flame ionisation detector (FID) and thermal conductivity detector (TC) responses were calibrated for each adsorbate by injecting a known amount of the sample. A linear relationship between the peak area and concentration was found for all the adsorbates. Figures 10 and 11 show the calibrations of the flame ionisation and thermal conductivity detectors respectively.

The pressure gauges were calibrated before and after the experiments. The pressure drop across the adsorption column was found to be negligible, (it was too small to register on the pressure gauge) over the range of flowrates used throughout the experiments.

10. Estimation of Errors Involved in the Measurements of the Amount adsorbed

Consider the repeated observation y, lying within the range $y' = y \pm dy$, where y' is the worst determination and dy is the absolute error. Let us now consider y as a function of dependent variables $x_1, x_2, \ldots x_n$:

$$y = f(x_1, x_2, \ldots x_n) \qquad (2.4)$$

In general the differential of the function y can be written as:

$$dy = \sum_{i=1}^{n} \frac{\partial y}{\partial x_i} dx_i \tag{2.5}$$

Now the worst possible value of dy will occur when all the terms on the right-hand side of equation (2.5) are either positive or negative. Therefore, equation (2.5) can be rewritten as:

$$dy = \sum_{i=1}^{n} \left|\frac{\partial y}{\partial x_i}\right| dx_i \tag{2.6}$$

Usually the experimental errors are reported as a percentage of relative error and defined as:

$$e\% = \frac{dy}{y} \times 100 = \left[\frac{1}{y} \sum_{i=1}^{n} \left|\frac{\partial}{\partial x_i}\right| dx_i\right] \times 100 \tag{2.7}$$

A similar analysis is used for the estimation of error in quantity adsorbed. In this study, quantity adsorbed was calculated using the following methods:-

(1) Instantaneous rate of adsorption

In this case, the quantity adsorbed was calculated by integrating the instantaneous rate of adsorption over the total time. Therefore:

$$q = \frac{\left[\int_0^t (F_i Y_i - F_o Y_o) + \int_t^{t_e} \{F_{i(t)} Y_{i(t)} - F_{o(t)} Y_{o(t)}\}\right] dt}{m} \tag{2.8}$$

When equilibrium between gas and solid is established rapidly, the quantity adsorbed is:

$$q = \frac{\int_0^t \Delta(FY)dt}{m} \tag{2.9}$$

or

$$q = \frac{FYt}{m} \qquad (2.10)$$

where F is the molar flowrate, calculated from the flowrate, which was measured by a flowmeter; Y is the mole fraction of the absorbate, calculated from the concentration which was measured by a pressure gauge.

The error involved in the calculation of quantity adsorbed is found by applying equation (2.7):

$$\frac{dq}{q} \times 100 = \left[\frac{dF}{F} + \frac{dY}{Y} + \frac{dt}{t} + \frac{dm}{m}\right] \times 100 \qquad (2.11)$$

The standard error, as given by the manufacturer for the following instruments, is as follows:-

(a) flowmeter 2-5% (the value of 3.5% was taken in this calculation)

(b) pressure gauge 1%

(c) electronic balance $2. \times 10^{-2}$%

(d) stop watch 0.3%

Therefore, equation (2.11) becomes:

$$\frac{dq}{q} \times 100 = [0.035 + 0.01 + 0.003 + 2. \times 10^{-4}] \times 100$$

$$\frac{dq}{q} \times 100 = 0.048 \times 100 \simeq 5.0\%$$

(2) Stoichiometric time

$$uct = mq + V_b \varepsilon c \qquad (2.12)$$

$$q = \frac{uct}{m} - \frac{V_b \varepsilon c}{m} \qquad (2.13)$$

The major error occurs in the first term of equation (2.13) ($\frac{uct}{m}$). The second term is too small and therefore the error is not significant and was neglected.

Hence

$$q = \frac{uct}{m} \qquad (2.14)$$

By applying equation (2.7), the error is given as:

$$\frac{dq}{q} \times 100 = \left[\frac{du}{u} + \frac{dc}{c} + \frac{dt}{t} + \frac{dm}{m}\right] \times 100$$

$$\frac{dq}{q} \times 100 = [0.035 + 0.01 + 0.003 + 2. \times 10^{-4}] \times 100$$

$$= 0.048 \times 100 \tilde{-} 5.0\%$$

CHAPTER 3

EXPERIMENTAL RESULTS AND MATHEMATICAL MODELLING OF METHANE, ETHANE AND PROPANE

This chapter contains experimental results for single and multicomponent mixtures of methane, ethane and propane on 5A molecular sieves at 25° C, and mathematical modelling for single components and ternary mixtures.

1. Single component adsorption isotherms

A concentration range (0.965 - 8.362 x 10^{-5} mol cm^{-3}) was used for each component. The quantity of single component adsorbed was calculated by (i) instantaneous rate of adsorption method [equations (1.8)-(1.12)] and (ii) stoichiometric time method [equations (1.18)-(1.19)]. There is a small difference between the adsorbed quantity calculated by these two methods. The first gives slightly higher results than the second. The discrepancy is attributed to the following:-

(a) Method (i) does not take into account the quantity of the fluid in the bed and is neglected.

(b) In method (ii), it is difficult to find the stoichiometric time with exact precision.

The comparison between the above two methods based on a Langmuir isotherm is shown in Figure 12.

In this study the instantaneous rate of adsorption [method (i)] was chosen for the calculations. The symbols in Figure 12 represent the experimental equilibrium data of methane, ethane and propane obtained by

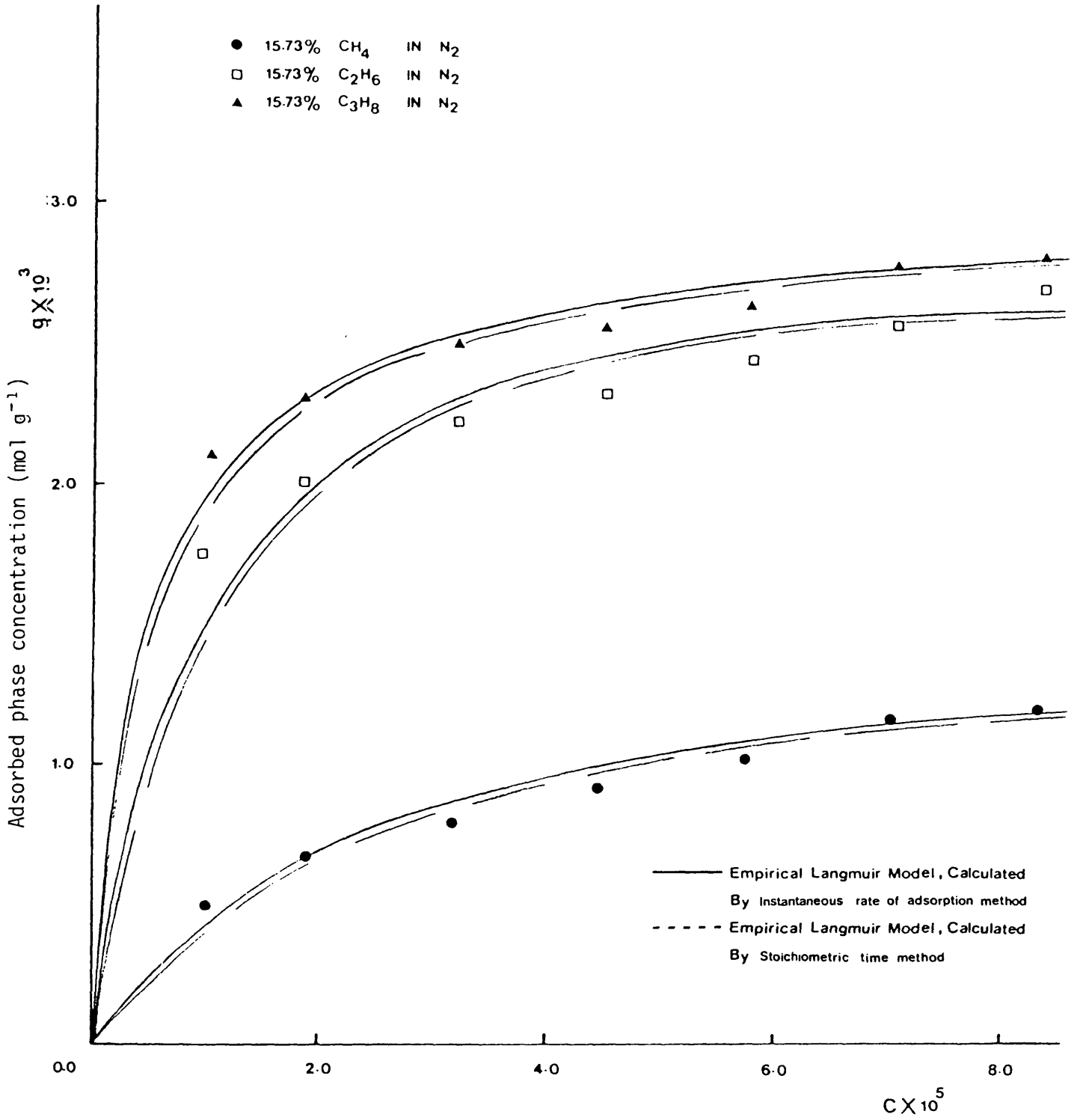

Figure 12 Single component isotherms at 25° C.

method (i). Propane is more strongly adsorbed than ethane, and ethane is more strongly adsorbed than methane.

1.1 Langmuir isotherm

The simple form of the Langmuir model may be written as:[10]

$$q = \frac{abc}{1+bc} \qquad (3.1)$$

By rearrangement, equation (3.1) gives:

$$\frac{c}{q} = \frac{1}{a}c + \frac{1}{ab} \qquad (3.2)$$

This is a linear equation relating $(\frac{c}{q})$ and (c), where a and b are constants.

The experimental equilibrium data for methane, ethane and propane correlated by equation (3.2) are presented in Figure 12. The data agree well with those calculated by the single component Langmuir model. The constants for this model, calculated by a least squares fit to the experimental data, are given in Table 3.1.

Table 3.1

Empirical Langmuir constant

Adsorbate	Temperature (° C)	a x 10^3 (mol g^{-1})	b x 10^{-4} (cm^3 mol)
methane	25	3.0	1.01
ethane	25	2.911	11.02
propane	25	2.96	18.25

1.2 Freundlich isotherm

The variation of adsorption with concentration can often be represented, over a limited range of concentration, at constant temperature, by the empirical equation:

$$q = K_f c^n \tag{3.3}$$

where K_f and n are constant, and the value of n is less than unity. On taking the logarithm of both sides, equation (3.3) becomes:

$$\log q = \log K_f + n \log c \tag{3.4}$$

so that a plot of log q, against log c should be a straight line. Therefore, the slope and the intercept are equal to n and log K_f respectively.

The experimental isotherms agree well with a Freundlich model over the whole range of adsorbate concentration, as shown in Figure 13. The values of the equilibrium constants, obtained by a least squares method, are given in Table 3.2.

Table 3.2

Empirical Freundlich constant

Adsorbate	Temperature (° C)	K_f*	n
methane	25	0.09121	0.458
ethane	25	0.0173	0.2
propane	25	0.00873	0.122

Many investigators have used this model to represent the equilibrium isotherm. Linderman and Williams[51] studied the sorption of nitrogen and methane on a 5A molecular sieve. The data they obtained could be fitted by both the Langmuir and Freundlich isotherms. They concluded that this was because the value of n in the Freundlich equation was near unity and the value of bc in the Langmuir equation was substantially less than unity, which causes the two expressions to be coincident. In this study the value

*The units of K_f depend on the magnitude of n. If n = 1 then the units of K_f are $cm^3\ g^{-1}$.

of n ranges from 0.122 to 0.458, while bc varies from 0.1 to 15.3 for all the adsorbates, which is inconsistent with the above conclusions. However, Dedrick and Beckmann[52] showed that the adsorption equilibrium data of 2,4-dichlorophenoxyacetic acid on activated carbon can be correlated by either a Freundlich or Langmuir type isotherm for both low and high concentrations, *i.e.*, when bc is in the range $0 \lesssim bc \lesssim 39.55$ and n is in the range $0.09 \lesssim n \lesssim 0.189$. This is in agreement with this study. Hence, it is not surprising that either the Freundlich or the Langmuir isotherms can both fit the data. By choosing appropriate values of K_f and n, a number of Type I isotherms[53] can be fitted by the Freundlich isotherm.[43]

1.3 Statistical thermodynamic model

Ruthven and Loughlin[18] presented an isotherm based on statistical thermodynamic for those molecular sieve adsorbents (such as the type A zeolites) which consist of discrete cavities interconnected through relatively small windows. Their expression for the equilibrium isotherm, for a single component is:

$$Q = \frac{Kxp + (Kxp)^2_x(1-2\beta/\nu)^2 + \ldots + \frac{(Kxp)^m}{(m-1)!} \times (1-m\beta/\nu)^m}{1 + Kxp + \frac{1}{2!} \times (Kxp)^2 \times (1-2\beta/\nu)^2 + \ldots + \frac{(Kxp)^m}{m!}(1-m\beta/\nu)^m} \qquad (3.5)$$

where Q is the average number of molecules adsorbed per cavity;

m is the saturation limit (an integer) determined by the condition $m \lesssim \nu/\beta$;

ν is the volume of the cavity (for a 5A sieve, 776 $\mathring{A}^3$);

β is the effective molecular volume of the adsorbate, which was estimated by linear interpolation between the van der Waal's b at the critical temperature and the molecular volume of the saturated liquid at the boiling point;[54]

K is Henry's constant, which was determined by (i) matching the theoretical isotherm equation [equation (4),[18]] to the experimental data,

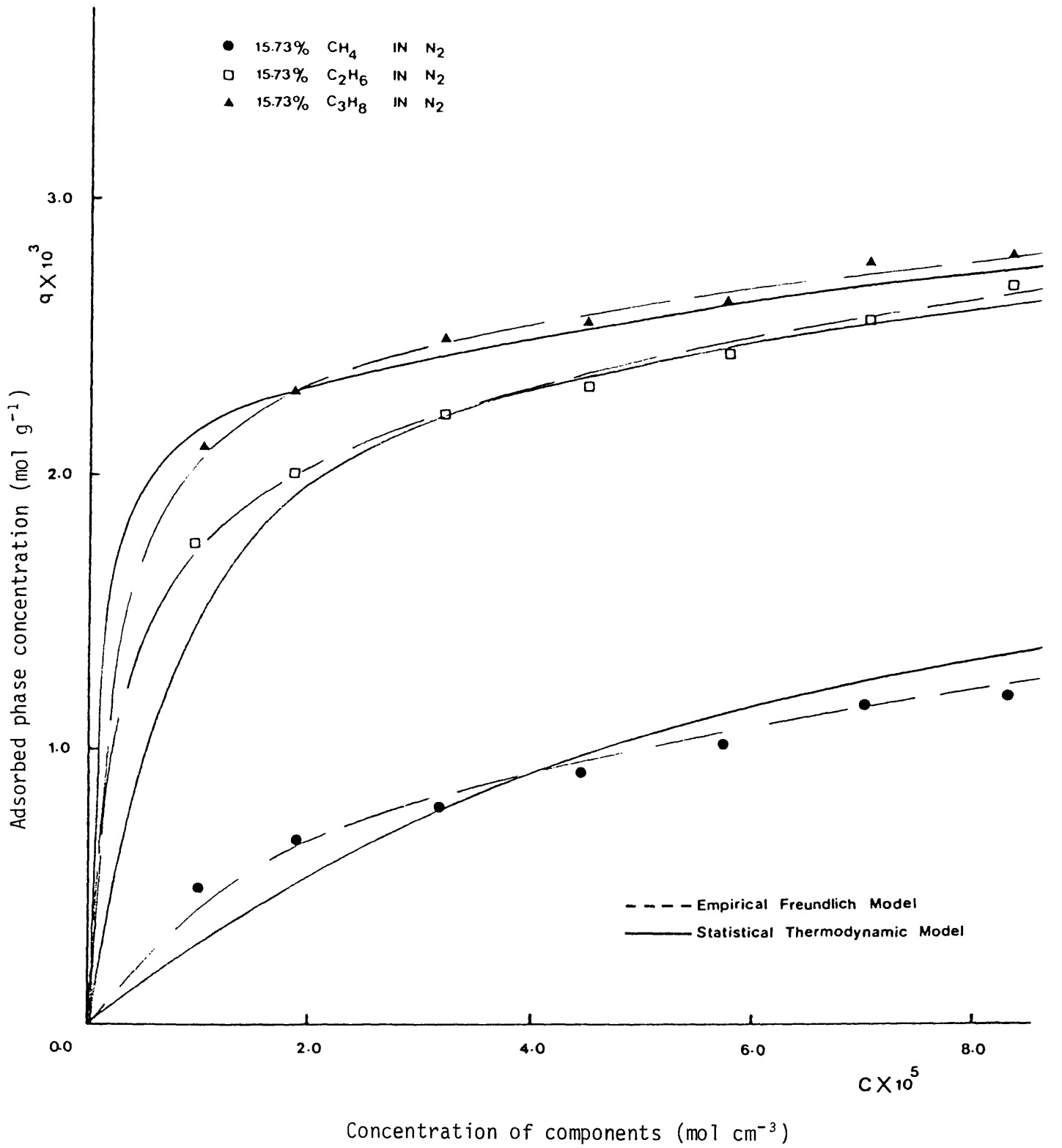

Figure 13 Single component isotherm at 25° C.

Table 3.3

Parameters for the statistical thermodynamic model

Cavity volume (ν, Å^3)	Component adsorbed at 25° C	Molecular volume (β) (Å^3 molecule^{-1})	No. of molecules per cavity ($m \leq \nu/\beta$)	Henry's constant calculated equation (4)[18] (molecule cavity^{-1} bar^{-1})	Henry's constant calculated equation (3.6) (molecule cavity^{-1} bar^{-1})
766	methane	82.1	9	2.58	2.18
	ethane	104.0	7	41.25	37.5
	propane	136.6	6	862.5	787.5

and (ii) taking into account the temperature dependence and expressing the Henry's law constant in the form of an Arrhenius equation:

$$K = K_0 \times \exp(\Delta H_0/RT) \qquad (3.6)$$

where ΔH_0 and K_0 are determined from the experimental data. There is a small discrepancy between the two methods. Henry's law constants determined by the first method were used in subsequent calculations. The parameters that were employed for this model are given in Table 3.3. The experimental data agree well with the model, except for methane, where the correlation is only moderately good, as shown in Figure 13.

2. Multicomponent adsorption isotherms

Two mixtures of methane, ethane and propane in nitrogen of different composition were used. The quantity adsorbed for multicomponent mixtures was calculated by the instantaneous rate of adsorption method (Chapter 1, section 2.1.1). The experimental data for ternary mixtures of methane, ethane and propane are shown in Figure 14. It can be seen that at constant pressure (concentration), a very small change in gas phase mole fraction of propane gives a strong change in adsorbed phase concentration. Similarly, but to a lesser extent, this is true for ethane. However, for methane a large change in the gas phase mole fraction is required before there is any significant effect on the adsorbed phase concentration. The inhibition of methane adsorption by ethane and propane can be seen from the amount of methane adsorbed (at the same gas phase concentration) decreasing with an increase in the gas phase concentration of both ethane and propane. In the same way it can be seen that propane inhibits the adsorption of ethane. However, the adsorption of propane is not inhibited by either methane or ethane (see Appendix 3). This behaviour can be explained from the breakthrough curves for two different mixtures

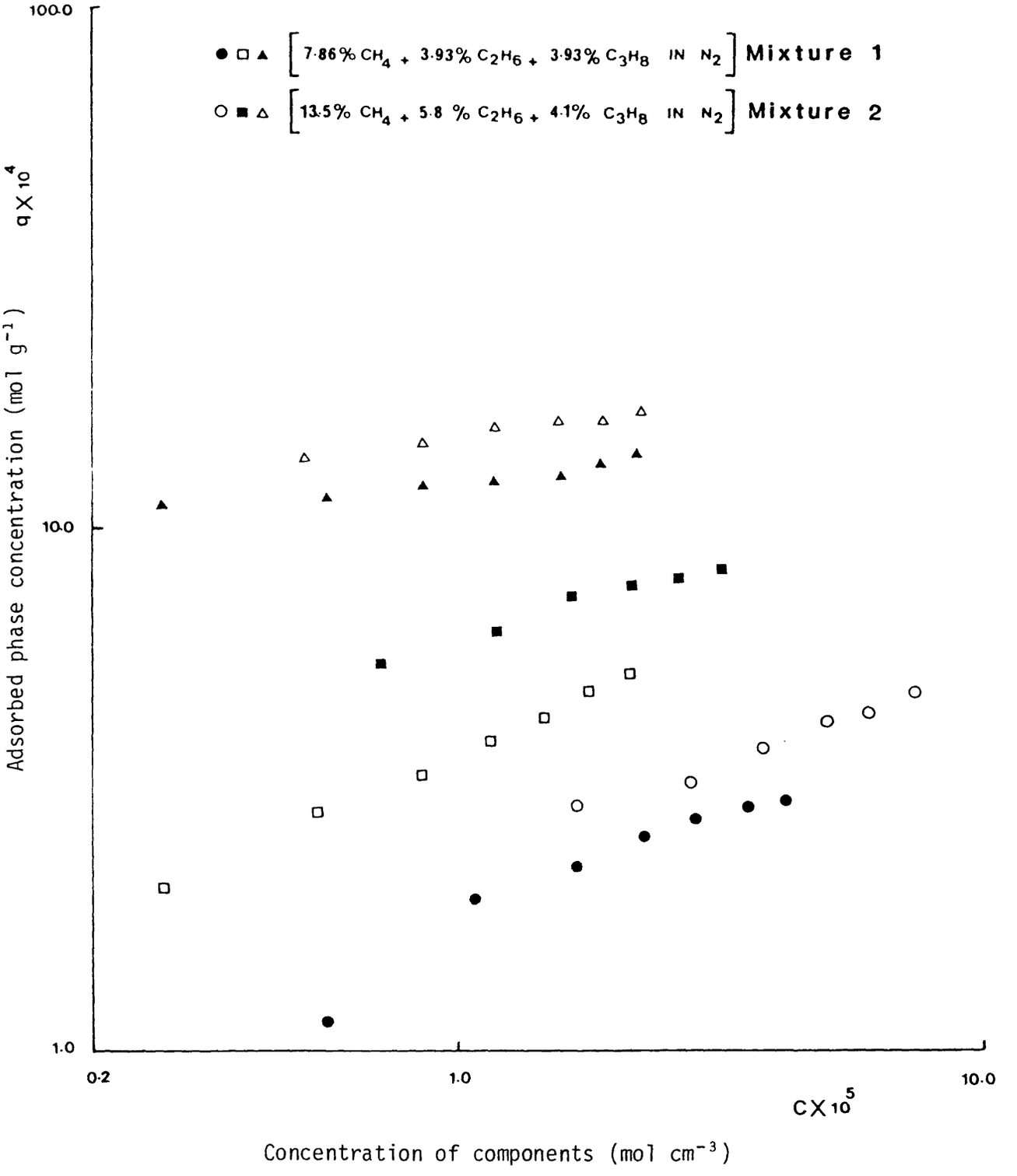

Figure 14 Ternary adsorption of methane, ethane and propane mixtures on 5A molecular sieve.

(of different composition) as shown in Figures 15 and 16. From Figure 16 (mixture 2), the fractional gas phase concentration for methane at the bed outlet is slightly greater than that for mixture 1, shown in Figure 15, in spite of the gas phase mole fraction being much greater. (The adsorption pressure for the two mixtures is the same, 10 atmos gauge.) For ethane, a smaller change in the gas phase mole fraction causes a much larger difference in the peaks for the breakthrouth curves of the two mixtures. Figures 15 and 17 show the breakthrough curves for mixture 1 at different adsorption pressures, 10 atmos and 0.5 atmos respectively. When the concentrations increase, the height of the peaks for methane and ethane increase, *i.e.*, a greater displacement of these components occurs. At high concentration, the strongest adsorbed component is adsorbed competitively and consequently more of the weakly adsorbed component is displaced. This displacement of the weakly adsorbed component is demonstrated by the desorption of a proportion of the less strongly adsorbed component during the period between its breakthrough and the breakthrough of the stronger adsorbed component. This phenomenon has also been demonstrated by Kast and Dreher[55] in the three component adsorption of benzene, water and methanol on silica gel, where water displaces benzene, and methanol displaces water. This raises the fluid phase composition of the weakly adsorbed component to such an extent that it rises to a peak composition above that of the inlet concentration. This phenomenon can be taken advantage of in the separation of components by suppressing adsorption prior to breakthrough of the next component. This technique will be discussed in Chapter 4.

Finally, by considering the area under the peaks above the initial (dimensionless) concentration (*i.e.*, above 1.0) for methane and ethane, it is shown that the displacement of ethane by propane is more than the displacement of methane by ethane. Furthermore, the total dis-

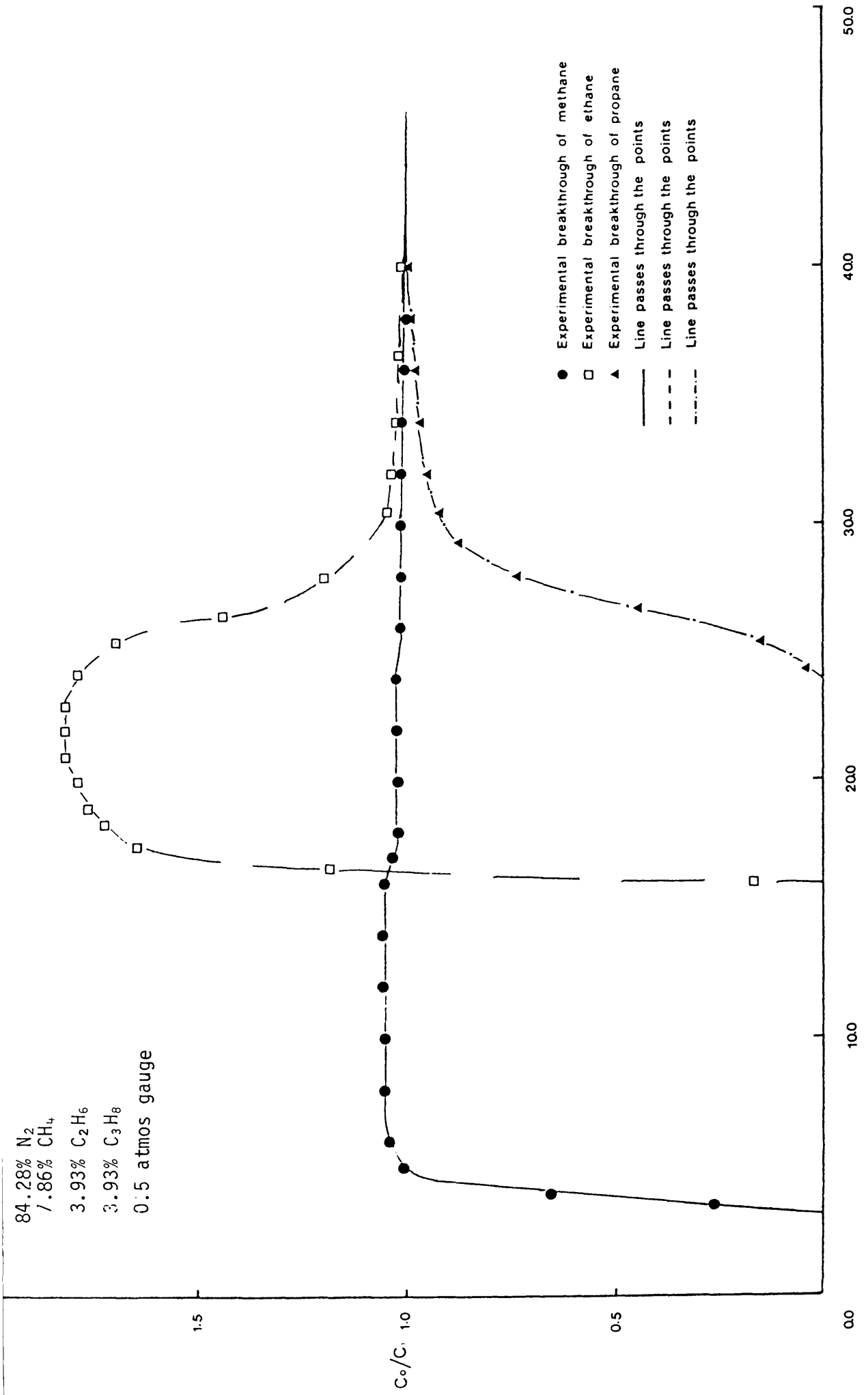

Figure 15 Experimental breakthrough of methane, ethane and propane from three-component mixture (mixture 1).

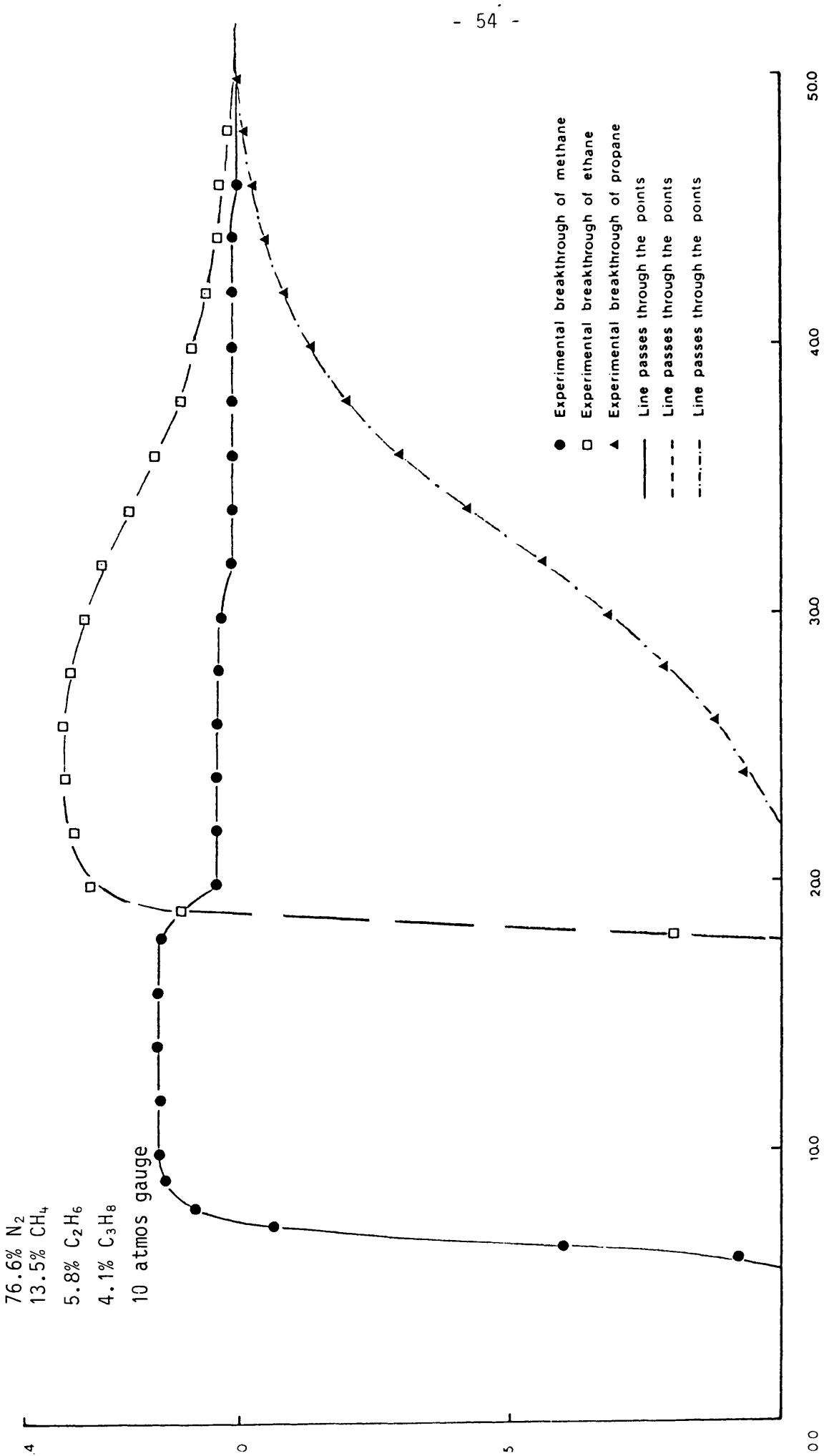

Figure 16 Experimental breakthrough of methane, ethane and propane from three-component mixture (mixture 2).

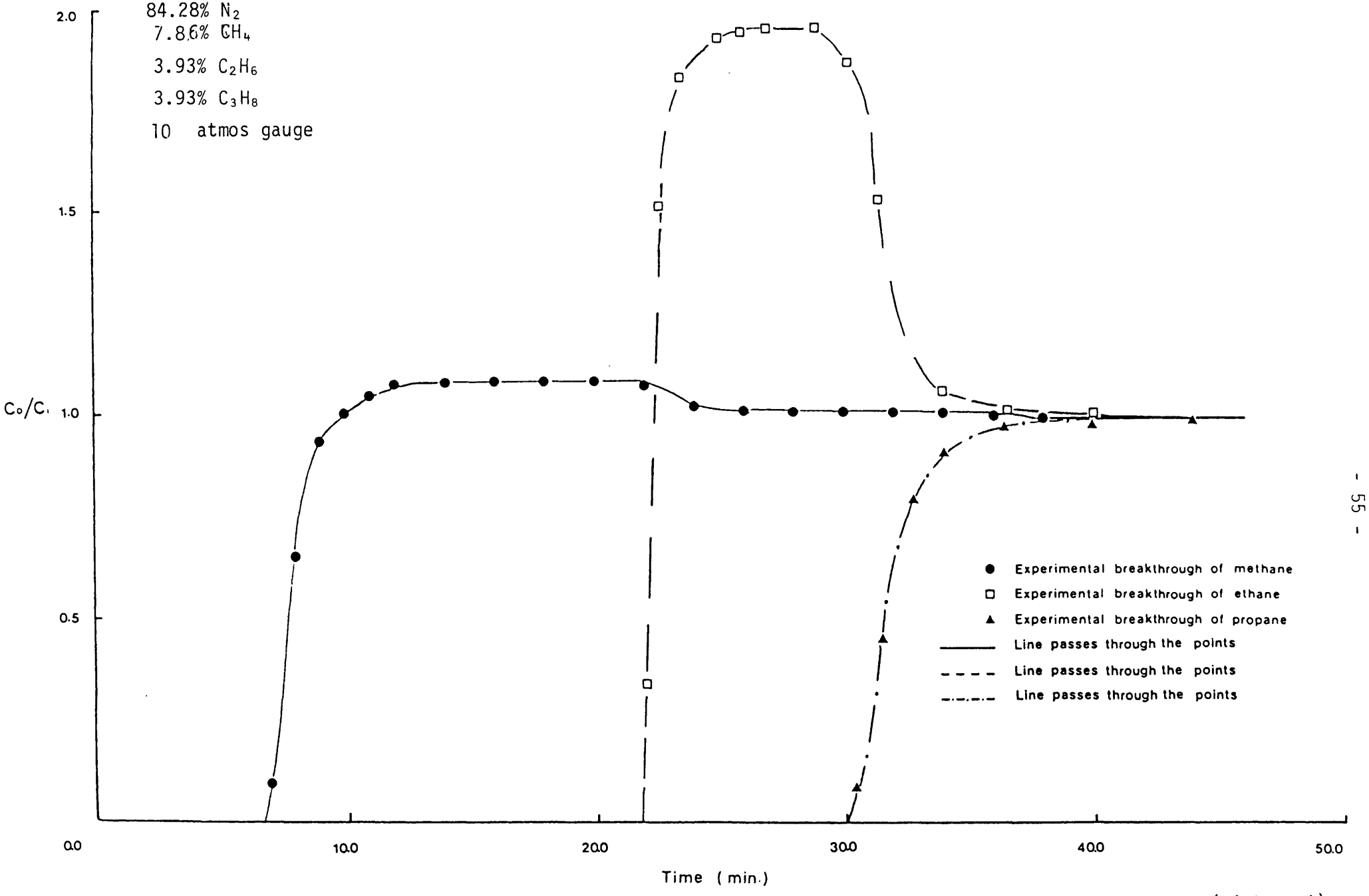

Figure 17 Experimental breakthrough curve of methane, ethane and propane from three-component mixture (mixture 1).

placement of ethane is greater than methane, whereas methane is not displaced to any extent by propane (see, for example, Figures 15-17).

3. Mathematical modelling of the ternary adsorption isotherm on 5A molecular sieves

In comparison with the studies on binary mixtures, those dealing with the prediction of ternary mixtures of gases are very few. Only one publication is concerned with the fitting of a Freundlich-type isotherm to a ternary mixtures of liquids[21,25-31] (see Chapter 1, section 1.2.2). The present study will therefore extend the procedure of prediction for binary mixtures to one for ternary mixtures in a similar way to the extension of the binary isotherm from the single component isotehrm. Moreover, there are no published results for ternary systems of the components employed for this study available for comparison.

3.1 Extended Langmuir model

The Langmuir model for mixed adsorption can be expressed in terms of the single component coefficients as:

$$q_i^* = \frac{a_i b_i c_i}{1+\sum_{i=1}^{n} b_i c_i} \qquad (3.7)$$

This implies that $a_1 = a_2 = a_3 \ldots\ldots\ldots a_n$. For ternary mixtures, equation (3.7) can be written as:

$$q_1 = \frac{a_1 b_1 c_1}{1+b_1c_1+b_2c_2+b_3c_3} \qquad (3.8)$$

with a similar expression for q_2 and q_3. The parameters used in this model were those employed for the single component isotherms, as noted in Table 3.1. Figure 18 shows the poor fit which was obtained, except at low gas phase concentrations of methane.

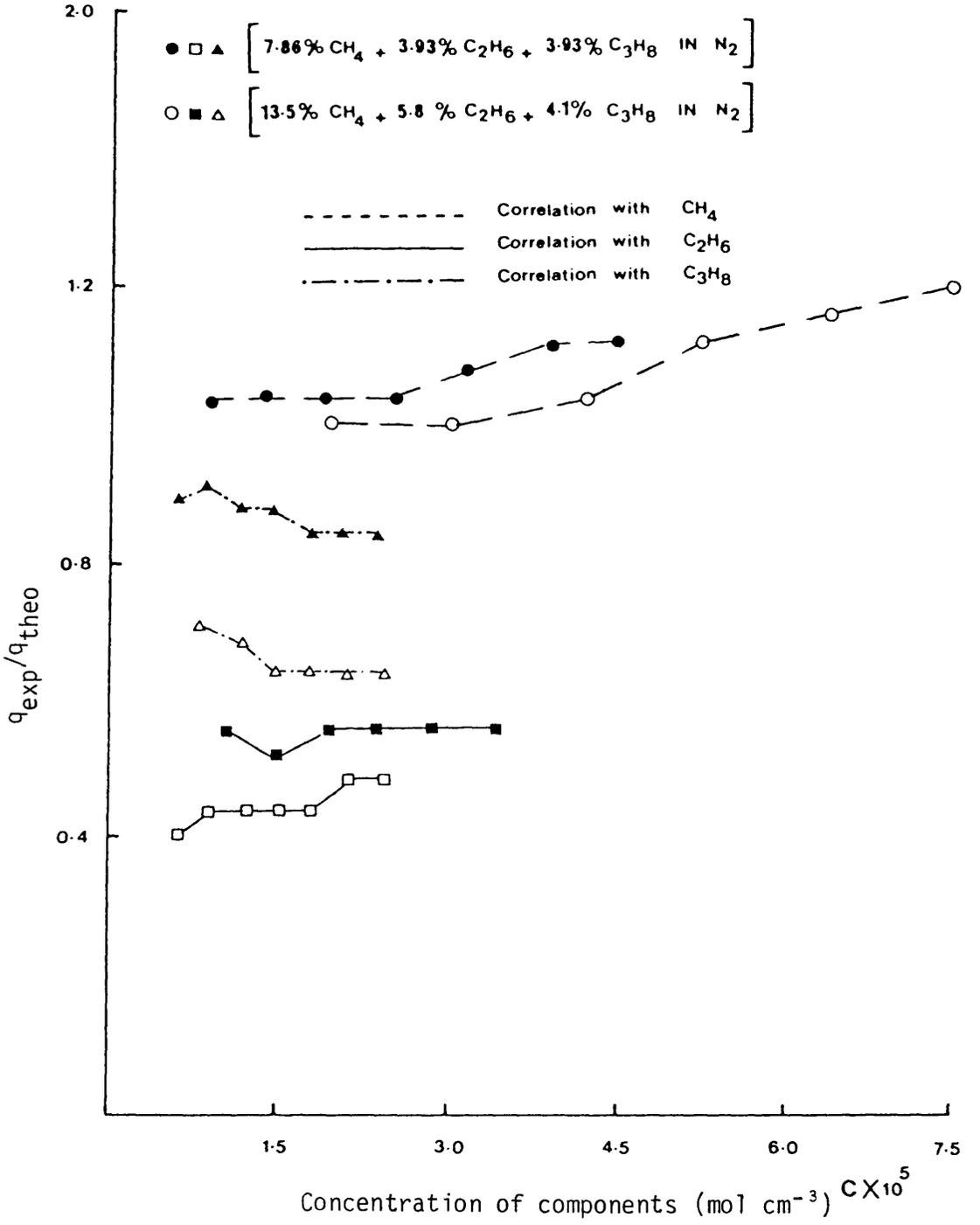

Figure 18 Ternary adsorption correlated with extended Langmuir model.

3.2 Ternary component statistical thermodynamic model

The binary adsorption model of Ruthven *et al.*[19,20] was extended to a ternary mixture as follows:

$$Q = \frac{K_1xp_1+\underset{hji}{\Sigma\Sigma\Sigma}(K_1xp_1)^i x(K_2xp_2)^i x(K_3xp_3)^h x\frac{(1-i\beta_1/\nu-j\beta_2/\nu-h\beta_3/\nu)^{i+j+h}}{(i-1)!xj!xh!}}{1+K_1xp_1+K_2xp_2+K_3xp_3+\underset{hji}{\Sigma\Sigma\Sigma}\frac{(K_1xp_1)^i x(K_2xp_2)^j x(K_3xp_3)^h x(1-i\beta_1/\nu-j\beta_2/\nu-h\beta_3/\nu)^{i+j+h}}{i!xj!xh!}} \qquad (3.9)$$

where $i+j+h \geq 3$, $i\beta_1+j\beta_2+h\beta_3 < \nu$, with similar expressions for Q_2 and Q_3. The coefficients obtained from single component isotherms were used to represent the ternary adsorption isotherm and are given in Table 3.3. Again, the model failed to predict the experimental data as shown in Figure 19.

3.3 Modified extended Langmuir model

The extended Langmuir model [equation (3.8)] was modified in two ways and solved as follows:

Case I. The modified extended Langmuir isotherm for a component M of a ternary mixture can be written as:

$$q_M = \frac{a_M b_M c_M}{1+b_M c_M+b'_E c_E+b'_p c_p} \qquad (3.10)$$

where the subscripts M, E and p denote methane, ethane and propane respectively, with a similar expression for q_E and q_p. Equation (3.10) was rearranged to calculate the value of the coefficients b'_E and b'_p as:

$$\frac{a_M b_M c_M}{q_M} - (1+b_M c_M) = b'_E c_E+b'_p c_p \qquad (3.11)$$

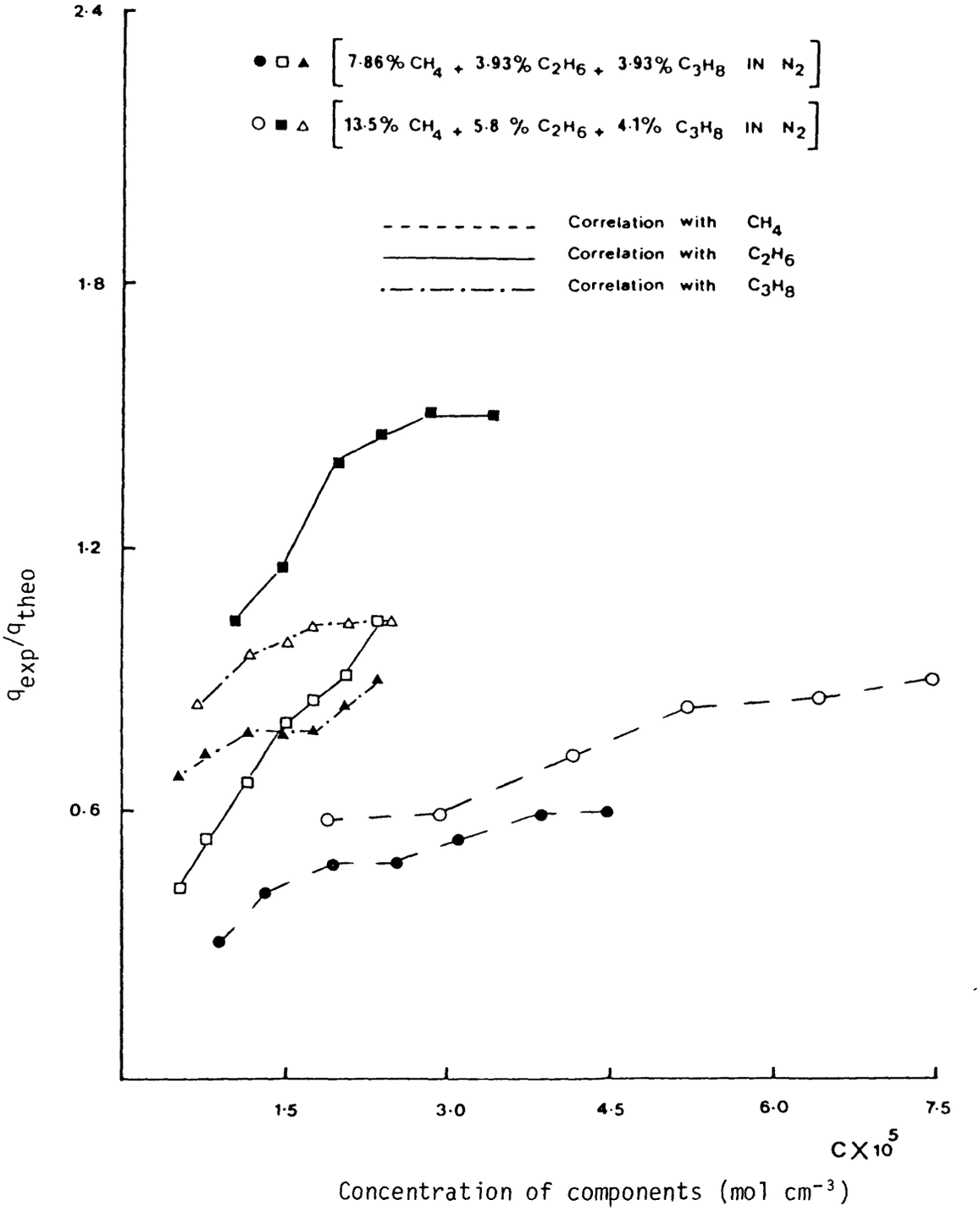

Figure 19 Ternary adsorption data correlated with statistical thermodynamic model.

The values of a_M and b_M are taken from the single component isotherm. The other constants, calculated by a least squares method, are summarised in Table 3.4.

Table 3.4

Modified extended Langmuir model coefficients

Case I:

i	adsorbate	$a_i \times 10^3$ (mol g^{-1})	$b_i \times 10^{-4}$ (cm^3 mol^{-1})	$b_{iM}' \times 10^{-4}$ (cm^3 mol^{-1})	$b_{iE}' \times 10^{-4}$ (cm^3 mol^{-1})	$b_{ip}' \times 10^{-4}$ (cm^3 mol^{-1})
1	methane	3.0	1.01	-	1.44	11.52
2	ethane	2.911	11.02	-12.26	-	77.74
3	propane	2.96	18.25	-30.57	77.7	-

Case II. The constants b_M, b_E and b_p from the single component isotherm will not be the same as those in the multicomponent equilibrium isotherm, so a more realistic approach would be to consider b_M, b_E and b_p as unknown in equation (3.8). By a rearrangement of equation (3.8), one obtains:

$$\left(\frac{c_M}{q_M} - \frac{c_M}{a_M}\right) = \frac{1}{a_M b_M'} + \frac{b_E'}{a_M b_M'} c_E + \frac{b_p'}{a_M b_M'} c_p \qquad (3.12)$$

A similar expression can be written for both ethane and propane. Equation (3.12) requires the value of a, which is taken from the single component isotherm and b_M', b_E' and b_p' are determined by a least squares method. This has the added advantage that there is an extra degree of freedom which will enable the resultant curve to give a closer fit to the data. The coefficients were determined, and are given in Table 3.5.

A good correlation was obtained by the above two methods, especially with Case II. Figures 20 and 21 show the correlation for Case I and Case II respectively.

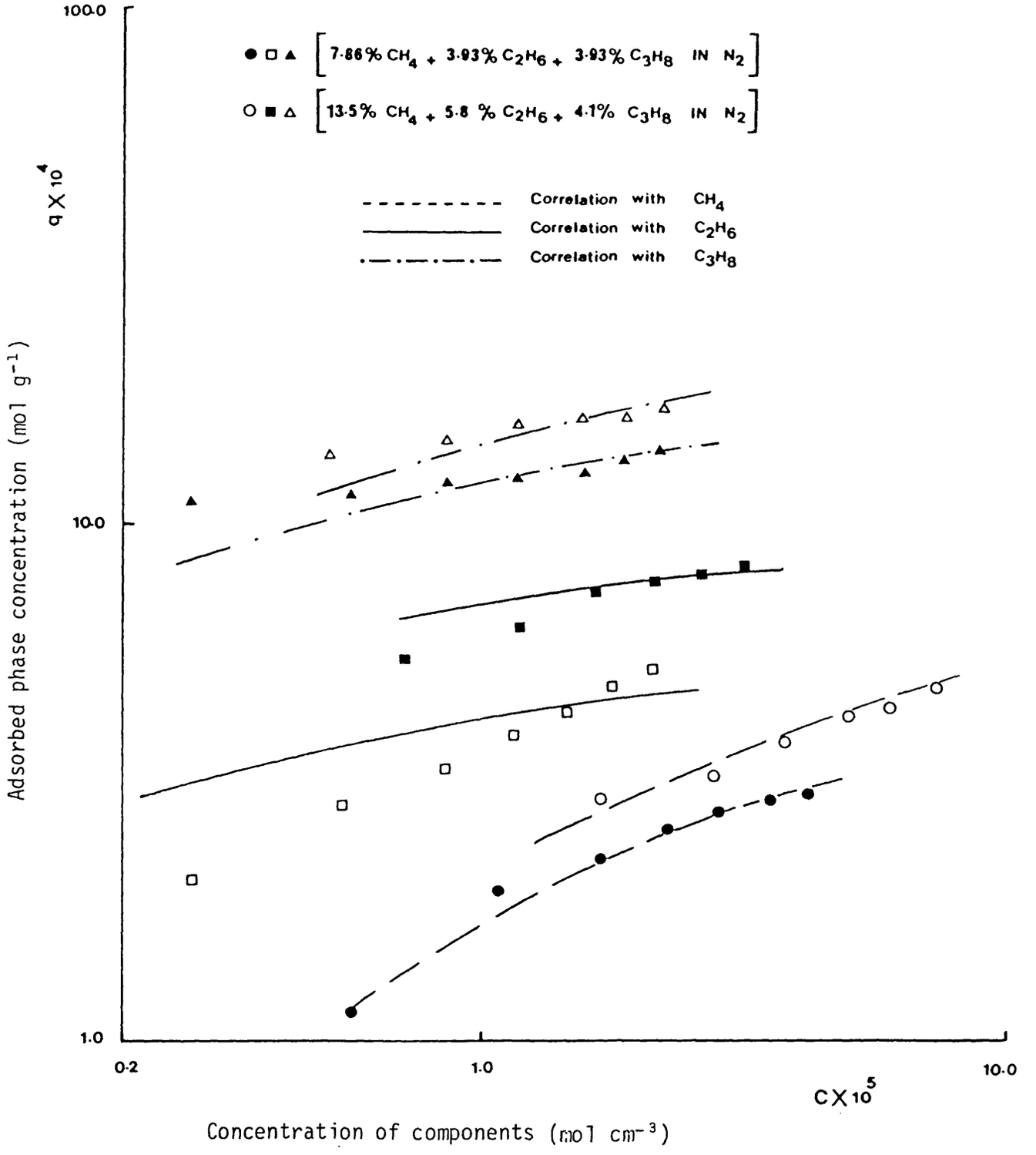

Figure 20 Isotherms for ternary mixtures of CH_4, C_2H_6 and C_3H_8 at 25° C, correlated by modified extended Langmuir model (Case I).

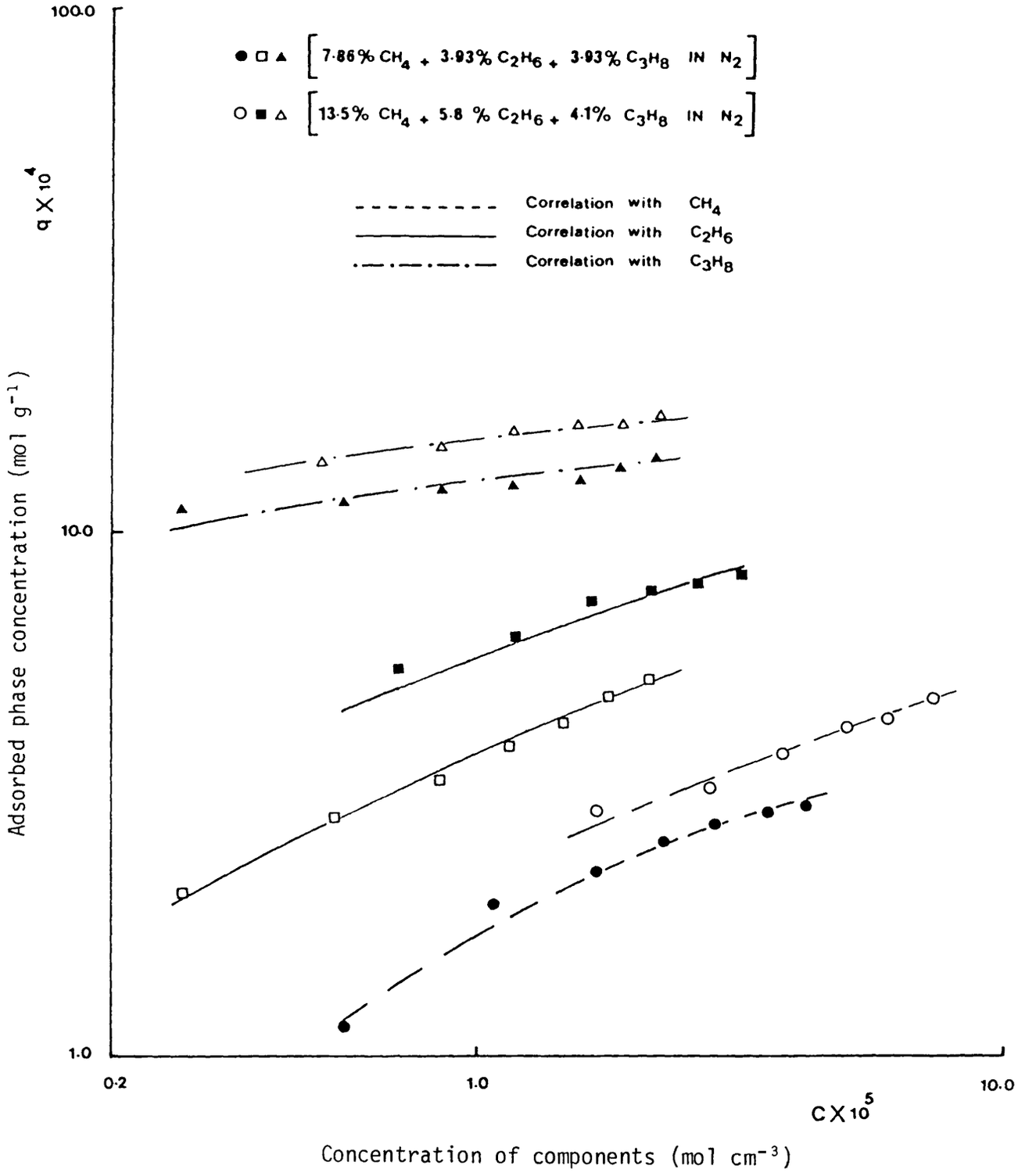

Figure 21 Isotherms for ternary mixtures of CH_4, C_2H_6 and C_3H_8 at 25° C, correlated by modified extended Langmuir model (Case II).

Table 3.5

Modified extended Langmuir model coefficients

Case II:

i	adsorbate	$a_i \times 10^3$ (mol g^{-1})	$b'_{iM} \times 10^{-4}$ (cm^3 mol^{-1})	$b'_{iE} \times 10^{-4}$ (cm^3 mol^{-1})	$b'_{ip} \times 10^{-4}$ (cm^3 mol^{-1})
1	methane	3.0	1.011	1.44	1.154
2	ethane	2.911	-3.89	3.67	20.98
3	propane	2.96	-73.59	190.47	39.19

The values of the coefficients b'_M (Tables 3.4 and 3.5) in the isotherms for ethane and propane are negative. No Langmuir correlation exists with respect to a ternary mixture for comparison. However, the equilibrium isotherm for ternary mixtures is more complicated, because firstly it will be a function of three independent concentrations, and secondly there will be mutual adsorbate interaction occuring under the influence of the adsorbent surface field. In the present study, the negative value for b'_M may be attributed to the presence of two strongly adsorbed components (ethane and propane), which might cause displacement of, or inhibit the adsorption of, the weakly adsorbed component (methane) (see section 2).

Finally, Dorfman and Danner[56] have studied the adsorption of a ternary mixture of nitrogen, oxygen and carbon monoxide on molecular sieve type 10X. They concluded that the Langmuir model for ternary systems gave qualitatively correct predictions, yet it was quantitatively too inaccurate to be acceptable. However, they did not give any reasons for their conclusions.

3.4 Freundlich-type multicomponent adsorption

Two methods have been proposed to describe the adsorption of multi-solutes (Chapter 1, section 1.2.2), which are as follows:

(1) Fritz and Schluender model.[21] An extended Freundlich isotherm model equation was used [Chapter 1, section 1.2.2, equation (1.5)]. For component 1 in a ternary mixture this equation becomes:

$$q_1 = \frac{K_{10}c_1^{n_{10}}}{c_1^{n_{11}} + K_{12}c_2^{n_{12}} + K_{13}c_3^{n_{13}}} \qquad (3.13)$$

with a similar expression for q_2 and q_3. K_{10} and $(n_{10}-n_{11})$ are the coefficients of the single component isotherm, while the other coefficients were calculated from multicomponent mixture experimental data by non-linear regression, and are listed in Table 3.6.

Non-linear regression.-The estimation of parameters by non-linear regression was undertaken because of the obvious non-linearity of the model [equation (3.13)]. The non-linear regression package chosen is available in the University of Bath Computer Unit through the services of the South Western Universities Computer Network. The program, known as 'BMDP3R' (a non-linear regression package for statistical analysis), was developed by the Biomedical Department of the University of California, Los Angeles.[57]

For methane and ethane a good correlation was obtained between the model and the experimental data over the range of gas phase adsorbate concentration investigated. For propane, the isotherm does not fit so well. These observations are illustrated in Figure 22.

Table 3.6

Freundlich-type multicomponent parameters (Fritz and Schluender model)

i	adsorbate	K_{io}*	n_{io}	K_{i1}*	n_{i1}	K_{i2}*	n_{i2}	K_{i3}*	n_{i3}
1	methane	0.0912	1.082	1.0	0.624	0.001	0.1	136.23	1.0
2	ethane	0.0173	1.946	0.001	1.7	1.0	1.75	0.2023	1.5
3	propane	0.00873	1.175	0.00001	0.5	0.00001	0.1	1.0	1.053

*Units of K_{io}, K_{i1}, K_{i2} and K_{i3} will obviously depend on values of n_{io}, n_{i1}, n_{i2} and n_{i3}.

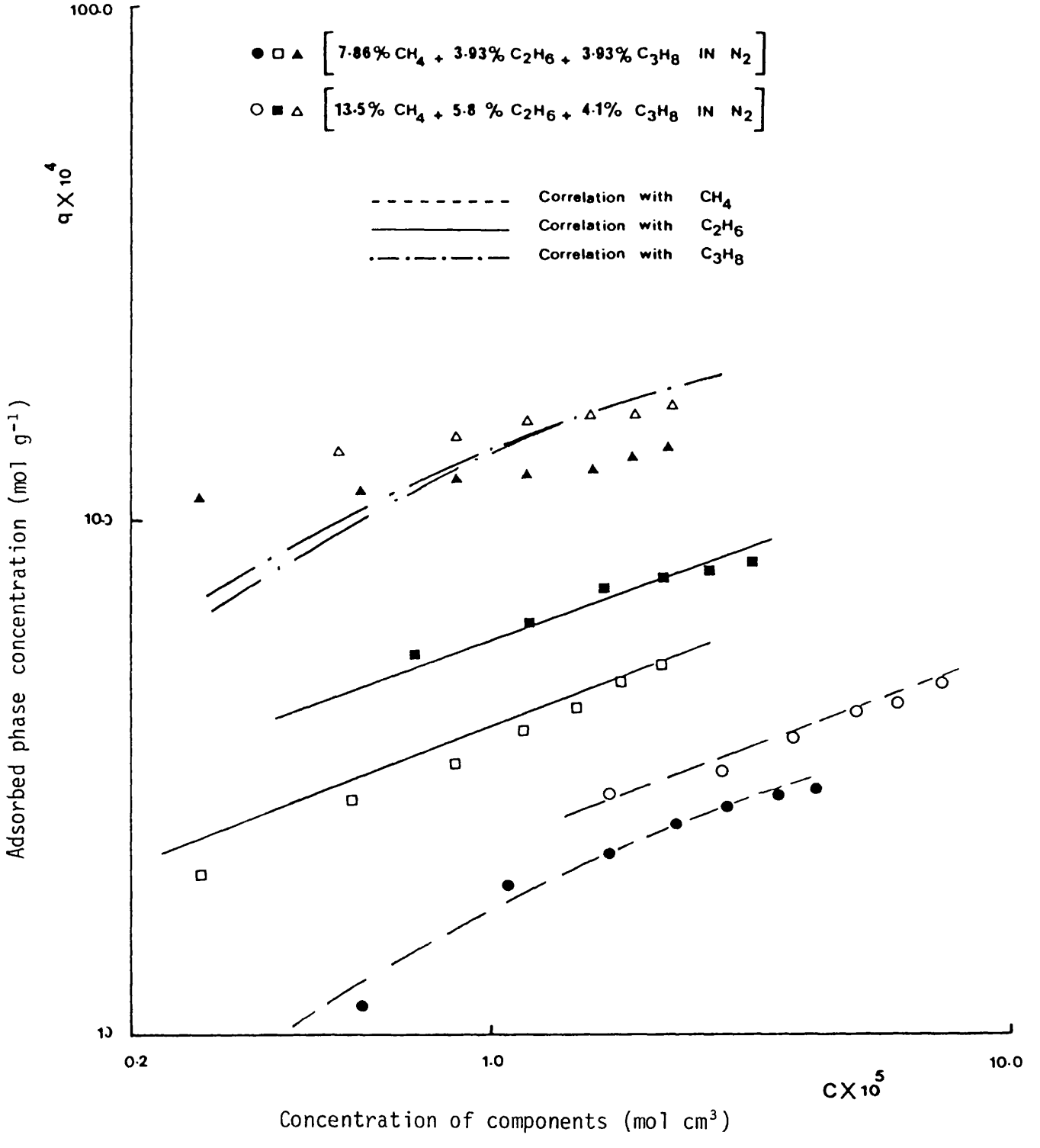

Figure 22 Isotherms for ternary mixtures of CH_4, C_2H_6 and C_3H_8 at 25° C, correlated by Fritz and Schluender model.

(2) Sheindorf *et al.* model.[29] The equilibrium adsorption of each component in a ternary mixture [equation (1.6), Chapter 1] may be written in polynomial form as:

$$q_1 = K_1c_1(c_1 + K_{12}c_2 + K_{13}c_3)^{n_1-1} \quad (3.14)$$

$$q_2 = K_2c_2(K_{21}c_2 + c_2 + K_{23}c_3)^{n_2-1} \quad (3.15)$$

$$q_3 = K_3c_3(K_{31}c_1 + K_{32}c_2 + c_3)^{n_3-1} \quad (3.16)$$

where K_1, K_2, K_3 and n_1, n_2, n_3 are the single component coefficients.

By linearisation, equation (3.14) gives:

$$\left(\frac{q_1}{K_1c_1}\right)^{\frac{1}{n_1-1}} - c_1 = K_{12}c_2 + K_{13}c_3 \quad (3.17)$$

The constants of equation (3.17) were obtained by a least squares method. The constants K_{21}, K_{23}, K_{31} and K_{32} in equations (3.15) and (3.16) can be calculated either by following the same procedure as in equation (3.14), or by caluation from the definition:

$$K_{ij} = \frac{1}{K_{ij}} \quad \left(\text{for example, } K_{21} = \frac{1}{K_{12}}\right)$$

obtained in the derivation of equations (3.14)-(3.16).[29-31] There is a small difference between the two methods. The coefficients obtained are talulated in Table 3.7.

Again, for methane and ethane the experimental data agree well, whereas for propane there is a discrepancy between the theoretical and experimental data. Figure 23 shows the correlation of the ternary mixture by this model.

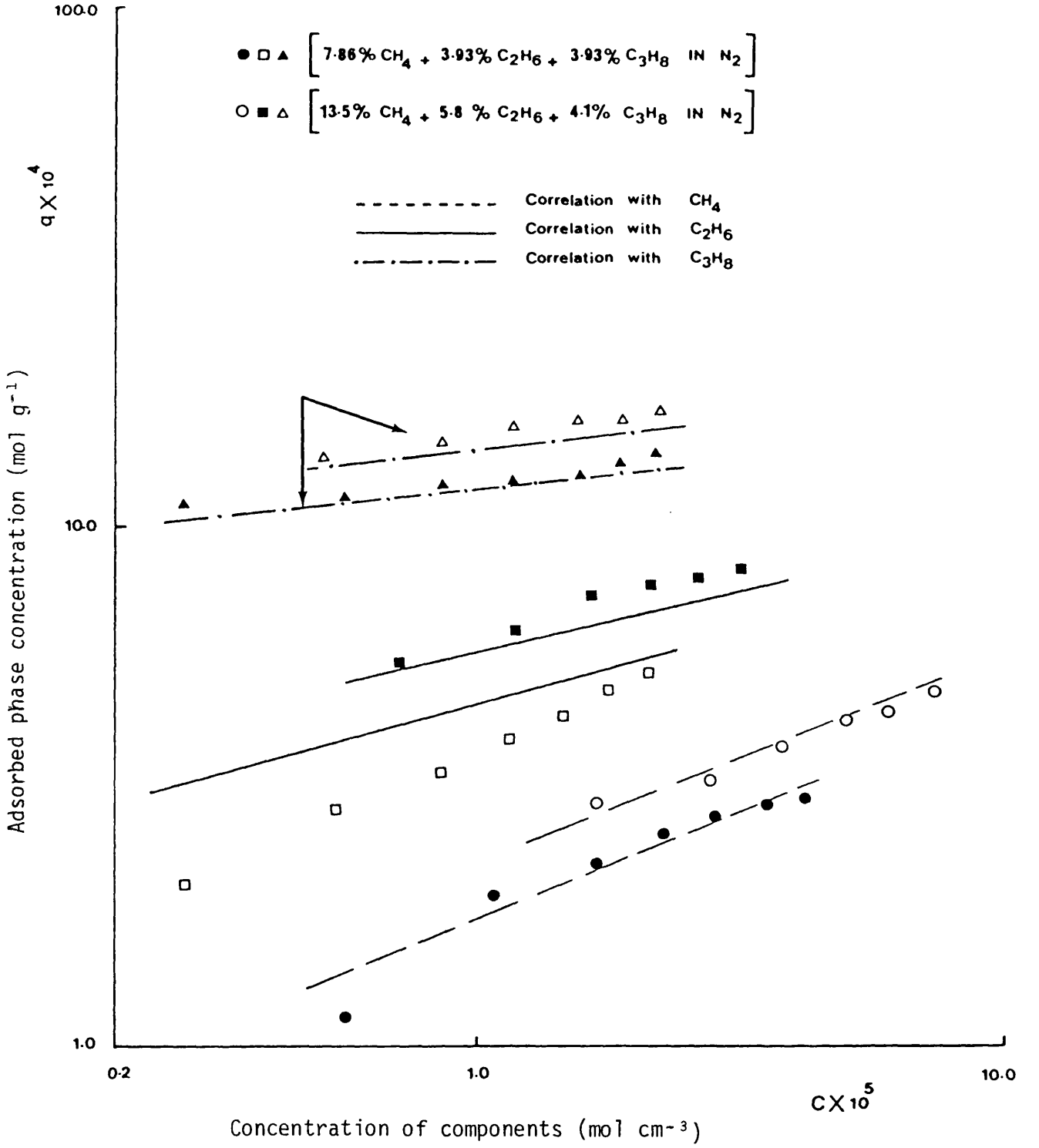

Figure 23 Isotherms for ternary mixtures of CH_4, C_2H_6 and C_3H_8 at 25° C, correlated by Sheindorf *et al.* model.

Table 3.7

Freundlich-type multicomponent parameters
(Sheindorf *et al.* model)

i	adsorbate	K_i*	K_{i1}*	K_{i2}*	K_{i3}*	n_i
1	methane	0.0912	1.0	2.74	8.91	0.458
2	ethane	0.0173	0.365	1.0	3.22	0.2
3	propane	0.00873	0.1122	0.31 - 0.4	1.0	0.12

4 Conclusions

Equilibrium isotherms for single component adsorption of methane, ethane and propane on 5A molecular sieves can be fitted by the empirical Langmuir and Freundlich models. The experimental data were well represented by these models. The statistical thermodynamic model was also represented fairly well by the experimental data. Both the extended Langmuir and the statistical thermodynamic models failed to predict the equilibrium isotherm for a ternary mixture. The modified extended Langmuir model, however, gave a good correlation. The extended Freundlich isotherm represented the data fairly well, except for propane, where there is some difference between the experimental and calculated values.

---

*Units of K_i, K_{i1}, K_{i2} and K_{i3} will obviously depend on values of n_i.

CHAPTER 4

FINITE DIFFERENCE TECHNIQUES

The prediction of the performance of a fixed bed adsorption column requires the solution of the appropriate differential rate equation describing the mass transfer process, subject to the boundary conditions imposed by the fluid phase mass balance. To predict the breakthrough curve for a given component, equation (1.25), representing concentration changes within the bed, is cast into difference form. A backward difference technique is used to approximate both the rates of change of gas phase adsorbate concentration with axial position and time. Therefore:

$$u\left.\frac{\partial c}{\partial z}\right|_t \simeq \frac{u_{(z,t)}[c_{(z,t)} - c_{(z-\Delta z,t)}]}{\Delta z} \tag{4.1}$$

$$\left.\frac{\partial c}{\partial t}\right|_z \simeq \frac{c_{(z,t)} - c_{(z,t-\Delta t)}}{\Delta t} \tag{4.2}$$

Substituting equations (4.1) and (4.2) into equation (1.25), an explicit solution for $c_{(z,t)}$ can be obtained from:

$$c_{(z,t)} = \frac{c_{(z,t-\Delta t)} + \frac{\Delta t}{\Delta z} \cdot u_{(z,t)} \cdot c_{(z-\Delta z,t)} - (\rho_{b/\varepsilon})\Delta q_{(z,t)}}{1 + \frac{\Delta t}{\Delta z} u_{(z,t)}} \tag{4.3}$$

The amount of component adsorbed within the adopted length and time increments is the calculated quantity. For this purpose, either an equilibrium or kinetic relationship between the adsorbed phase component concentration and the gas phase concentration is employed. This can be written as:

$$q_{(z,t)} = f(z,t) \tag{4.4}$$

Clearly then, all the terms in equation (4.3) are either known experimentally or can be calculated from the experimental data. Hence stepwise computation in both the length and time parameters can be initiated to generate breakthrough data.

1. Breakthrough of Single Component

Various rate models which are proposed to describe the different type of adsorption mechanisms (Chapter 1, section 3) are substituted into equation (4.4). The breakthrough curves obtained (theoretically) are then compared with the experimental curves for different experimental conditions and all the adsorbates to test the applicability of the proposed model.

1.1 Equilibrium model

The quantity adsorbed of a component can be calculated from:

$$\Delta q_{(z,t)} = q_{(z-\Delta z,t)} - q_{(z,t-\Delta t)} \tag{4.5}$$

Assuming the equilibrium condition can be expressed by the Langmuir equation (3.1), then:

$$q_{(z-\Delta z,t)} = \frac{abc_{(z-\Delta z,t)}}{1+bc_{(z-\Delta z,t)}} \tag{4.6}$$

and

$$q_{(z,t-\Delta t)} = \frac{abc_{(z,t-\Delta t)}}{1+bc_{(z,t-\Delta t)}} \tag{4.7}$$

As both $c_{(z-\Delta z,t)}$ and $c_{(z,t-\Delta t)}$ are known from the information obtained at previous length and time steps, equations (4.3), (4.6) and (4.7) can be solved numerically.

The calculation procedure was as follows:

a - Set $t = 0$

b - Set $t = t+\Delta t$

c - Set $z = \Delta z$ ($z = 0$ contained the boundary conditions)

d - Calculate $\Delta q_{z,t}$

e - Calculate $c_{z,t}$

f - Set $z = z+\Delta z$

g - Return to d until the end of the bed is reached

h - Return to b until complete breakthrough

A computer program was written to solve the above set of equations to generate a fixed bed breakthrough curve for a single component and is given in Appendix 4. This model has been applied to all the adsorbates (methane, ethane and propane). Figure 24 shows the experimental points and computed breakthrouth curve for methane. It can be seen that the equilibrium model failed to predict the experimental breakthrough. Similarly, it failed for ethane and propane, as shown in Figures 25 and 26 respectively. Therefore, the equilibrium model does not determine the rate of adsorption for any of the adsorbates.

1.2 Linear driving force model

In this case, the overall rate of adsorption is limited by the rate of transfer of material into the adsorbent particles, as given by Glueckauf and Coates [equation (1.29)], then:

$$\Delta q_{(z,t)} = K_G \Delta t [q^*_{(z,t)} - q_{(z-\Delta z, t-\Delta t)}] \tag{4.8}$$

where

$$q^*_{(z,t)} = \frac{abc_{(z,t)}}{1+bc_{(z,t)}} \tag{4.9}$$

and

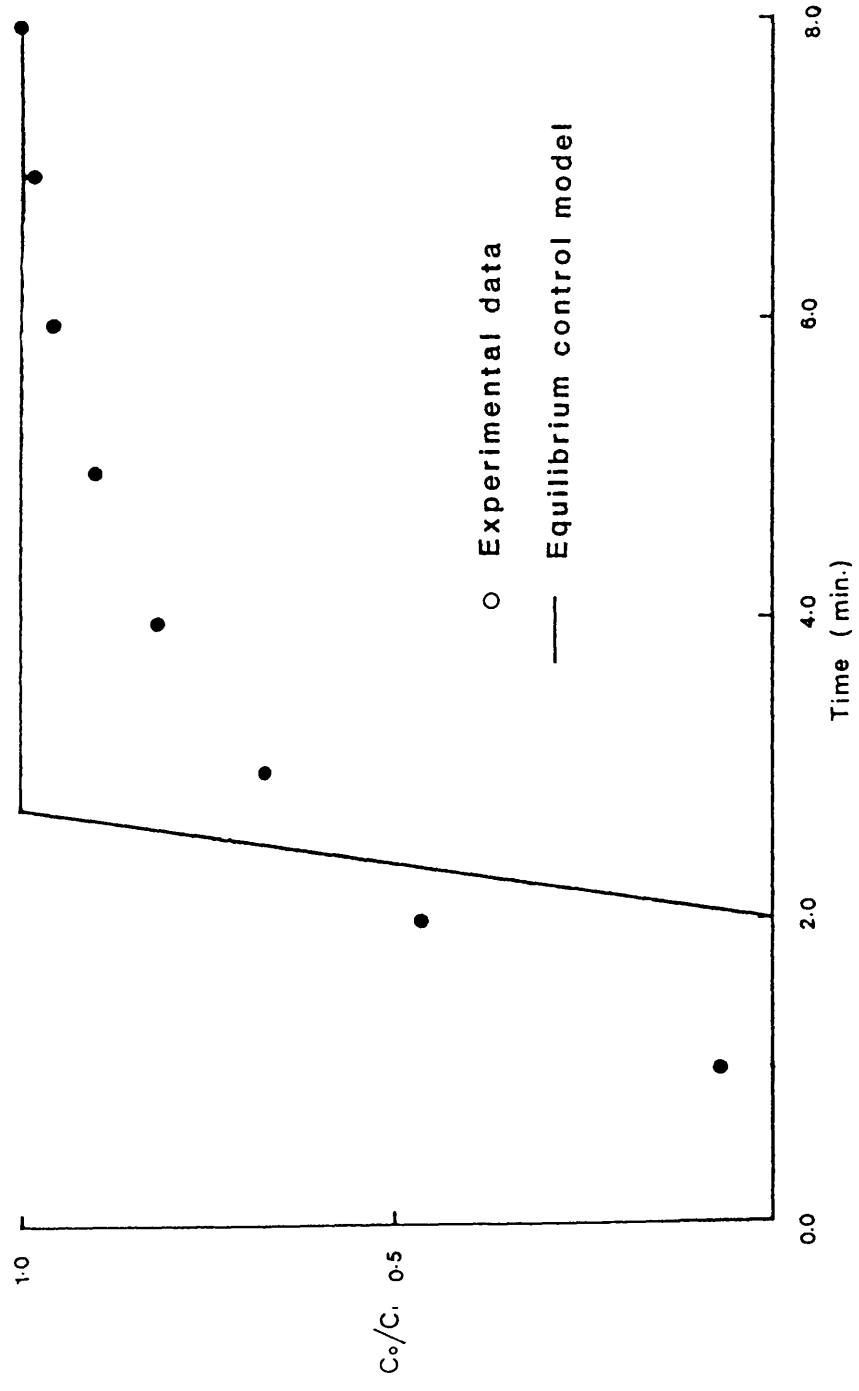

Figure 24 Breakthrough of methane.

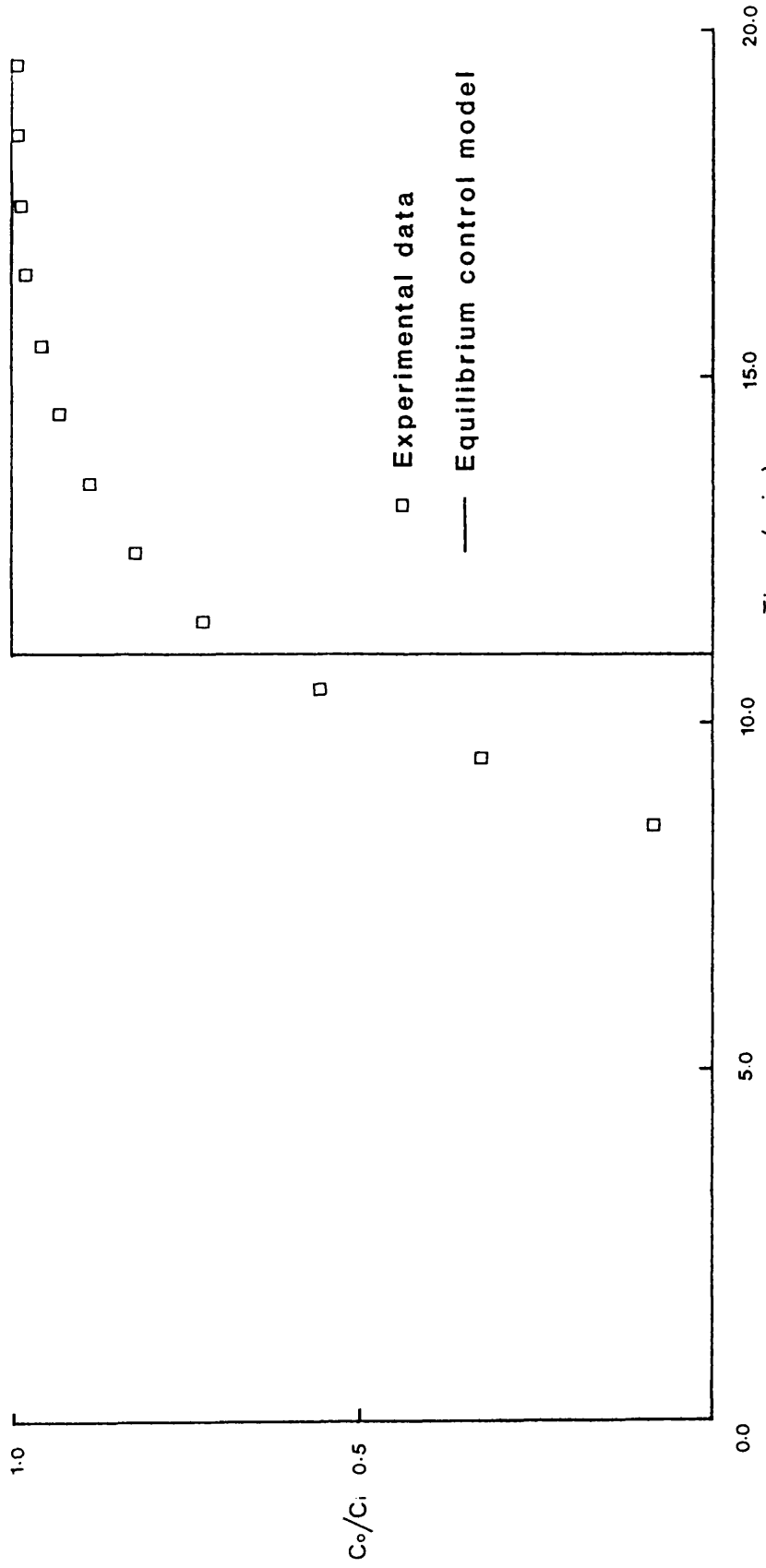

Figure 25 Breakthrough of ethane.

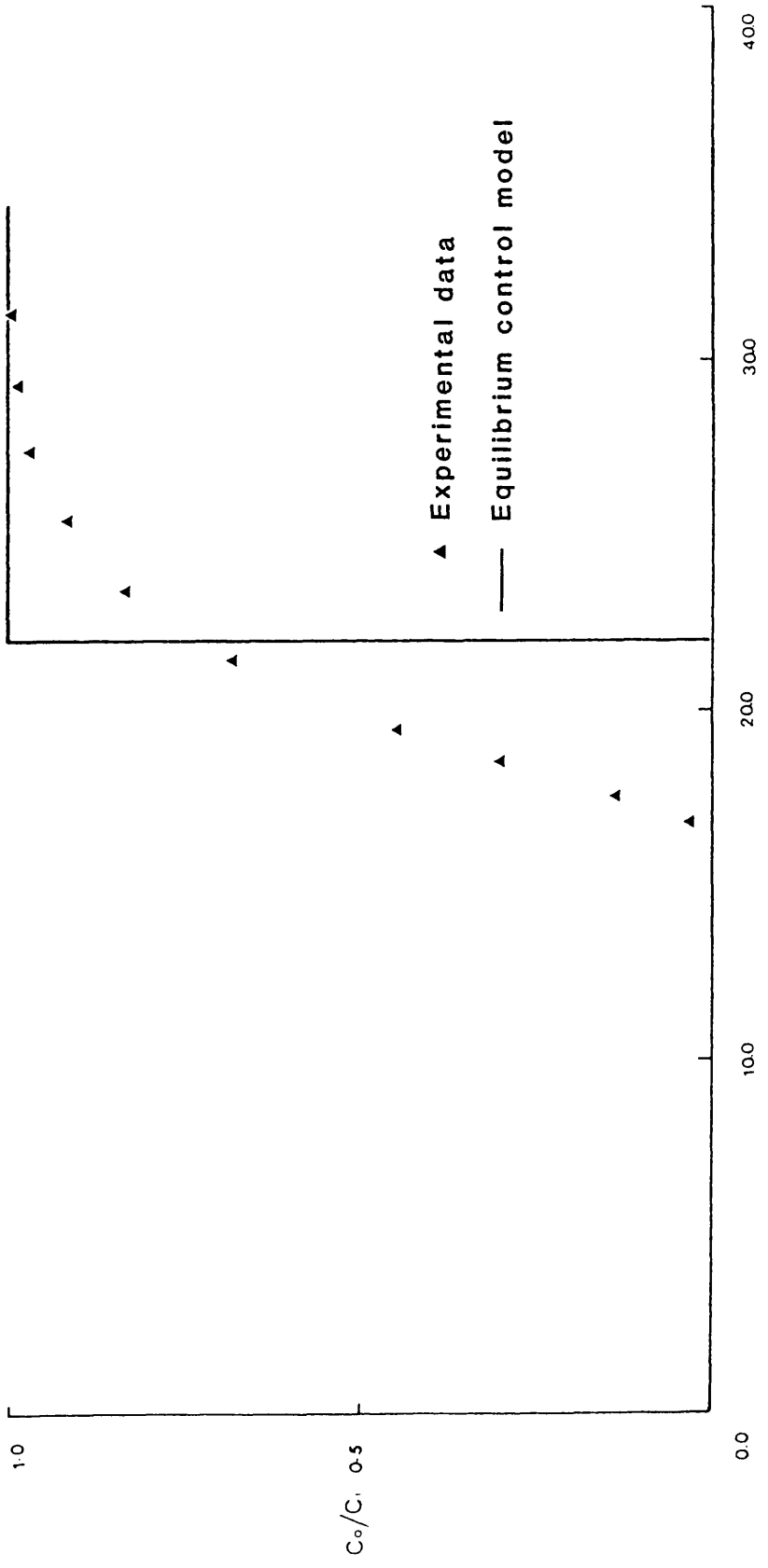

Figure 26 Breakthrough of propane.

$$q_{(z-\Delta z,t-\Delta t)} = \frac{abc_{(z-\Delta z,t-\Delta t)}}{1+bc_{(z-\Delta z,t-\Delta t)}} \qquad (4.10)$$

K_G is the linear driving force kinetic parameter, which is determined by fitting the model to the experimental column breakthrough data. Equations (4.3), (4.8), (4.9) and (4.10) were solved numerically. Appendix 5 gives the computer program for this model.

At low gas phase concentrations of methane (9.65×10^{-6} mol cm^{-3}), the model does predict the experimental data fairly well, as shown in Figure 27. However, for ethane, propane and high gas phase concentrations of methane, the model does not predict the experimental data. Figures 28-30 show the experimental and computed breakthrough curves for methane, ethane and propane respectively. The values of K_G are listed in Table 4.1.

Table 4.1

Linear driving force parameters

Adsorbate	Temperature (° C)	K_G (min^{-1})
Methane	25	0.65
Ethane	25	0.10
Propane	25	0.06

1.3 Micropore diffusion model

If intraparticle diffusion is rate-controlling, then the differential form of equation (4.4) would be, for spherical particles, equation (1.27).

Rosen[58,59] integrated the differential material balance equation for the case of linear equilibrium, where the rate of adsorption is determined by the combined effect of a film resistance and solid diffusion into spherical particles. He used an effective diffusion coefficient which can be interpreted

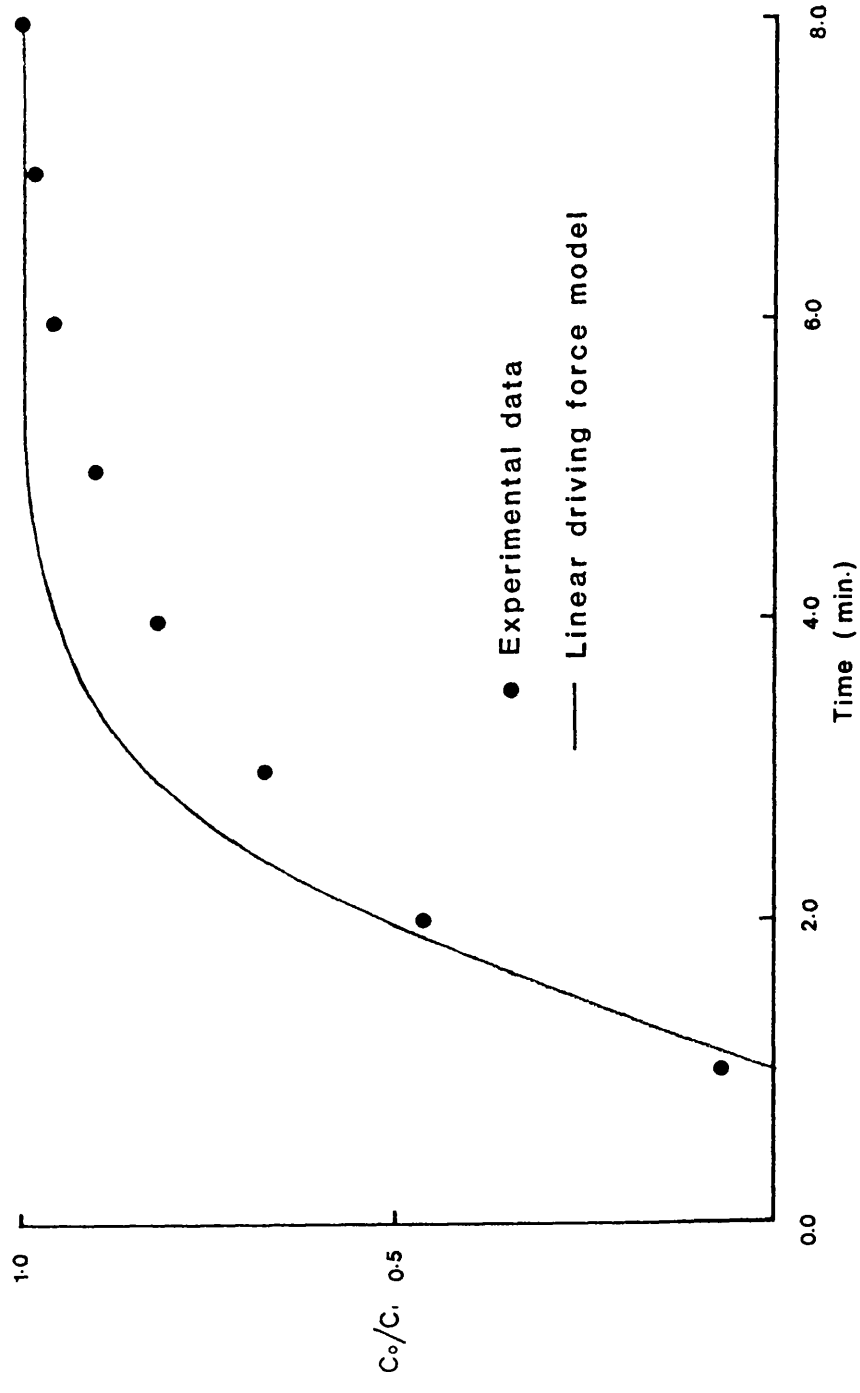

Figure 27 Breakthrough curve of methane ($C = 9.65 \times 10^{-6}$ mol cm^{-3}).

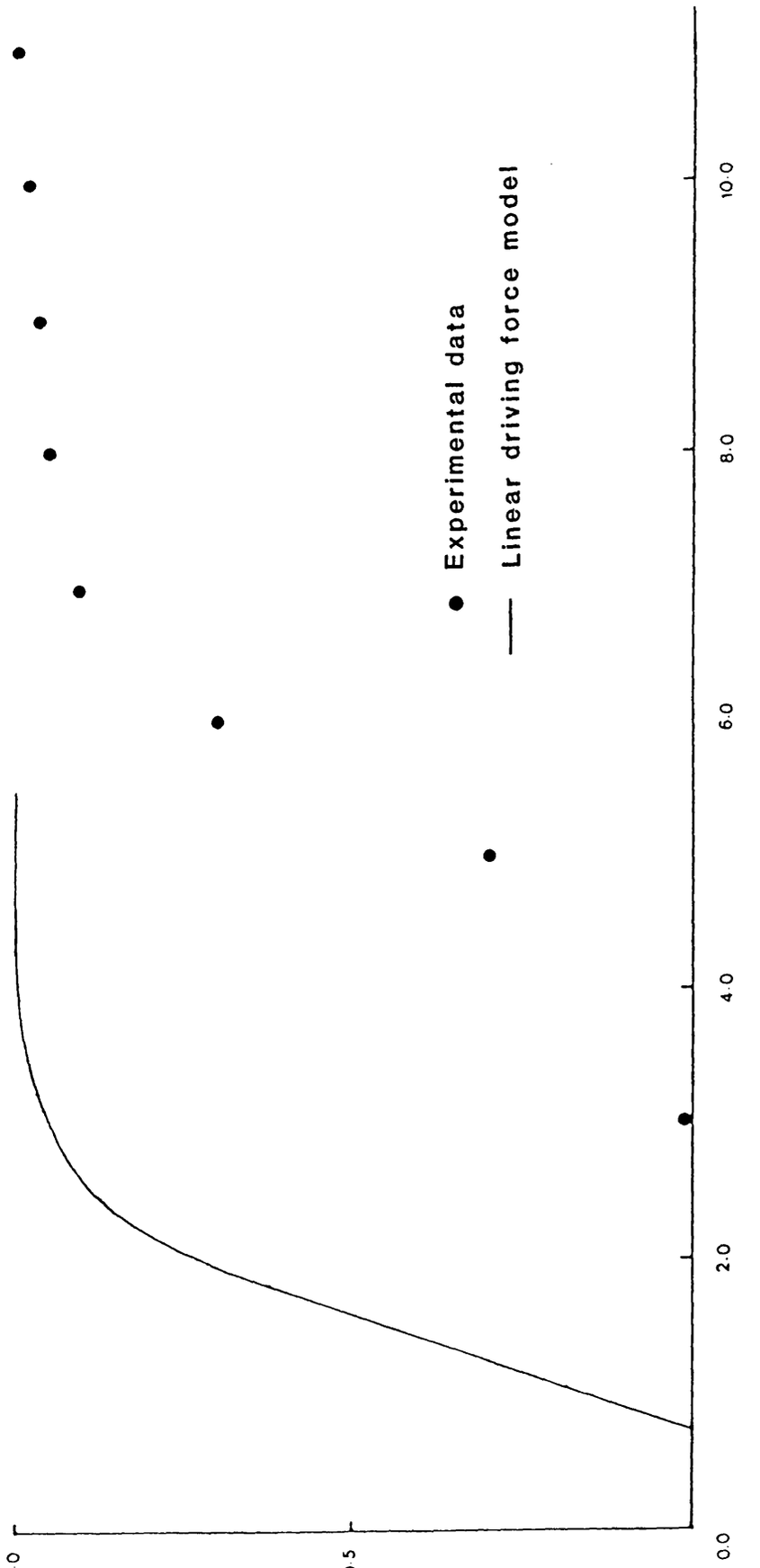

Figure 28 Breakthrough curve of methane.

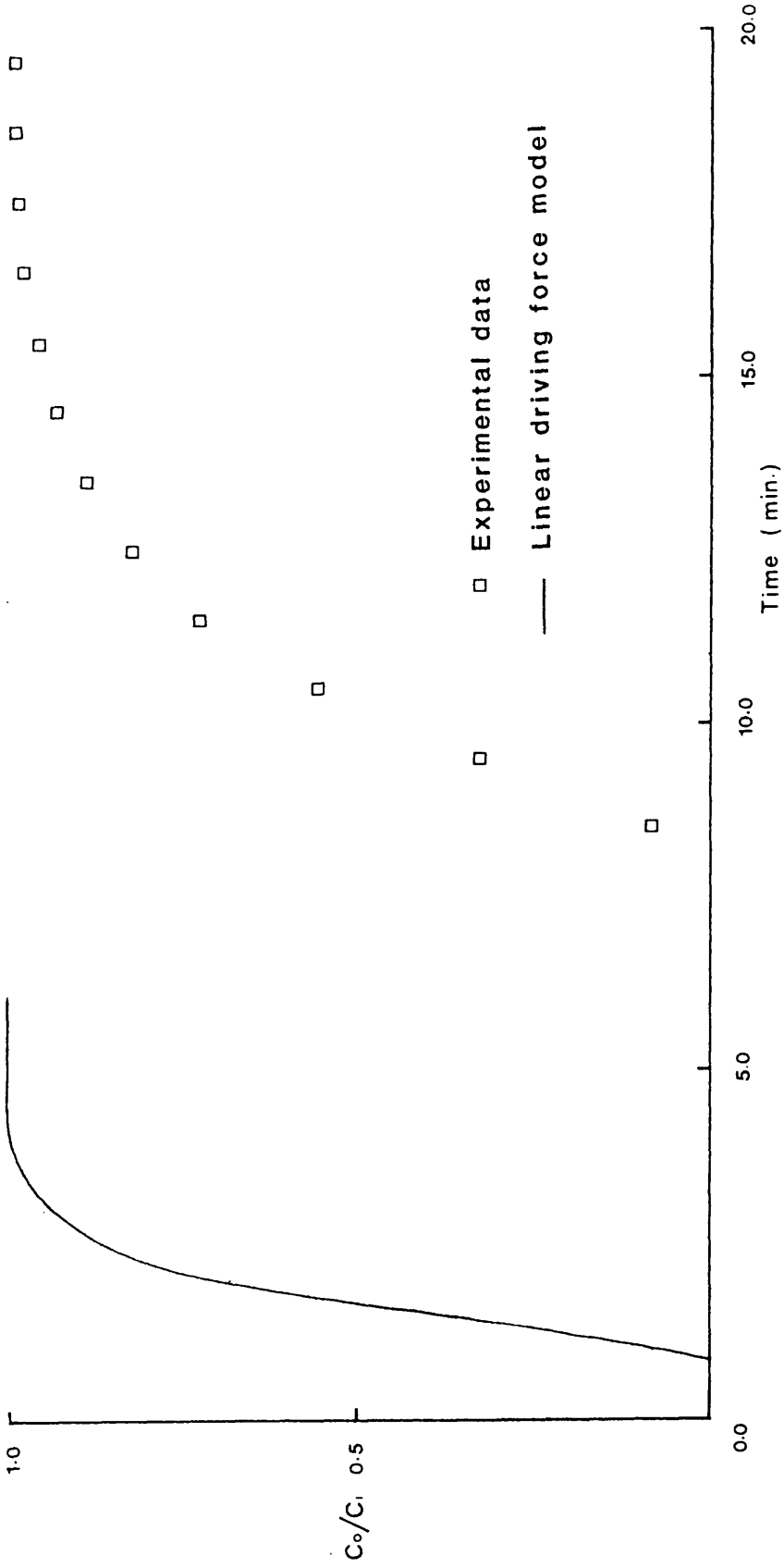

Figure 29 Breakthrough curve of ethane.

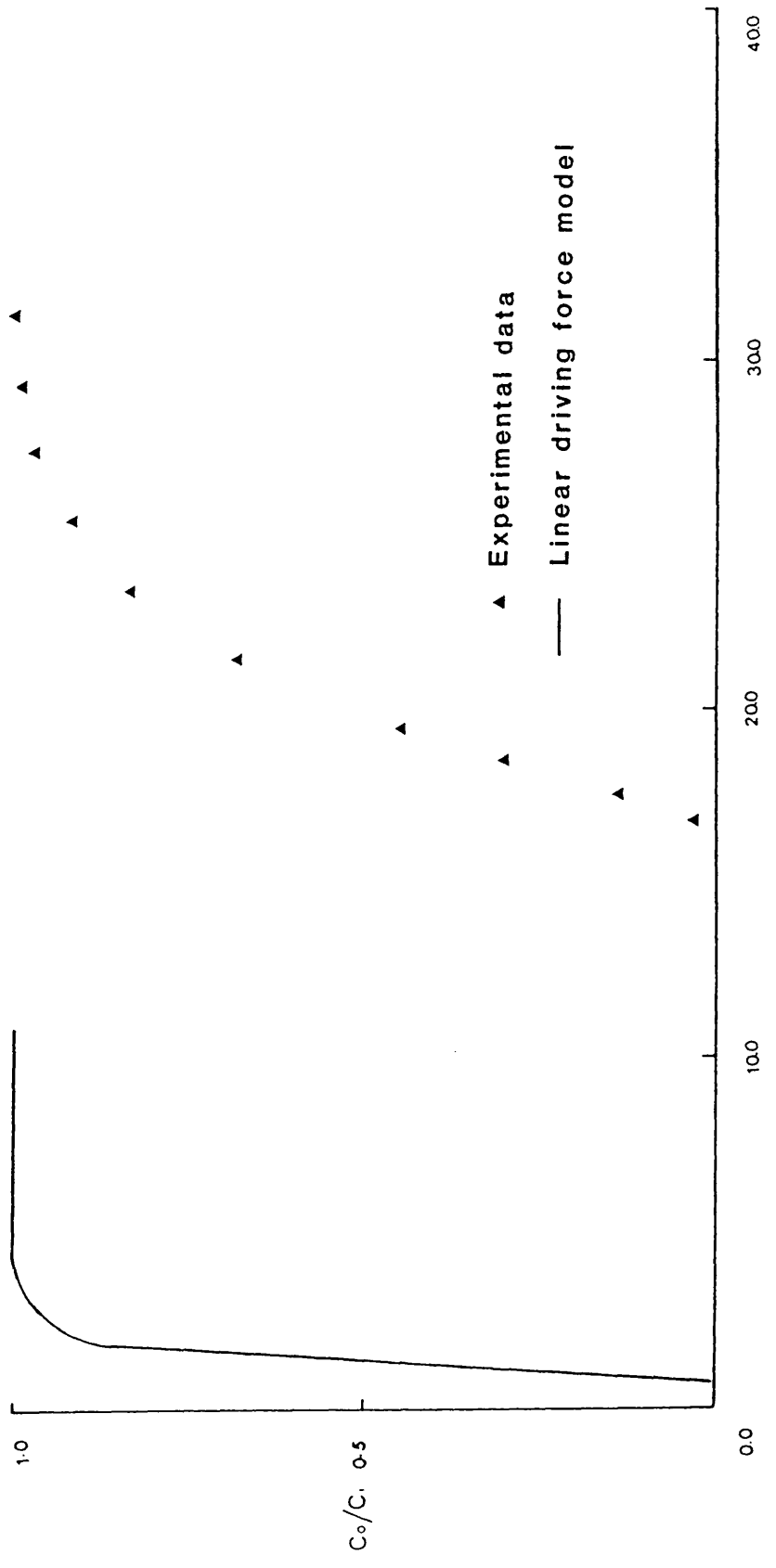

Figure 30 Breakthrough curve of propane.

as including both the effect of pore and surface diffusion. By the following change of variables in equation (1.25), t-z/u for t and $z(1-\varepsilon)/ux\varepsilon$ for z, and lengthy mathematical manipulation of equations (1.25) and (1.27), the general expression for the breakthrough curve can be derived:

$$c_o/c_i = \tfrac{1}{2}[1 + \mathrm{erf}(\frac{\frac{3}{2}\tau - 1}{2\sqrt{\frac{1}{5}\mu+\theta}})] \qquad (4.11)$$

which is a function of three dimensionless parameters, as follows:

$$\text{Bed length parameter } (\mu) = \frac{3D_m(1-\varepsilon)abl}{\varepsilon u r^2}$$

$$\text{Film resistance parameter } (\theta) = \frac{\varepsilon u}{Tkga(1-\varepsilon)}$$

$$\text{Time parameter } (\tau) = \frac{2\varepsilon[(ut/l) - 1]}{3(1-\varepsilon)ab}$$

When micropore diffusion is the rate-controlling step, the film resistance parameter (θ) is set to zero in equation (4.11).

Dranoff and Antonson[60] have studied the adsorption of ethane on a 5A molecular sieve using this model, modified for non-linear equilibrium and non-spherical particles. Their investigation has shown that ethane adsorption can be well described by intraparticle diffusion controlling the rate. The same literature source was used to obtain a value of D_m/r^2 for ethane, which is equal to 6.0×10^{-4} s^{-1} at 25° C. There is a lack of values of D_m/r^2 in the literature for methane and propane. However, Satterfield and Frabetti[61] studied the crystal diffusivity (D_c) of methane, ethane and propane on molecular sieves (sodium mordenite). The value of D_c which was found is nearly equal,

and of the same order of magnitude for each of these gases. Therefore, it is reasonable to use the same value of D_m/r^2 for methane and propane as given for ethane above.

This model does not fit the experimental data. Figures 31-35 show the experimental and computed breakthrough curves obtained by the method of Rosen for methane, ethane and propane respectively.

1.4 Surface diffusion model

If surface diffusion were the overall rate-controlling mechanism, the rate of adsorption term in equation (1.25) would correspond to equation (1.28). In the absence of numerical estimates for surface diffusion coefficients in zeolites, the value of D_S/r^2 was assumed to be 6.0×10^{-3} s^{-1}, an order of magnitude greater than pore diffusion.[46,62]

At gas phase concentrations of methane of 4.503×10^{-5} mol cm^{-3}, the model predicts the breakthrough curve fairly well. As the concentration increases, (8.362×10^{-5} mol cm^{-3}), the computed curve moves far from the experimental points. Figures 31 and 32 show the comparison between the experimental and computed curves for these two concentrations.

At low gas phase concentrations of ethane of 9.65×10^{-6} mol cm^{-3}, the model predicts the experimental breakthrough data fairly well, as shown in Figure 33. At high gas phase concentrations, the computed curve departs from the experimental points, but nevertheless gives virtually the same shape as the experimental data and is shown in Figure 34.

At low gas phase concentrations of propane of 9.65×10^{-6} mol cm^{-3}, the computed curve departs, but has the same shape as, the experimental breakthrough data. Figure 35 shows the comparison between the experimental and computed breakthrough curves.

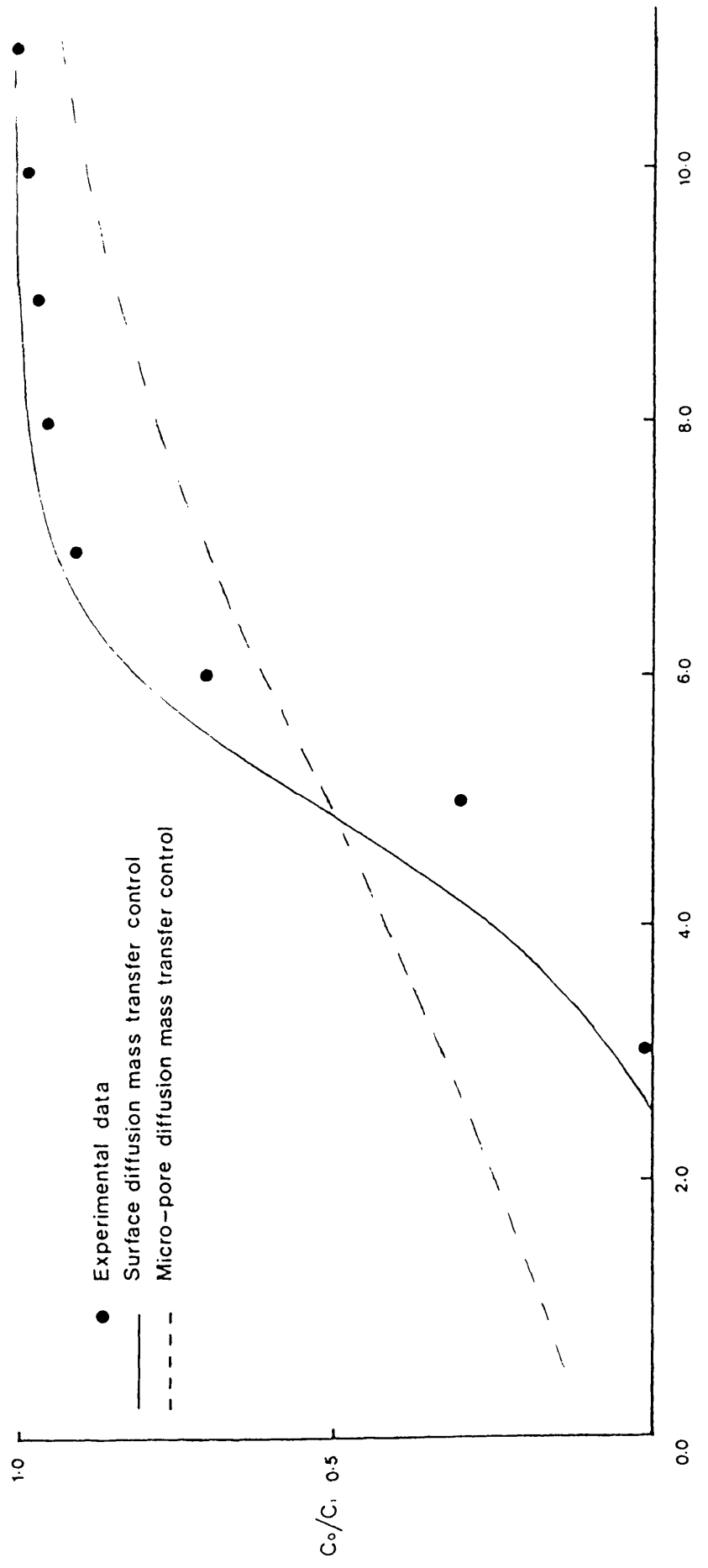

Figure 31 Breakthrough curve of methane ($C = 4.503 \times 10^{-5}$ mol cm^{-3})

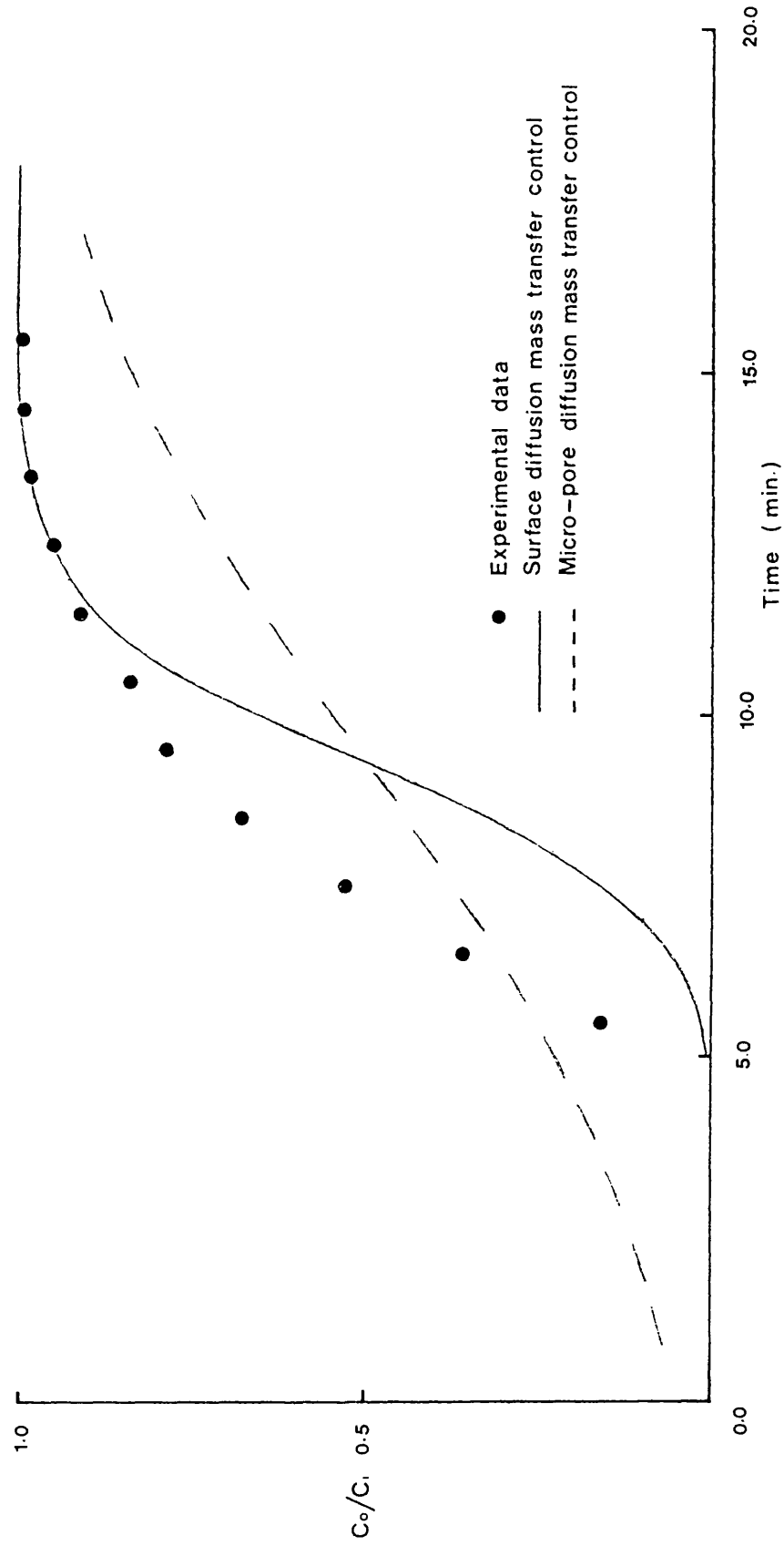

Figure 32 Breakthrough curve of methane ($C = 8.362 \times 10^{-5}$ mol cm^{-3})

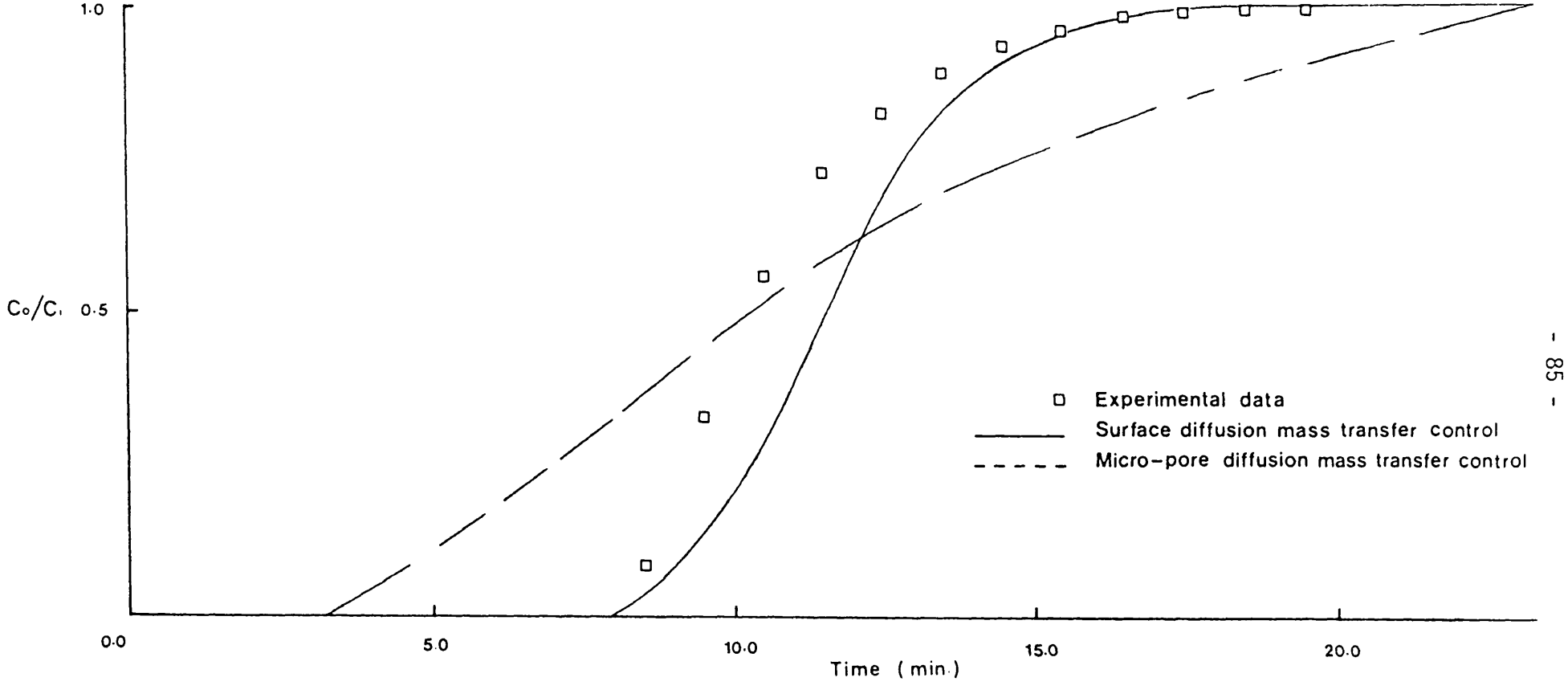

Figure 33 Breakthrough curve of ethane ($C = 9.65 \times 10^{-6}$ mol cm^{-3})

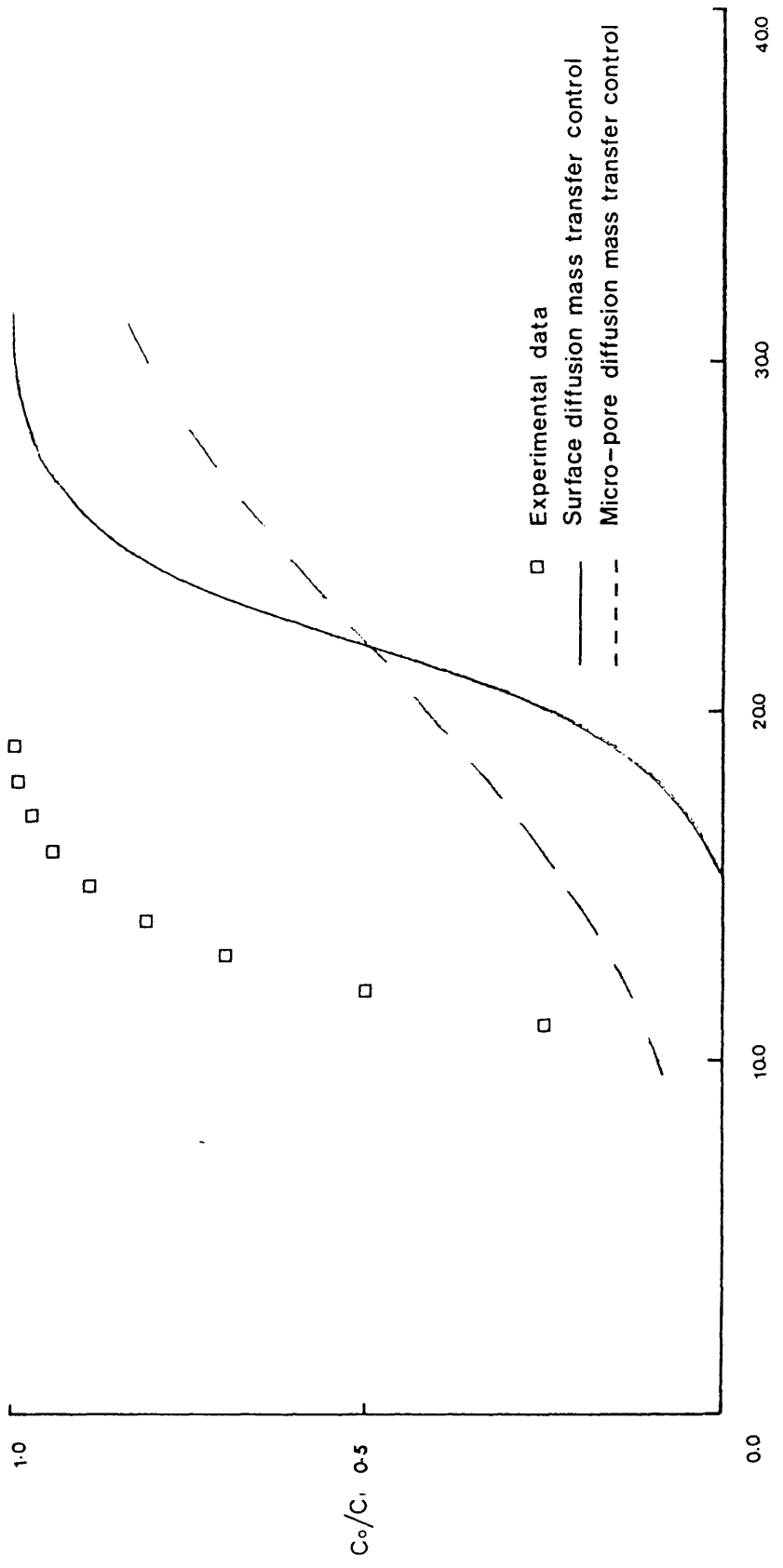

Figure 34 Breakthrough curve of ethane ($C = 1.93 \times 10^{-5}$ mol cm^{-3})

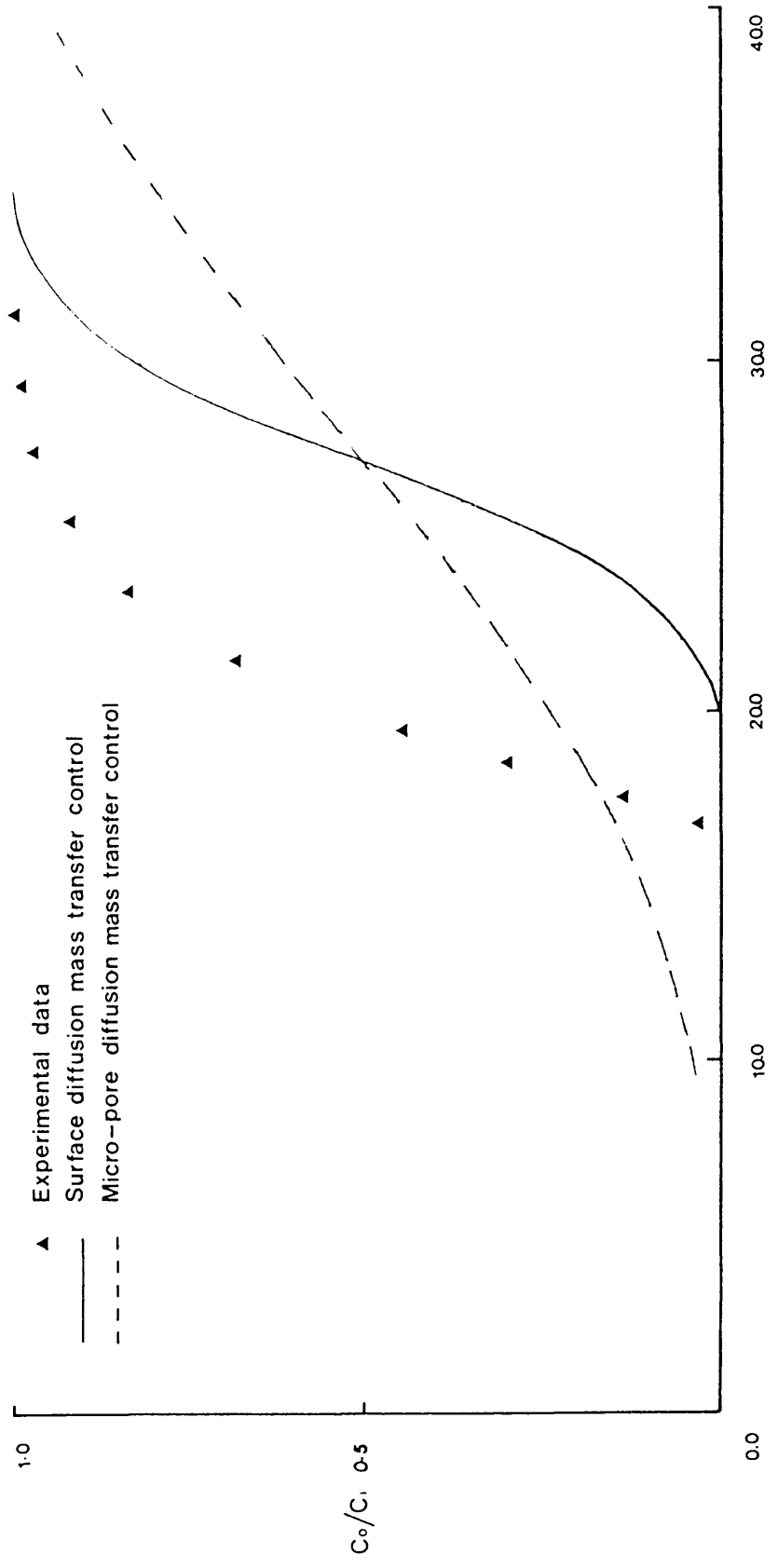

Figure 35 Breakthrough curve of propane ($C = 9.65 \times 10^{-6}$ mol cm^{-3})

1.5 External mass transfer control

If the overall rate of adsorption is limited by the transfer of adsorbate between the bulk of the fluid phase and the outer surface of the adsorbent particle, then equation (1.26) has to be solved with equation (1.25).

The fluid film mass transfer coefficient (K_G) was calculated by Wilke and Hougen[63] using the gas phase diffusion coefficient calculated by the method of Wilke and Lee.[64]

The value of the Rosen film resistance parameter (θ) was calculated from the experimental conditions and found to be less than 10^{-3} for all the adsorbates (methane, ethane and propane). Inspection of the breakthrough curves calculated by Rosen, given in Figure 36, reveals that for values of the film parameter which are less than 0.025, mass transfer has no significant effect on the breakthrough curves. Therefore, it was concluded that the effect of film resistance could be ignored. Experimentally, the effect of external mass transfer was studied by changing the flowrate of the feed, as well as the length of the bed. Figures 37-39 show that there is little or no change in the shape of the breakthrough for methane, ethane and propane respectively. Hence it is concluded that there is no resistance due to gas phase mass transfer.

1.6 Conclusions

Equilibrium, external mass transfer and micropore diffusion models do not fit the experimental data for each of the adsorbates, methane, ethane and propane. The linear driving force model is applicable only to methane at low concentration.

A surface diffusion model, however, fits the data over a wide range of concentration for methane, but only at low gas phase concentration for ethane.

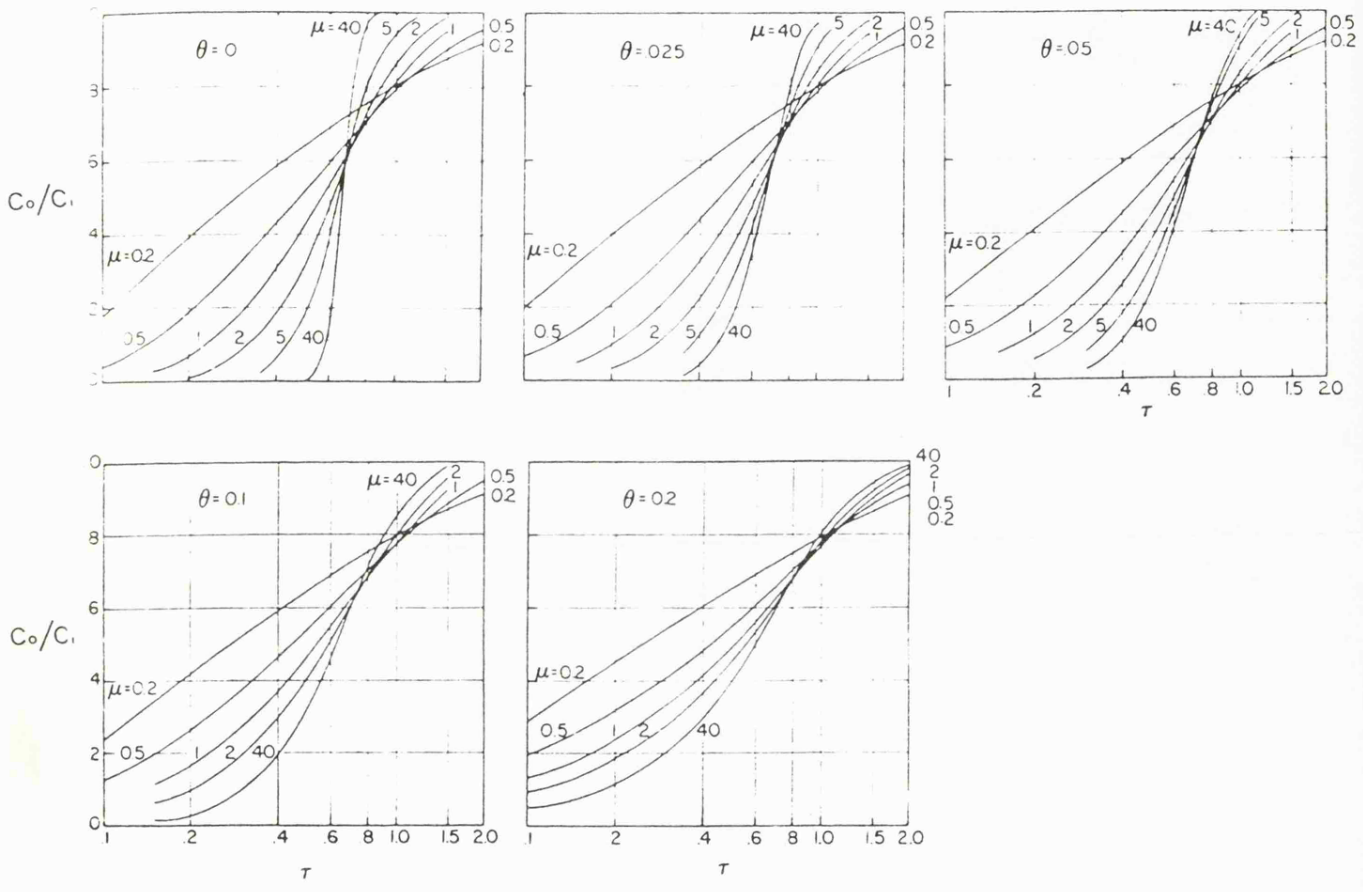

Figure 36 Effluent Concentration versus Time Parameter for Selected Values of Bed Length and Film Resistance Parameters

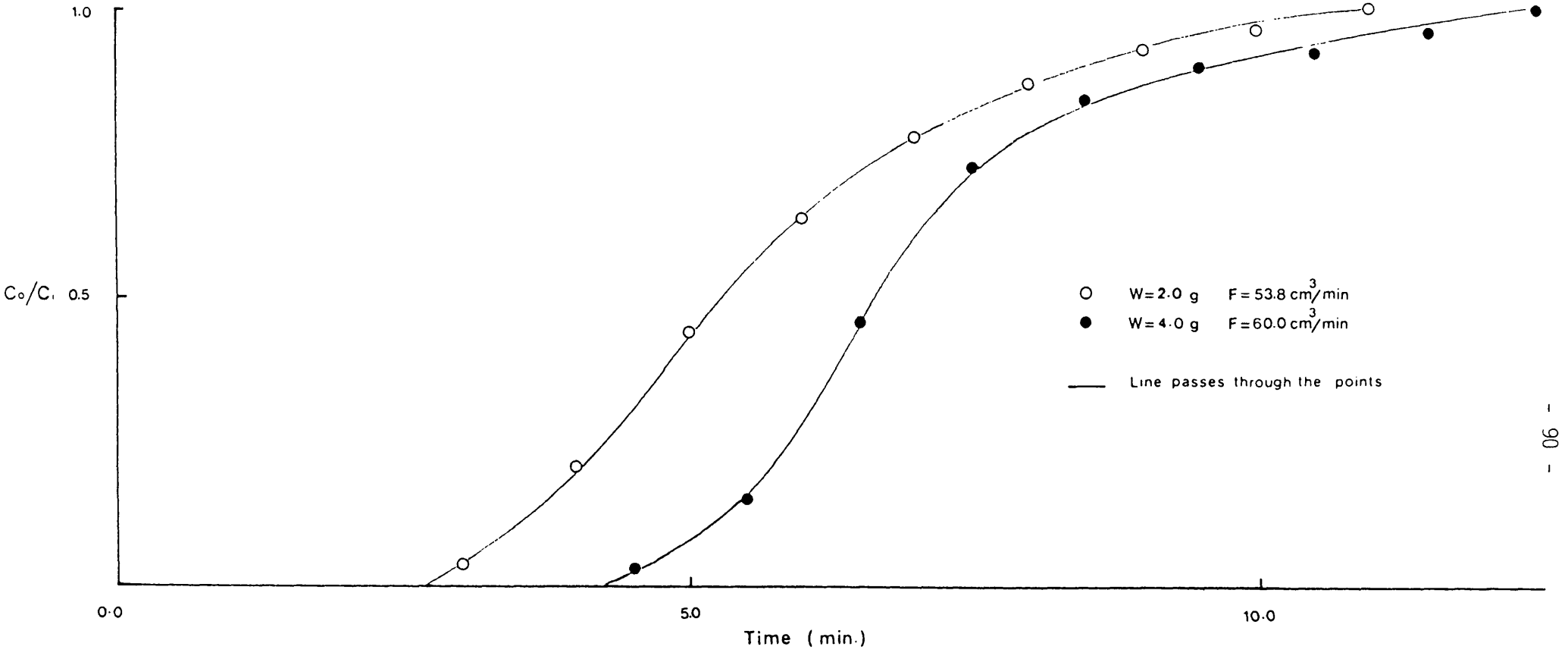

Figure 37 Constant pattern behaviour for methane.

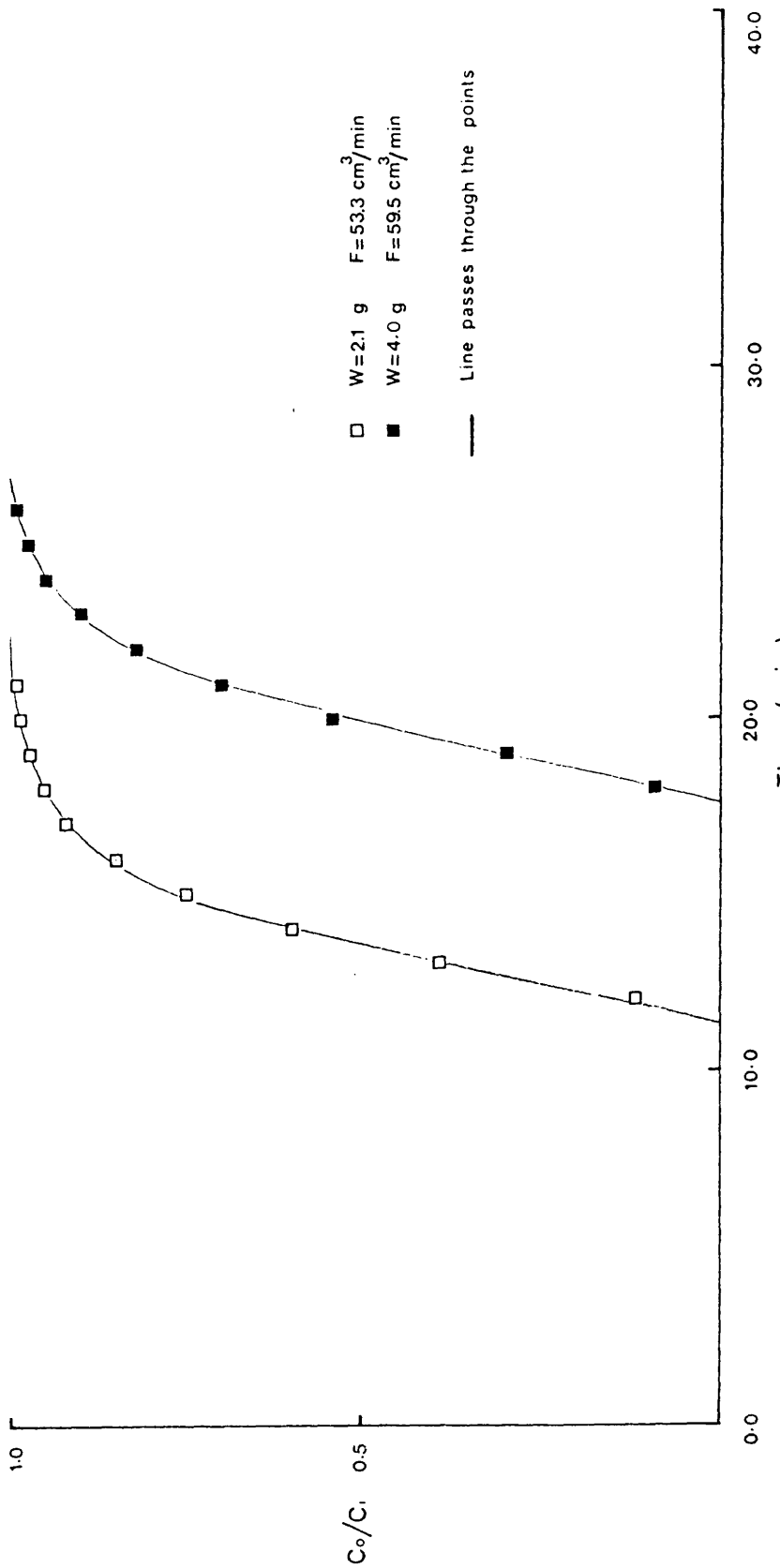

Figure 38 Constant pattern behaviour for ethane.

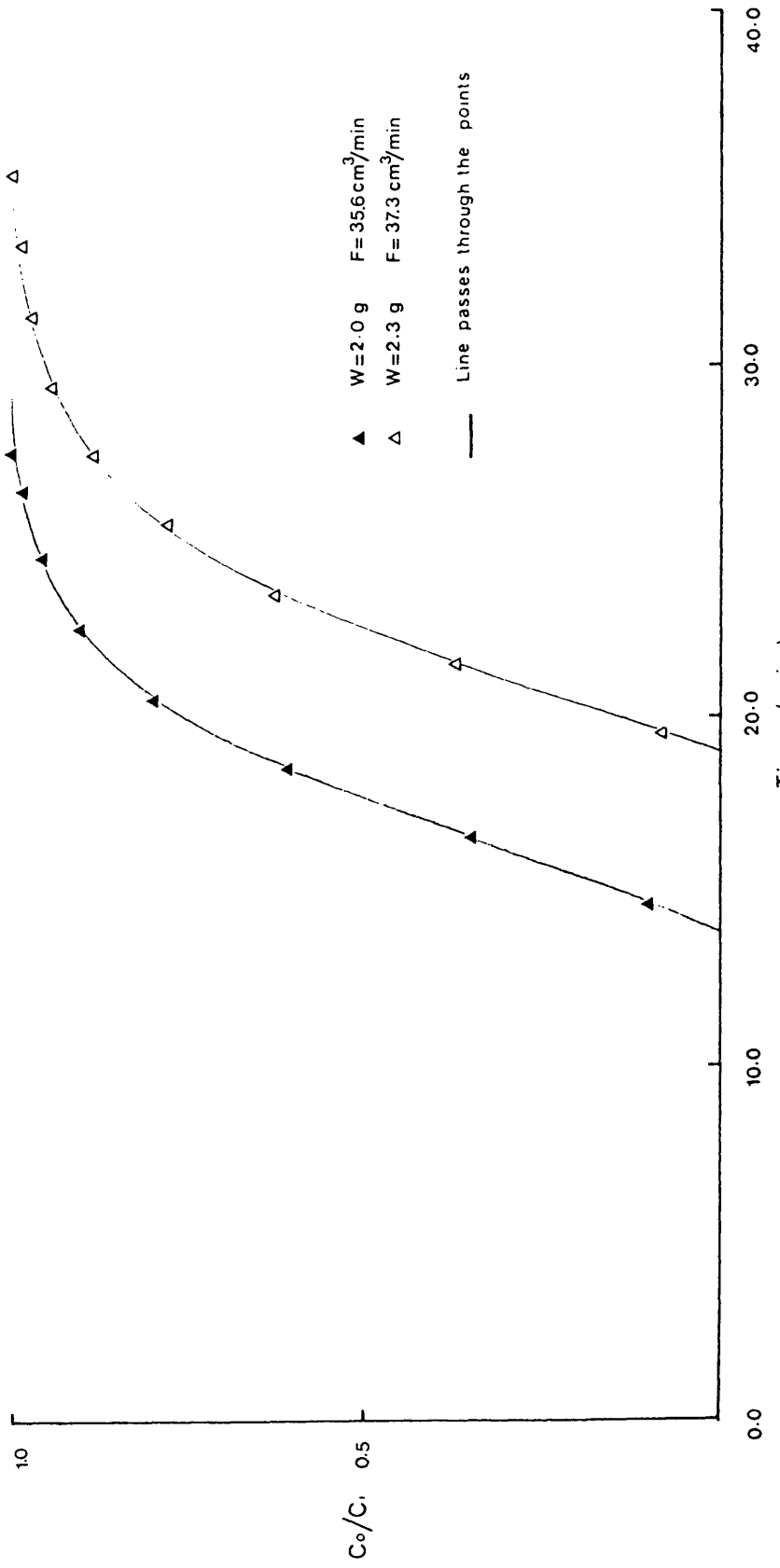

Figure 39 Constant pattern behaviour for propane.

The shape of the theoretical curves for propane and ethane at high gas phase concentrations are similar to the experimental ones, but are somewhat displaced.

This discrepancy may be attributed to the fact that diffusivity of gases in zeolites is concentration-dependent.[65-67] However, there are studies[60,61,68] which show that diffusivity is independent of gas phase concentration. As the computed breakthrough curves for all the adsorbates virtually resembles the shape of the experimental data, it may therefore be concluded that surface diffusion is a dominant factor in mass transfer for all the three adsorbates considered.

2. Breakthrough of Ternary Component Mixtures

2.1 Constant pattern behaviour

The adsorption of a single component in a bed produces a comparatively simple type of concentration history curve (*e.g.*, S-shape), unlike the concentration profiles for ternary mixtures, which consist of several successive plateau and transfer zones. Multi-component adsorption is characterised by interactive and competitive effects involving the various adsorbable species. These effects may manifest themselves in two ways, competition in the mass transfer process (within and surrounding the adsorbent), and displacement from the adsorbent of those species possessing lower adsorption affinities in favour of those with higher values.

For a given inlet concentration, the shape of the breakthrough curve for a single component remains approximately constant for variations of the bed length. Therefore, a series of experiments was performed to investigate whether a constant shape concentration profile is also obtained for a ternary component mixture. For a given inlet concentration, it appears that the shortest bed used (*ca.* 1.0 g) is insufficiently long to allow the concentration

profiles to develop and that the transfer and plateau zones for methane and for ethane overlap. For the second bed length (*ca.* 2.0 g), there is still an overlap between the zones for methane. For the longest bed (*ca.* 4.0 g), the plateau and transfer zones for all the adsorbates are well developed. The results of this investigation are presented in Figures 40-42.

Typical breakthrough curves for pure and dilute ternary component mixtures are shown in Figures 43 and 44 respectively.

2.2 Prediction of breakthrough curves

The prediction of breakthrough curves for multi-component mixtures requires the solution of the finite difference representation of the bed equation (1.25) for each component, together with an appropriate equilibrium or kinetic relationship between the gas phase and adsorbed phase concentration. The same finite difference mathematical method which was used for the single component adsorption work (see section 1 of this chapter), was modified to account for ternary component adsorption. Two kinetic models that describe the adsorption mechanism are considered. These are a linear driving force model and an equilibrium model. Both models require an equilibrium isotherm. The extended modified Langmuir isotherm for ternary mixtures failed to predict the breakthrough curves. This is because of the negative value for some parameters obtained (see Chapter 3, section 3.3). Therefore, the Freundlich-type[21] multi-component isotherm by Fritz and Schluender (Chapter 3, section 3.4) is used for the multi-component adsorption.

The linear driving force model does not predict the experimental breakthrough curves. Figure 45 shows the computed breakthrough curves of a ternary mixture of methane, ethane and propane employing alternative equi-

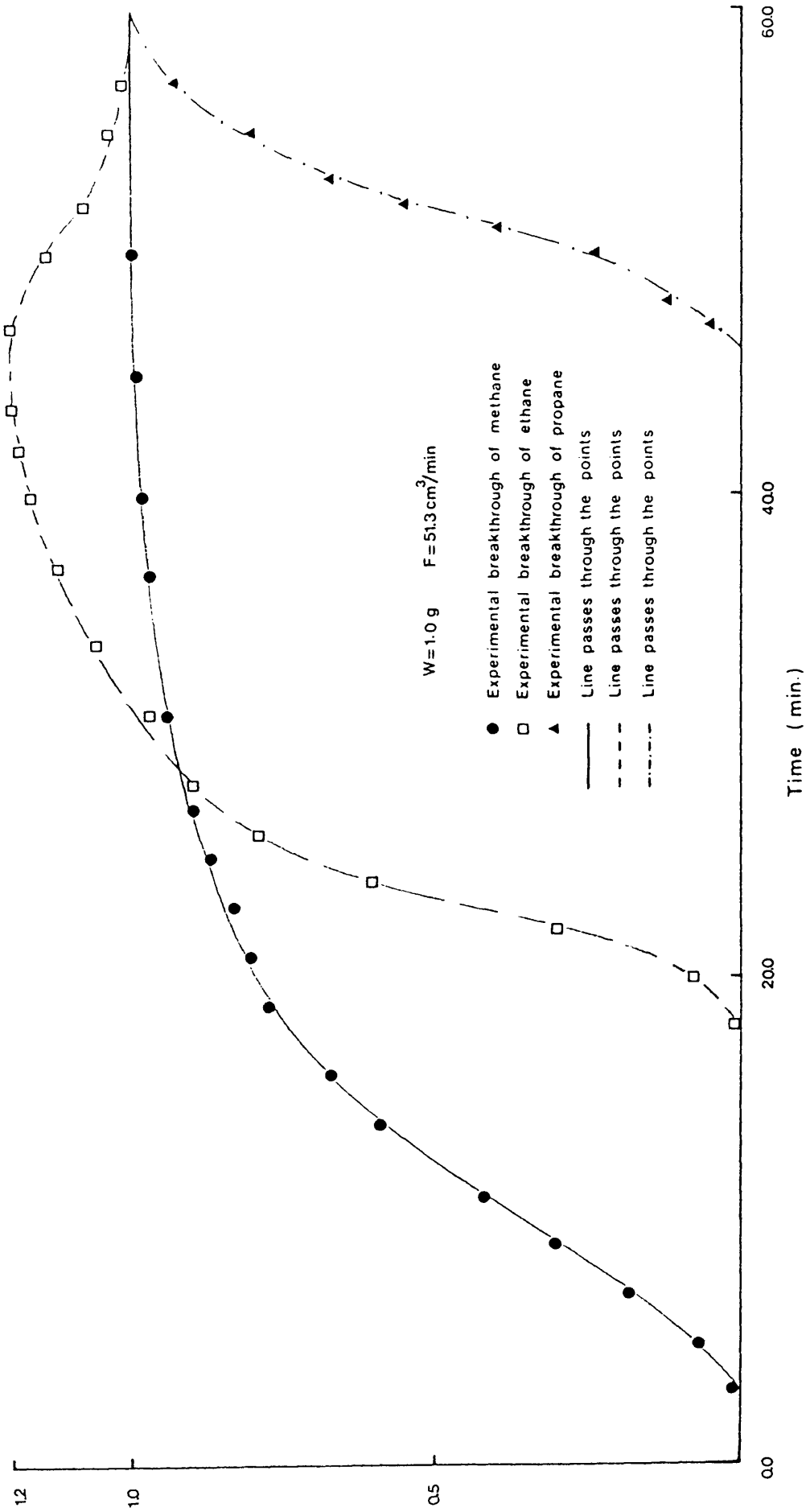

Figure 40 Constant pattern behaviour of a ternary mixture of methane-ethane and propane. 92.9% N_2, 3.9% CH_4, 1.6% C_2H_6, 1.6% C_3H_8, 81.6 atmos gauge.

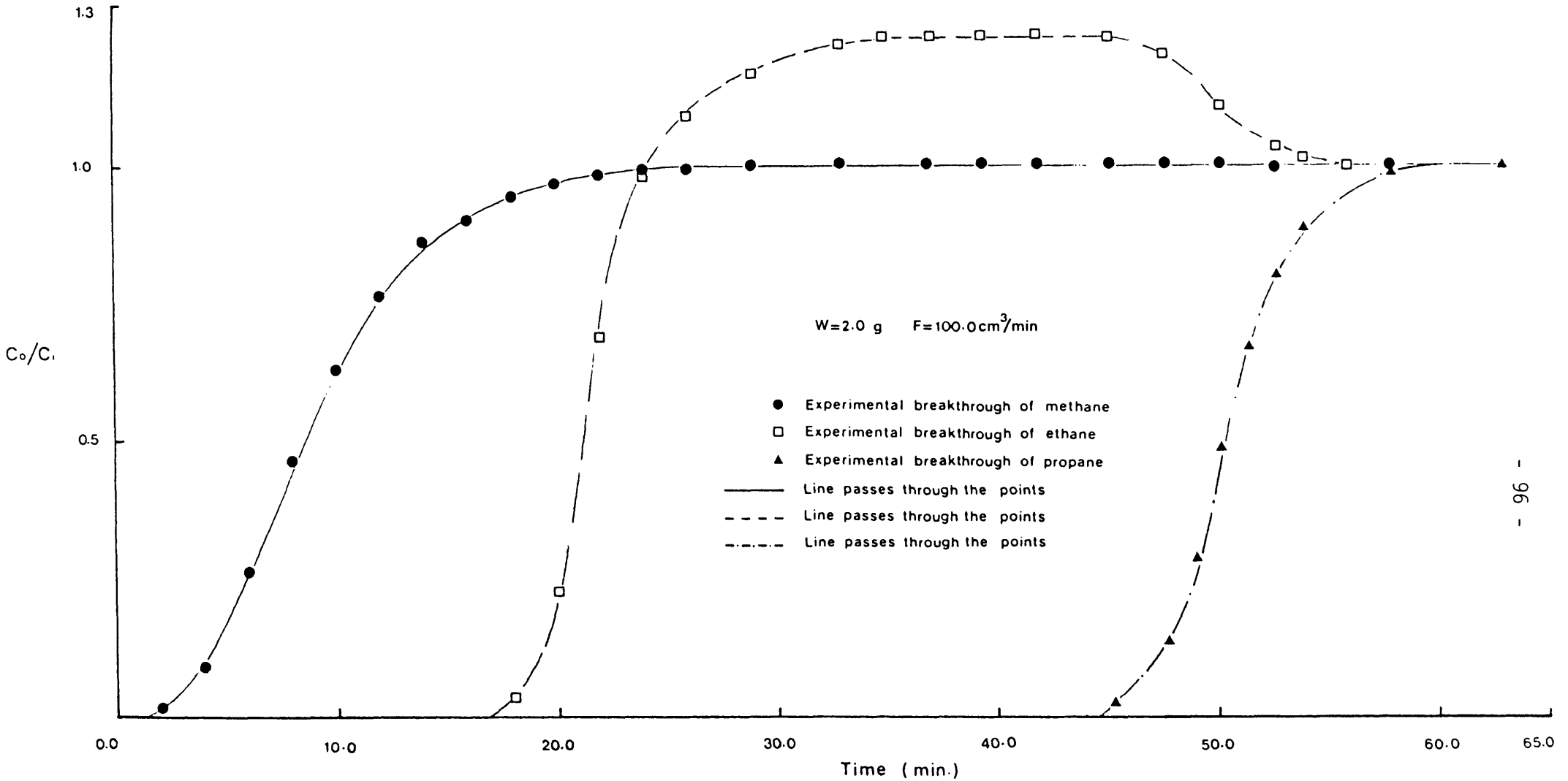

Figure 41 Constant pattern behaviour for a ternary mixture of methane-ethane and propane. 92.9% N_2, 3.9% CH_4, 1.6% C_2H_6, 1.6% C_3H_8, 81.6 atmos gauge.

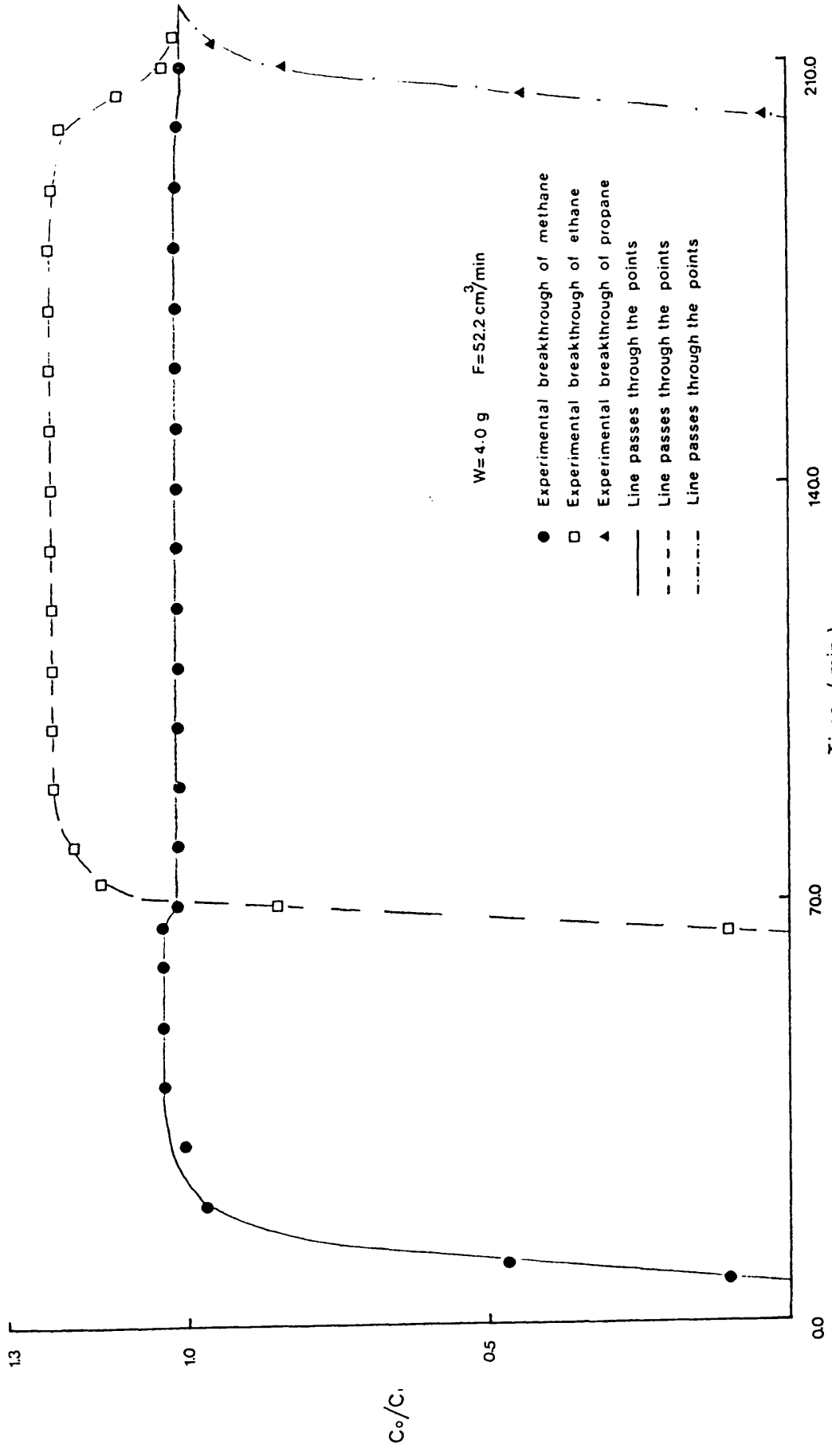

Figure 42 Constant pattern behaviour of a ternary mixture of methane-ethane and propane. 92.9% N_2, 3.9% CH_4, 1.6% C_2H_6, 1.6% C_3H_8 81.6 atmos gauge.

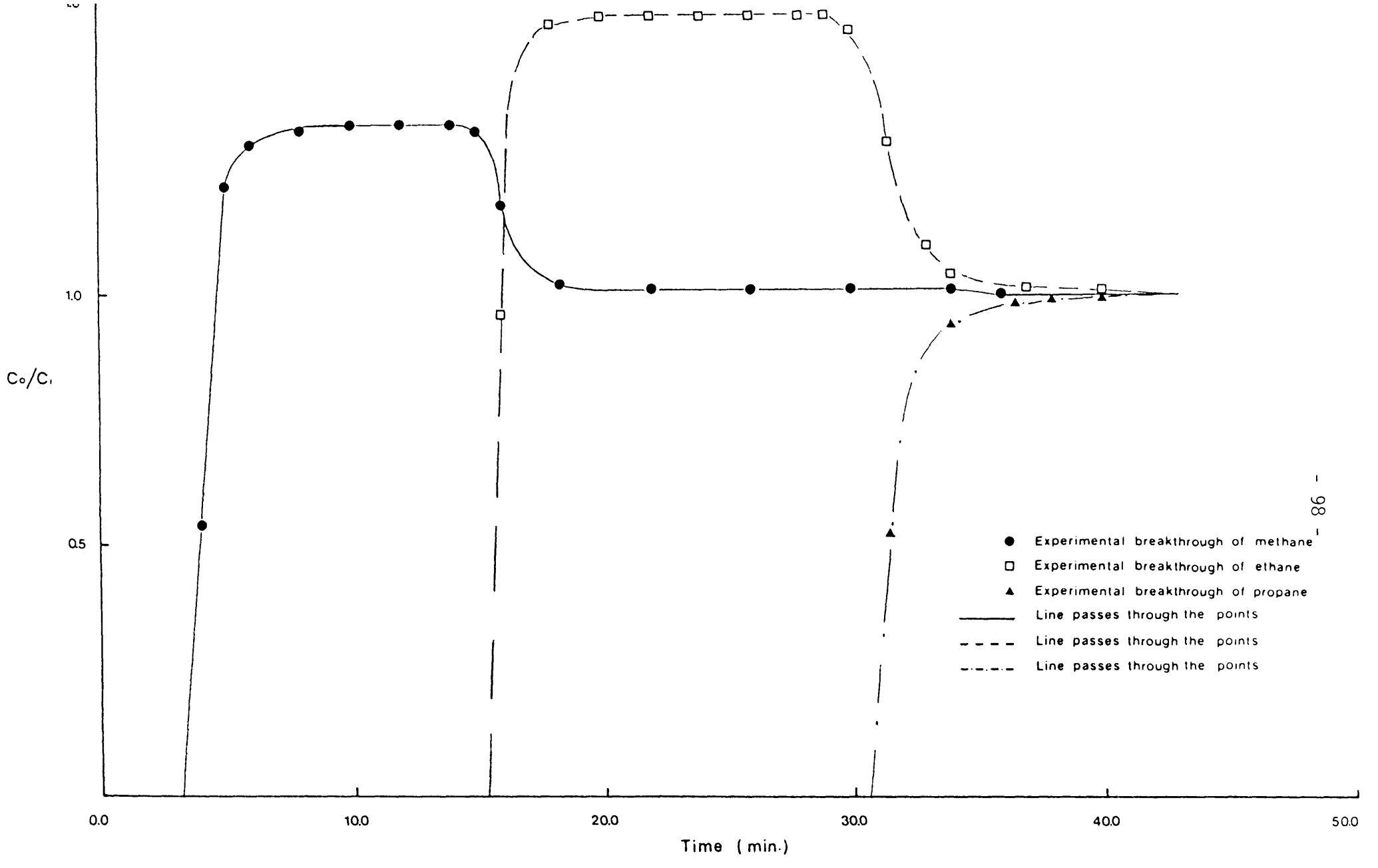

Figure 43 Typical breakthrough curve for a pure ternary mixture of methane-ethane and propane. 69.0% CH_4, 15.5% C_2H_6, 15.5% C_3H_8, 2.25 atmos gauge

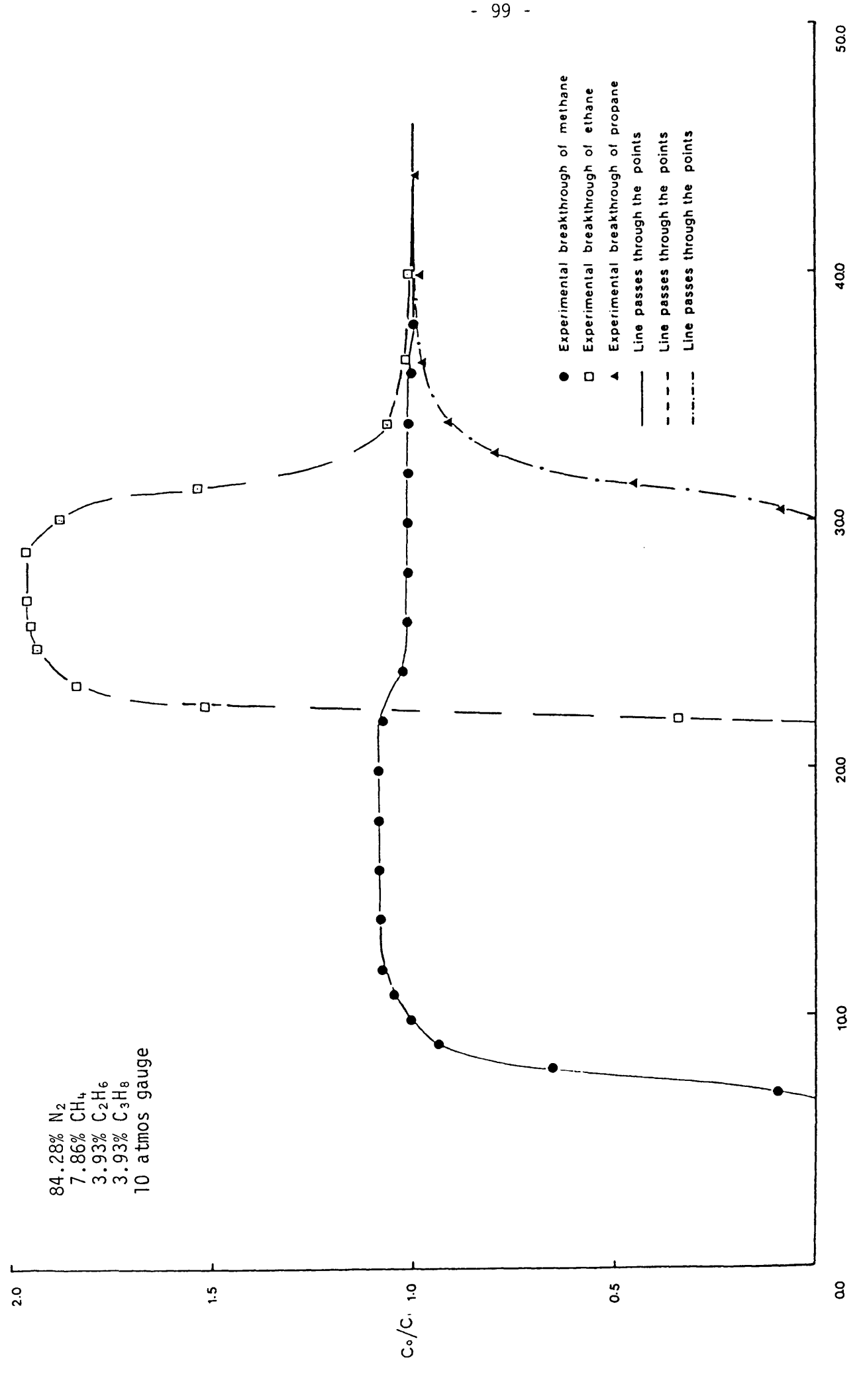

Figure 44 Typical breakthrough curve for a dilute ternary mixture of methane-ethane and propane.

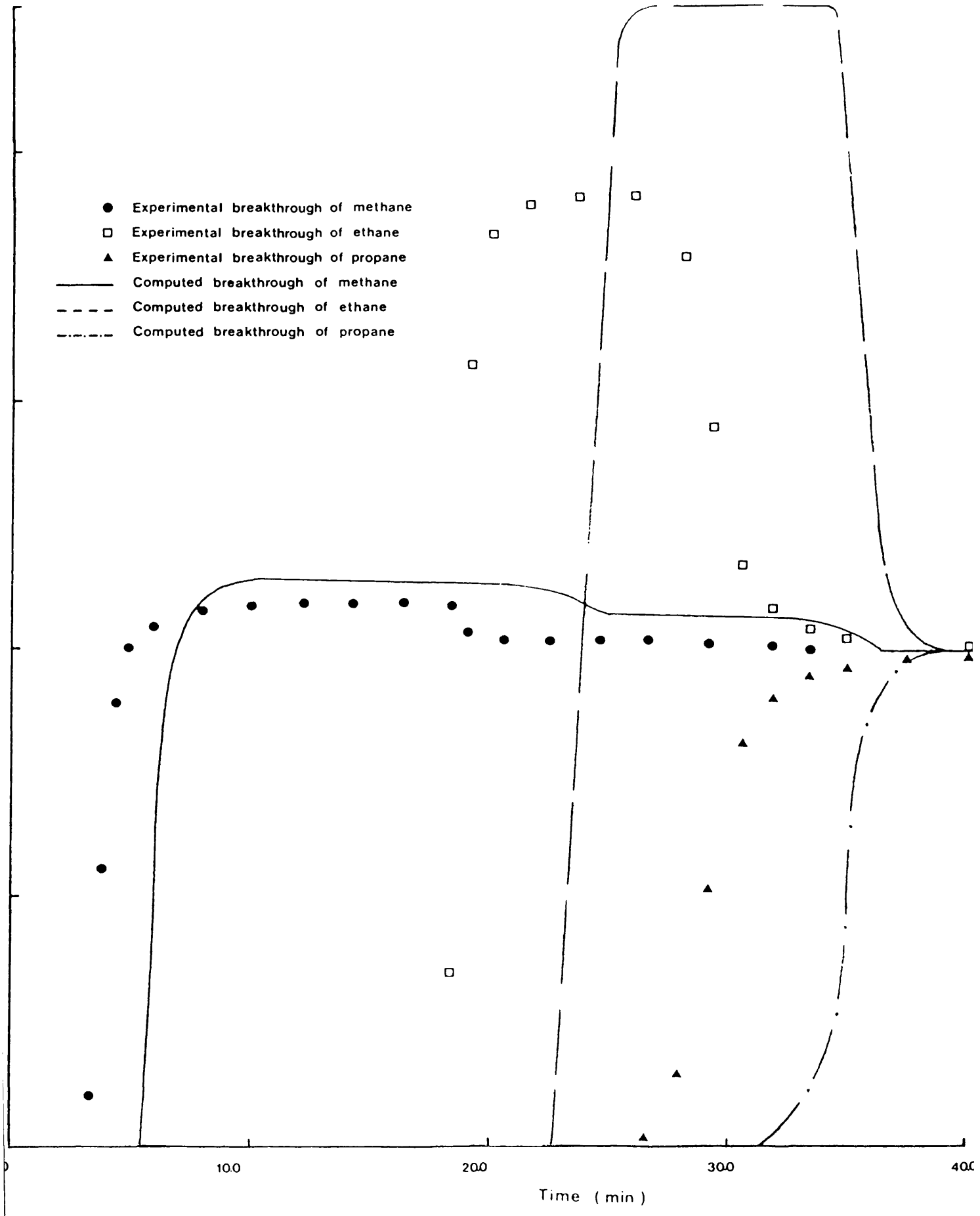

Figure 45 Breakthrough of methane-ethane and propane from three-component mixture, composition: 84.28% N_2, 7.86% CH_4, 3.93% C_2H_6, 3.93% C_3H_8, 4.3 atmos gauge.

librium model. It can be seen that the shape of the computed curves is similar to the experimental breakthrough curves. However, they are shifted along the time axis. This failure accurately to predict the experimental data may be due to the poor correlation of Freundlich-type multi-components for propane (see Chapter 3, section 3.4).

The computer program used for these predictions is summarised in Appendix 6.

3. Adsorption-desorption Cycle of Ternary Mixtures on a 5A Molecular Sieve

In order to study the possibility of separation by an adsorption-desorption cycle, a series of experiments was carried out for pure and dilute mixtures of methane, ethane and propane. An appropriate cycle of adsorption-desorption operations is one in which adsorption is followed by desorption initiated at a time when all of the first component is desorbed, but before breakthrough of the second component has occurred. In the case of ternary mixtures, this method can be applied in two ways to separate out different components, *i.e.*, before the breakthrough of the second component (ethane) to separate out ethane, or before the breakthrough of the third component (propane) to separate propane from a methane, ethane and propane mixture. These cycles may lead to an effluent sufficiently rich in either ethane or propane for it to be used for subsequent processing.

4. Experimental Procedures

The adsorption experiments were carried out by passing a mixture of methane, ethane and propane to the adsoprtion column *via* valve v_8 (see Chapter 2, section 5). On completion of the adsorption run before breakthrough of the next component, the mixture supply was cut off. Nitrogen was then supplied *via* valve v_9 to the bed until the adsorbate was completely removed from the adsorbent. This was indicated by the analyser units (see

Chapter 2, section 3).

5. Results

Typical experimental adsorption-desorption cycles for pure methane, ethane and propane mixtures are illustrated in Figures 46 and 47. Figure 46 shows the desorption initiated before breakthrough of ethane has occurred. Figure 47 shows the desorption initiated before breakthrough of propane has occurred.

Another adsorption-desorption cycle is illustrated in Figure 48 for pure methane-ethane mixtures, desorption being initiated before ethane breakthrough. For dilute mixtures and for a given inlet concentration, two experiments were performed, in which the desorption was initiated at different times before breakthrough of ethane. Similarly, two experiments were performed for desorption initiated before the breakthrough of propane. In all cases the rate of desorption was slower than the rate of adsorption for methane, ethane and propane. The rate of desorption of methane is much faster than the rate of desorption of ethane, which itself is much faster than that for propane. When desorption was initiated before the breakthrough of ethane or propane, the desorption rate of methane remained constant for a considerable period, then rapidly decreased as the amount in the adsorbed phase decreased. Similarly, ethane followed a similar pattern with the exception that desorption started before the breakthrough of propane.

6. Mathematical Modelling of the Experimental Adsorption-desorption Cycle

The desorption of a single component has been studied for ethane[68] on 4A molecular sieves, where micropore diffusion is the mass transfer controlling rate process. There have been other studies for some adsorbates, ethane and carbon dioxide on 5A and 4A molecular sieves, where the rate of desorption is either micropore or macropore diffusion controlled.[69] No reference has been

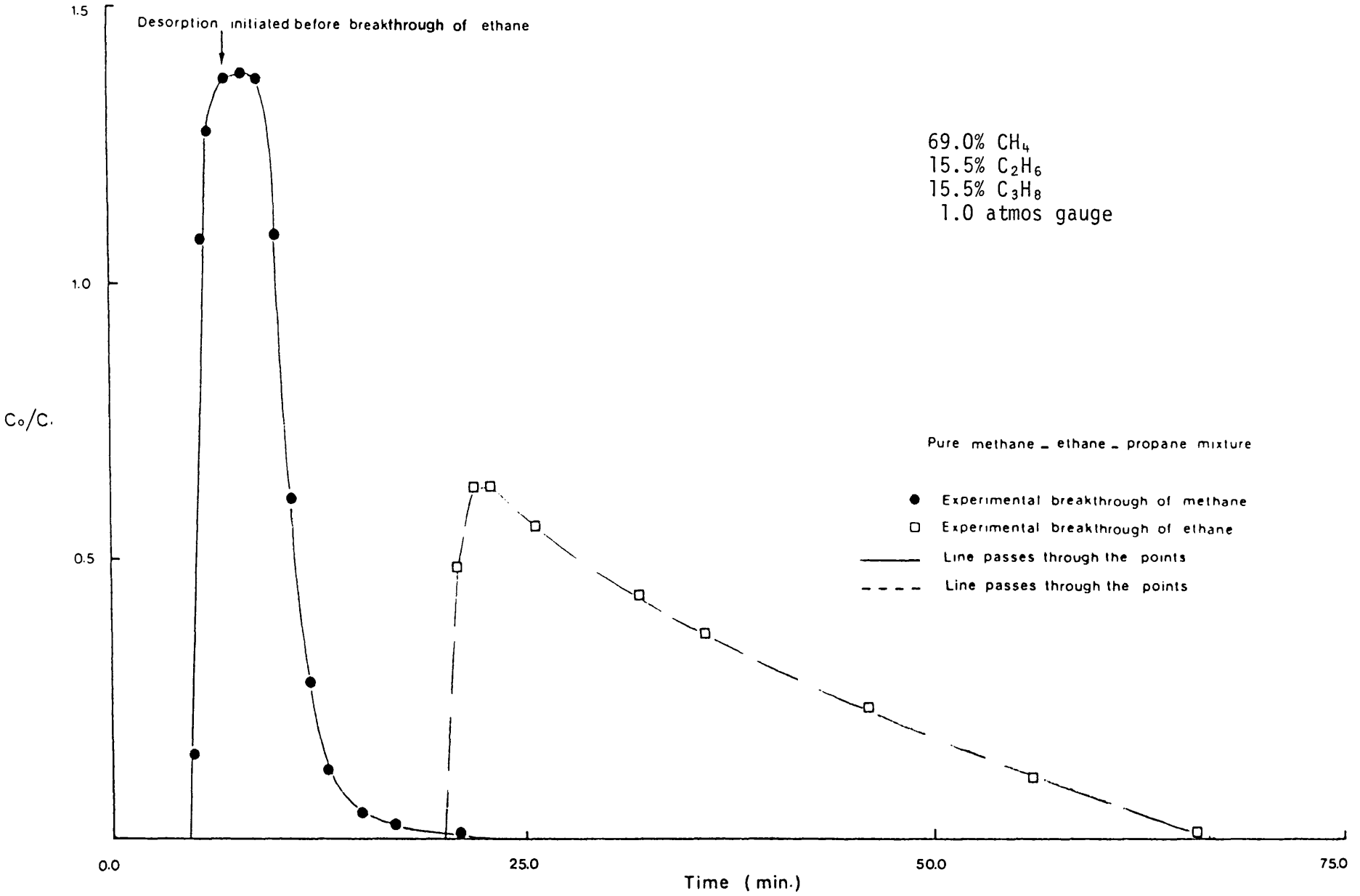

Figure 46 Ternary gas mixture adsorption-desorption cycle.

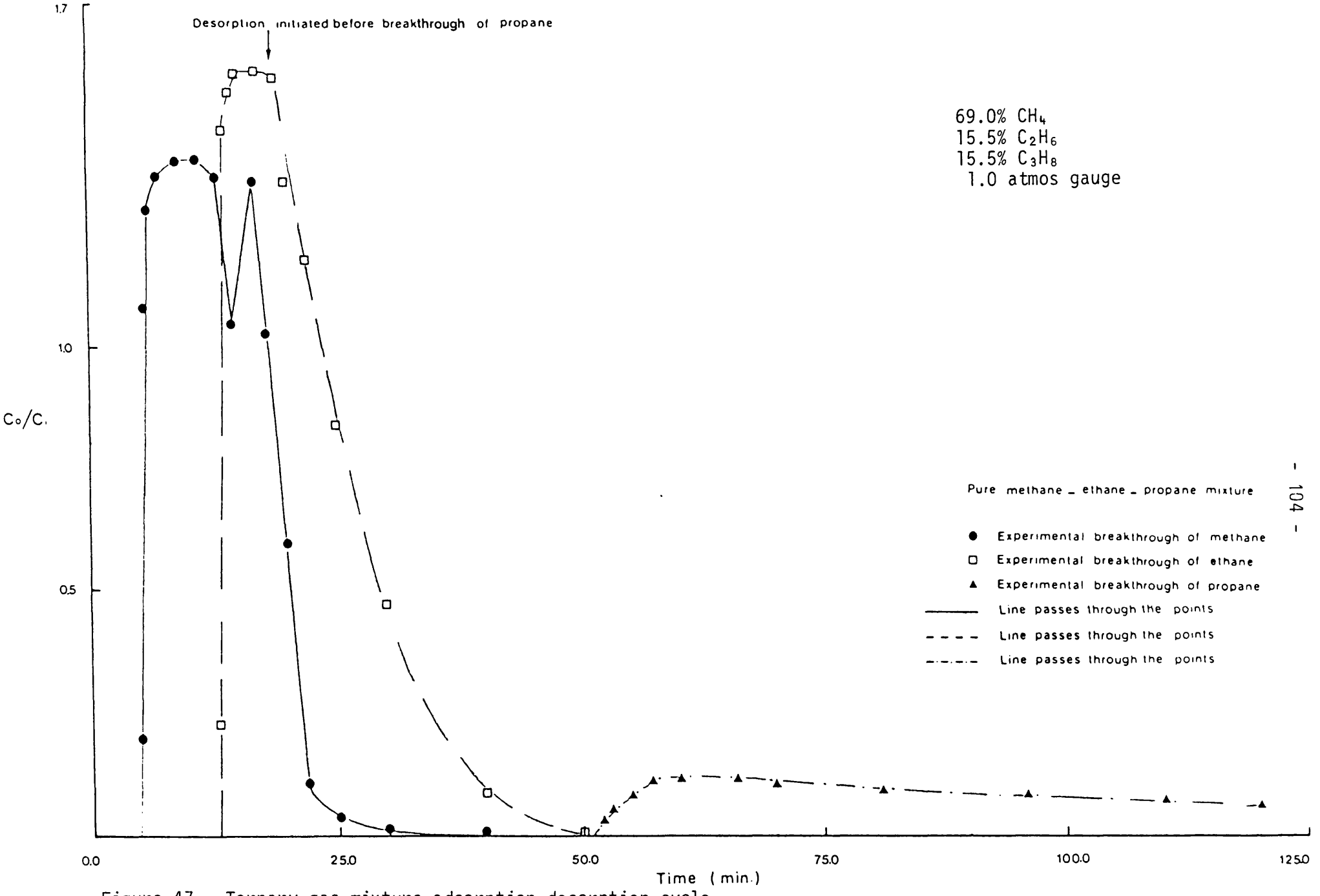

Figure 47 Ternary gas mixture adsorption-desorption cycle.

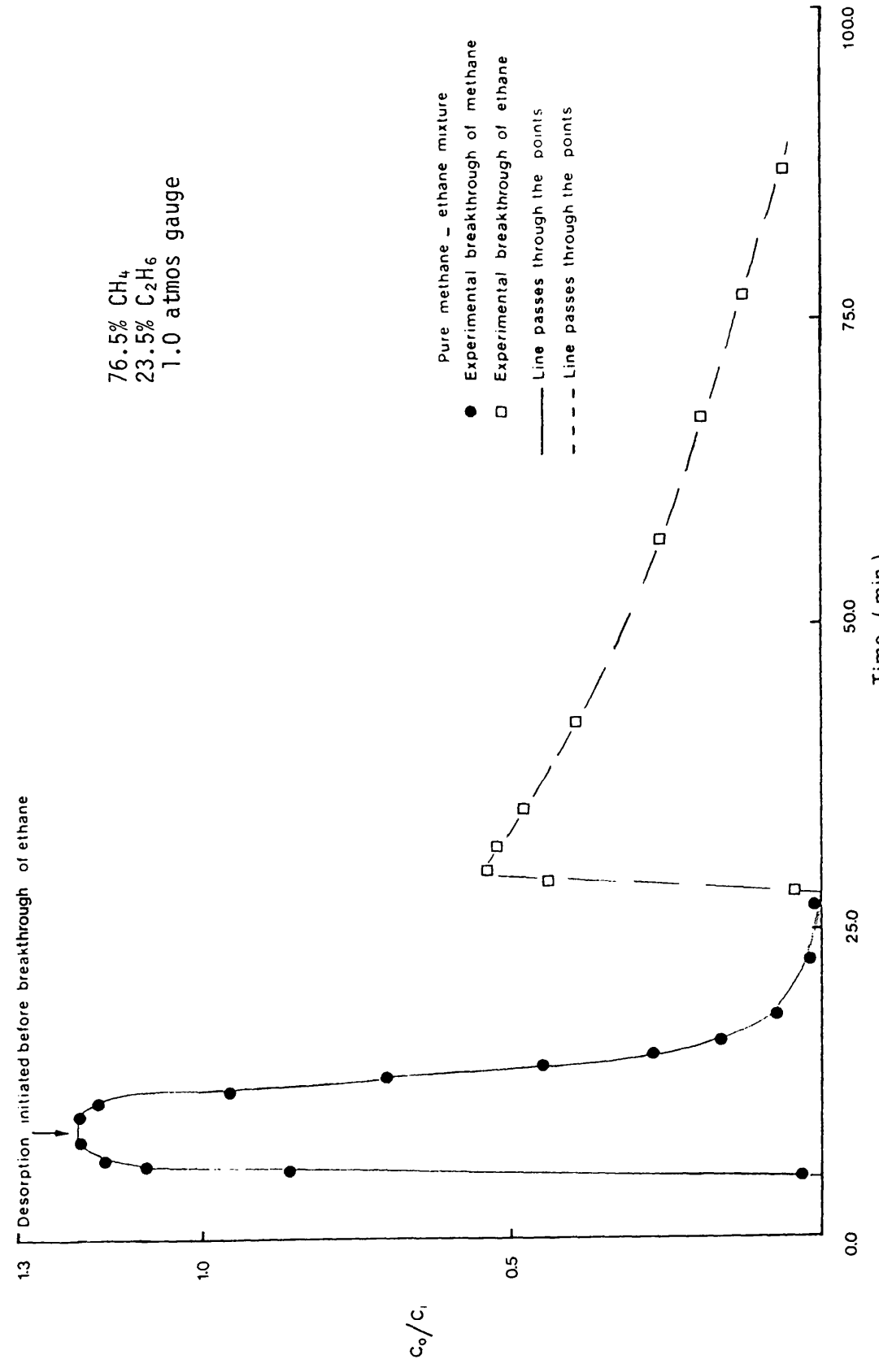

Figure 48 Binary gas mixture adsorption-desorption cycle.

found which deals with ternary mixtures. Recently, Robinson and Thomas[70] studied the binary separation of methane-ethane on 5A molecular sieves employing adsorption-desorption cycles. Two kinetic models were used, an equilibrium model for adsorption, and a linear lumped model for desorption to predict successfully the experimental data.

The equilibrium model was used to describe the multi-component adsorption (see section 2.2 of this chapter). For desorption, a linear driving force model was used, but it failed to fit the experimental data. Therefore, it was decided to use the equilibrium model to describe the whole adsorption-desorption cycle.

The procedure adopted for computation of the cycle was therefore to run the adsorption computation, as previously described (see section 2.2 of this chapter), and then, at a given time, to set the inlet gas phase concentration equal to zero, *i.e.*,

$$\text{for adsorption} \quad c_{(o,t)} = c_o$$

$$\text{for desorption} \quad c_{(o,t)} = 0.0$$

Appendix 7 represents the computer program for the adsorption-desorption cycle.

It was found that the equilibrium model did not fit the experimental data very well. This is attributed to the fact that the experimental equilibrium data were not well correlated by the Freundlich-type multi-component model (see Chapter 3, section 3.4). Figures 49-52 show the experimental and computed adsorption-desorption cycle, with the desorption started at different times before the breakthrough of ethane or propane respectively. Figures 49 and 50 show the desorption started after 5 and 7 min of adsorption respectively and before the breakthrough of ethane, while Figures 51 and 52 show the desorption started after 15 and 18 min of adsorption respectively and before

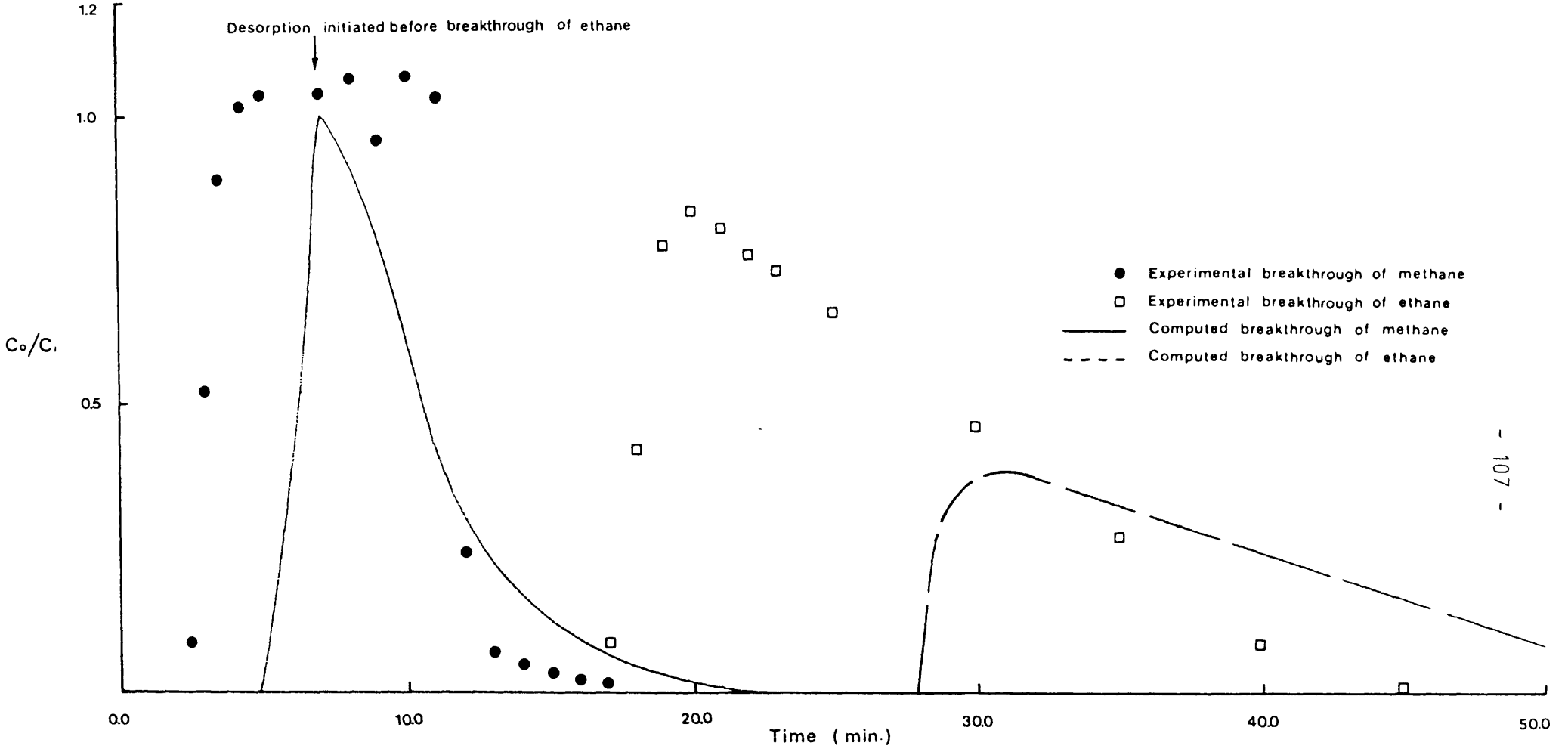

Figure 49 Methane-ethane and propane adsorption-desorption cycle, mixture composition: 76.6% N_2, 13.5% CH_4, 5.8% C_2H_6, 4.1% C_3H_8, 6.0 atmos gauge.

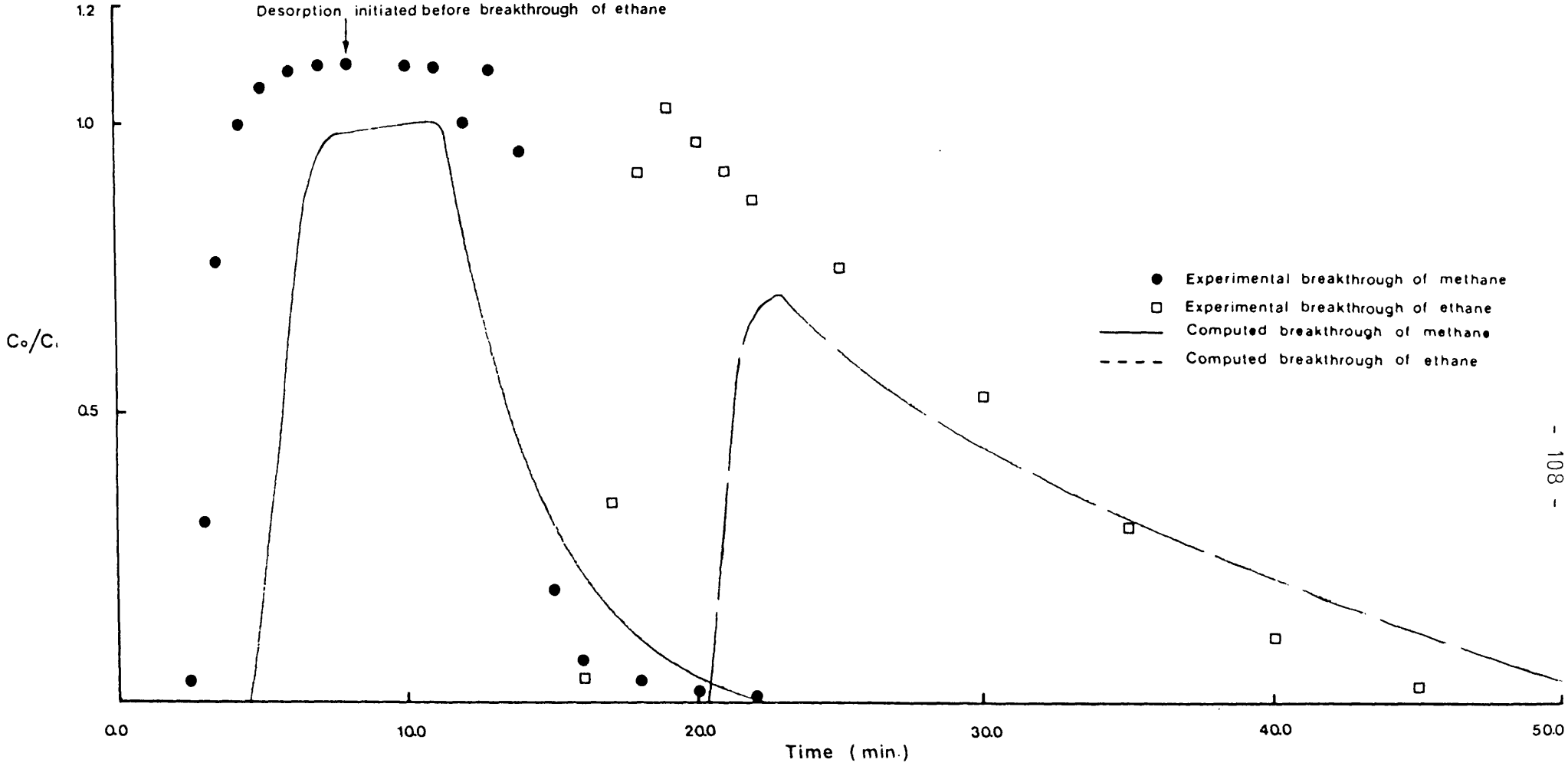

Figure 50 Methane-ethane and propane adsorption-desorption cycle, mixture composition: 76.6% N_2, 13.5% CH_4, 5.8% C_2H_6, 4.1% C_3H_8, 6.0 atmos gauge.

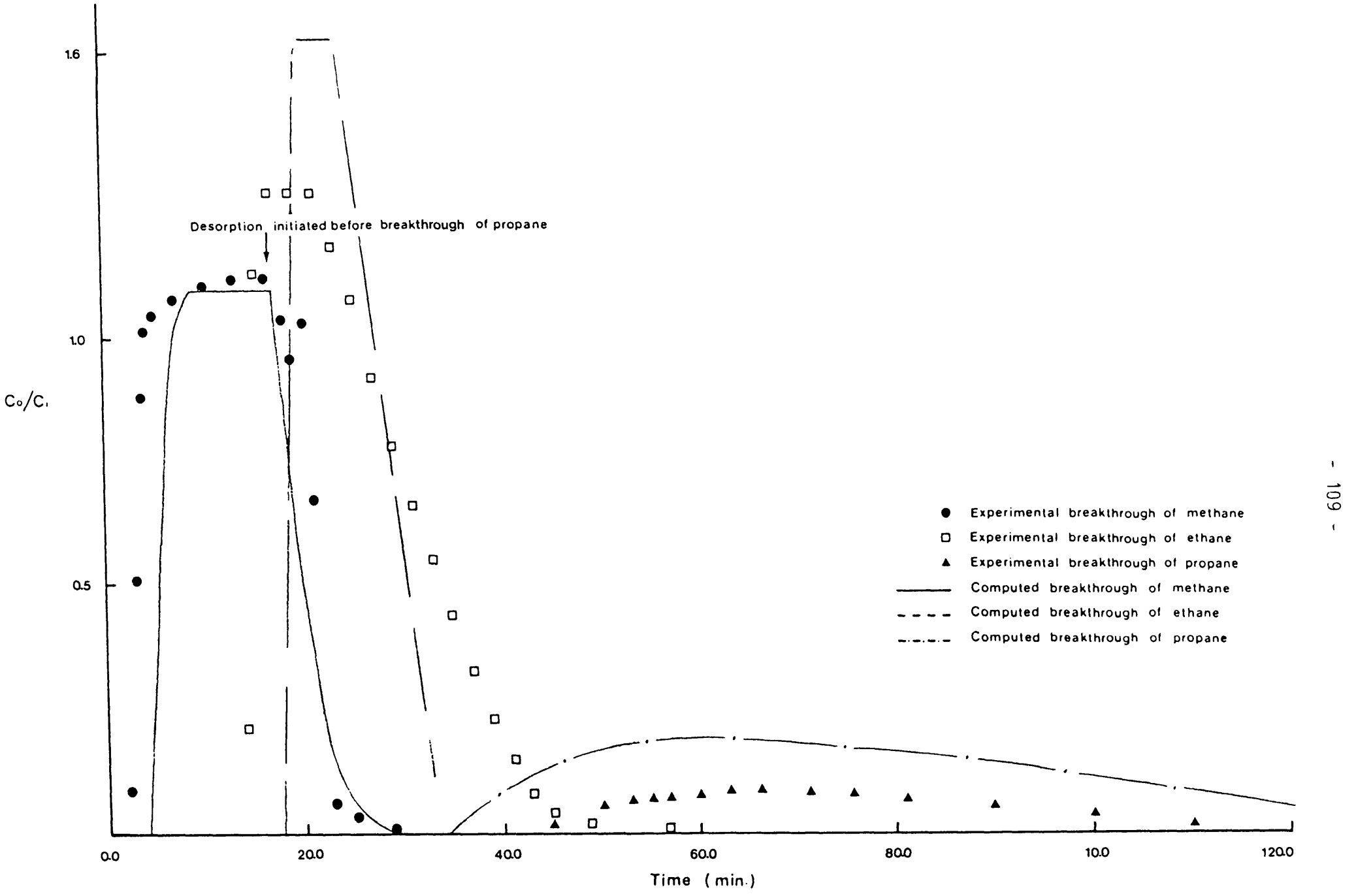

Figure 51 Methane-ethane and propane adsorption-desorption cycle, mixture composition 76.6% N_2, 13.5% CH_4, 5.8% C_2H_6, 4.1% C_3H_8, 6.0 atmos gauge.

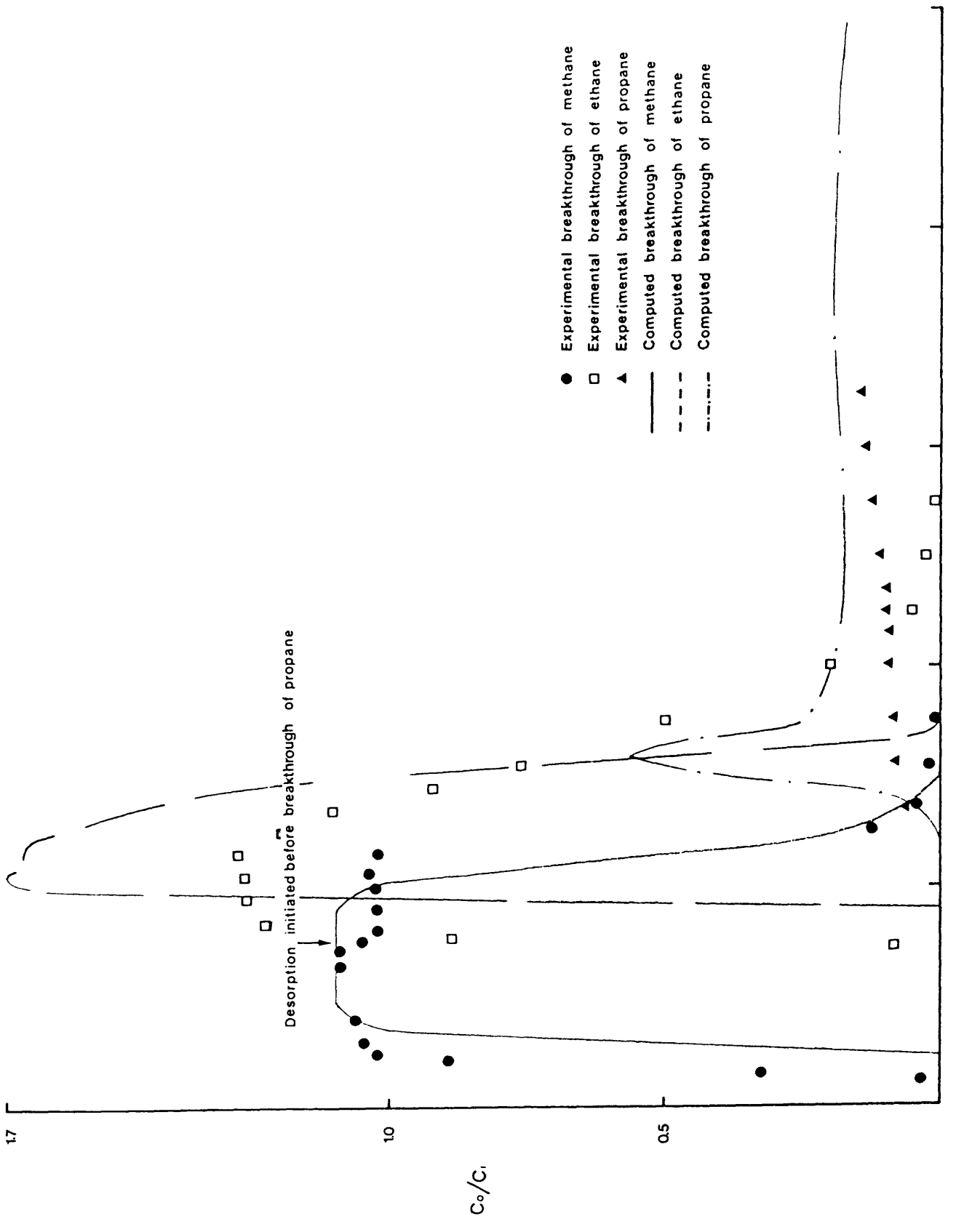

Figure 52 Methane-ethane and propane adsorption-desorption cycle, mixture composition: 76.6% N_2, 13.5% CH_4, 5.8% C_2H_6, 4.1% C_3H_8, 6.0 atmos gauge.

the breakthrough of propane for a mixture of methane, ethane and propane. It can be seen from Figures 50 and 52 that as the adsorption time increases, an overlap between the components occurs. Therefore, the time of desorption should be carefully chosen.

6.1 Conclusions

The experimental adsorption-desorption cycles for pure and dilute ternary mixtures showed that it is possible to separate ethane as well as propane from methane-ethane and propane mixtures. Also, it was shown that it is possible to separate ethane from a methane-ethane mixture. Experimental adsorption-desorption cycles indicated that good separation is dependent on the instant at which desorption is initiated.

CHAPTER 5

EXPERIMENTAL RESULTS AND MATHEMATICAL MODELLING OF METHANE AND CARBON DIOXIDE

1. Single component adsorption isotherm results

A concentration range (6.4-36.4 x 10^{-5} mol cm^{-3} for methane and 2.94-16.65 x 10^{-5} mol cm^{-3} for carbon dioxide) was used. The quantity adsorbed was calculated by equations (1.8)-(1.12) and (1.18)-(1.19) (see Chapter 1, Sections 2.1.1 and 2.1.2). Figure 53 illustrates the curves obtained in this way for the adsorption of methane and carbon dioxide as single components on 4A and 5A molecular sieves. The quantity adsorbed on the 5A sieve is greater than on the 4A sieve for both methane and carbon dioxide. The latter is more strongly adsorbed than the former on each adsorbent.

1.1 Methane

For methane adsorption on a 5A molecular sieve, Langmuir's, Freundlich's and the statistical thermodynamic models are all successful in predicting the experimental data. The parameters for each model are those used in the first part (Chapter 3) and are listed in Tables 3.1-3.3 and 5.1-5.3.

Figure 54 shows the experimental data for methane at 25° C on the 5A molecular sieve with the mole fraction 0.1074 at various concentrations, along with that obtained in the previous work (Chapter 3), with a mole fraction 0.1473, correlated by the above-mentioned models. For methane on the 4A molecular sieve, the three models gave good agreement. Figures 53 and 55 show the correlation for methane on 5A and 4A molecular sieves at 25° C. The parameters employed for the Langmuir and Freundlich models, obtained by the least squares method, are given in Tables 5.1-5.3, while

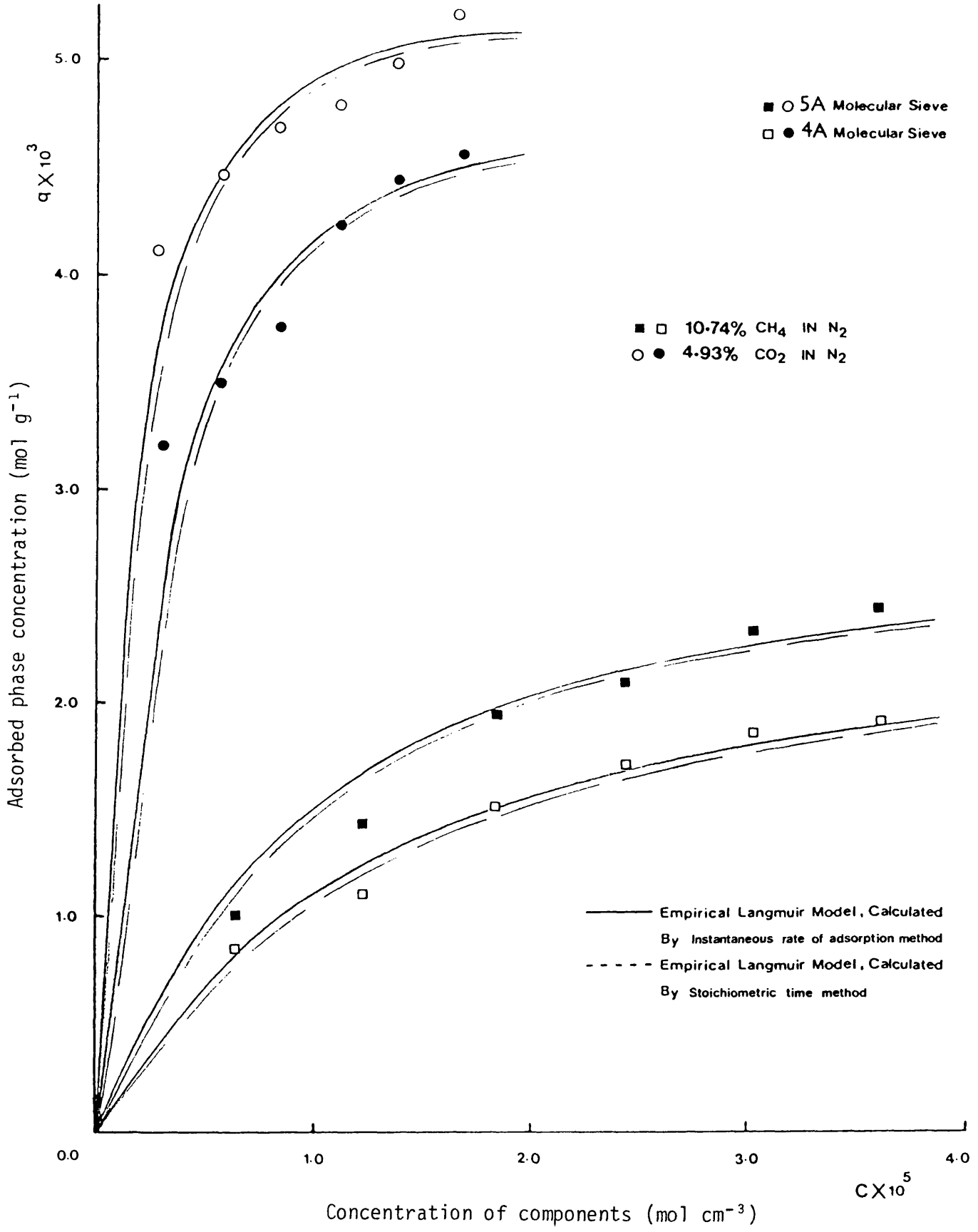

Figure 53 Single component isotherms at 25° C on 4A and 5A molecular sieves.

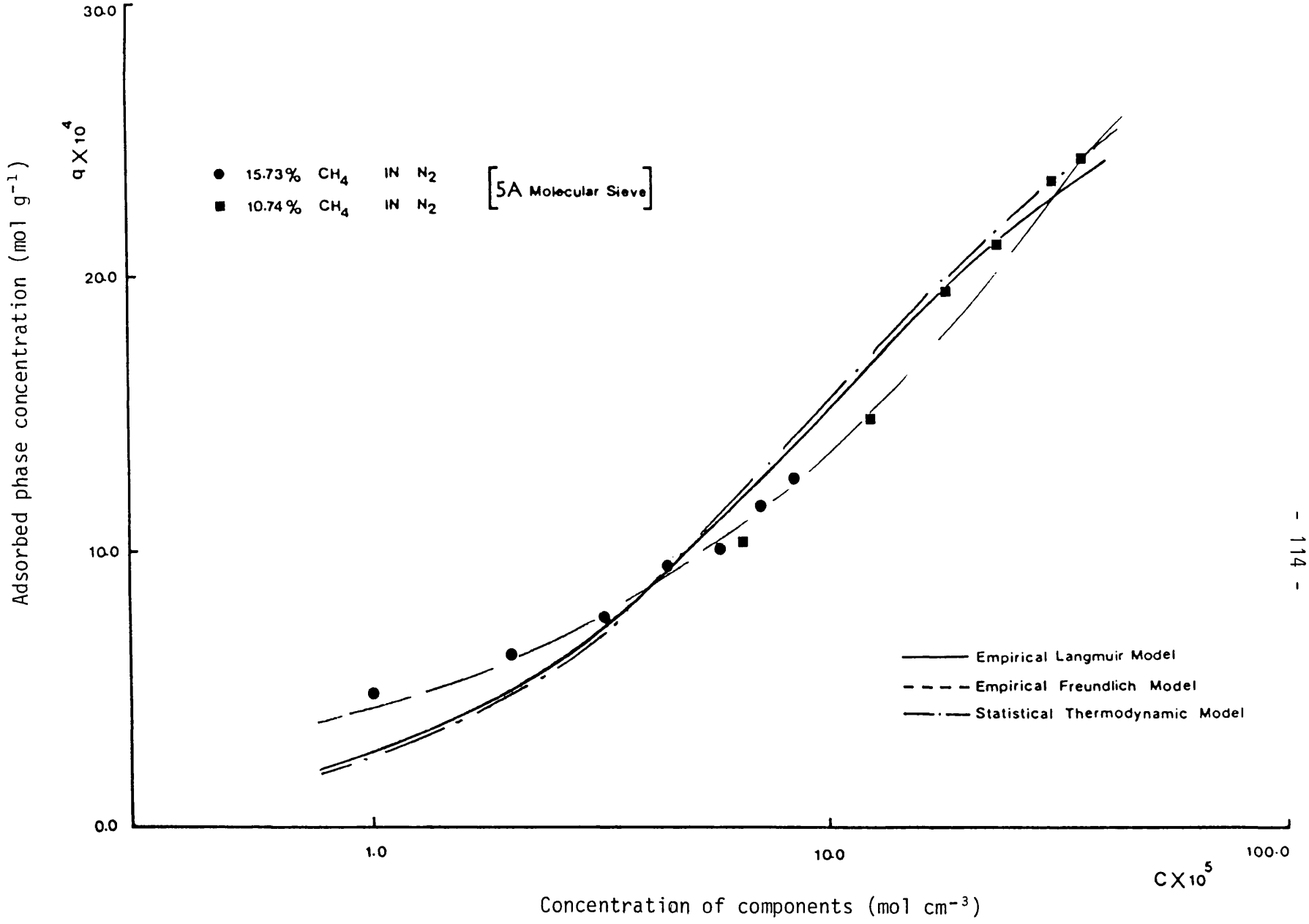

Figure 54 Single component isotherm of methane at 25° C and on 5A molecular sieve.

Table 5.1

Empirical Langmuir constants

Adsorbent	Temperature (° C)	Component	a x 10^{3} (mol g^{-1})	b x 10^{-4} (cm^{3} mol^{-1})
5A	25	methane	3.0	1.01
5A	25	carbon dioxide	5.5	7.982
4A	25	methane	2.78	0.62
4A	25	carbon dioxide	5.15	4.137

Table 5.2

Empirical Freundlich constants

Adsorbent	Temperature (° C)	Component	K_f*	n
5A	25	methane	0.0912	0.458
5A	25	carbon dioxide	0.0157	0.1388
4A	25	methane	0.1023	0.497
4A	25	carbon dioxide	0.0295	0.2155

*The units of K_f depend on the magnitude of n. If n = 1, then the units of K_f are cm^{3} g^{-1}.

Table 5.3

Parameters for the statistical thermodynamic model

Adsorbent	Cavity volume (ν, Å^3)	Component adsorbed at 25° C	Molecular volume (β) (Å^3 molecule^{-1})	No. of molecules per cavity $m \leqslant \nu/\beta$ (molecule cavity^{-1})	Henry's constant (K) [equation (4)[18]] (molecule cavity^{-1} bar^{-1})	Henry's constant* (molecule cavity^{-1} bar^{-1})
5A	776	methane	82.1	9	2.58	2.18
5A	776	carbon dioxide	70.0	11	825	675
4A	776	methane	82.1	9	1.73	-
4A	776	carbon dioxide	70.0	11	112.5	-

*Calculated by $K=K_0 \exp \Delta H_0/RT$

the coefficients for the statistical thermodynamic model were calculated by the methods described in Chapter 3 (Section 1.3).

1.2 Carbon dioxide

The experimental data for carbon dioxide on 4A and 5A molecular sieves are well represented by the Langmuir and Freundlich adsorption isotherms. The correlation obtained by the two models is illustrated in Figures 53 and 55. Tables 5.1 and 5.2 give the models coefficients calculated by a least squares method. Figure 55 shows that the statistical thermodynamic model represents the experimental data reasonably well. The parameters employed by this model are summarised in Table 5.3.

2. Binary adsorption isotherm results

Two mixtures of methane and carbon dioxide in nitrogen of different composition were used to study binary mixture isotherms. The quantity of carbon dioxide adsorbed on 5A molecular sieves is greater than that adsorbed on 4A molecular sieves, whereas the amount of methane adsorbed on 5A sieves is only slightly greater than that adsorbed on 4A sieves. Figures 56 and 57 show the experimental data for binary mixtures of methane and carbon dioxide on 5A and 4A molecular sieves respectively.

The inhibition of methane adsorption by carbon dioxide can be seen from the amount of methane adsorbed (at the same gas phase concentration) decreasing with an increase in the gas phase concentration of carbon dioxide, while for the adsorption of carbon dioxide there is slight inhibition by methane (see Appendix 8).

For engineering design calculations, the separating factor ($K_{1,2}$) plays a very important role. It is a measure of competitive selectivity for the adsorbates 1 and 2.

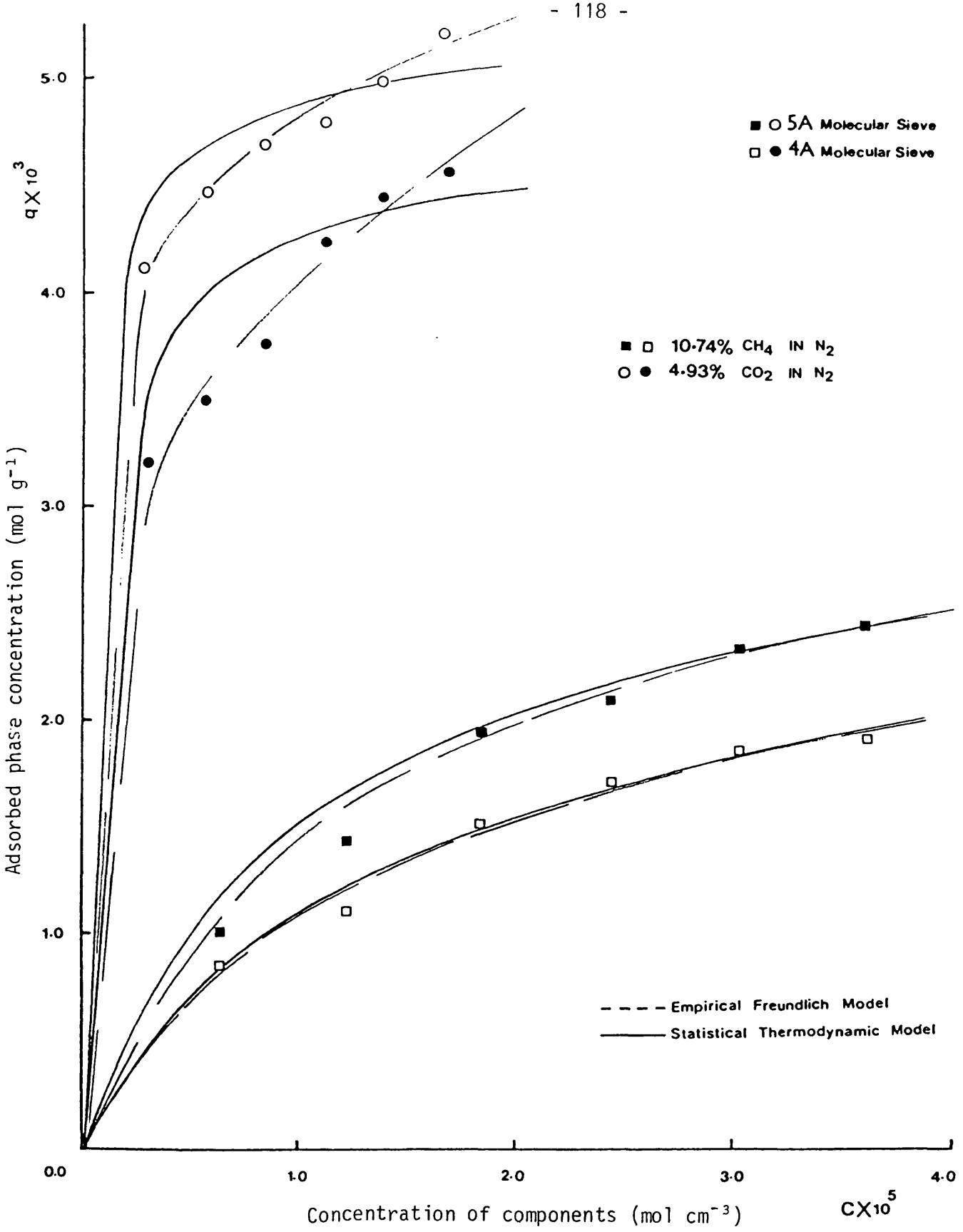

Figure 55 Single component isotherm of CH_4 and CO_2 at 25° C and on 4A and 5A molecular sieves.

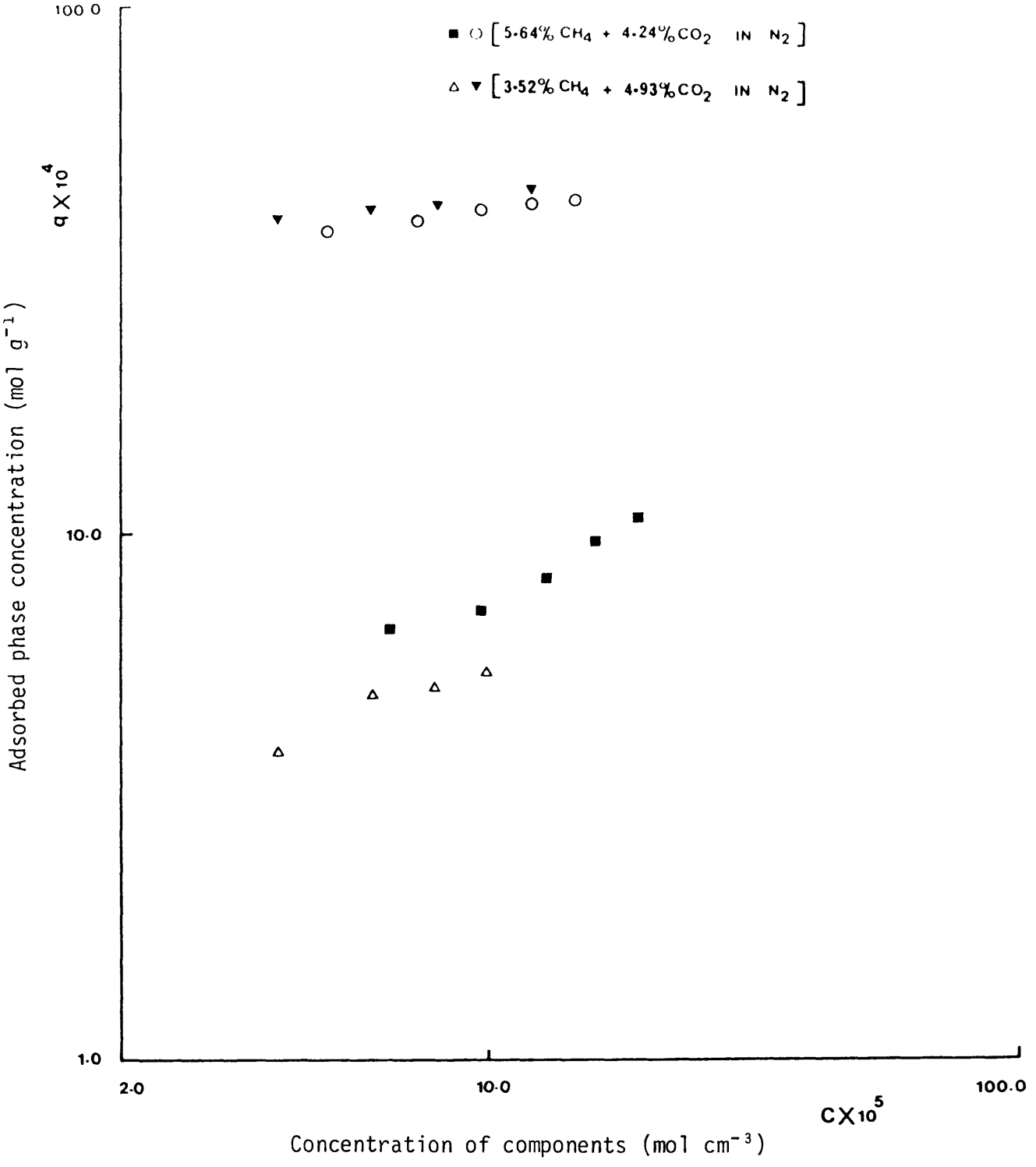

Figure 56 Binary adsorption of methane and carbon dioxide on 5A molecular sieve.

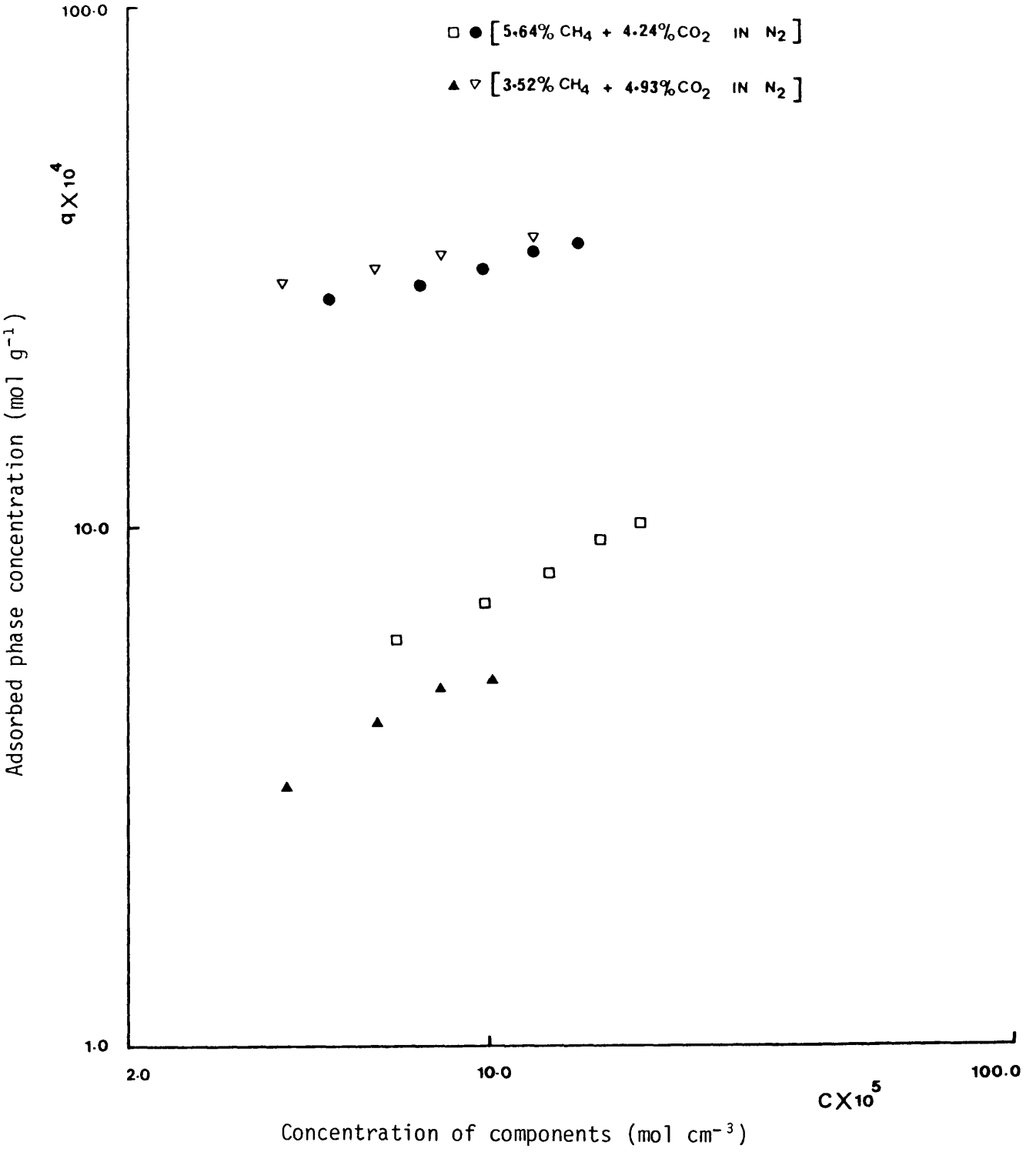

Figure 57 Binary adsorption of methane and carbon dioxide on 4A molecular sieve.

$$K_{1,2} = \frac{q_1^*/c_1}{q_2^*/c_2} \tag{5.1}$$

Different types of equilibrium may be indicated by the values of $K_{1,2}$ as follows:

$K_{1,2} > 1.0$ Component 1 is preferentially adsorbed

$K_{1,2} < 1.0$ Component 2 is preferentially adsorbed

The total concentrations of the two components in the gas phase (C) and the adsorbed phase (Q), are defined as follows:

$$C = c_1 + c_2 \tag{5.2}$$

$$Q = q_1 + q_2 \tag{5.3}$$

Equations (3.7), (5.1)-(5.3) yield another form of the isotherm equation:

$$\frac{c_2/C}{q_2/Q} = K_{1,2} + (1 - K_{1,2})\frac{c_2}{C} \tag{5.4}$$

This equation is useful for correlation if the adsorption is governed by a Langmuir isotherm. By plotting $c_2/C \Big/ q_2/Q$ against c_2/C, the intercept is equal to the separation factor ($K_{1,2}$). This was obtained by a least squares fit to the experimental data, as illustrated in Figures 58 and 59 for 5A and 4A molecular sieves respectively. However, the scattering of the data suggests that the separation factor is not constant (*i.e.*, it varies from 5.5 to 7.7 for 5A and 4.5 to 6.7 for 4A molecular sieves). The separation factor for both the adsorbents is the same and equal to 5.7. In this chapter, only the theoretical modelling of adsorption on a 5A molecular sieve is considered.

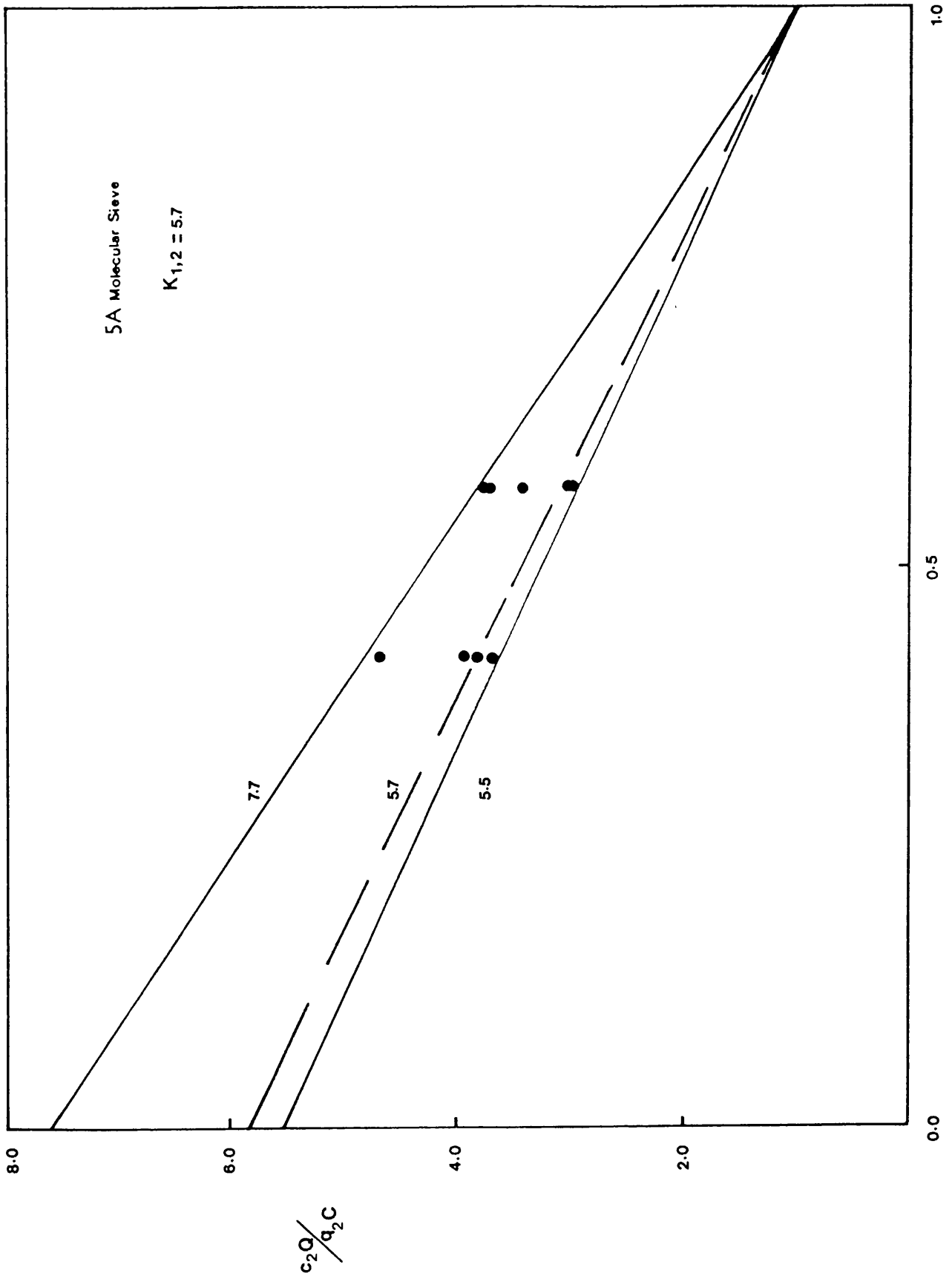

Figure 58 Binary adsorption data expressed in terms of separation factor.

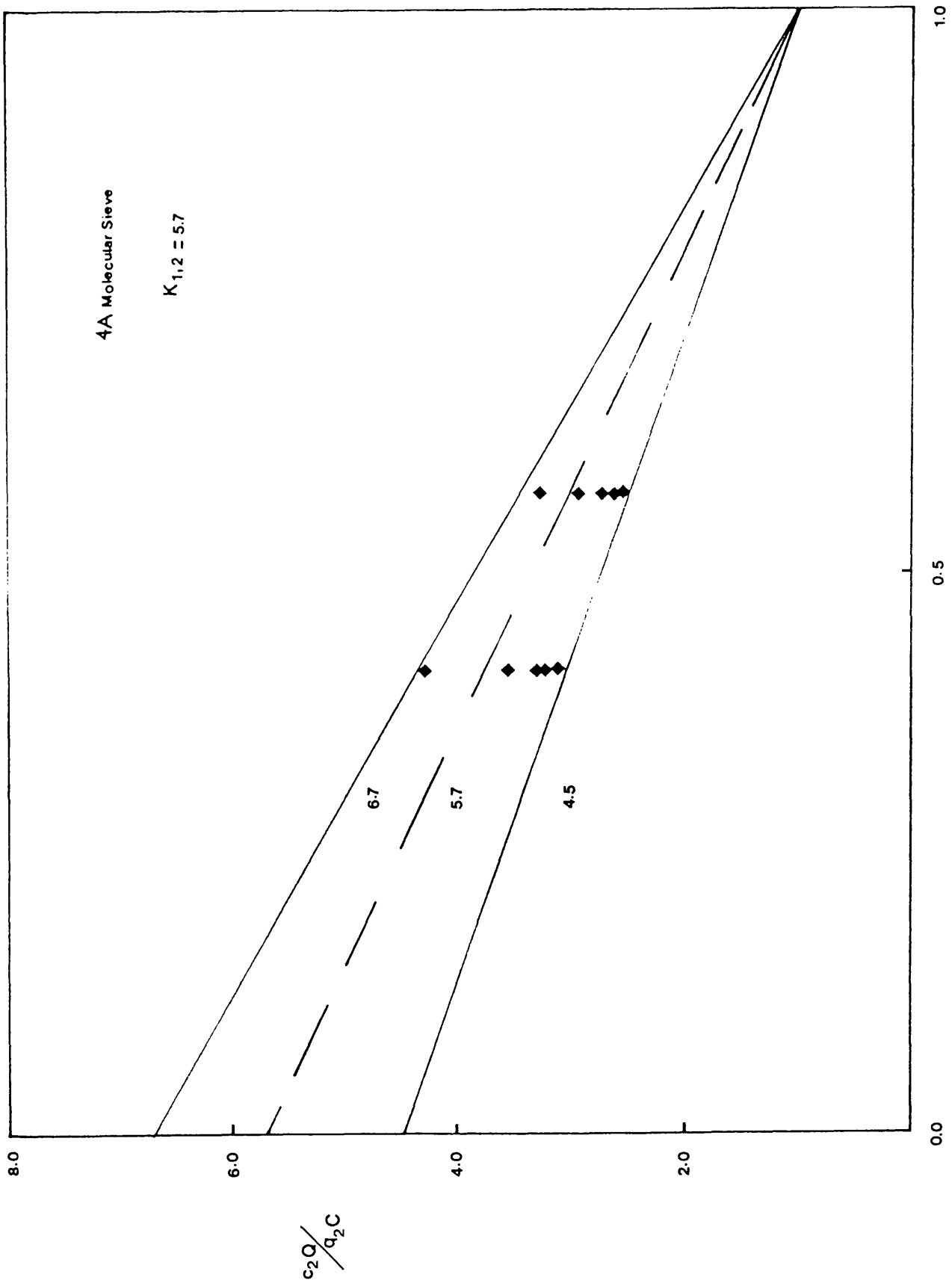

Figure 59 Binary adsorption data expressed in terms of separation factor.

2.1 The extended Langmuir model

For binary adsorption mixtures equation (3.7) can be written as:

$$q_1 = \frac{a_1 b_1 c_1}{1+b_1 c_1+b_2 c_2} \tag{5.5}$$

with a similar expression for q_2.

A comparison between the experimental equilibrium data and that predicted from equation (5.5) is shown in Figure 60, using the coefficient of the single component isotherms, as given in Table 5.1. The calculated solid phase adsorbate concentration of methane was less than the experimental value in all cases. In the case of carbon dioxide the calculated adsorbed phase concentration was slightly greater than the experimental data, giving a fairly reasonable fit. The experimental equilibrium data, however, are not well correlated by this model.

2.2 Statistical thermodynamic model

Ruthven and Loughlin[19,20] have extended the single component model to include binary adsorption on type A zeolites, thus:

$$Q_1 = \frac{K_1 p_1 \times \sum_{i=1} \sum_{j=1} \frac{(K_1 p_1)^i (K_2 p_2)^j (1-i\beta_1/\nu-j\beta_2/\nu)^{i+j}}{(i-1)!j!}}{1+K_1 p_1+K_2 p_2+ \frac{\sum\sum_{ij} (K_1 p_1)^i (K_2 p_2)^j (1-i\beta_1/\nu-j\beta_2/\nu)^{i+j}}{i!j!}} \tag{5.6}$$

with a similar expression for Q_2,

where $i + j \leqslant 2$ and $i\beta_1 + j\beta_2 \leqslant \nu$

The parameters used in this model are those obtained from the single component equilibrium isotherms, and are given in Table 5.3. The model failed to predict the experimental data. The results are shown in Figure 61.

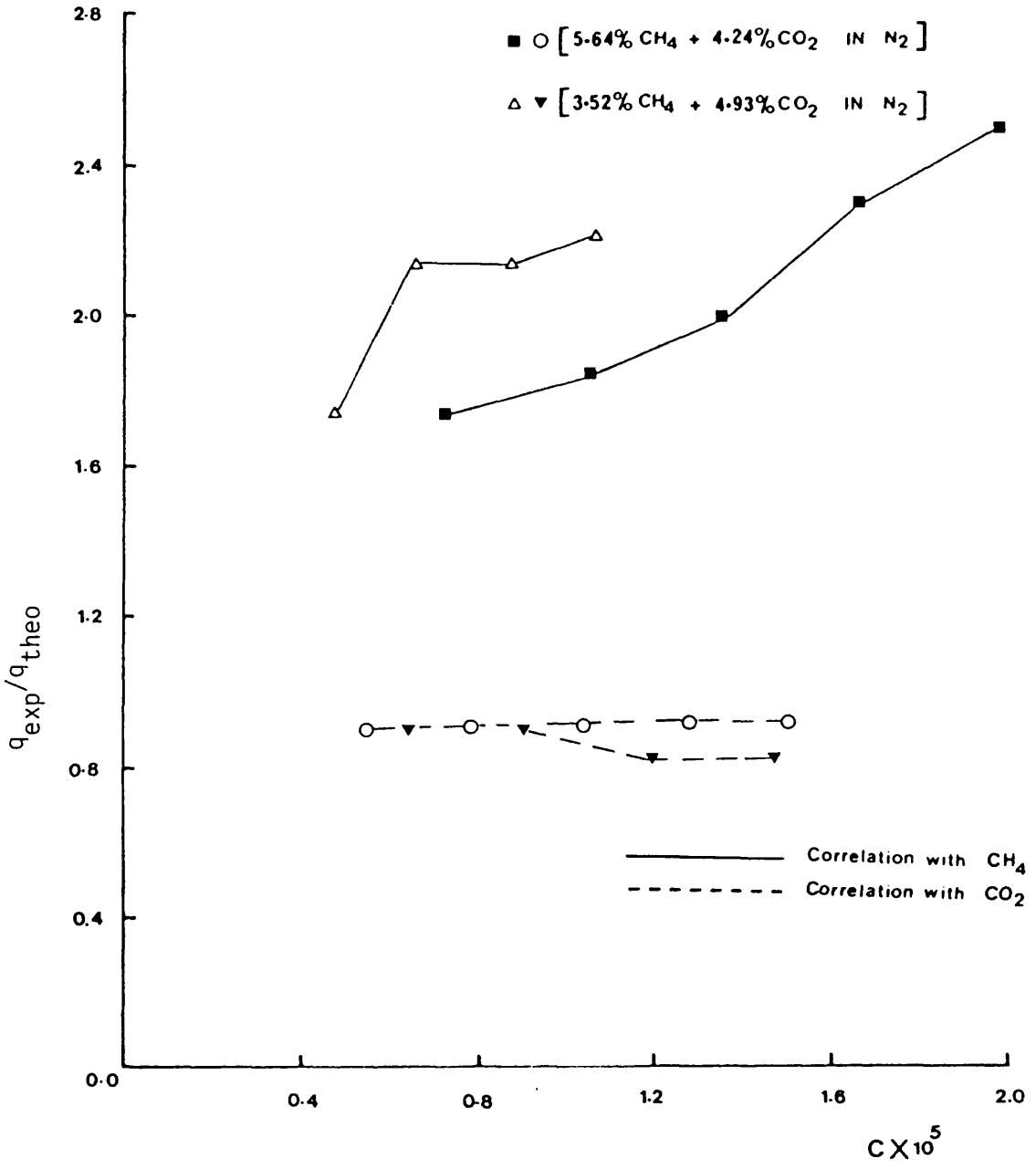

Figure 60 Binary adsorption of methane and carbon dioxide correlated with extended Langmuir model.

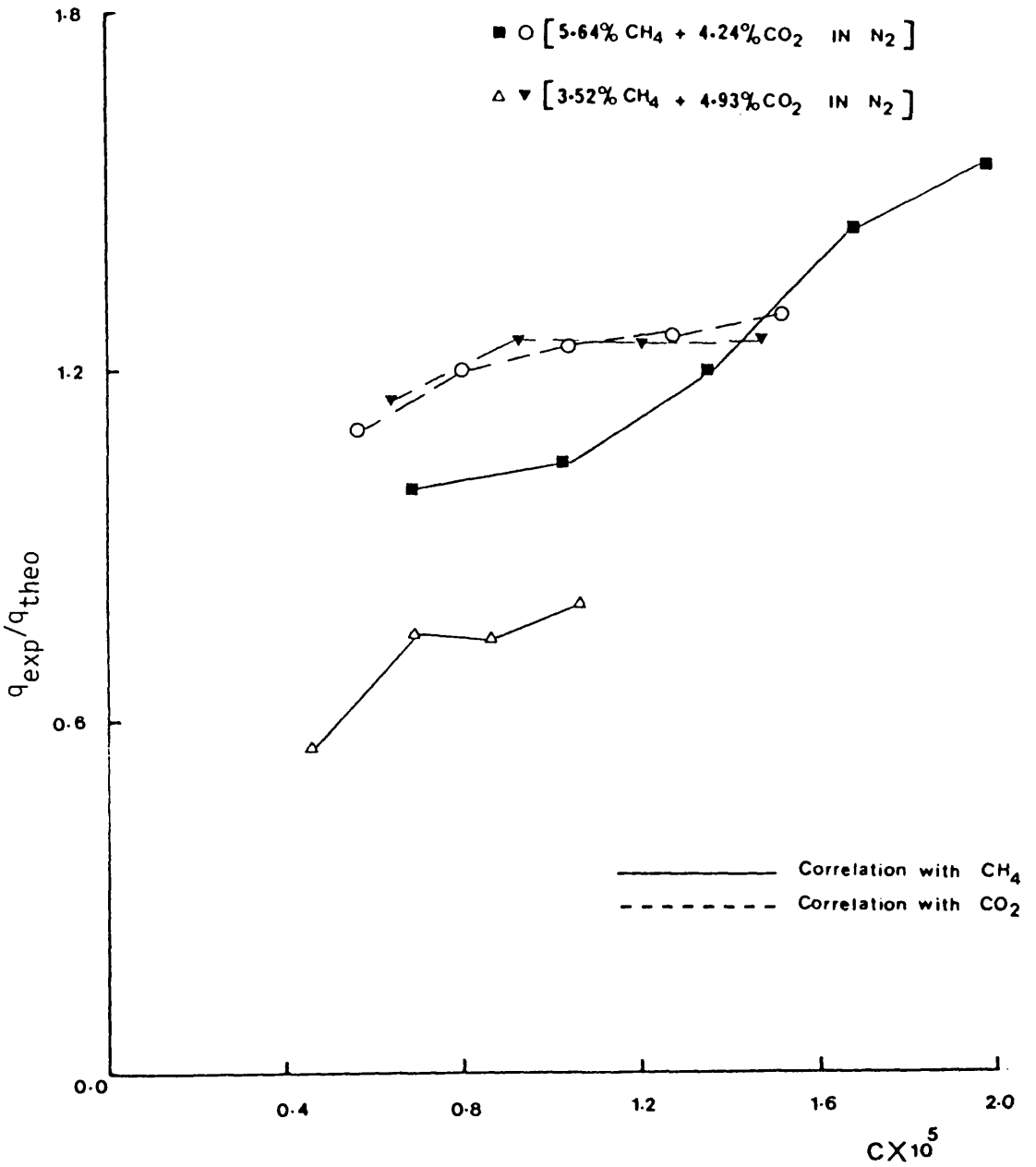

Figure 61 Binary adsorption of methane and carbon dioxide correlated with extended statistical thermodynamic model.

2.3 The ideal adsorbed solution theory

Myers and Prausnitz[15] have proposed a method which is based on an analogy to Raoult's law: the partial pressure of an adsorbate is equal to the product of the adsorbed mole fraction and the equilibrium pressure that would be exerted by the pure component at the same temperature and spreading pressure as the mixture, as is given by:

$$pY_i = p_i^0(\pi)X_i \tag{5.7}$$

Furthermore, at equilibrium, all adsorbates have the same spreading pressure. The spreading pressure (π) is calculated from the pure component data as:

$$\pi = \frac{RT}{A_s}\int_0^{p_i^0} \frac{q}{p}\,dp \tag{5.8}$$

where π = spreading pressure of pure component,

A_s = specific surface area of the adsorbent

p = total pressure

p_i^0 = equilibrium vapour pressure for pure adsorbate i.

The experimental values for the integral ($^q/_p$) become very large as the pressure approaches zero.

Kidnay and Myers[17] showed that the problem described above may often be alleviated by changing the variable of integration. By changing the independent variable from p to q, equation (5.8) becomes:

$$\pi = \frac{RT}{A_s}\int_0^{q} \frac{d\log p}{d\log q}\,dq \tag{5.9}$$

They also suggested that if the plots of log c against log q for the individual isotherms are parallel, then the adsorbates have the same relationship between the spreading pressure and adsorbed phase concentration. The

individual isotherms for methane and carbon dioxide are plotted in Figure 62, and it can be seen that the curves obtained are not parallel. Thomas and Lombardi[32] derived an equation relating gas and solid phase adsorbate concentration, using the single component empirical coefficients:

$$q_M = \frac{a_M b_M c_M [1 + (1 - \frac{a_{CO_2}}{a_M}) b_{CO_2} c_{CO_2}]}{1 + b_M c_M + b_{CO_2} c_{CO_2}} \qquad (5.10)$$

with a similar expression for q_{CO_2}. The model, however, does not correlate the experimental data, as shown in Figure 63.

2.4 Modified extended Langmuir model

For a component in a binary mixture, equation (3.7) becomes:

$$q_M = \frac{a_M b_M c_M}{1 + b_M c_M + b_{CO_2} c_{CO_2}} \qquad (5.11)$$

with a similar expression for q_{CO_2}.

The same procedure of calculation was used as had been employed to correlate the experimental equilibrium isotherm data for ternary mixtures (see Chapter 3, Section 3.3) and is as follows:

Case I By modification of equation (5.11) according to the procedure previously outlined (see Chapter 3, Section 3.3), one may write:

$$\frac{a_M b_M c_M}{q_M} - (1 + b_M c_M) = b'_{CO_2} c_{CO_2} \qquad (5.12)$$

with a similar expression for CO_2. The parameters were calculated by a least squares method, and are given in Table 5.4.

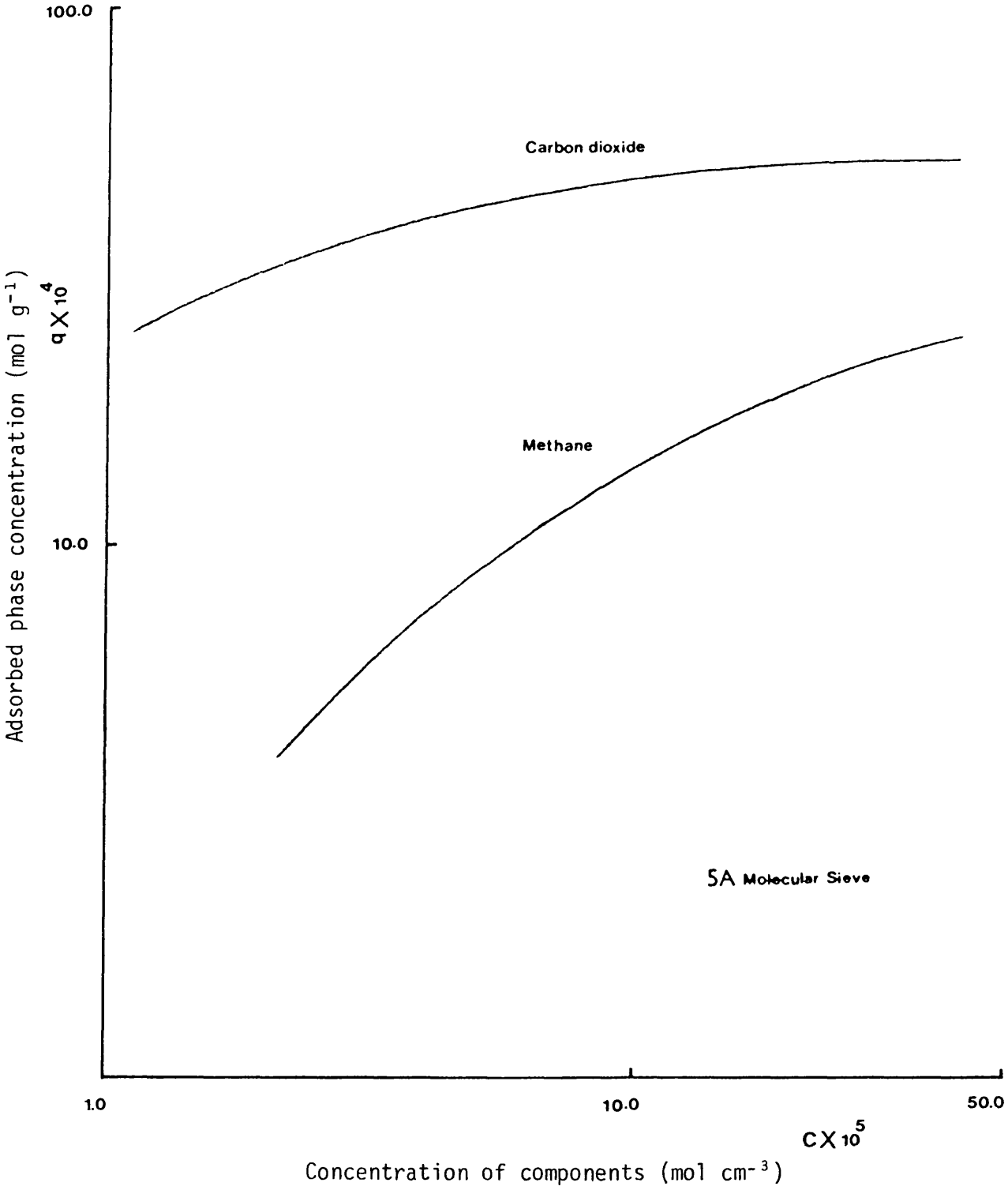

Figure 62 Single component isotherm logarithmic plots displaying variation of separation factor $K_{1,2}$.

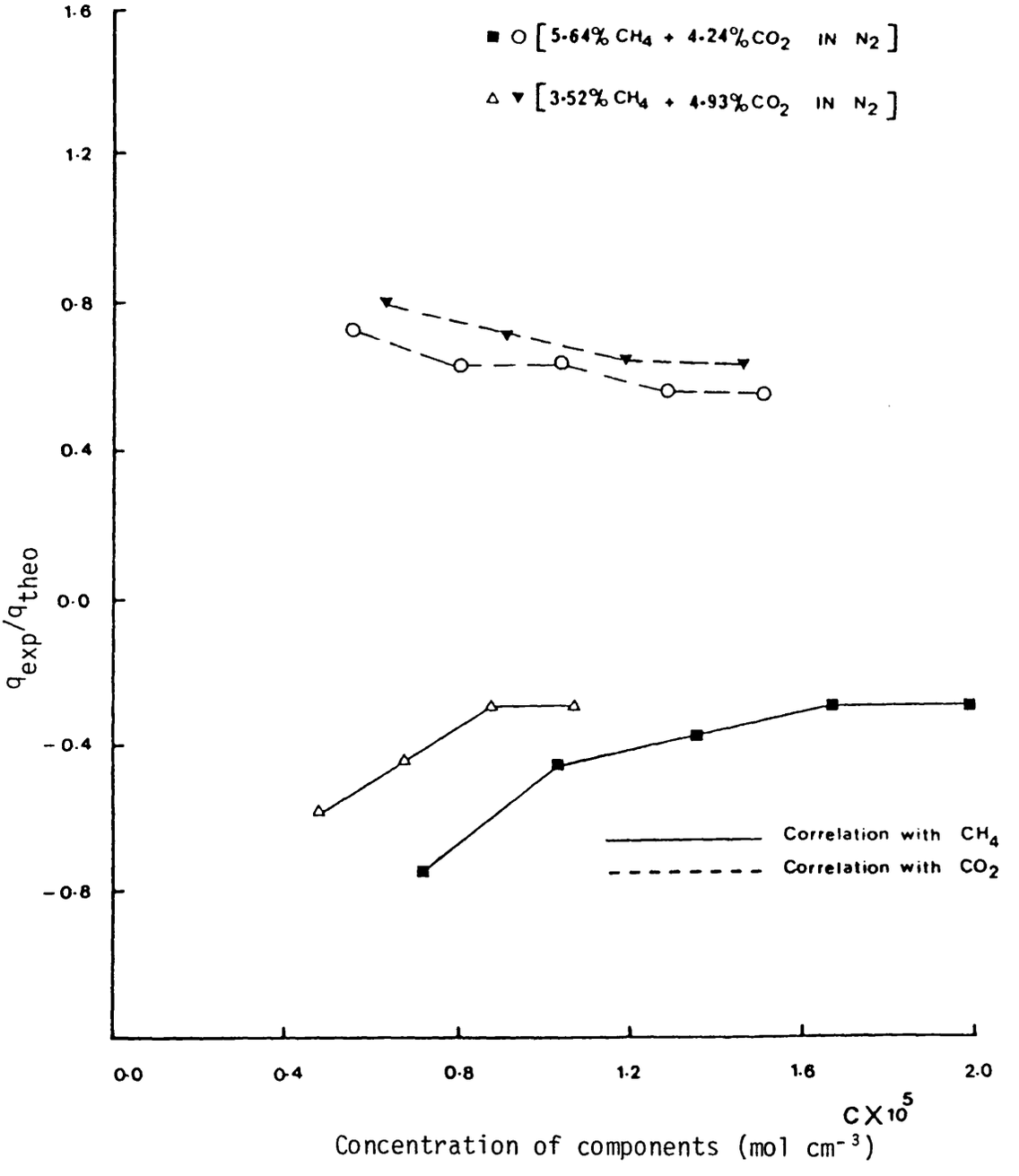

Figure 63 Binary adsorption of methane and carbon dioxide correlated with Kidnay and Myers model.

Table 5.4

Modified extended Langmuir model parameters: Case I

i	adsorbate	$a_i \times 10^3$ (mol g^{-1})	$b_i \times 10^{-4}$ (cm^3 mol^{-1})	$b_{i_M}' \times 10^{-4}$ (cm^3 mol^{-1})	$b_{i_{CO}}' \times 10^{-4}$ (cm^3 mol^{-1})
1	methane	3.0	1.01	-	2.32
2	carbon dioxide	5.5	7.983	1.385	-

Case II Equation (5.11) may be modified in an alternative way (see Chapter 3, Section 1.3.3), thus:

$$\left(\frac{c_M}{q_M} - \frac{c_M}{a_M}\right) = \frac{1}{a_M b_M'} + \frac{b_{CO_2}'}{a_M b_M'} c_{CO_2} \qquad (5.13)$$

with a similar expression for CO_2. Again the constants b_M' and b_{CO_2}' were calculated by a least squares fit to the experimental data, and are listed in Table 5.5.

Table 5.5

Modified extended Langmuir model parameters: Case II

i	adsorbate	$a_i \times 10^3$ (mol g^{-1})	$b_{i_M}' \times 10^{-4}$ (cm^3 mol^{-1})	$b_{i_{CO}}' \times 10^{-4}$ (cm^3 mol^{-1})
1	methane	3.0	0.568	o.9276
2	carbon dioxide	5.5	0.4775	4.687

A good correlation was obtained by the two methods. Figures 64 and 65 show the correlation of the experimental equilibrium data for binary mixtures of methane and carbon dioxide by Case I and Case II respectively.

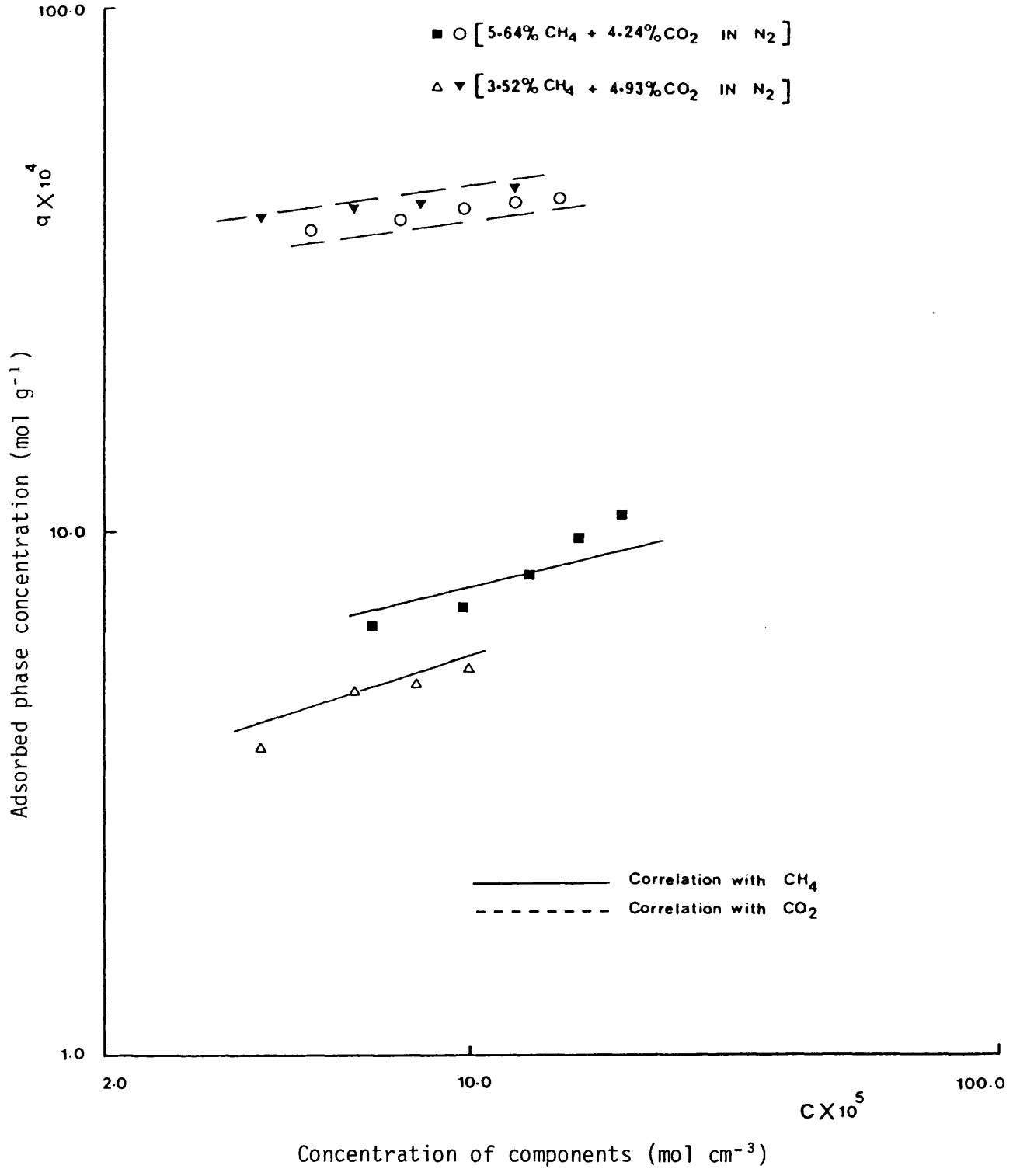

Figure 64 Isotherms for binary mixture of CH_4 and CO_2 at 25° C, correlated by modified extended Langmuir model (Case I).

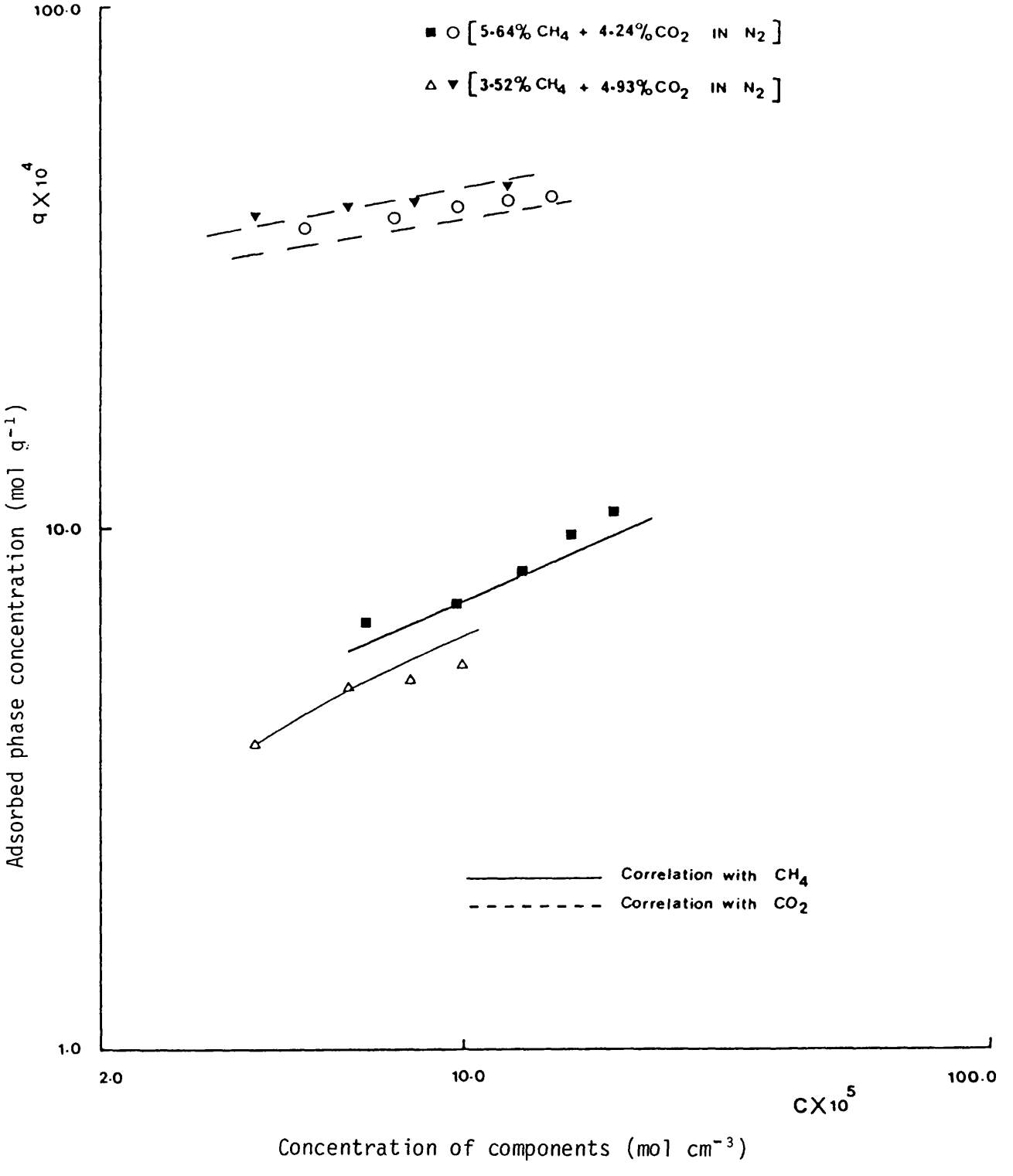

Figure 65 Isotherms for binary mixture of CH_4 and CO_2 at 25° C, correlated by modified extended Langmuir model (Case II).

2.5 The Freundlich-type multicomponent adsorption isotherm

This model has been applied for a ternary mixture (see Chapter 3, Section 3.4). The same procedure of correlation was used for a binary mixture.

(a) Fritz and Schluendermodel

For a component 1 in a binary mixture, equation (1.5) becomes:

$$q_1 = \frac{K_{10} c_1^{n_{10}}}{c_1^{n_{11}} + K_{12} c_2^{n_{12}}} \qquad (5.14)$$

with a similar expression for q_2, where K_{10} and $(n_{10}-n_{11})$ are the single component parameters. The other coefficients were obtained by non-linear regression and are given in Table 5.6. The experimental data are well correlated by this model, as shown in Figure 66.

Table 5.6

Freundlich-type multicomponent parameters (Fritz and Schluendermodel)

i	adsorbate	K_{io}*	n_{io}	K_{i1}*	n_{i1}	K_{i2}*	n_{i2}
1	methane	0.0912	0.958	1.0	0.5	2.5	0.6
2	carbon dioxide	0.0157	0.229	0.1	0.1	1.0	0.1

*Unit of K_{io}, K_{i1} and K_{i2} will obviously depend on values of n.

(b) Sheindorf *et al.* model

For a binary system the adsorption by each component from equation (1.6) is given by:

$$q_1 = K_1 c_1 (c_1 + K_{12} c_2)^{n_1 - 1} \qquad (5.15)$$

$$q_2 = K_2 c_2 (K_{21} c_1 + c_2)^{n_2 - 1} \qquad (5.16)$$

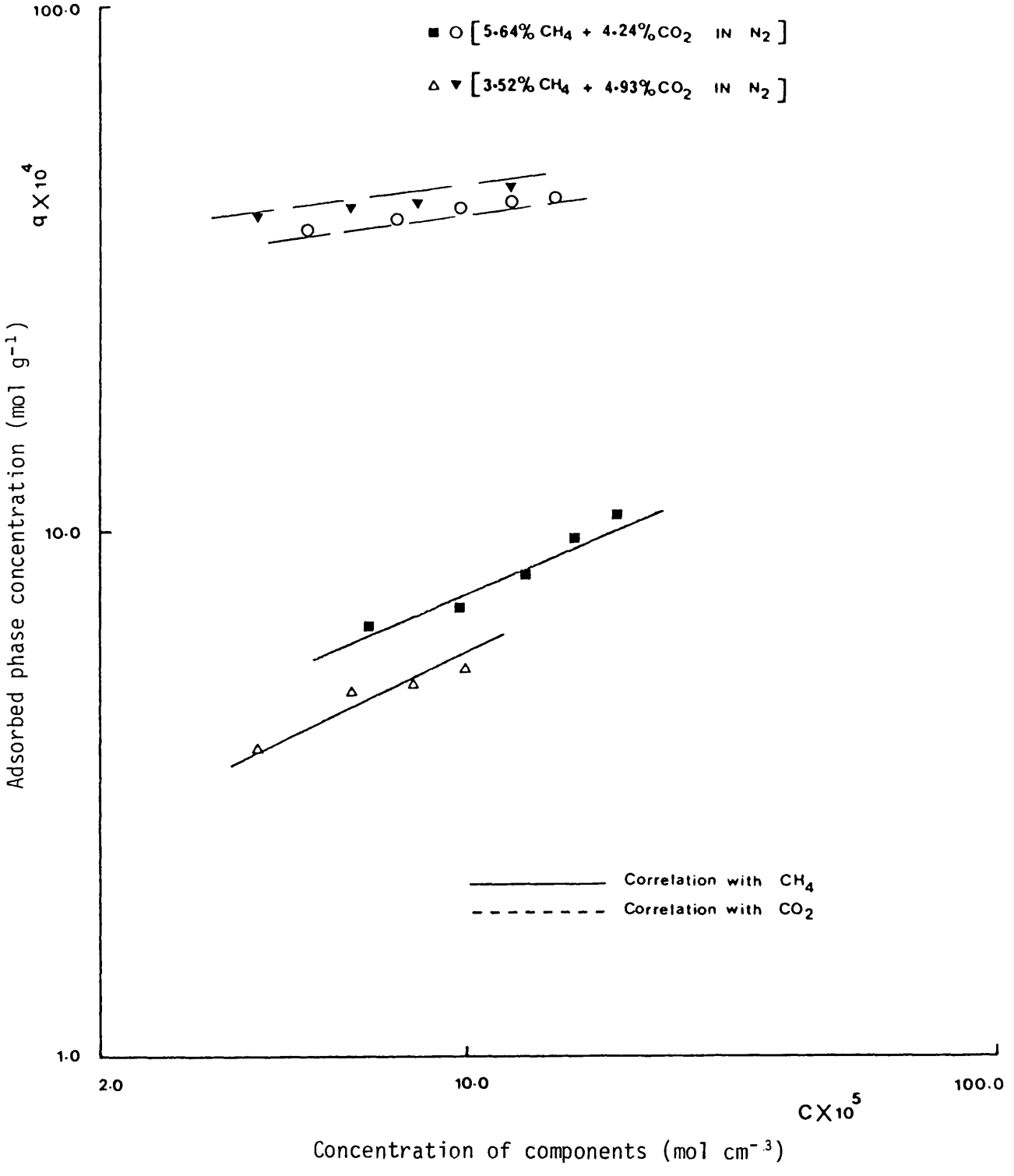

Figure 66 Isotherms of binary mixture of CH_4 and CO_2 at 25° C, correlated by Fritz and Schluender model.

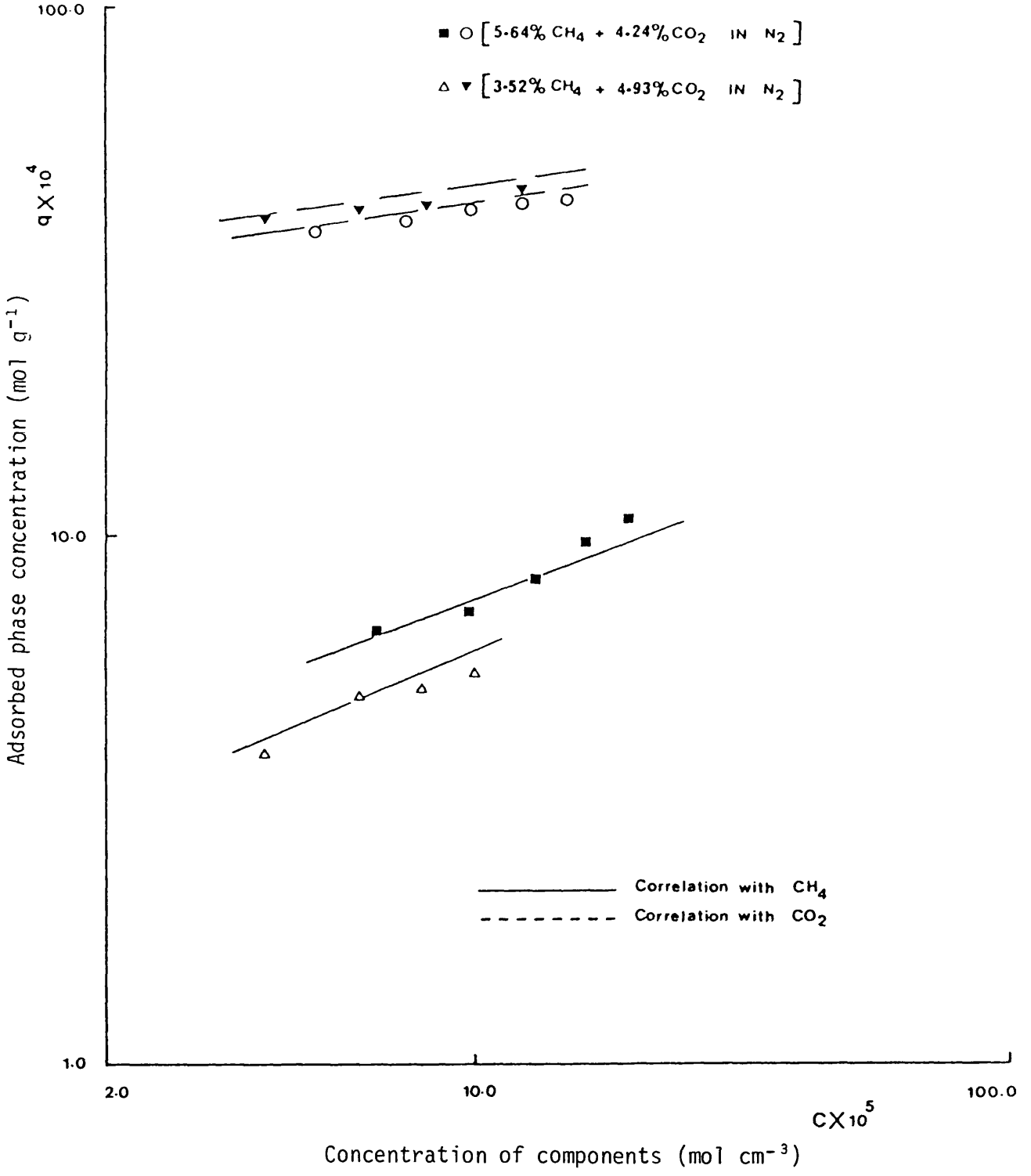

Figure 67 Isotherms for binary mixture of CH_4 and CO_2 at 25° C, correlated by Sheindorf *et al*, model.

By linearisation of equation (5.15),

$$\left(\frac{q_1}{K_1 c_1}\right)^{\frac{1}{n_1-1}} - c_1 = K_{12} c_2 \qquad (5.17)$$

The constant K_{12} was obtained by a least squares method, while the constant K_{21} in equation (5.16) is calculated by:

$$K_{21} = \frac{1}{K_{12}}$$

or by linearising equation (5.16) and obtaining the value of K_{21} by a least squares method. The parameters were calculated, and are listed in Table 5.7. The experimental equilibrium data are well correlated by this model. Figure 67 shows the correlation.

Table 5.7

Freundlich-type multicomponent parameters: Sheindorf *et al.* model

i	adsorbate	K_i*	K_{i1}*	K_{i2}*	n_i
1	methane	0.0912	1.0	2.64	0.458
2	carbon dioxide	0.0157	0.17-0.38	1.0	0.1288

*Unit of K_{i0}, K_{i1} and K_{i2} will obviously depend on values of n_i.

3. Conclusions

Experimental equilibrium adsorption isotherms for the single component of methane or carbon dioxide on 5A and 4A molecular sieves can be fitted by the empirical Langmuir and Freundlich models. A statistical thermodynamic model also represents the data fairly well. For the adsorption of binary mixtures of methane and carbon dioxide, the extended Langmuir, statistical

thermodynamic and Kidnay and Myers models all failed to correlate the experimental results. Good correlations were obtained, however, by the modified extended Langmuir, extended Freundlich by Fritz and extended Freundlich by Sheindorf models.

Miura *et al.*[71] studied the adsorption of a binary mixture for an aqueous solution of *p*-nitrophenol and dodecylbenzenesulphonate and gaseous mixtures of benzene and toluene on activated carbon. Their experimental data also agreed well with the extended models of Langmuir and Freundlich (Fritz). However, Miura *et al.* did not clearly mention the conditions required for the application of these models. In addition, they did not specify the concentrations of the adsorbates. In the present work, the experimental results of a binary mixture of methane and carbon dioxide were well presented by Langmuir and Freundlich type multicomponents. This is because the concentrations of the adsorbates could be in the range where the two models are applicable.

CHAPTER 6

BREAKTHROUGH CURVES

The methods of predicting the breakthrough curves (theoretically) for single and multicomponent mixtures of methane and carbon dioxide are the same as those that were employed earlier and described in Chapter 4.

1. Single Component Breakthrough Curve

1.1 Equilibrium model

A comparison between the computed and the experimental breakthrough curves for methane and carbon dioxide are shown in Figures 68 and 69 respectively. An equilibrium model does not predict the experimental data for either adsorbate. The computer program used for this prediction is given in Appendix 4.

1.2 Linear driving force model

Results for methane have already been discussed in Chapter 4, Section 1.2. For carbon dioxide, the experimental data were compared with the theoretical curves calculated from Glueckuaf and Coates'[34] linear driving force model [equation (1.29)]. The model does not match the experimental breakthrough curve as shown in Figure 70. Appendix 5 gives the computer program for this model.

1.3 Micro-pore diffusion model

The breakthrough curves of methane predicted by this model, along with the experimental points, are shown in Figures 71 and 72. The value of D_m/r^2 used is the same as that employed in Chapter 4 (see Section 1.3.).

For carbon dioxide, Sargent and Whitford[72] have suggested that crystal diffusion plays an important role in determining the overall rate of sorption

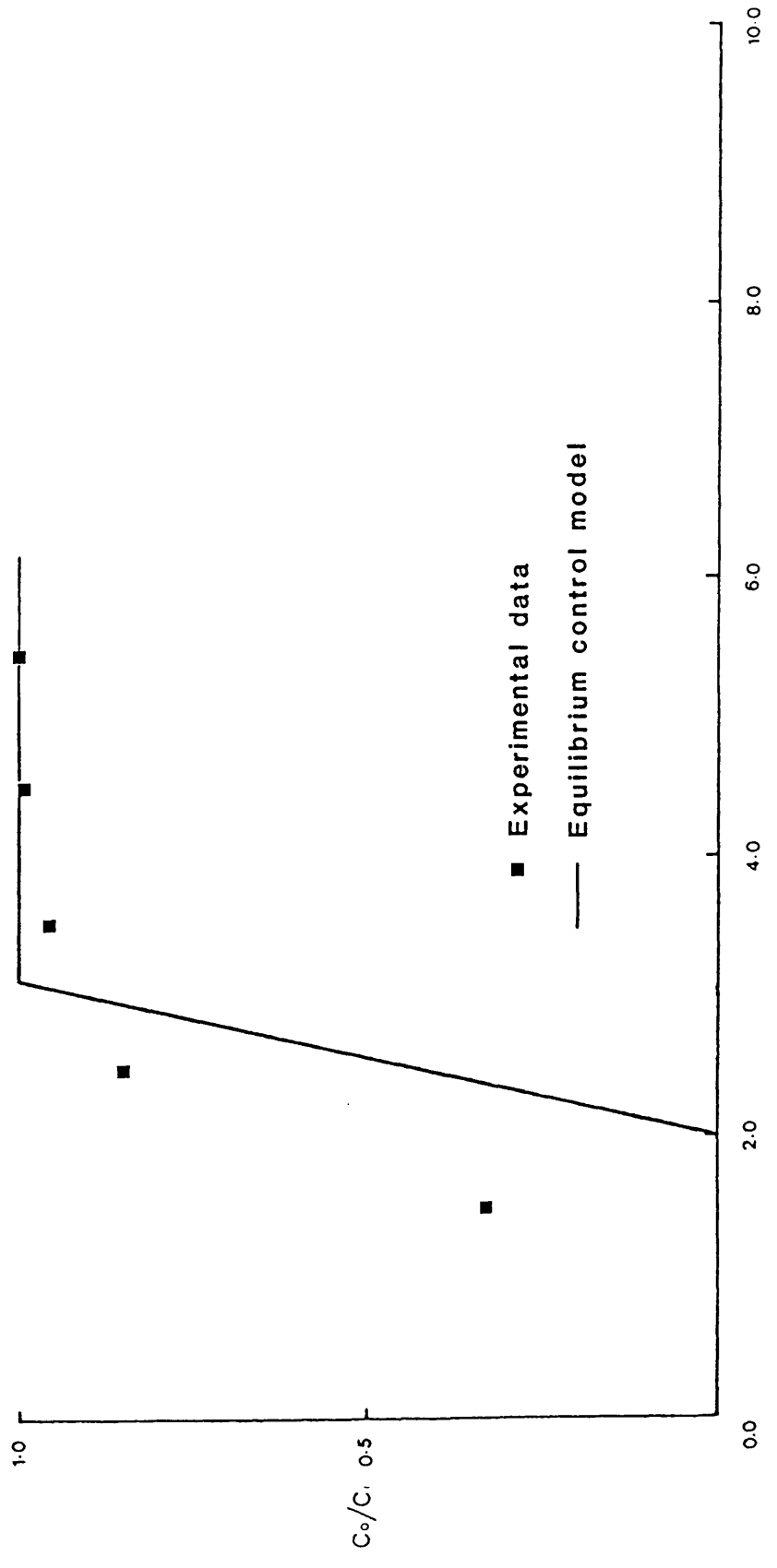

Figure 68 Breakthrough curve of methane.

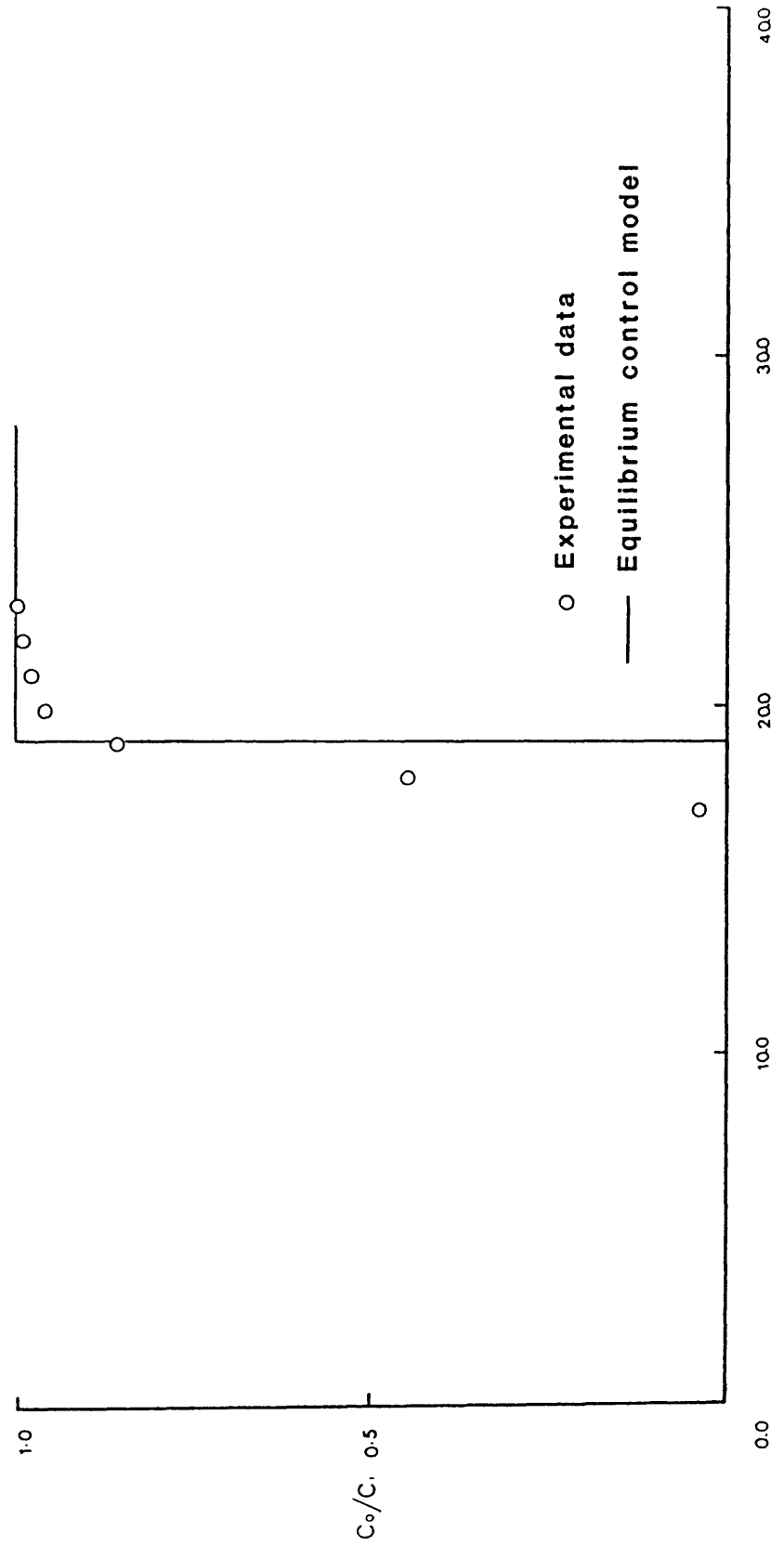

Figure 69 Breakthrough curve of carbon dioxide.

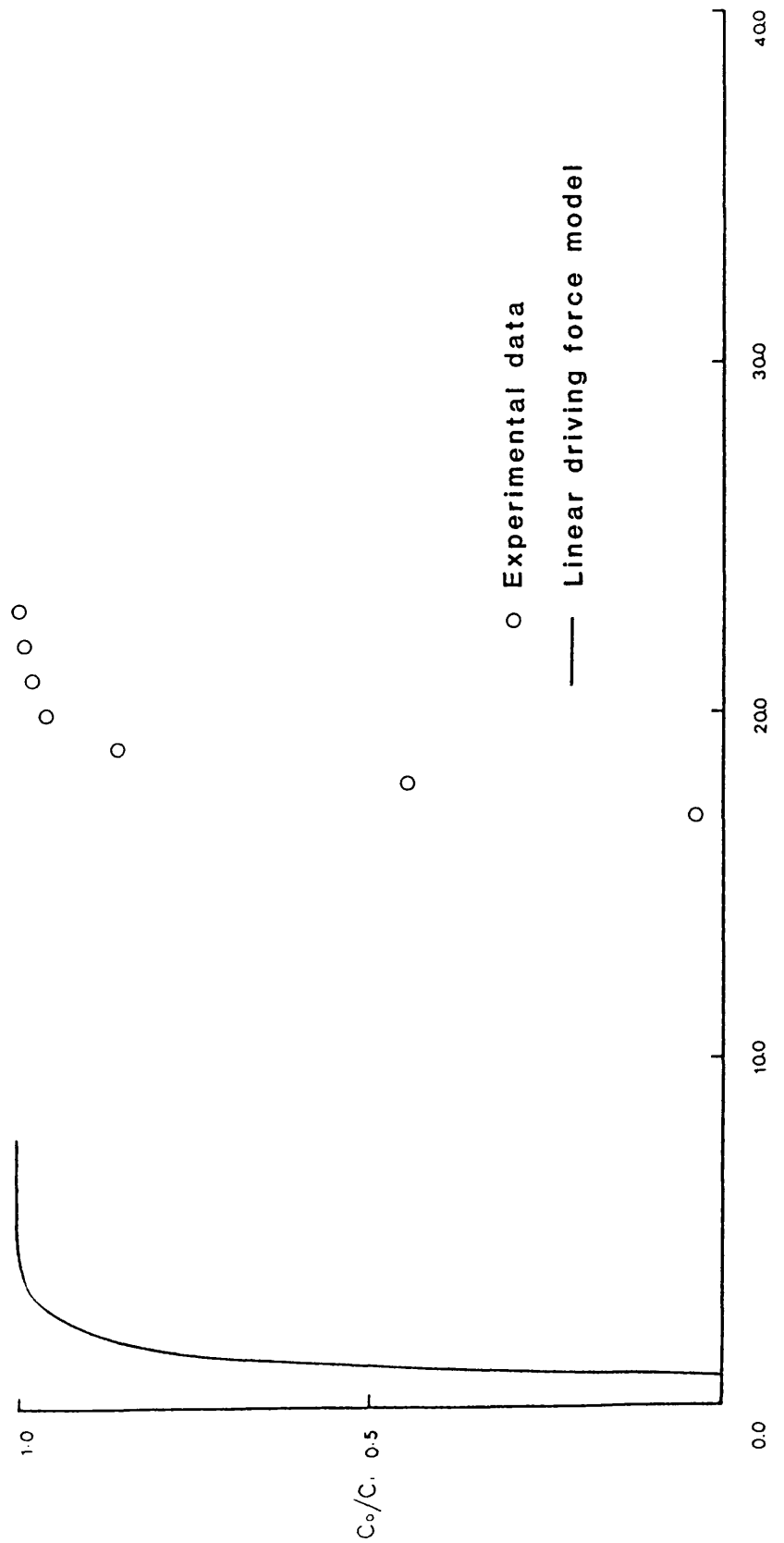

Figure 70 Breakthrough curve of carbon dioxide.

of carbon dioxide on 5A molecular sieves in the temperature range -25° C to 25° C. The same reference quotes the value of D_c as $1.39 \times 10^{-11} cm^2 sec^{-1}$, with the crystal size (diameter) equal to 1 μ.

Figure 73 shows the breakthrough curve for carbon dioxide calculated on the basis of these values. The pore diffusion model [Chapter 1, equation (1.27)] does not fit the experimental breakthrough for either adsorbate.

1.4 Surface diffusion model

At a concentration of 6.42×10^{-5} mol cm^{-3} for methane, Figure 71 shows the comparison between the experimental breakthrough curves and results computed on the basis of a surface diffusion model [Chapter 1, equation (1.28)]. A surface diffusion model is seen to give a fairly reasonable fit. As the concentration increases, the computed curve departs from the experimental data, as shown in Figure 72 for a concentration of 18.38×10^{-5} mol cm^{-3} (see, also, Chapter 4, Section 1.4).

For carbon dioxide, at low concentration, 2.94×10^{-5} mol cm^{-3}, the computed breakthrough has a similar shape to the experimental data, but is displaced along the time axis, as shown in Figure 73.

1.5 Conclusion

The results obtained for the equilibrium control, micropore and linear driving force models suggest that there is no resistance to mass transfer, and hence do not determine the shape of the breakthrough curve for both methane and carbon dioxide. However, the match between experimental data and the surface diffusion model suggested that resistance, due to surface diffusion, occurs over a wide range of gas phase concentration of methane. The computed breakthrough for carbon dioxide has a similar shape to the experimental breakthrough, but there is some departure (see the conclusion in Chapter 4). Therefore, it is concluded that surface diffusion is the

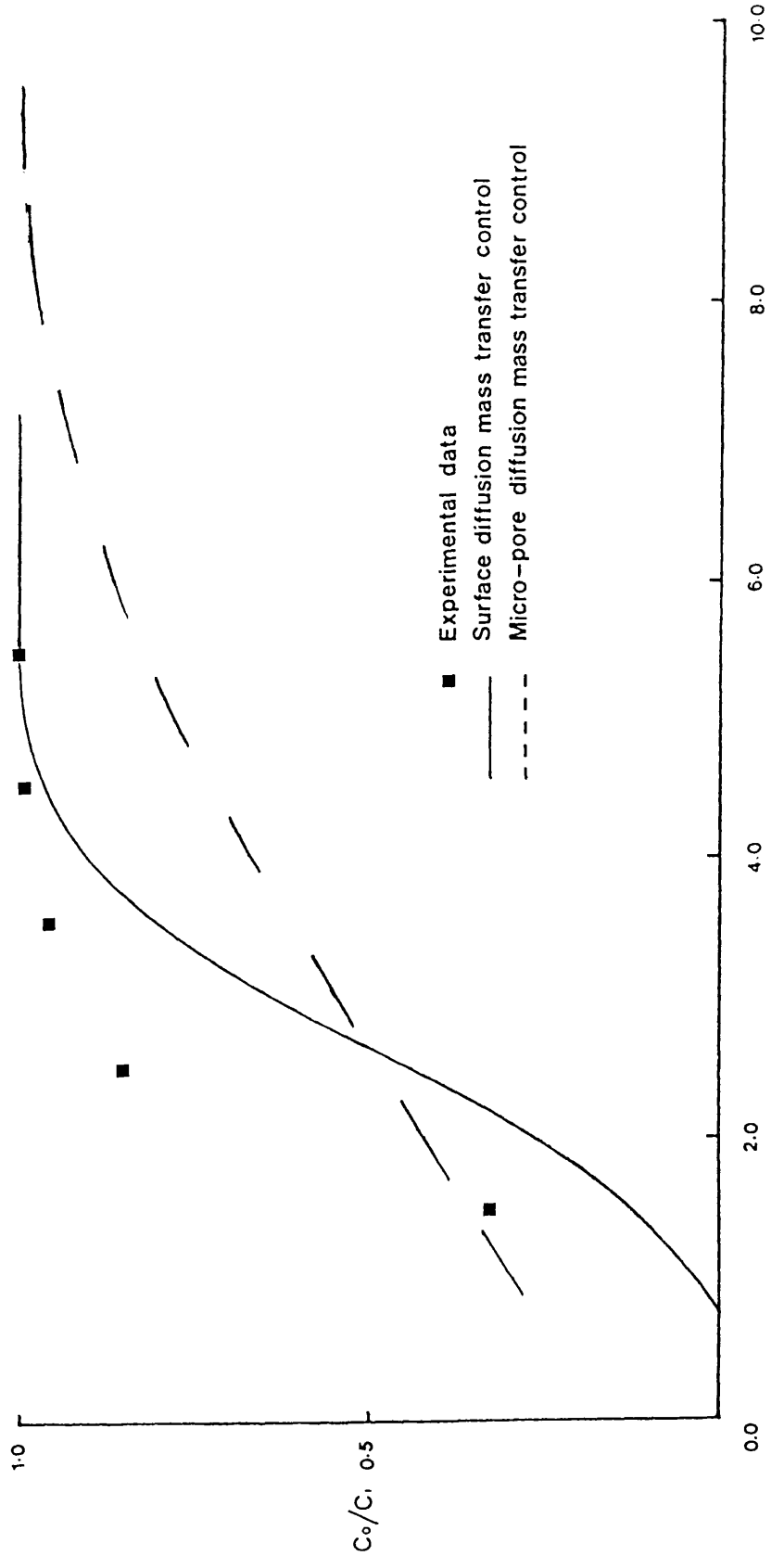

Figure 71 Breakthrough curve of methane ($C = 6.42 \times 10^{-5}$ mol cm^{-3}).

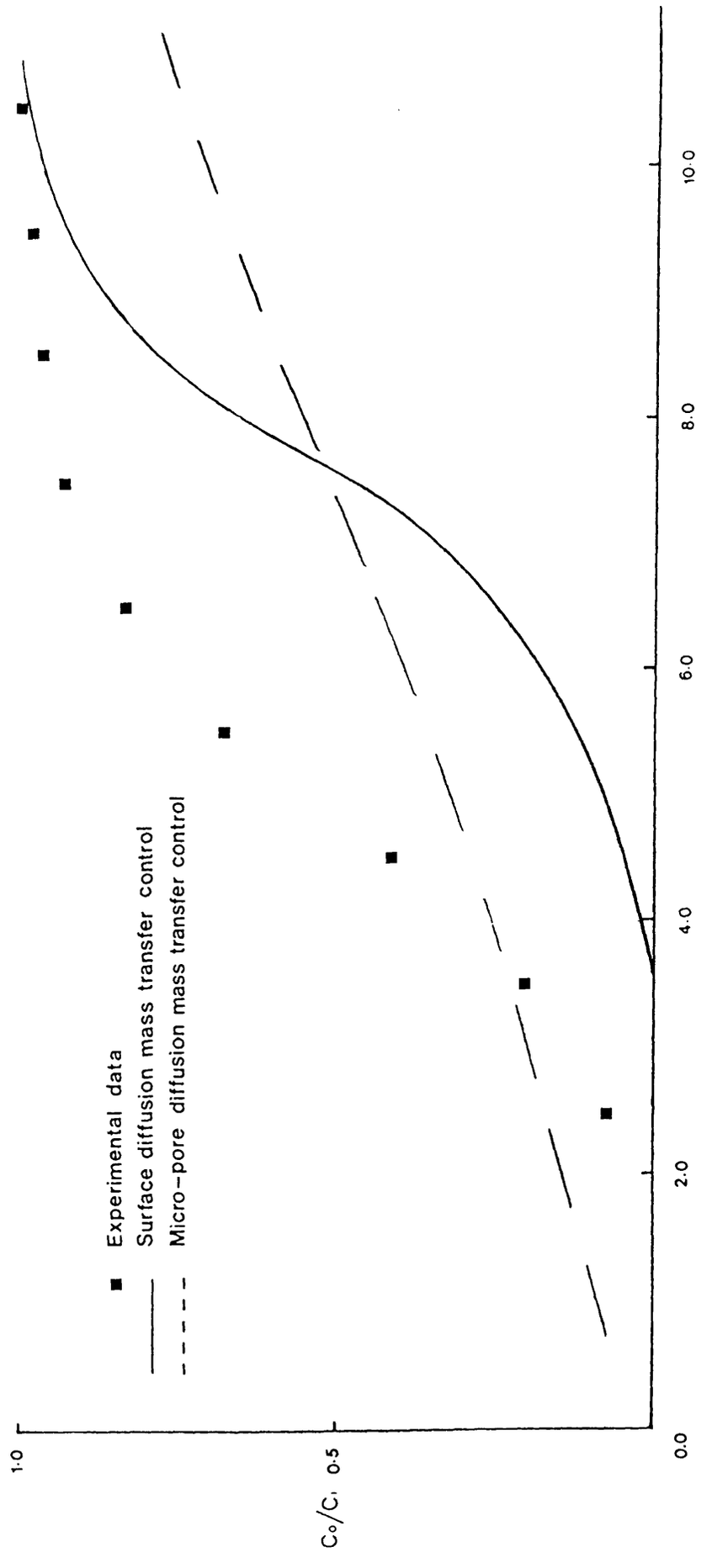

Figure 72 Breakthrough curve of methane ($C = 18.4 \times 10^{-5}$ mol cm^{-3}).

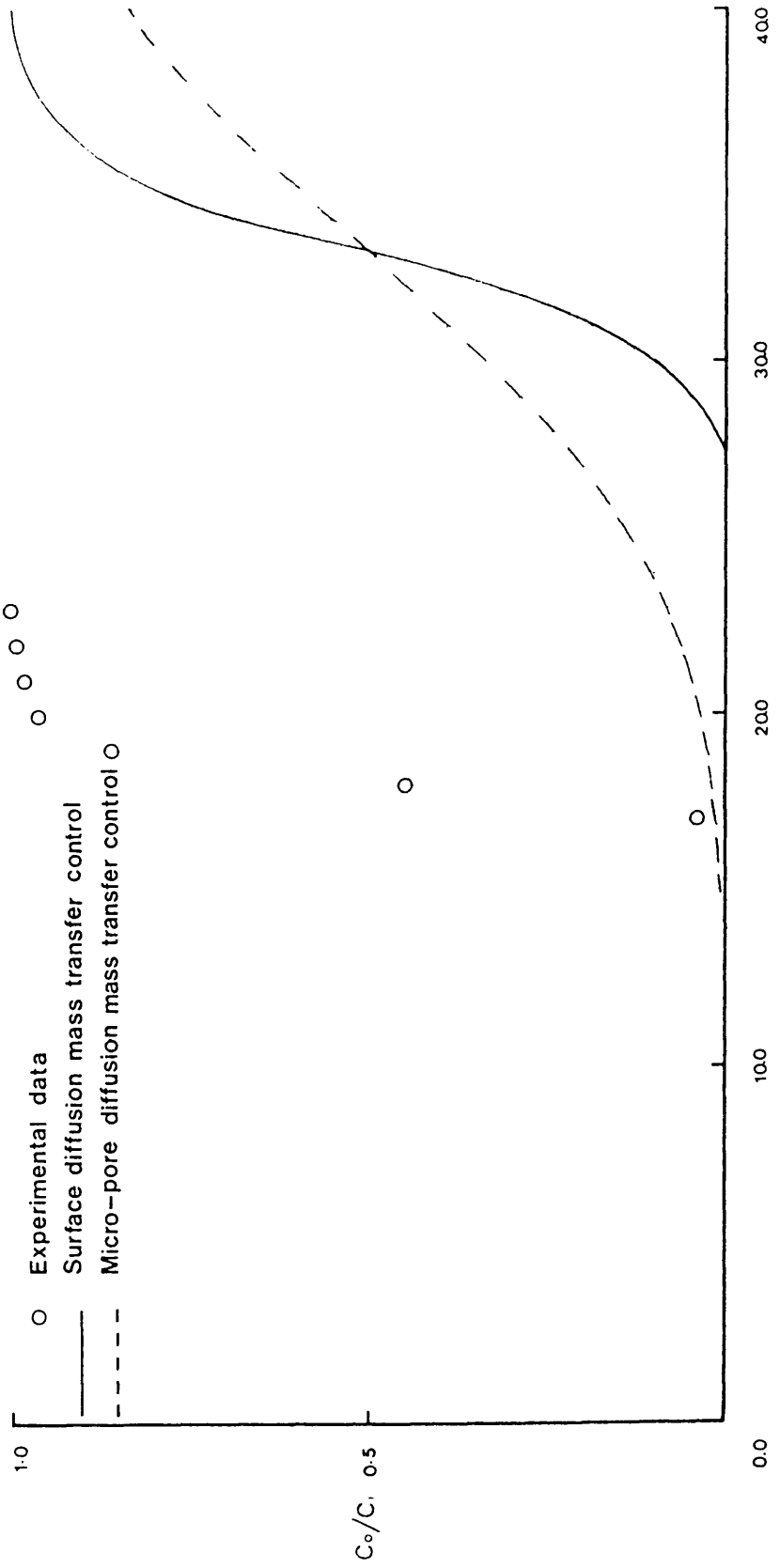

Figure 73 Breakthrough curve of carbon dioxide ($C = 2.0 \times 10^{-5}$ mol cm^{-3}).

rate determining step.

2. Binary Component Breakthrough Curves

The finite difference mathematical approximation which was used for single component adsorption (see Chapter 4), was modified for binary component adsorption. Two kinetic models which describe the adsorption of each component in the mixture were employed, together with the differential equation describing gas phase and adsorbed phase concentrations as a function of bed position and time. The numerical solution of these equations was then compared with the experimental results. The modified extended Langmuir and Freundlich-type multicomponent models successfully predicted the experimental data for binary mixtures (Chapter 5, Sections 2.4 and 2.5), and are applicable to computation of binary breakthrough curves for the equilibrium relation. In this work, the modified extended Langmuir model was chosen for this purpose.

Accordingly, equations (4.3) and (4.4), with the modified extended Langmuir isotherm serving to define the relationship of equation (4.4), were utilised to compute the breakthrough curves of both components (methane and carbon dioxide) from the experimental data. The linear driving force model failed to predict the experimental breakthrough curves for the binary adsorption of methane and carbon dioxide. Therefore, the equilibrium model was used to describe the binary adsorption. Figure 74 shows the comparison between the computed and experimental breaktbrough of a methane and carbon dioxide binary mixture. The model gives a reasonable fit.

The computer program used for this prediction is summarised in Appendix 9.

3. Adsorption-desorption Cycle of Binary Mixtures on 5A Molecular Sieves

A series of experiments was studied for pure and dilute mixtures of methane and carbon dioxide. The experiments were performed by passing a

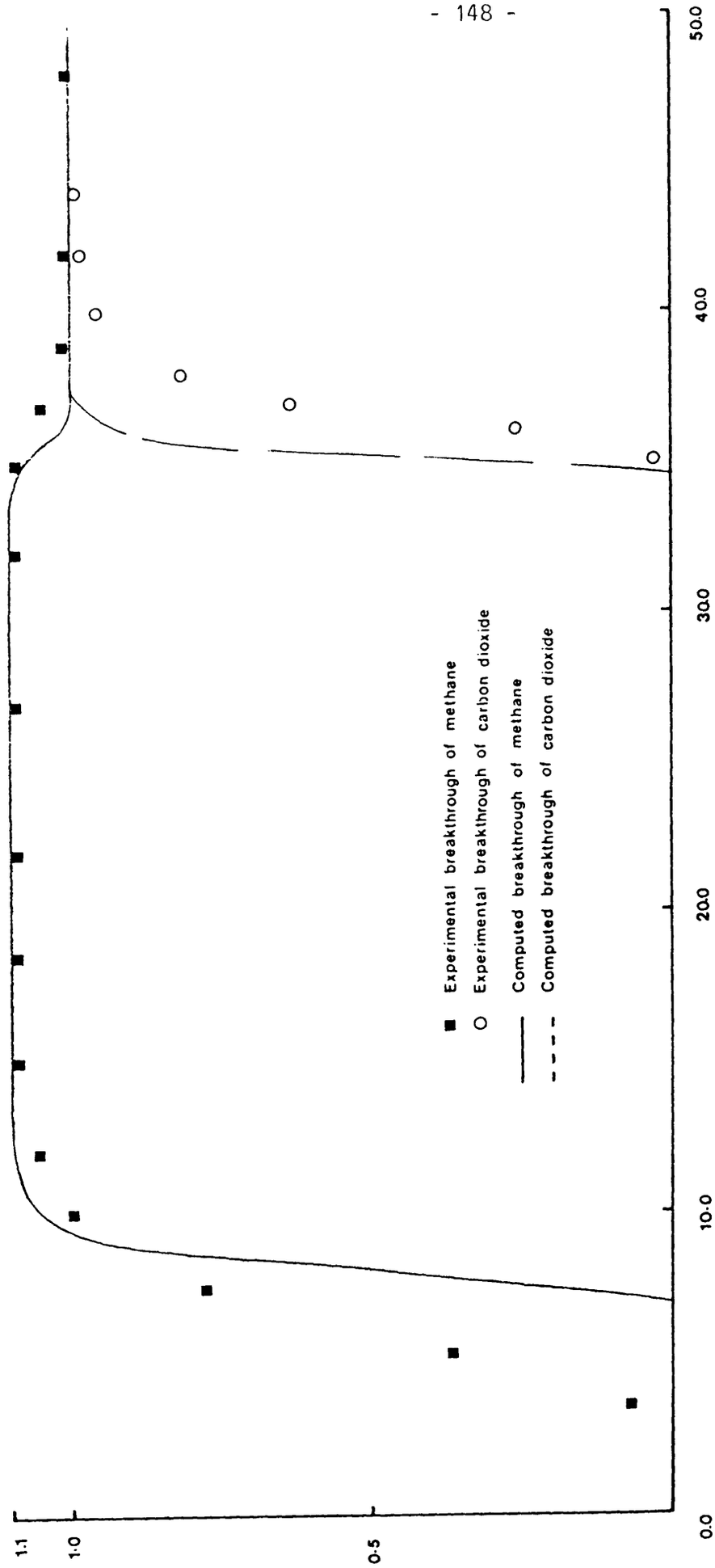

Figure 74 Breakthrough curve for a binary mixture of methane and carbon dioxide, composition: 90.12% N_2, 5.64% CH_4, 4.24% CO_2, p = 81,6 atmos gauge.

mixture of methane and carbon dioxide through the adsorbent bed at 25° C and initiating desorption by passing only nitrogen at a time soon after the breakthrough of methane had occurred, but well before the inevitable breakthrough of carbon dioxide. Desorption was accomplished by means of a step decrease to zero of adsorbate concentration, with only nitrogen carrier gas being fed to the adsorbent bed from that moment until all the carbon dioxide had been desorbed. This may have significance in practical application for the separation of gases.

4. Experimental Procedure

The experimental procedure is the same as that employed for ternary mixtures (see Chapter 4, Section 4).

5. Results

Figure 75 shows the experimental adsorption-desorption cycle for a pure methane-carbon dioxide mixture. For a dilute mixture, Figures 76 and 77 show the separation cycles that were performed under identical conditions, with the exception that nitrogen carrier gas was reconnected to the bed inlet at different times.

In all cases, the rate of desorption was slower than the rate of adsorption for both methane and carbon dioxide. The rate of desorption of methane is much faster than the rate of desorption of carbon dioxide. Also, the adsorption rate of methane remains constant during the initial period, then rapidly decreases as the amount in the adsorbed phase decreases.

6. Mathematical Modelling of the Experimental Adsorption-desorption Cycle

The equilibrium control model was used to predict the adsorption part of the cycle for binary mixtures of methane and carbon dioxide, whilst for desorption, two models were used. These are the linear driving force and the equilibrium models (Chapter 1, Sections 3.4 and 3.5). The linear

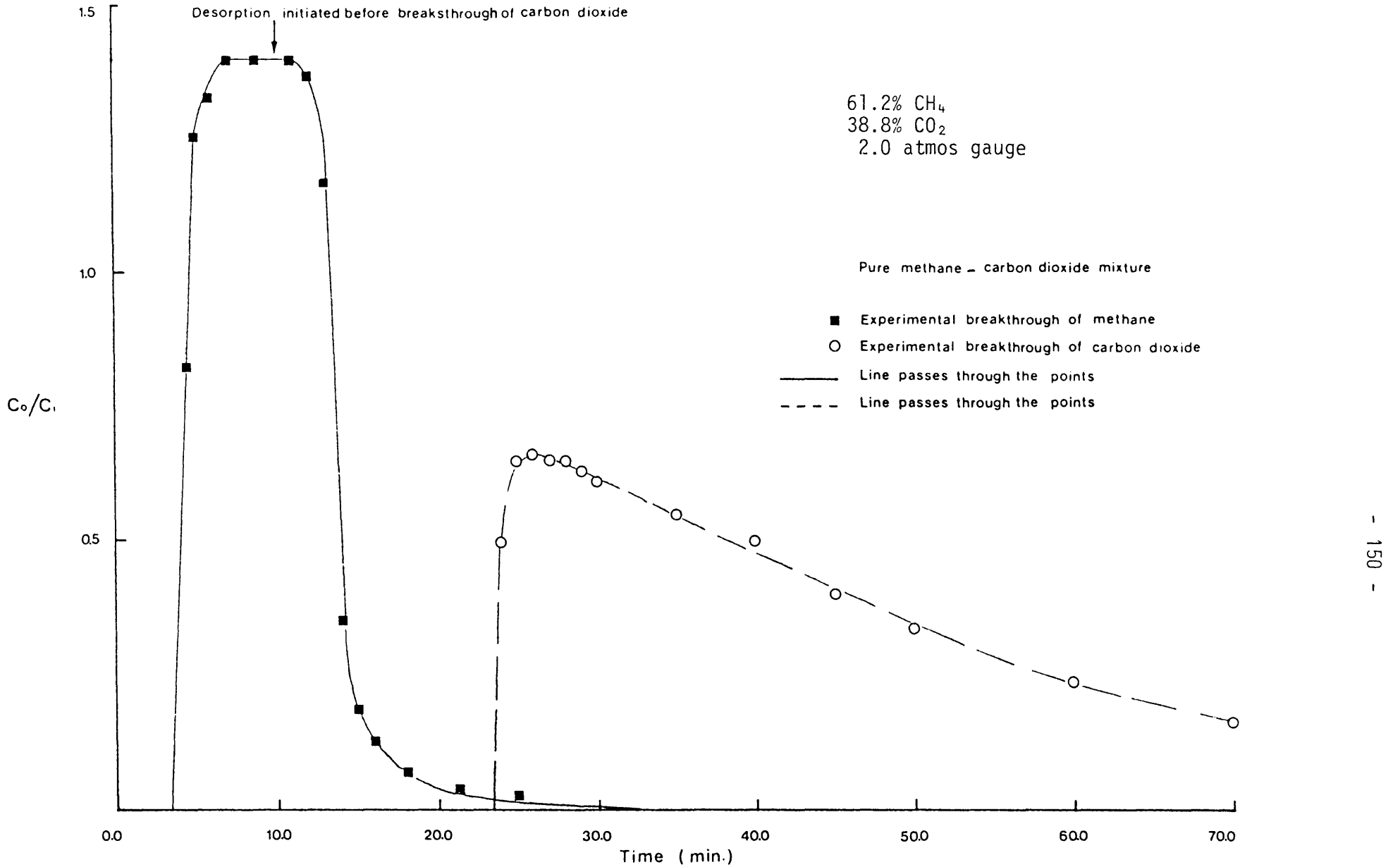

Figure 75 Experimental adsorption-desorption cycle for a pure binary mixture of methane and carbon dioxide.

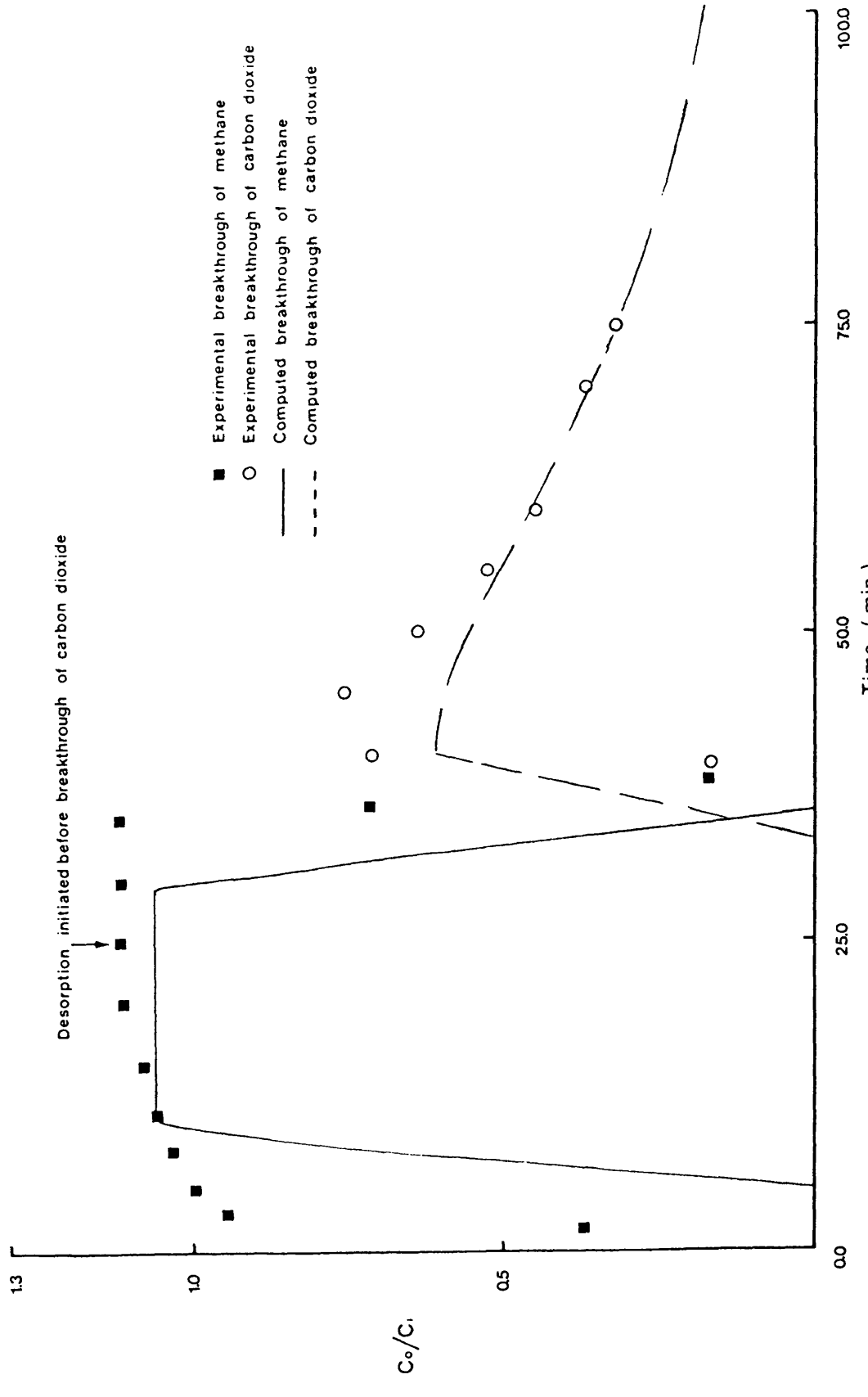

Figure 76 Binary gas mixture adsorption-desorption cycle, composition: 90.12% N_2, 5.64% CH_4, 4.24% CO_2, p = 13.6 atmos gauge.

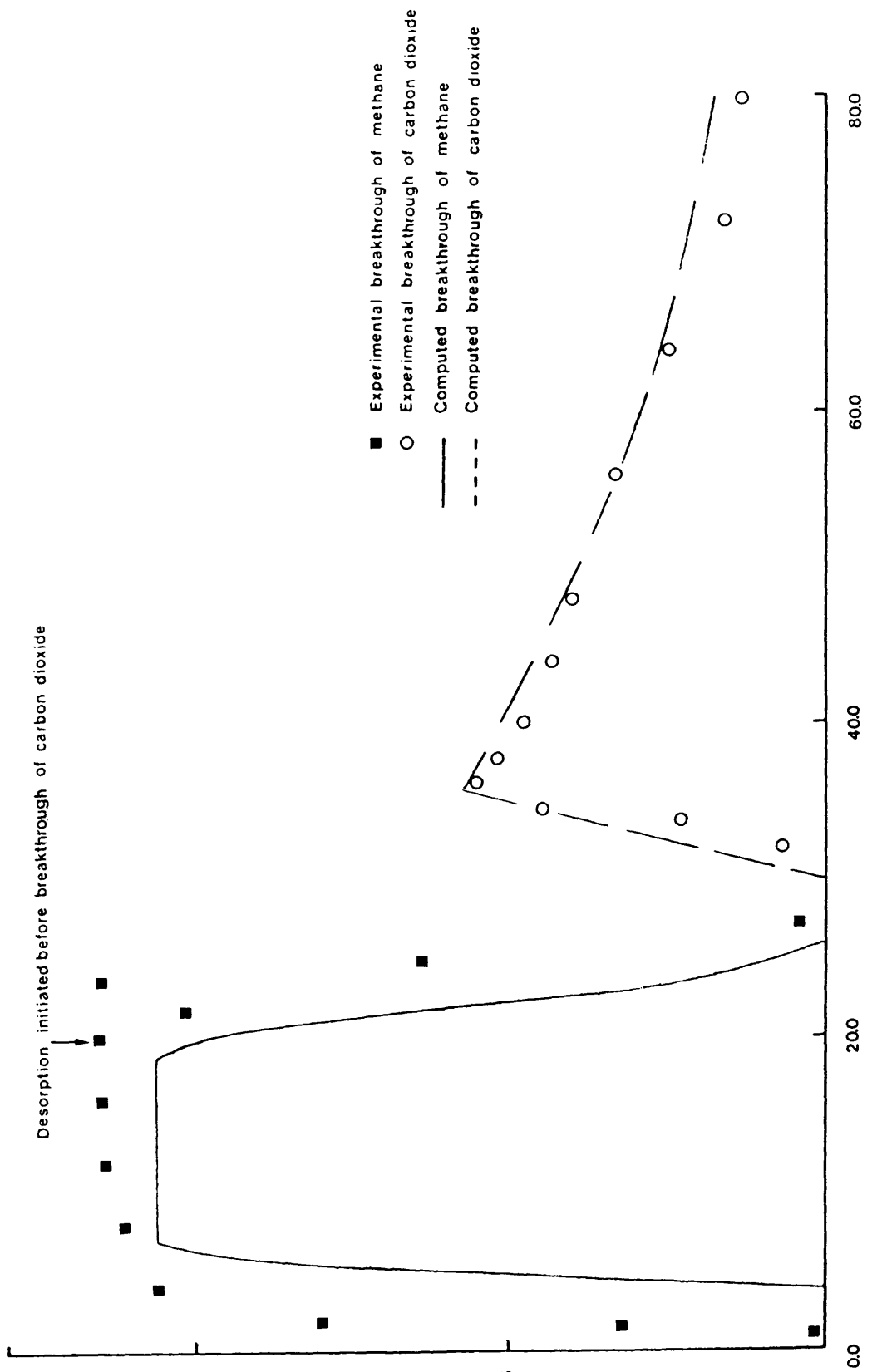

Figure 77 Binary gas mixture adsorption-desorption cycle, composition: 90.12% N_2, 5.64% CH_4, 4.24% CO_2, p = 13.6 atmos. gauge.

driving force model failed to describe the desorption part of the cycle. Therefore, the equilibrium model was used to describe the whole adsorption-desorption cycle.

Figures 76 and 77 show the experimental and computed adsorption-desorption cycles for a binary mixture of methane and carbon dioxide, where desorption starts after 20 and 25 minutes respectively of adsorption and before the breakthrough of carbon dioxide. The model satisfactorily described the experimental results. An overlap between the components occurs, as the desorption time increases, as shown in Figure 76.

Appendix 10 gives the computer program used for the adsorption-desorption cycle prediction.

Conclusion

The experimental adsorption-desorption cycles for both pure and dilute mixtures showed that carbon dioxide can be separated from a binary mixture of methane and carbon dioxide, provided the time at which desorption is initiated is carefully chosen.

APPENDIX 1

Calculation of the allowable flowrate

The maximum gas flowrate in a packed bed for different conditions of temperature and pressure may be calculated by the correlation given by Ledoux.[49]

$$\frac{G^2}{dg.da.D.g} = 0.0167 \qquad (A.1)$$

where: G = mass velocity of gas g cm^{-2} s^{-1};

dg = gas density g cm^{-3};

da = adsorbent bed density = 0.732 g cm^{-3};[46]

D = average particle diameter = 0.0427 cm; and

g = acceleration due to gravity = 980.1 cm s^{-2}.

The density of a gas can be calculated as:

$$\rho = \frac{p \times M\ wt}{ZRT} \qquad \text{(for high pressure)} \qquad (A.2)$$

at pressure = 90 atmos and t = 25° C.

The average density of gas mixtures, for different concentrations of adsorbate in nitrogen, calculated from equation (A.2) is 0.1 g cm^{-3}. Therefore:

$$\frac{G^2}{0.1 \times 0.732 \times 0.0427 \times 980.1} = 0.0167$$

$$G = 0.226 \text{ g cm}^{-2} \text{ s}^{-1}$$

$$\text{Maximum flowrate} = \frac{\text{mass velocity of gas} \times \text{cross-sectional area of adsorption column}}{\text{density of the gas}}$$

$$= \frac{0.226 \times \pi(\frac{0.493}{2})^2 \times 60}{0.1} = 25.88 \text{ cm}^3 \text{ min}^{-1} \text{ at 90 atmos.} \qquad (A.3)$$

Assuming ideal gas behaviour:

$$p_1 v_1 = p_2 v_2 \qquad (A.4)$$

$$90 \times 25.88 = 1 \times v_2$$

$v_2 = 2329.2$ cm^3 min^{-1} (flowrate at atmospheric pressure, *i.e.*, outlet flowrate)

At low pressure p = 1 atmos, t = 25^0 C

The average density of the gas mixture, for different concentrations of adsorbate in nitrogen = 0.0012 g cm^{-3}.

By applying equations (A.1) and (A.3), the maximum flowrate is 237.0 cm^3 min^{-1} (*i.e.*, the outlet flowrate).

Hence, the outlet flowrate ranges from 2329.2-237.0 for high and low pressure. Actual design velocities should be somewhat lower than might be indicated by equation (A.1), because of uncertainties inherent in the use of an average particle size and bed density for the adsorbents, as well as the density of the gas mixture. Therefore the outletflowrate used during the experiments was between 35-100 cm^3 min^{-1}.

APPENDIX 2

Determination of the thickness of the pipes

The minimum wall thickness may be estimated[50] from the following equation:

$$t_m = \frac{P_b \times D_m}{2S_T} \qquad (A.5)$$

where t_m = minimum wall thickness in.

P_b = bursting pressure (difference between internal and external pressure), psi.

S_T = tensile strength, psi

D_m = mean diameter, in.

The stainless steel used was of type 316S with a tensile strength of 75000 psi.

The dimension of the adsorption column used was 0.194" and 0.25" inside and outside diameters respectively. For the other pipes used at high pressure, the dimensions were 0.055" and 0.125" inside and outside diameters respectively.

By applying equation (A.5) to the adsorption column, at pressure = 100 atmos and inside diameter = 0.194", $t_m = \frac{100 \times 14.7 \times 0.194}{2 \times 75000} = 0.0019"$ the minimum thickness. The wall thickness used for the desorption column $= \frac{0.25-0.194}{2} = 0.028"$, which is much higher than the calculated value.

The inside diameter for the other pipes was 0.055", $t_m = \frac{100 \times 14.7 \times 0.055}{2 \times 75000} = 0.00054"$ the minimum thickness. The wall thickness used for the other pipes $= \frac{0.125-0.055}{2} = 0.035"$, which is much greater than the calculated value, (see Table 2.3, Chapter 2).

APPENDIX 3

Mixture 1

P (atmos)	c_{CH_4} (mol $cm^{-3} \times 10^5$)	$c_{C_2H_6}$ (mol $cm^{-3} \times 10^5$)	$c_{C_3H_8}$ (mol $cm^{-3} \times 10^5$)	q_{CH_4} (mol $g^{-1} \times 10^4$)	$q_{C_2H_6}$ (mol $g^{-1} \times 10^4$)	$q_{C_3H_8}$ (mol $g^{-1} \times 10^4$)
12	4.1810	2.0905	2.0905	3.0366	5.2800	13.7500
10	3.5380	1.7690	1.7690	2.9717	4.8500	13.0700
8	2.8950	1.4475	1.4475	2.7573	4.2940	12.5440
6	2.2920	1.1460	1.1460	2.5123	3.8890	12.4000
4	1.7000	0.8500	0.8500	2.2522	3.3200	12.0000
2	1.0450	0.5225	0.5225	1.9874	2.8525	11.5300
0.5	0.5400	0.2700	0.2700	1.1500	2.0400	11.0144
Mixture 2						
12	7.1936	3.0840	2.1533	4.8100	8.2000	16.3300
10	6.0870	2.6100	1.8220	4.5300	8.0000	16.2400
8	4.9800	2.1350	1.4907	4.2640	7.9000	16.0000
6	3.8735	1.6600	1.1594	3.7800	7.5000	15.6000
4	2.7670	1.1860	0.8282	3.2000	6.2000	14.7100
2	1.6600	0.7120	0.4969	2.9400	5.5000	13.6000

APPENDIX 4

Equilibrium control model

```
      implicit real*8(a-h,o-z)
      real*8 A,B,C
      external condition_(descriptors),nothing
      common c(k),clast(k),u,delq
      call condition_("underflow",nothing)
      read (70,100) k,n,delt,delz,rowb,pros
      read (70,100) a,b,u,c
      100 format(v)
      do 333 i=1,k
      c(i)=0.0d0
      clast(i)=0.0d0
  333 continue
      c(1)=c
      clast(1)=c
      j=1
      do 4 i=2,k
      delq=a*b*c(i-1)/(1.0+b*c(i-1))-(a*b*clast(i)/(1.0+b*clast(i)))
      al=clast(i)+(delt/delz)*u*c(i-1)-(rowb/pros)*delq
      cl=1.0+(delt/delz)*u
      c(i)=(al/cl)
    4 continue
      do 20 i=2,k
      clast(i)=c(i)
   20 continue
      write(2,101) j,c(k)
  101 format (5x,i5,3x,d11.4)
      do 7 j=2,n
      do 8 i=2,k
      delq=a*b*c(i-1)/(1.0+b*c(i-1))-(a*b*clast(i)/(1.0+b*clast(i)))
      al=clast(i)+(delt/delz)*u*c(i-1)-(rowb/pros)*delq
      cl=1.0+(delt/delz)*u
      c(i)=(al/cl)
    8 continue
      do 11 i=2,k
      clast(i)=c(i)
   11 continue
      write(2,104) j,c(k)
      104format(5x,i5,3x,d11.4)
    7 continue
      stop
      end
```

APPENDIX 5

Linear driving force model

```
      implicit real*8(a-h,o-z)
      external condition_(descriptors),nothing
      common c(k),clast(k),u,delq
      call condition_("underflow",nothing)
      read (80,100) k,n,delt,delz,rowb,pros
      read (80,100) a,b,u,c,gf
      qstar=a*b*c/(1.0+b*c)
      do 333 i=1,k
      c(i)=0.0d0
      clast(i)=0.0d0
  333 continue
      c(1)=c
      clast(1)=c
      j=1
      do 4 i=2,k
      delq=delt*gf*(qstar-(a*b*clast(i-1)/(1.0+b*clast(i-1))))
      al=clast(i)+(delt/delz)*u*c(i-1)-(rowb/pros)*delq
      cl=1.0+(delt/delz)*u
      c(i)=(al/cl)
    4 continue
      do 20 i=2,k
      clast(i)=c(i)
   20 continue
      write(6,101) j,c(k)
  101 format (5x,i5,3x,d11.4)
      do 7 j=2,n
      do 8 i=2,k
      delq=delt*gf*(qstar-(a*b*clast(i-1)/(1.0+b*clast(i-1))))
      al=clast(i)+(delt/delz)*u*c(i-1)-(rowb/pros)*delq
      cl=1.0+(delt/delz)*u
      c(i)=(al/cl)
    8 continue
      do 11 i=2,k
      clast(i)=c(i)
   11 continue
      write(6,104) j,c(k)
  104 format(5x,i5,3x,d11.4)
    7 continue
      stop
      end
```

APPENDIX 6

Equilibrium control model for a ternary mixture

```
      implicit real*8(a-h,o-z)
      real*8 A,B,C
      external condition_(descriptors),nothing
      common cm(k),ce(k),cmlast(k),celast(k),cp(k),cplast(k)
      common u,delqm,delqe,delqp
      call condition_("underflow",nothing)
      read (82,100) k,n,delt,delz,rowb,pro
      read (82,100) u,cm,ce,cp
      read (82,100) ao,alo,all,al2,al3,al4,al5
      read (82,100) bo,b2o,b21,b22,b23,b24,b25
      read (82,100) po,p3o,p31,p32,p33,p34,p35
      do 111 i=1,k
      cm(i)=0.0d0
      cmlast(i)=0.0d0
      ce(i)=0.0d0
      celast(i)=0.0d0
      cp(i)=0.0d0
      cplast(i)=0.0d0
111   continue
      cm(1)=cm
      cmlast(1)=cm
      ce(1)=ce
      celast(1)=ce
      cp(1)=cp
      cplast(1)=cp
      j=1
      do 20 i=2,k
      w1=cm(i-1)**all+al2*(ce(i-1)**al3)+al4*(cp(i-1)**al5)
      w2=cmlast(i)**all+al2*(celast(i)**al3)+al4*(cplast(i)**al5)
      delqm=ao*(cm(i-1)**alo)/w1-(ao*(cmlast(i)**alo)/w2)
      v1=b21*(cm(i-1)**b22)+ce(i-1)**b23+b24*(cp(i-1)**b25)
      v2=b21*(cmlast(i)**b22)+celast(i)**b23+b24*(cplast(i)**b25)
      delqe=bo*(ce(i-1)**b2o)/v1-(bo*(celast(i)**b2o)/v2)
      f1=p31*(cm(i-1)**p32)+p33*(ce(i-1)**p34)+(cp(i-1)**p35)
      f2=p31*(cmlast(i)**p32)+p33*(celast(i)**p34)+(cplast(i)**p35)
      delqp=po*(cp(i-1)**p3o)/f1-(po*(cplast(i)**p3o)/f2)
      alm=cmlast(i)+(delt/delz)*u*cm(i-1)-(rowb/pros)*delqm
      ale=celast(i)+(delt/delz)*u*ce(i-1)-(rowb/pros)*delqe
      alp=cplast(i)+(delt/delz)*u*cp(i-1)-(rowb/pros)*delqp
      clm=1.0+(delt/delz)*u
      cle=1.0+(delt/delz)*u
      clp=1.0+(delt/delz)*u
      cm(i)=alm/clm
      ce(i)=ale/cle
      cp(i)=alp/clp
 20   continue
      do 25 i=2,k
      cmlast(i)=cm(i)
      celast(i)=ce(i)
      cplast(i)=cp(i)
```

```
 25 continue
    write(2,101) j,cm(k),ce(k),cp(k)
101 format (5x,i5,3x,f14.10,3x,f14.10,3x,f14.10)
    do 21 j=2,n
    do 22 i=2,k
    w1=cm(i-1)**a11+a12*(ce(i-1)**a13)+a14*(cp(i-1)**a15)
    w2=cmlast(i)**a11+a12*(celast(i)**a13)+a14*(cplast(i)**a15)
    delqm=ao*(cm(i-1)**alo)/w1-(ao*(cmlast(i)**alo)/w2)
    v1=b21*(cm(i-1)**b22)+ce(i-1)**b23+b24*(cp(i-1)**b25)
    v2=b21*(cmlast(i)**b22)+celast(i)**b23+b24*(cplast(i)**b25)
    delqe=bo*(ce(i-1)**b2o)/v1-(bo*(celast(i)**b2o)/v2)
    f1=p31*(cm(i-1)**p32)+p33*(ce(i-1)**p34)+(cp(i-1)**p35)
    f2=p31*(cmlast(i)**p32)+p33*(celast(i)**p34)+(cplast(i)**p35)
    delqp=po*(cp(i-1)**p3o)/f1-(po*(cplast(i)**p3o)/f2)
    alm=cmlast(i)+(delt/delz)*u*cm(i-1)-(rowb/pros)*delqm
    ale=celast(i)+(delt/delz)*u*ce(i-1)-(rowb/pros)*delqe
    alp=cplast(i)+(delt/delz)*u*cp(i-1)-(rowb/pros)*delqp
    clm=1.0+(delt/delz)*u
    cle=1.0+(delt/delz)*u
    clp=1.0+(delt/delz)*u
    cm(i)=alm/clm
    ce(i)=ale/cle
    cp(i)=alp/clp
 22 continue
    do 11 i=2,k
    cmlast(i)=cm(i)
    celast(i)=ce(i)
    cplast(i)=cp(i)
 11 continue
    write(2,101) j,cm(k),ce(k),cp(k)
 21 continue
    stop
    end
```

APPENDIX 7

Adsorption_desorption cycle for a ternary mixture

```
      implicit real*8(a-h,o-z)
      real*8 A,B,C
      external condition_(descriptors),nothing
      common cm(k),ce(k),cmlast(k),celast(k),cp(k),cplast(k)
      common u,delqm,delqe,delqp
      call condition_("underflow",nothing)
      read (82,100) k,n1,n2,delt,delz,rowb,pro
      read (82,100) u,cm,ce,cp
      read (82,100) ao,alo,a11,a12,a13,a14,a15
      read (82,100) bo,b2o,b21,b22,b23,b24,b25
      read (82,100) po,p3o,p31,p32,p33,p34,p35
      do 111 i=1,k
      cm(i)=0.0d0
      cmlast(i)=0.0d0
      ce(i)=0.0d0
      celast(i)=0.0d0
      cp(i)=0.0d0
      cplast(i)=0.0d0
111   continue
      cm(1)=cm
      cmlast(1)=cm
      ce(1)=ce
      celast(1)=ce
      cp(1)=cp
      cplast(1)=cp
      j=1
      do 20 i=2,k
      w1=cm(i-1)**a11+a12*(ce(i-1)**a13)+a14*(cp(i-1)**a15)
      w2=cmlast(i)**a11+a12*(celast(i)**a13)+a14*(cplast(i)**a15)
      delqm=ao*(cm(i-1)**alo)/w1-(ao*(cmlast(i)**alo)/w2)
      v1=b21*(cm(i-1)**b22)+ce(i-1)**b23+b24*(cp(i-1)**b25)
      v2=b21*(cmlast(i)**b22)+celast(i)**b23+b24*(cplast(i)**b25)
      delqe=bo*(ce(i-1)**b2o)/v1-(bo*(celast(i)**b2o)/v2)
      f1=p31*(cm(i-1)**p32)+p33*(ce(i-1)**p34)+(cp(i-1)**p35)
      f2=p31*(cmlast(i)**p32)+p33*(celast(i)**p34)+(cplast(i)**p35)
      delqp=po*(cp(i-1)**p3o)/f1-(po*(cplast(i)**p3o)/f2)
      alm=cmlast(i)+(delt/delz)*u*cm(i-1)-(rowb/pros)*delqm
      ale=celast(i)+(delt/delz)*u*ce(i-1)-(rowb/pros)*delqe
      alp=cplast(i)+(delt/delz)*u*cp(i-1)-(rowb/pros)*delqp
      clm=1.0+(delt/delz)*u
      cle=1.0+(delt/delz)*u
      clp=1.0+(delt/delz)*u
      cm(i)=alm/clm
      ce(i)=ale/cle
      cp(i)=alp/clp
 20   continue
      do 25 i=2,k
      cmlast(i)=cm(i)
      celast(i)=ce(i)
      cplast(i)=cp(i)
```

```
 25 continue
    write(2,101) j,cm(k),ce(k),cp(k)
101 format (5x,i5,3x,f14.10,3x,f14.10,3x,f14.10)
    do 21 j=2,n2
    do 22 i=2,k
    w1=cm(i-1)**a11+a12*(ce(i-1)**a13)+a14*(cp(i-1)**a15)
    w2=cmlast(i)**a11+a12*(celast(i)**a13)+a14*(cplast(i)**a15)
    delqm=ao*(cm(i-1)**a1o)/w1-(ao*(cmlast(i)**a1o)/w2)
    v1=b21*(cm(i-1)**b22)+ce(i-1)**b23+b24*(cp(i-1)**b25)
    v2=b21*(cmlast(i)**b22)+celast(i)**b23+b24*(cplast(i)**b25)
    delqe=bo*(ce(i-1)**b2o)/v1-(bo*(celast(i)**b2o)/v2)
    f1=p31*(cm(i-1)**p32)+p33*(ce(i-1)**p34)+(cp(i-1)**p35)
    f2=p31*(cmlast(i)**p32)+p33*(celast(i)**p34)+cplast(i)**p35
    delqp=po*(cp(i-1)**p3o)/f1-(po*(cplast(i)**p3o)/f2)
    alm=cmlast(i)+(delt/delz)*u*cm(i-1)-(rowb/pros)*delqm
    ale=celast(i)+(delt/delz)*u*ce(i-1)-(rowb/pros)*delqe
    alp=cplast(i)+(delt/delz)*u*cp(i-1)-(rowb/pros)*delqp
    clm=1.0+(delt/delz)*u
    cle=1.0+(delt/delz)*u
    clp=1.0+(delt/delz)*u
    cm(i)=alm/clm
    ce(i)=ale/cle
    cp(i)=alp/clp
 22 continue
    do 11 i=2,k
    cmlast(i)=cm(i)
    celast(i)=ce(i)
    cplast(i)=cp(i)
 11 continue
    write(2,101) j,cm(k),ce(k),cp(k)
    if (j.lt.n1) go to 21
    cm(1)=0.0d0
    ce(1)=0.0d0
    cp(1)=0.0d0
 21 continue
    stop
    end
```

APPENDIX 8

Mixture 1:

p	c_{CH_4}	c_{CO_2}	q_{CH_4}	q_{CO_2}
(atmos gauge)	(mol $cm^{-3} \times 10^5$)	(mol $cm^{-3} \times 10^5$)	(mol $g^{-1} \times 10^4$)	(mol $g^{-1} \times 10^4$)
82.633	19.060	14.330	10.35	43.0
69.030	15.923	11.970	9.63	42.1
55.422	12.784	9.611	8.20	41.6
41.816	9.646	7.251	7.12	39.7
28.211	6.507	4.892	6.60	37.7

Mixture 2:

69.03	9.940	13.920	5.40	42.3
55.422	7.980	11.175	5.11	41.9
41.816	6.020	8.430	4.89	41.3
28.211	4.061	5.700	3.81	39.2

APPENDIX 9

Equilibrium control model for a binary mixture

```
      implicit real*8(a-h,o-z)
      real*8 A,B,C
      external condition_(descriptors),nothing
      common cm(k),ce(k),u,delqm,delqe,cmlast(k),celast(k)
      call condition_("underflow",nothing)
      read (81,100) k,n,delt,delz,rowb,pros
      read (81,100) am,ae,bm1,bm2,be1,be2,cm,ce,u
      100 format(v)
      do 111 i=1,k
      cm(i)=0.0d0
      cmlast(i)=0.0d0
      ce(i)=0.0d0
      celast(i)=0.0d0
  111 continue
      cm(1)=cm
      cmlast(1)=cm
      ce(1)=ce
      celast(1)=ce
      j=1
      do 20 i=2,k
      w1=1.0+bm1*cm(i-1)+be1*ce(i-1)
      w2=1.0+bm1*cmlast(i)+be1*celast(i)
      delqm=(am*bm1*cm(i-1)/w1)-(am*bm1*cmlast(i)/w2)
      v1=1.0+bm2*cm(i-1)+be2*ce(i-1)
      v2=1.0+bm2*cmlast(i)+be2*celast(i)
      delqe=(ae*be2*ce(i-1)/v1)-(ae*be2*celast(i)/v2)
      alm=cmlast(i)+(delt/delz)*u*cm(i-1)-(rowb/pros)*delqm
      ale=celast(i)+(delt/delz)*u*ce(i-1)-(rowb/pros)*delqe
      clm=1.0+(delt/delz)*u
      cle=1.0+(delt/delz)*u
      cm(i)=alm/clm
      ce(i)=ale/cle
   20 continue
      do 5 i=2,k
      cmlast(i)=cm(i)
      celast(i)=ce(i)
    5 continue
      write(7,101) j,cm(k),ce(k)
  101 format (5x,i5,3x,f14.10,3x,f14.10)
      do 21 j=2,n
      do 22 i=2,k
      w1=1.0+bm1*cm(i-1)+be1*ce(i-1)
      w2=1.0+bm1*cmlast(i)+be1*celast(i)
      delqm=(am*bm1*cm(i-1)/w1)-(am*bm1*cmlast(i)/w2)
      v1=1.0+bm2*cm(i-1)+be2*ce(i-1)
      v2=1.0+bm2*cmlast(i)+be2*celast(i)
      delqe=(ae*be2*ce(i-1)/v1)-(ae*be2*celast(i)/v2)
      alm=cmlast(i)+(delt/delz)*u*cm(i-1)-(rowb/pros)*delqm
      ale=celast(i)+(delt/delz)*u*ce(i-1)-(rowb/pros)*delqe
      clm=1.0+(delt/delz)*u
```

```
      cle=1.0+(delt/delz)*u
      cm(i)=alm/clm
      ce(i)=ale/cle
   22 continue
      do 11 i=2,k
      cmlast(i)=cm(i)
      celast(i)=ce(i)
   11 continue
      write(7,101) j,cm(k),ce(k)
   21 continue
      stop
      end
```

APPENDIX 10

Adsorption_desorption cycle for a binary mixture

```
      implicit real*8(a-h,o-z)
      real*8 A,B,C
      external condition_(descriptors),nothing
      common cm(k),ce(k),u,cmlast(k),celast(k),delqm,delqe
      call condition_("underflow",nothing)
      read (81,100) k,n1,n2,delt,delz,rowb,pros
      read (81,100) am,ae,bm1,bm2,be1,be2,cm,ce,u
      100 format(v)
      do 111 i=1,k
      cm(i)=0.0d0
      cmlast(i)=0.0d0
      ce(i)=0.0d0
      celast(i)=0.0d0
111   continue
      cm(1)=cm
      cmlast(1)=cm
      ce(1)=ce
      celast(1)=ce
      j=1
      do 20 i=2,k
      w1=1.0+bm1*cm(i-1)+be1*ce(i-1)
      w2=1.0+bm1*cmlast(i)+be1*celast(i)
      delqm=(am*bm1*cm(i-1)/w1)-(am*bm1*cmlast(i)/w2)
      v1=1.0+bm2*cm(i-1)+be2*ce(i-1)
      v2=1.0+bm2*cmlast(i)+be2*celast(i)
      delqe=(ae*be2*ce(i-1)/v1)-(ae*be2*celast(i)/v2)
      alm=cmlast(i)+(delt/delz)*u*cm(i-1)-(rowb/pros)*delqm
      ale=celast(i)+(delt/delz)*u*ce(i-1)-(rowb/pros)*delqe
      clm=1.0+(delt/delz)*u
      cle=1.0+(delt/delz)*u
      cm(i)=alm/clm
      ce(i)=ale/cle
 20   continue
      do 5 i=2,k
      cmlast(i)=cm(i)
      celast(i)=ce(i)
 5    continue
      write(7,101) j,cm(k),ce(k)
 101  format (5x,i5,3x,f14.10,3x,f14.10)
      do 21 j=2,n2
      do 22 i=2,k
      w1=1.0+bm1*cm(i-1)+be1*ce(i-1)
      w2=1.0+bm1*cmlast(i)+be1*celast(i)
      delqm=(am*bm1*cm(i-1)/w1)-(am*bm1*cmlast(i)/w2)
      v1=1.0+bm2*cm(i-1)+be2*ce(i-1)
      v2=1.0+bm2*cmlast(i)+be2*celast(i)
      delqe=(ae*be2*ce(i-1)/v1)-(ae*be2*celast(i)/v2)
      alm=cmlast(i)+(delt/delz)*u*cm(i-1)-(rowb/pros)*delqm
      ale=celast(i)+(delt/delz)*u*ce(i-1)-(rowb/pros)*delqe
      clm=1.0+(delt/delz)*u
```

```
      cle=1.0+(delt/delz)*u
      cm(i)=alm/clm
      ce(i)=ale/cle
   22 continue
      do 11 i=2,k
      cmlast(i)=cm(i)
      celast(i)=ce(i)
   11 continue
      write(7,101) j,cm(k),ce(k)
      if (j.lt.nl) go to 21
      cm(1)=0.0d0
      ce(1)=0.0d0
   21 continue
      stop
      end
```

REFERENCES

1. H.W. Collins Jr. and K.C. Chao, *A.I.Chem.E. Symp. Series*, 1973, 69, No.134, 9.
2. W.K. Lewis, E.R. Gilliland, B. Chertow and W.P. Cadogan, *Ind. Eng. Chem.*, 1950, 42, No.7, 1326.
3. D.W. Breck and T.B. Reed, *J. Am. Chem. Soc.*, 1956, 78, 5972.
4. E. Guccione, *Chem. Eng.*, 1965, 72, No.9, 104.
5. K.P. Tapan, R. Josef, F. Fritz and R.N. Mukherjea, *Ger. Chem. Eng.*, 1983, 6, 371.
6. R.A. Anderson, *A.C.S. Symp. Series*, *"Molecular Sieve II"*, 1977, 637.
7. R.A. Anderson and H.J. Springett, *I.Chem.E. Symp. Series*, 1976, 44, 1.
8. G.M. Barrow, "Physical Chemistry", 4th Ed., McGraw-Hill, New York, 1979.
9. H. Freundlich, *Z. Phys. Chem.*, 1906, 57, 385.
10. I. Langmuir, *J. Am. Chem. Soc.*, 1918, 40, 1361.
11. D.M. Young and A.D. Crowell, "Physical Adsorption of Gases", Butterworth, London, 1962.
12. E.C. Markham and A.F. Benton, *J. Am. Chem. Soc.*, 1931, 53, 497.
13. R.J. Grant and M. Manes, *Ind. Eng. Chem. Fundamentals*, 1964, 3, No.3. 221.
14. R.J. Grant and M. Manes, *Ind. Eng. Chem. Fundamentals*, 1966, 5, No.4, 490.
15. A.L. Myers and J.M. Prausnitz, *A.I.Chem.E. J.*, 1965, 11, No.1, 121.
16. A.L. Myers, *Ind. Eng. Chem.*, 1968, 60, 5.
17. A.J. Kidnay and A.C. Myers, *A.I.Chem.E. J.*, 1966, 12, No.5, 981.
18. D.M. Ruthven and K.F. Loughlin, *J. Chem. Soc., Faraday Trans.*, 1972, 68, 696.
19. D.M. Ruthven, K.F. Loughlin and K.A. Holborrow, *Chem. Eng. Sci.*, 1973, 28, 701.

20. D.M. Ruthven, *A.I.Chem.E. J.*, 1976, 22, No.4, 753.

21. W. Fritz and E.U. Schluender, *Chem. Eng. Sci.*, 1974, 29, 1279.

22. J.A.V. Butler and C. Ockrent, *J. Phys. Chem.*, 1930, 34, 2841.

23. E. Erdös and L. Jäger, *Coll. Czech. Chem. Commun.*, 1959, 24, 2851.

24. L. Jäger and E. Erdös, *Coll. Czech. Chem. Commun.*, 1959, 24, 3019.

25. A.I. Liapis and D.W.T. Rippin, *Chem. Eng. Sci.*, 1977, 32, 619.

26. A.I. Liapis and D.W.T. Rippin, *Chem. Eng. Sci.*, 1978, 33, 593.

27. M.W. Balzli, PhD Thesis, Eidgenössiche Technische Hochschüle, Zurich, 1977.

28. M.W. Balzli, A.L. Liapis and D.W.T. Rippin, *Trans. I. Chem. E.*, 1978, 56, 145.

29. C. Sheindorf, M. Rebhun and M. Sheintuch, *J. Coll. Interface Sci.*, 1981, 79, No.1, 136.

30. C. Sheindorf, M. Rebhun and M. Sheintuch, *Water Research*, 1982, 16, 357.

31. C. Sheindorf and M. Rebhun, *Chem. Eng. Sci.*, 1983, 38, No.2, 335.

32. W.J. Thomas and I. Lombardi, *Trans. I. Chem. E.*, 1971, 49, 240.

33. K.S. Siddiqi, PhD Thesis, University of Bath, 1980.

34. W.J. Thomas, *Chem. Ind.*, 1980, 366.

35. E. Glueckauf and J.I. Coates, *J. Chem. Soc.*, 1947, 1315.

36. D. De Vault, *J. Am. Chem. Soc.*, 1943, 65, 532.

37. L.C. Eagleton and H. Bliss, *Chem. Eng. Progr.*, 1953, 49, No.10, 543.

38. K.R. Hall, L.C. Eagleton, A. Acrivos and T. Vermeulen, *Ind. Eng. Chem. Fundamentals*, 1966, 5, No.2, 212.

39. D.O. Cooney and E.N. Lightfoot, *Ind. Eng. Chem. Fundamentals*, 1965, 4, No.2, 233.

40. D.O. Cooney and F. Paolo Strusi, *Ind. Eng. Chem. Fundamentals*, 1972, 11, No.1, 123.

41. A. Acrivos, *Chem. Eng. Sci.*, 1960. 13, No.1, 1.

42. L. Lapidus and J.B. Rosen, *Chem. Eng. Progr., Symp. Series*, 1954, 50, No.14, 97.

43. J.M. Coulson and J.F. Richardson, "Chemical Engineering", 2nd Ed., Vol.3, Pergamon Press, 1979, pp.497-593.

44. C. Tien and G. Thodos, *A.I.Chem.E. J.*, 1959, 5, No.3, 373.

45. N.K. Heister, S. Radding, R. Nelson and T. Vermeulen, *A.I.Chem.E. J.*, 1956, 2, No.3, 404.

46. K.S. Robinson, PhD Thesis, University of Bath, 1978.

47. S. Masamune and J.M. Smith, *A.I.Chem.E. J.*, 1965, 11, No.1, 34 and 41.

48. P.R. Kasten, L. Lapidus and N.R. Amundson, *J. Phys. Chem.*, 1952, 56, 683.

49. E. Ledoux, *Chem. Eng.*, 1948, 55, 118.

50. M.S. Peters and K.D. Timmerhaus, "Plant Design and Economics for Chemical Engineers", 2nd Ed., McGraw-Hill, New York, 1968, P 430.

51. P.B. Lederman and B. Williams, *A.I.Chem. J.*, 1964, 10, No.1, 30.

52. R.L. Dedrick and R.B. Beckmann, *Chem. Eng. Progr., Symp. Series*, 1967, 63, No.74, 68.

53. S. Brunauer, "The Adsorption of Gases and Vapours", University Press, Princeton, 1943.

54. M.M. Dubinin, *Chem. Rev.*, 1960, 60, 235.

55. W. Kast, *Ger. Chem. Eng.*, 1981, 4, 265.

56. L.R. Dorfman and R.P. Danner, *A.I.Chem.E. Symp. Series*, 1975, 71, No.152, 30.

57. W.J. Dixon, "BMDP Statistical Software", University of California Press, Berkeley, 1981.

58. J.B. Rosen, *J. Chem. Phys.*, 1952, 20, No.3, 387.

59. J.B. Rosen, *Ind. Eng. Chem.*, 1954, 46, No.8, 1590.

60. C.R. Antonson and J.S. Dranoff, *Chem. Eng. Progr., Symp. Series*, 1969, 65, No.96, 27.

61. C.N. Satterfield and A.J. Frabetti, *A.I.Chem.E. J.*, 1967, 13, No.4, 731.

62. D.T. Camp and L.N. Canjar, *A.I.Chem.E. J.*, 1966, 12, No.2, 339.

63. C.R. Wilke and O.A. Hougen, *Trans. Am. Inst. Chem. Engrs*, 1945, 41, 445.

64. C.R. Wilke and C.Y. Lee, *Ind. Eng. Chem.*, 1955, 47, No.6, 1253.

65. R.M. Barrer and B.E.F. Fender, *J. Phys. Chem. Solids*, 1961, 21, 12.

66. H.W. Habgood, *Can. J. Chem.*, 1958, 36, 1384.

67. D.M. Ruthven and K.F. Loughlin, *Trans. Faraday Soc.*, 1971, 67, 1661.

68. E.F. Kondis and J.S. Dranoff, *A.I.Chem.E. Symp. Series*, 1971, 67, No.117, 25.

69. D.M. Ruthven, *A.I.Chem.E. J.*, 1978, 24, No.3, 540.

70. W.J. Thomas and K.S. Robinson, *Trans. I. Chem. E.*, 1980, 58, 219.

71. K. Miura, H. Kurahashi, Y. Inokuchi and K. Hashimoto, *J. Chem. Eng. Japan*, 1979, 12, No.4, 281.

72. R.W.H. Sargent and C.J. Whitford, *Adv. Chem. Series*, 1971, 102, 155.

73. K. Hashimoto, K. Miura and M. Tsukano, *J. Chem. Eng. Japan*, 1977, 10, No.1, 27.